UNCLASSIFIED

AD NUMBER
AD517696
NEW LIMITATION CHANGE
TO Approved for public release, distribution unlimited
FROM Distribution authorized to U.S. Gov't. agencies and their contractors; Administrative/Operational Use; SEP 1971. Other requests shall be referred to Naval Ship Systems Command, Washington, DC 20360.
AUTHORITY
ONR ltr, 31 Jan 2006

THIS PAGE IS UNCLASSIFIED

UNCLASSIFIED

AD NUMBER
AD517696
CLASSIFICATION CHANGES
TO unclassified
FROM confidential
AUTHORITY
30 Sep 1983, DoDD 5200.10

THIS PAGE IS UNCLASSIFIED

GROUP 4

Downgraded at 3-year intervals;
declassified after 12 years.

CONFIDENTIAL

NUC TP 257

ADAPTIVE BEAMFORMING ANALYSIS FOR DIRECTIONALITY USING DATA FROM A VERTICAL ARRAY IN THE MEDITERRANEAN (U)

by

Craig G. Anderson
Dorothy A. Anderson
Gerald L. Kinnison

Ocean Sciences Department

September 1971

CONFIDENTIAL

NAVAL UNDERSEA RESEARCH AND DEVELOPMENT CENTER, SAN DIEGO, CA. 92132

AN ACTIVITY OF THE NAVAL MATERIAL COMMAND

CHARLES B. BISHOP, Capt., USN
Commander

Wm. B. McLEAN, Ph.D.
Technical Director

The work reported was sponsored by NAVAIR (533) Project Number W-2140 and NAVSHIPS (00V) Project Number F 11-121 and was done from December 1970 to April 1971.

Released by
R. S. GALES, Head
Passive Acoustics Division

Under Authority of
G. B. ANDERSON, Head
Ocean Sciences Department

This document contains information affecting the National Defense of the United States within the meaning of the Espionage Laws, Title 18, U. S. C., Sections 793 and 794. The transmission or the revelation of its contents in any manner to an unauthorized person is prohibited by law.

SUMMARY

PROBLEM

Analyze the vertical directionality of the ambient noise in the Ionian Basin of the Mediterranean Sea. Record and analyze data for directional content using adaptive and conventional beamforming techniques.

RESULTS

It was found that the amount of uncorrelated (circuit) noise has a strong influence on the measured directionality of the noise field. It was also found that adaptive beamforming improves the resolving power of the array at any frequency over conventional beamforming, but more especially at low frequencies.

RECOMMENDATIONS

1. Array-independent vertical directionality of ambient noise should be attempted using adaptive beamforming techniques as an analytical tool. Minimal ambiguity in directionality conclusions will result from careful attention to uncorrelated (circuit) noise, suspension noise, and verticality of the array.
2. The resolving power of the array should be tested in advance using propagation theory and assumed shipping and sea state distributions.
3. Only then can measurement results help in our understanding of the acoustic environment and allow us to establish system performance modeling as a basis for future system decisions with adequate confidence.

CONTENTS

INTRODUCTION	1
RESULTS	6
Directional-Response Computations at 97 Hz	6
Array Gain Versus Frequency (AGVF) Curves	13
Frequency Versus Depression/Elevation Angle Plots	14
REFERENCES	15
APPENDIX A: ACTUAL DATA RESULTS	17
APPENDIX B: SIMULATED DATA RESULTS	31
APPENDIX C: ARRAY GAIN FOR ACTUAL DATA	105
APPENDIX D: ARRAY GAIN FOR SIMULATED DATA	113

INTRODUCTION

(U) In January, 1970, under contract N00019-70-C-0468, extensive data were taken in the Mediterranean Sea by Sanders Associates, Inc. of Nashua, N. H. Data were recorded from each of the four major deep water basins. The only one of these samples treated in this report was recorded on 28 January from the vertical array suspended from the surface of the Ionian Sea; this sample, chosen from that day's recordings, was recorded during a period with no especially close merchant traffic. This was verified by aircraft surveillance as shown in figure 1.

(U) Figure 2 shows the array as deployed during the data acquisition. It consisted of 10 omnidirectional hydrophones suspended vertically from a surface buoy along a 200-foot cable. These sensors were recorded as two separate arrays: one designed for high frequencies (300-1000 Hz) and the other for low frequencies (< 300 Hz). Data from the latter array were selected for analysis by NUC. The sensors of this array were regularly spaced at 16.4-foot intervals along the line configuration; of the seven sensors recorded, the elements at top and bottom failed to operate during the tests, so only the remaining five constituted the array from which data were analyzed for this report.

(U) From the surface float, the array was hardwired to recording equipment aboard the U. S. S. Hoist at the end of a 2000-foot cable run. This tether suspension caused numerous problems, since the strong frequency lines from rotating machinery aboard the Hoist interfered with far-field inputs. Other than Hoist, the nearest merchant vessel at 1400 on 28 January, the period taken for our analysis, was about 20 nautical miles away (see figure 1).

(U) The analog outputs from the five sensors were passed through a 30- to 1000-Hz bandpass filter aboard the Hoist just prior to recording. During playback, before digitization, antialiasing filters that have an 18 dB per octave roll-off with the cornering frequency set at 300 Hz are applied. Digitization was then set at 1285 samples per second per channel, ten significant bits per sample. With the data in the time-domain digital form, the next operation was 1024-point fast Fourier transformation (FFT) with about 20 significant bits of accuracy, using a computer software algorithm. This yielded 512 complex frequency coefficients with approximately 1.25-Hz resolution.

(U) Owing to the regular sensor spacing along the 65.6-foot line array, not all of these frequency bins were useful for analysis. If we assume 5000 feet per second as the speed of sound in sea water, and use the 16.4-foot sensor separation as half wavelength for the upper frequency of interest, we find that the array performance will gradually degrade until at 152.4 Hz, directional ambiguity will prevent adequate resolution of the directional character of the noise field. Hence, we lack confidence in any conclusions about results above 152.4 Hz. After FFT, the complex frequency coefficients were multiplied to yield spectral crosspower matrices by adding successive sensor pair multiples until an effective 8.5 minutes of time integration was achieved.

(U) These matrices were "interrogated" for the directional character of the field by pre- and post-multiplication by a directional pointing vector which describes the expected

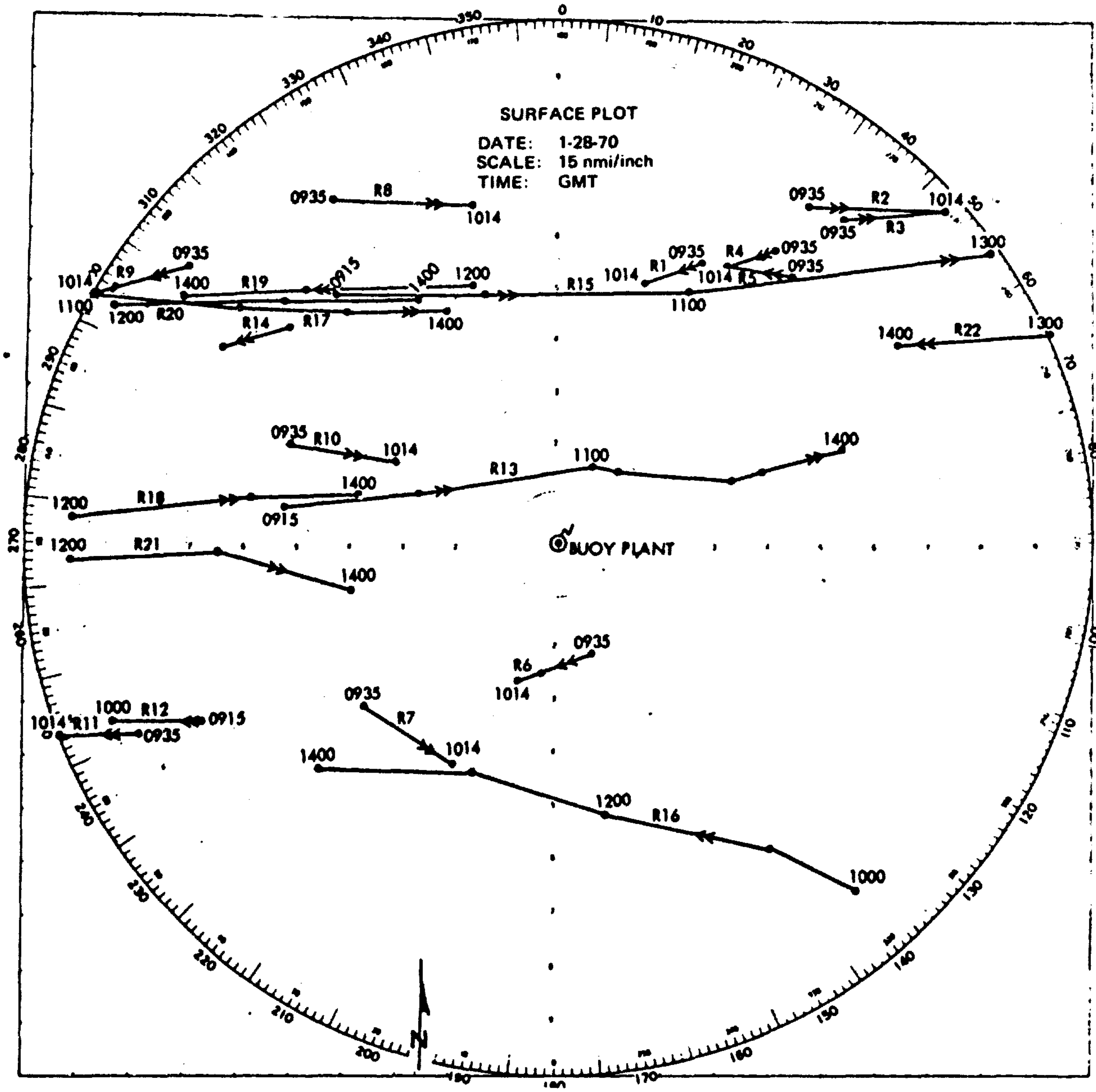

(C) Figure 1. Surface traffic plot.

wavefront of acoustical energy from a single direction and at a single frequency. The resultant integrated beam power outputs, by repeated interrogation over all directions and all frequencies, can be plotted as shown in figures 3 (adaptive) and 4 (conventional) to show an overall measure of the actual data noise-field directionality. For single frequency consideration, however, the plots (figures A1 -- A12) from actual data can be better compared with

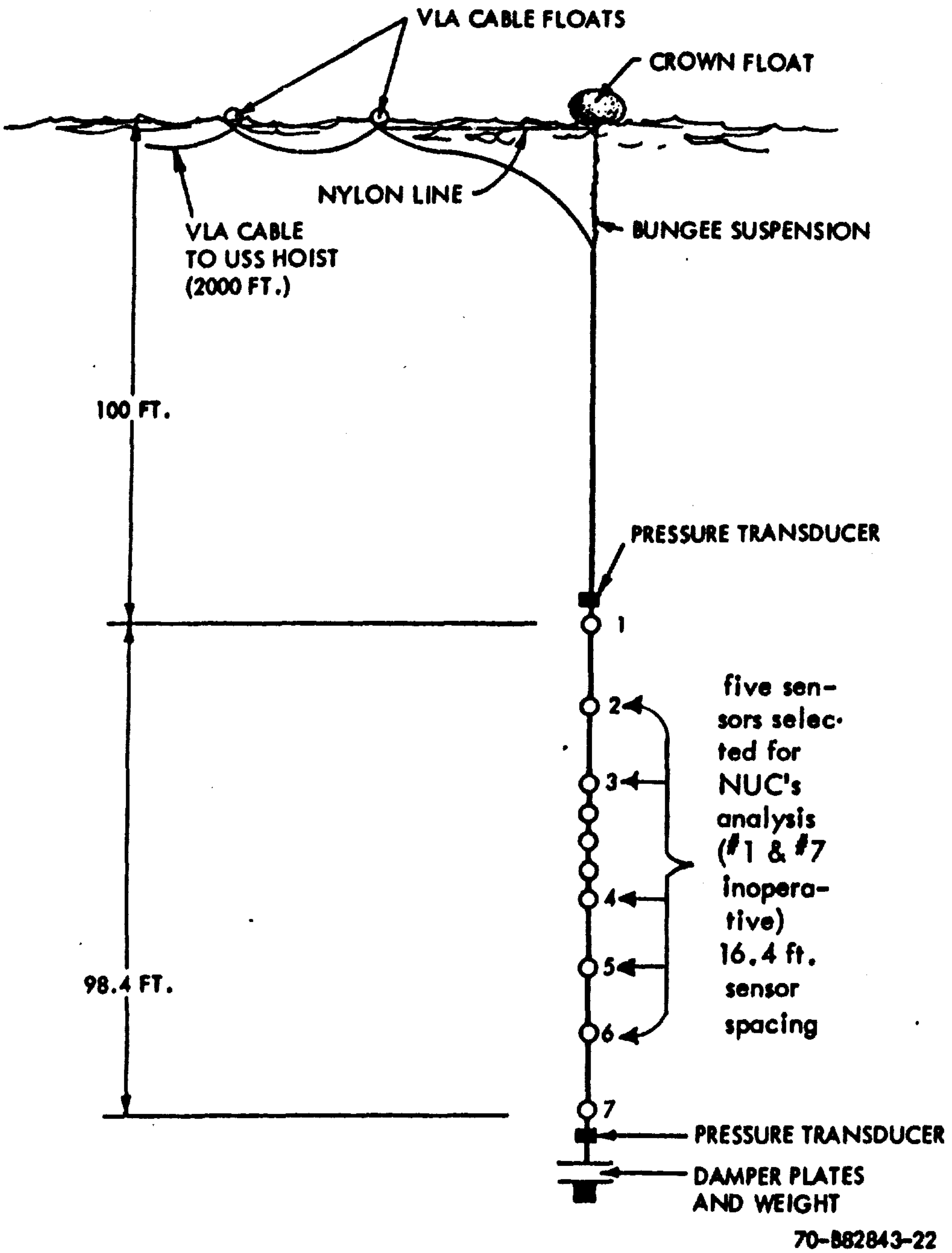

(U) Figure 2. Vertical line array.

a priori assumptions about the vertical directionality (see figures B1 – B72). All the above computations were based upon the same well-established theory found in reference 3, and the reader is referred there for more detailed information about the beamforming techniques employed for this analysis. For further details regarding the array and data collection procedures see the final Sanders, Inc. report (reference 4).

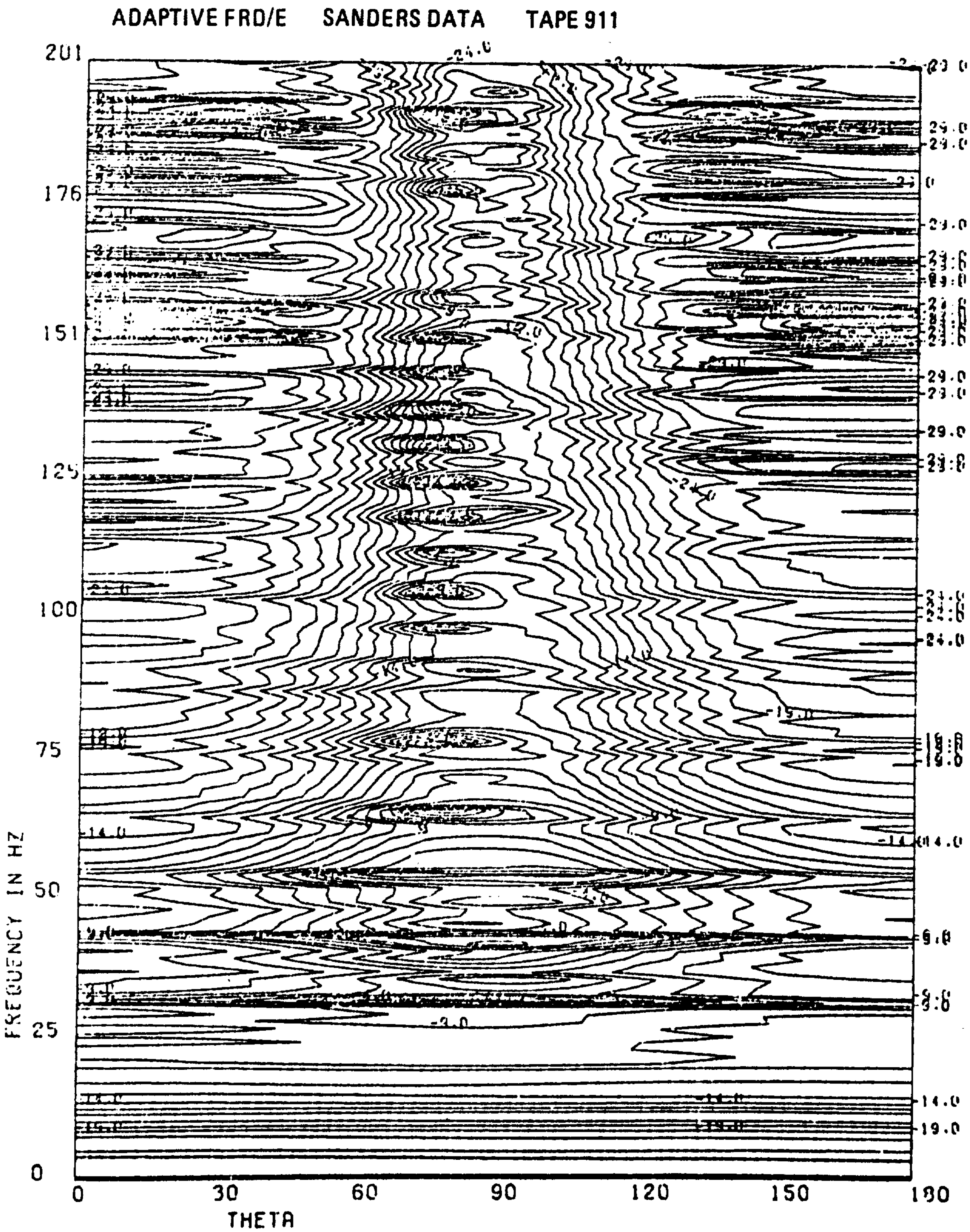

(U) Figure 3. Adaptive FRD/E.

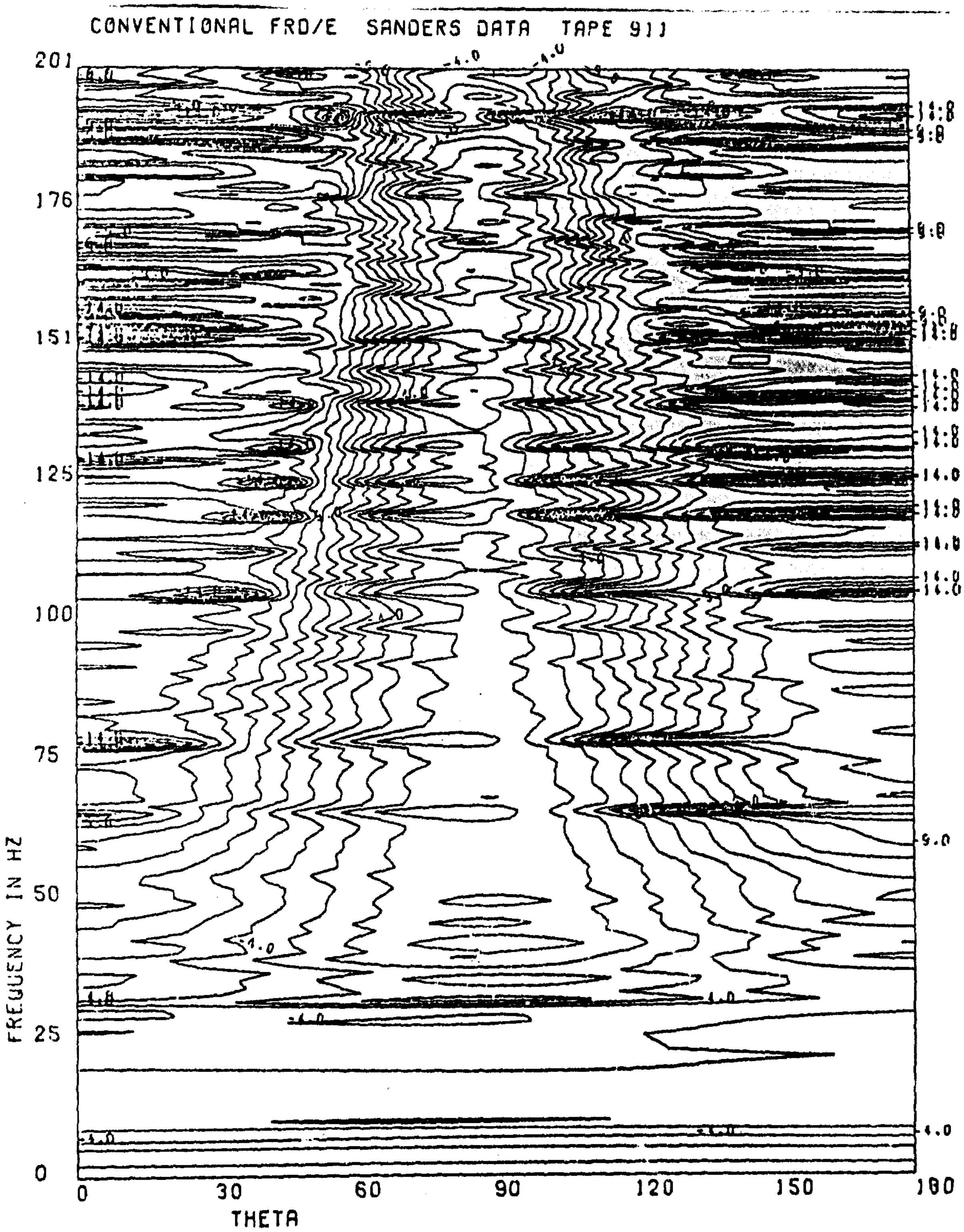

(U) Figure 4. Conventional FRD/E.

RESULTS

(U) Prior to the analysis of actual array data, we tested the ability of the array to resolve vertically directional simulated noise. To do so, we chose the upper solid curves in figures B1 through B72 as the simulated directionality. We then employed two beamforming schemes to resolve this known directional character: adaptive (or optimal) combination of the five sensors, and conventional (or time-shift-and-sum). Results of the application of these two beamformer outputs are shown in figures B1 through B72 as the middle and lower curves, respectively. Note that at the lower frequencies (< 64 Hz) the resolving power decreases sharply, as indicated by the lower (conventional beamforming) curve, which is no doubt due to the array's short (65.4-foot) length. Note also that at frequencies above the half-wavelength frequency (152.4 Hz) degradation can be seen (especially in the conventional response) as a waviness in the baseline in directions away from the directionality peak, which becomes progressively worse as frequency is increased. In this upper frequency band the array is sensor-limited and the regular spacing between sensors leads to "grating lobe" behavior or directional ambiguity at higher frequencies. Adaptive beamforming improves the resolving power of the array at any frequency, but is especially effective at low frequencies. Figures 5-10, A1-A12, and B1-B72 present the data as "bearing response", plotting relative bearing (0° straight up, 90° horizontal, and 180° straight down) and relative power out in dB along the ordinate. No attempt is made to indicate absolute power levels, and the curves are arbitrarily clamped to 0 dB at 180°. This type of output is intended for directionality conclusions only: other outputs (array gain versus frequency) are more useful for array S/N improvement conclusions.

(U) Actual data results to be compared with the above a priori, simulated data results are found as figures A1 through A12. Note that they all show broader directional response than any of the simulated data results (figures B1 through B72). Note also that the beam power response humps in the actual data (figures A1 through A12) suggest that the actual data field is best approximated by either noise field 1 (figures B1 through B12) or 2 (figures B13 through B24), depending upon the frequency being considered. However, the separation between the adaptive and conventional beam power output response curves is less for the actual data than for the corresponding simulated data response curves. This observation caused us to examine the conditions from which this result would follow. We concluded that this was probably due to high levels of uncorrelated (circuit) noise, and we present the following sample computational results to document this conclusion and to arrive at a reasonable estimate of the vertical angle arrival structure of the actual noise field.

Directional-Response Computations at 97 Hz

(U) In figure 5 we show a family of four simulated directional response curves (the upper four) so constructed that they could account for the actual data directional response at 97 Hz (which is presented in figure 6 and shown superimposed on the simulated directional response curves in figure 7) under different assumptions about the fraction of uncorrelated noise on each sensor channel. In figure 5, the top curve in the family portrays the actual vertical character of noise in the water, which could account for the response shown in the two lower curves if 0.1 or - 10 dB of the single sensor voltage-squared input had been contaminated with uncorrelated (from channel to channel) noise such as that from thermal or

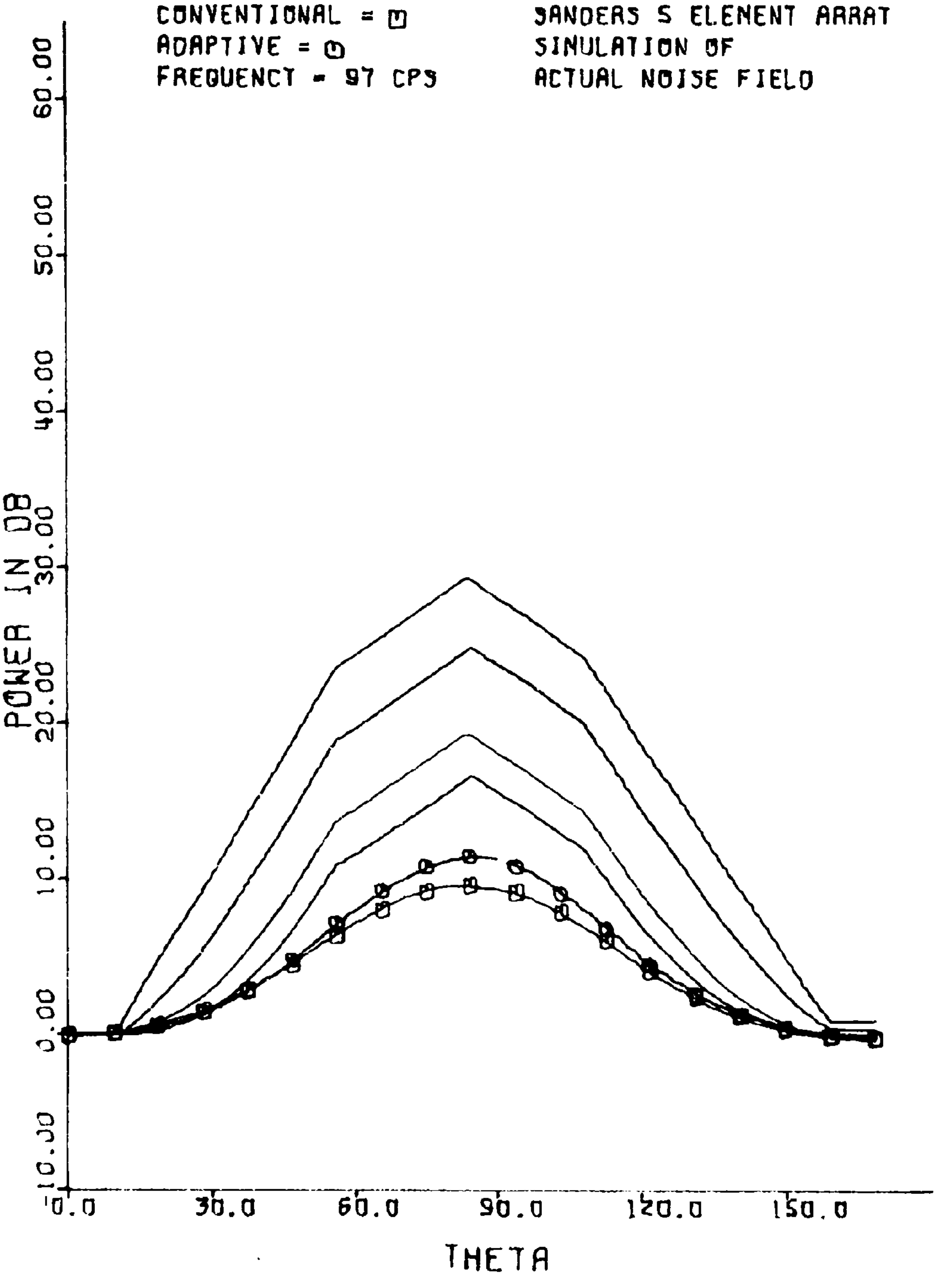

(U) Figure 5. Bearing response (BR) Simulation of actual noise field 97 cps.

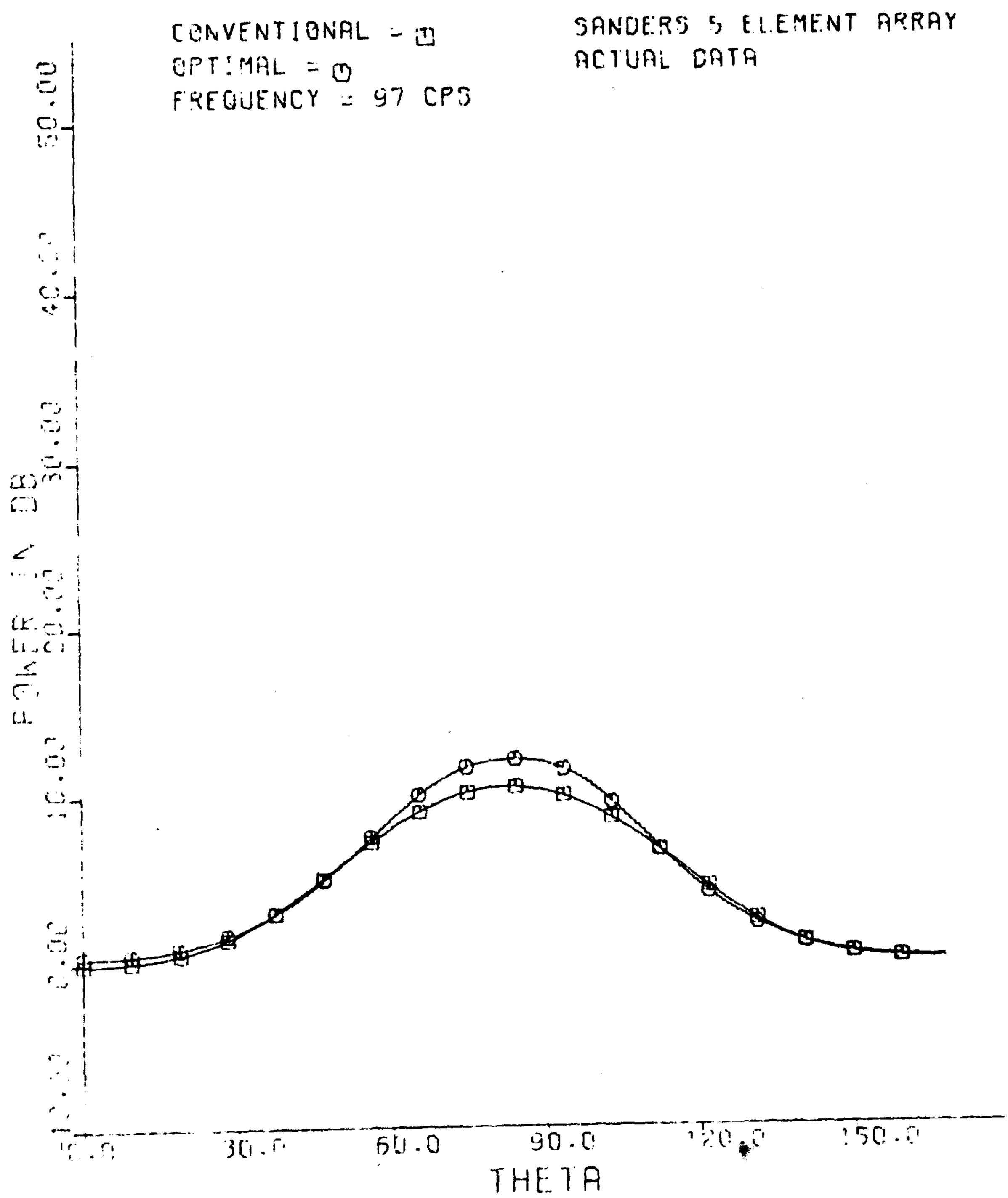

(U) Figure 6. BR – actual noise field – 97 cps. "Optimal" has the same meaning as "adaptive."

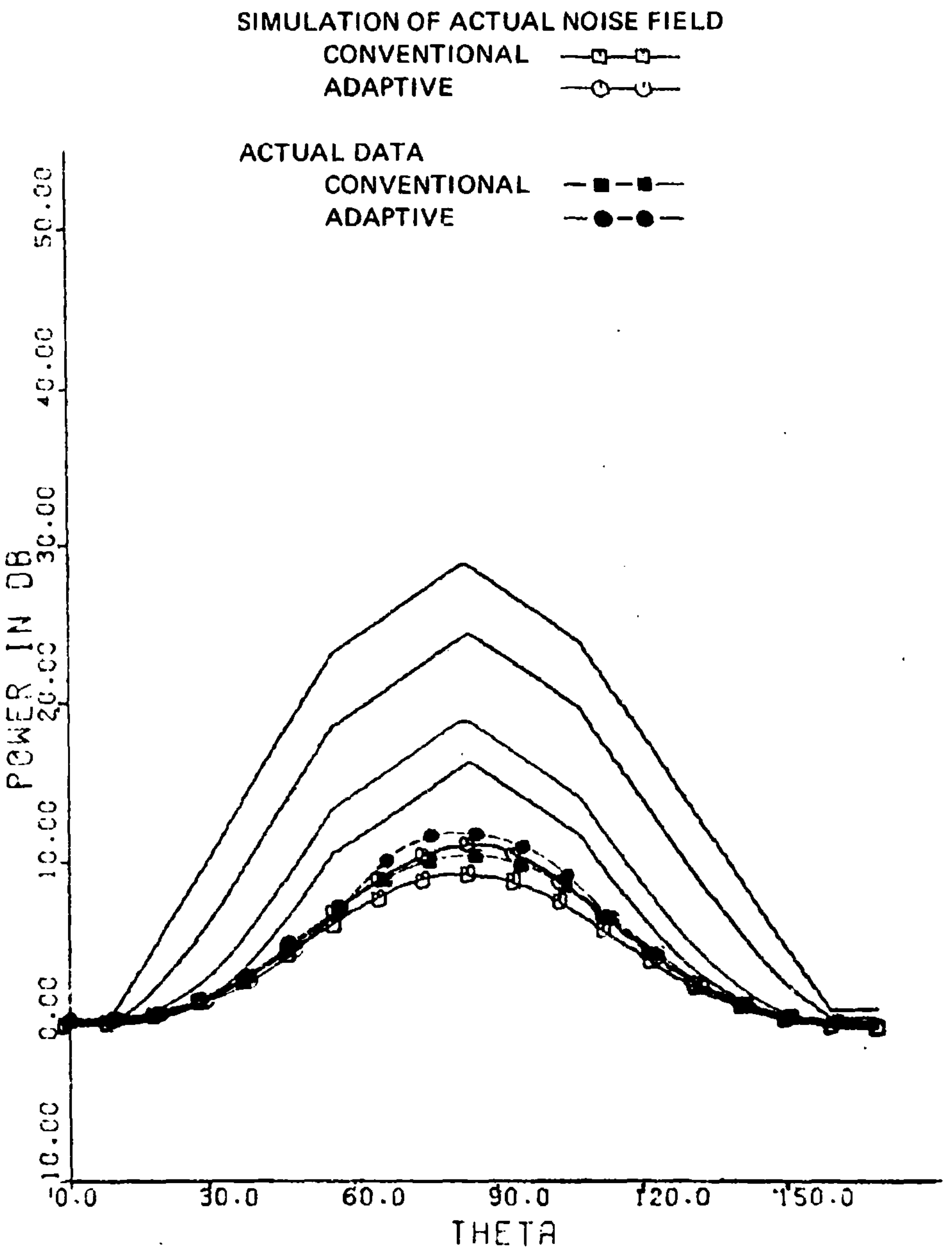

(U) Figure 7. BR actual noise field and simulation 97 cps.

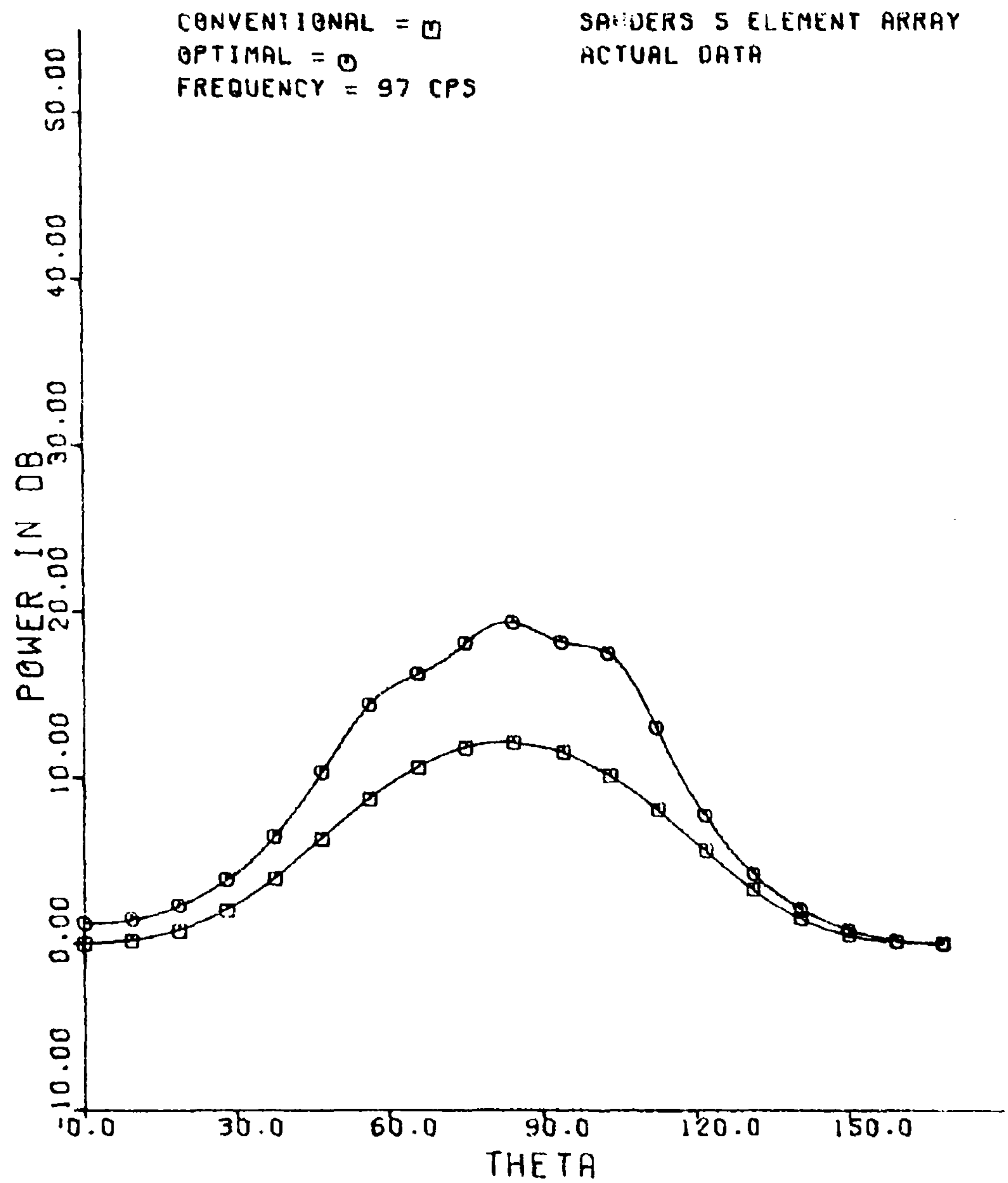

(U) Figure 8 BR actual noise field 97 cps 10 percent uncorrelated noise deleted. "Optimal" has the same meaning as "adaptive."

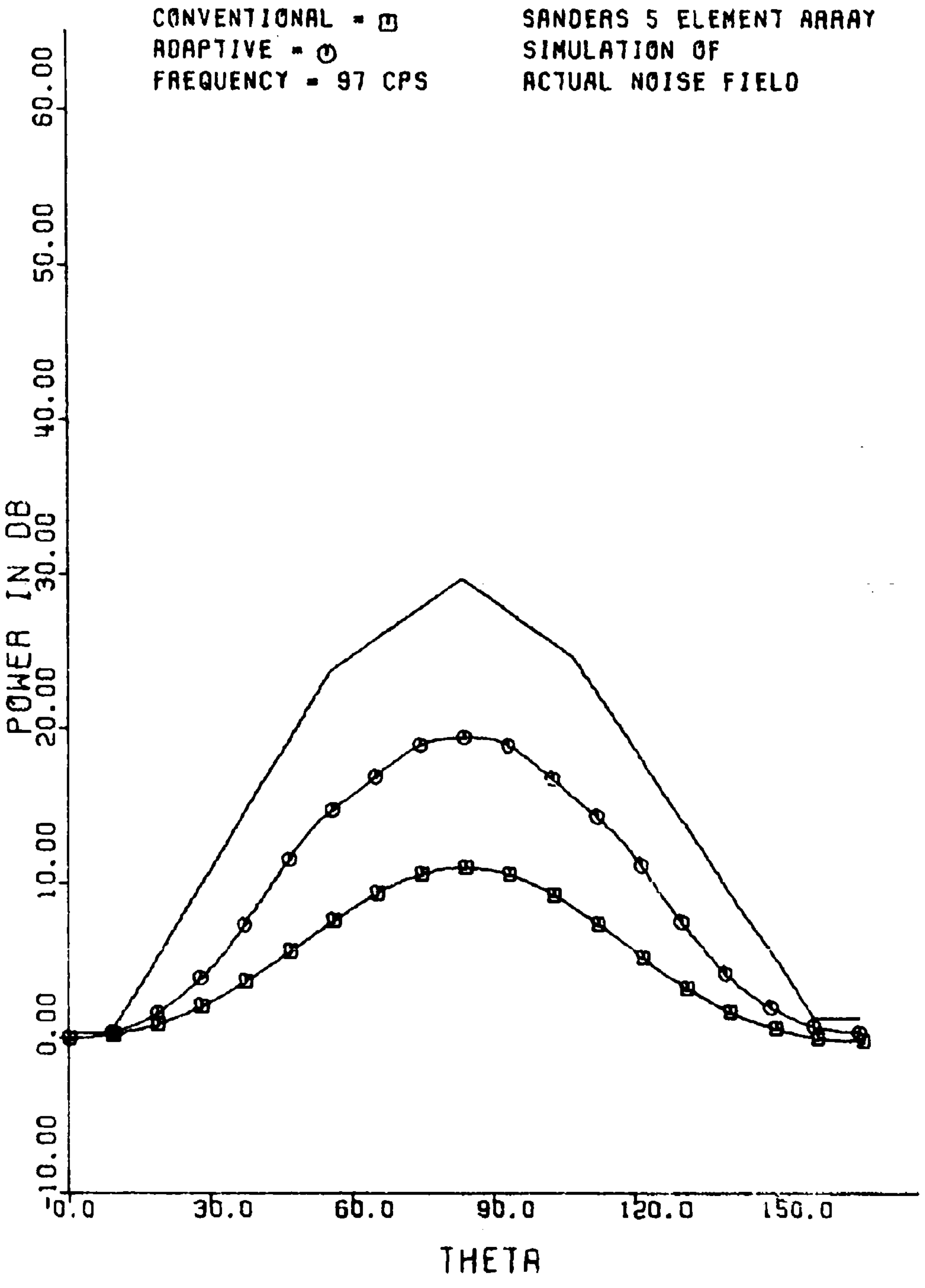

(U) Figure 9. BR – simulation of actual noise field with –40 dB uncorrelated 97 cps.

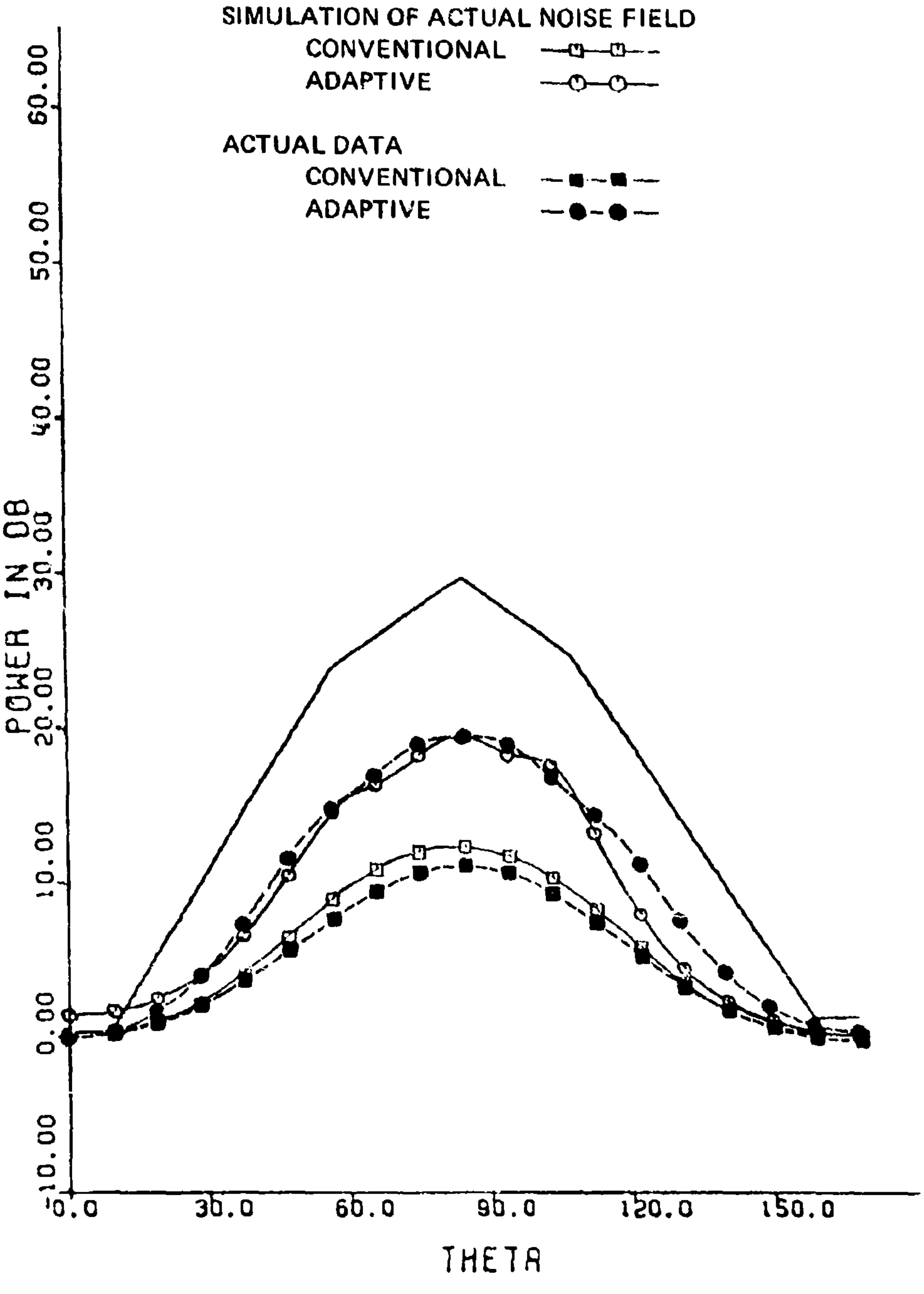

(U) Figure 10. BR - ctual noise field with 10 percent uncorrelated noise deleted and simulation of actual noise field with -40 dB incorrelated 97 cps.

circuit-noise sources. The next-lower curve of the family is the constructed response (not unique) appropriate for 9-percent contamination, the next for 5-percent contamination, and the lowest family member for no contamination. Which curve of this family best represents the true directional character of the vertical noise field at the time and location of the deployed Sanders array cannot be conclusively established, which underscores the need for high quality array recording (low circuit noise) if directionality conclusions are to be drawn from such measurements.

(U) A check with Sanders, Inc., revealed that the spectral circuit noise level had been measured at only about 10 dB below the single sensor power at the recording time, so we continued our analytical investigation. We took the actual data spectral cross power matrix at 97 Hz and subtracted from the main diagonal terms a scalar amount equivalent to 10 dB uncorrelated noise. Upon interrogation, this matrix yielded the curves of figure 8, which are to be compared with the simulated curves of figure 9. Figure 9 shows the simulated beamformer output responses assuming a very small fraction (0.0001 or −40 dB) of uncorrelated noise. When we tried to subtract 12-percent uncorrelated noise the resultant matrix was singular. For the above reasons, the upper solid curve of figure 9 is presented as the most reasonable estimate for the shape for the actual noise field's vertical arrival structure, bearing in mind that the width of the response near horizontal may be artificially broad, if the array had significant tilt. Tilt was not measured. The curves of figures 8 and 9 are shown superimposed in figure 10 to facilitate comparison.

Array Gain vs Frequency (AGVF) Curves

(C) If the noise field were completely uncorrelated, these curves (see figures C1-C7) would be straight lines at 10 log N, where N is the number of sensors. For this data there were 5 sensors, so 10 log 5 = 7 dB for uncorrelated noise. As can be seen by examining the sequence of figures C1 through C7, the least gain is realized at D/E = 0 (figure C1), and progressively greater array gain results from steering beams progressively farther up, or down, from horizontal (D/E = 0). The term D/E indicates the depression/elevation angle with positive angles up from the horizontal and negative angles down from the horizontal. Only beginning at D/E = 30 does the optimal array gain curve begin to exceed the 10 log N (7 dB) level. The anomalous peak in the optimal gain curve at 105 Hz was due to noise radiated from the nearby surface vessel, which at this time was only 700 feet from the suspension buoy. For the closer-in targets which are expected to have arrival angles up to 60° D/E (figure C5), improvements of up to 15 dB are possible using adaptive beamforming at frequencies above 80 Hz. For conventional beamforming, improvements of only 3 or 4 dB less are possible.

(U) For a theoretical description of array gain the reader is referred to references 1 and 2.

(U) Figures D1 through D42 present calculated array gains for the same simulated noise fields as for the directional response computations above, showing significant gains which were possible even from this array without close attention to array tilt, vertical motion, and array tether.

Frequency Versus Depression/Elevation Angle Plots

(U) An overall view of the recorded noise field is presented in the FRequency vs Depression/Elevation angle (FRD/E) plots. These plots are collections of single line-bearing responses at many frequencies. All of the lines on a plot are normalized to a common maximum power point; the contour lines represent areas of equal power. On the FRD/E plots presented in this report, these contours are 1-dB apart. Figure 3 is the FRD/E plot for the adaptive processor. The dynamic range of the plot is approximately 30 dB with the maximum power response occurring at about $\theta = 85$ (near horizontal) and frequency = 76 Hz. The noise field above 50 Hz is fairly directional. The power for θ near 90° appears 13 dB higher than the powers at $\theta = 0°$ and $\theta = 180°$. The harmonic content of noise at $\theta = 85°$ is also revealed by the adaptive bearing response. (Note that the dark areas near 0° (straight up) and 180° (straight down) at frequencies above 150 Hz are dips in the power response.) The apparent isotropic nature of the noise field below 30 Hz is artificial; it is caused by the bandpass filters applied to the data (as mentioned earlier). Figure 4 is the FRD/E plot for the conventional (time-shift-and-sum) processor. Its dynamic range is approximately 16 dB with a maximum response at $\theta = 72°$ and frequency = 76 Hz. Almost all of the dark areas on this plot are dips rather than peaks. Also, the frequency content present in the conventional FRD/E is not as well defined. The field does not appear so directional on the conventional FRD/E as on the adaptive. There is only a 10 dB separation between power at $\theta = 90°$ and power at $\theta = 0°$ and $\theta = 180°$. This generally agrees with the single frequency results (figures A1 through A12).

(U) Figures A1 through A12 were generated from the actual data at frequencies selected from the FRD/E contour plots. The same array configuration was used in several simulated noise fields at approximately the same frequencies. Figures B1 through B72 were generated from simulated, vertically-directional noise fields. Comparison of the actual data figures with the latter figures allows conclusions regarding the directionality of the actual noise field.

(U) Figures B1 through B72 show the potential resolving power as calculated from the array geometry (at the frequencies indicated) by plotting bearing vs power responses for conventionally and adaptively processed beamforming with simulated, directional noise fields. These simulated noise fields were obtained from Naval Air Development Center (NADC). The simulated noise field is the solid curve on the graph, while the output of the conventional processor is the curve with the squares and the output of the adaptive processor is the curve with the circles. −40 dB of uncorrelated noise was added to each of the simulated noise fields. As stated earlier, the unusually high level of uncorrelated circuit noise apparently prevented the actual array implementation from realizing its potential for resolving directionality.

(U) The analysis output which quantifies the improvement that can be realized by using a vertical array of sensors compared with using only a single omnidirectional sensor is ARRAY GAIN vs FREQUENCY. An example of this output is shown for the January 1970 Mediterranean data (as described earlier) as figures C1 through C7.

(U) Figures D1 through D42 show the array gains for the simulated noise fields. −40 dB of uncorrelated noise was added to each of the simulated noise fields.

REFERENCES

1. D. J. Edelblute, J. M. Fisk, and G. L. Kinnison. Criteria for Optimum Signal Detection Theory for Arrays. Acoustical Society of America, Journal, v. 41:199-205, no. 1, January 1967.

2. Naval Undersea Warfare Center. NUWC TP 101, Array-Analysis of Data from 12 BQS-6 Transducers for Passive Sonar Purposes, January 1969. CONFIDENTIAL

3. D. J. Edelblute, J. M. Shapard, and G. L. Kinnison. Beam to Beam Normalization for Adaptive and Conventional Preformed Beams, *Proceedings of the Optimal/Adaptive Space Processing Seminar,* 12-14 August 1969. CONFIDENTIAL

4. Sanders Associates, Inc. Acoustic Survey and Data Reduction Phase II. Final report under Contract N00019-70-C-0468 for Naval Air Systems Command and ASW Systems Project Office, PM-4. SECRET.

APPENDIX A

ACTUAL DATA RESULTS

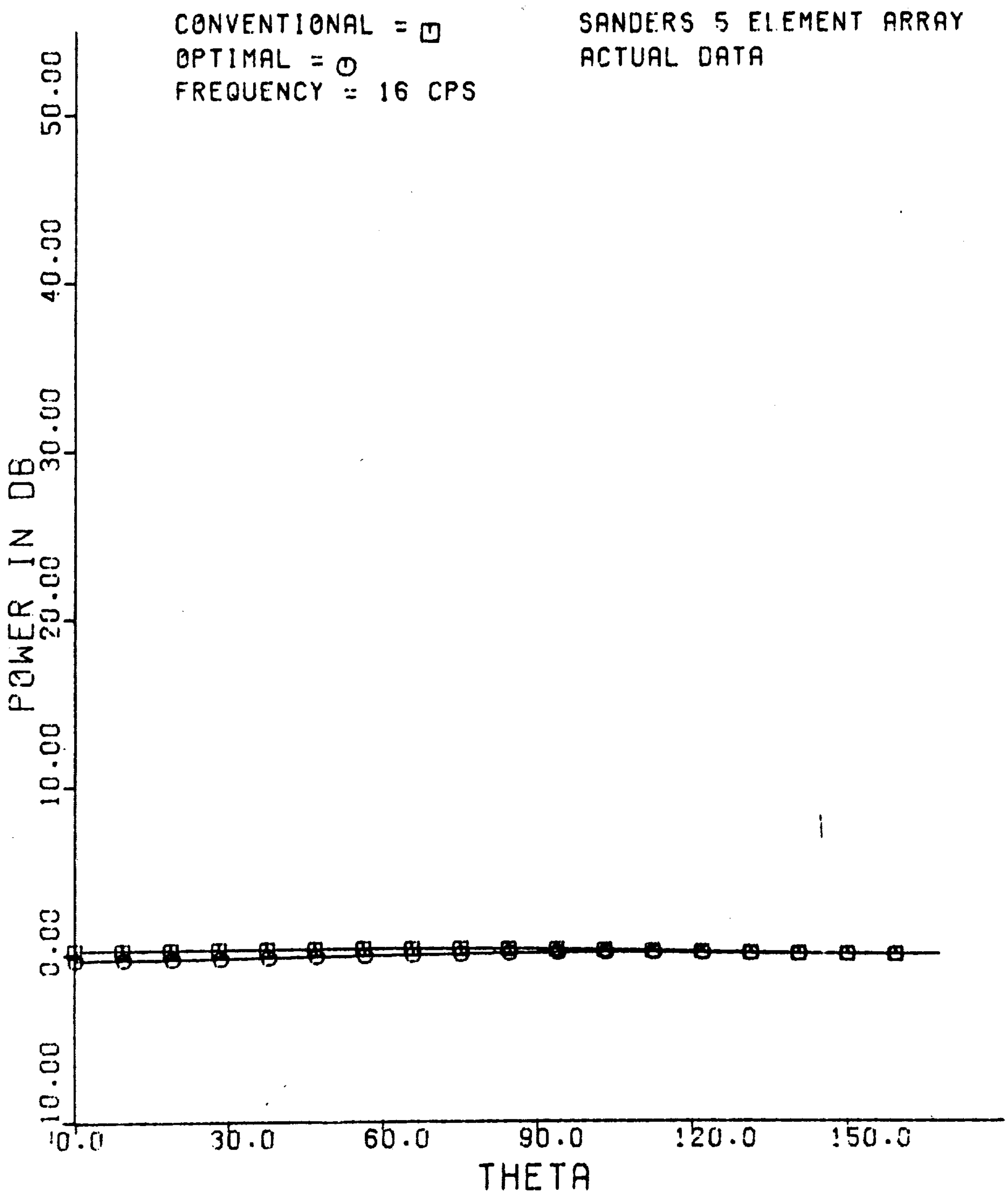

(U) Figure A1. BR – actual data – 16 cps. "Optimal" appears in figures A1 through A12 and has the same meaning as "adaptive."

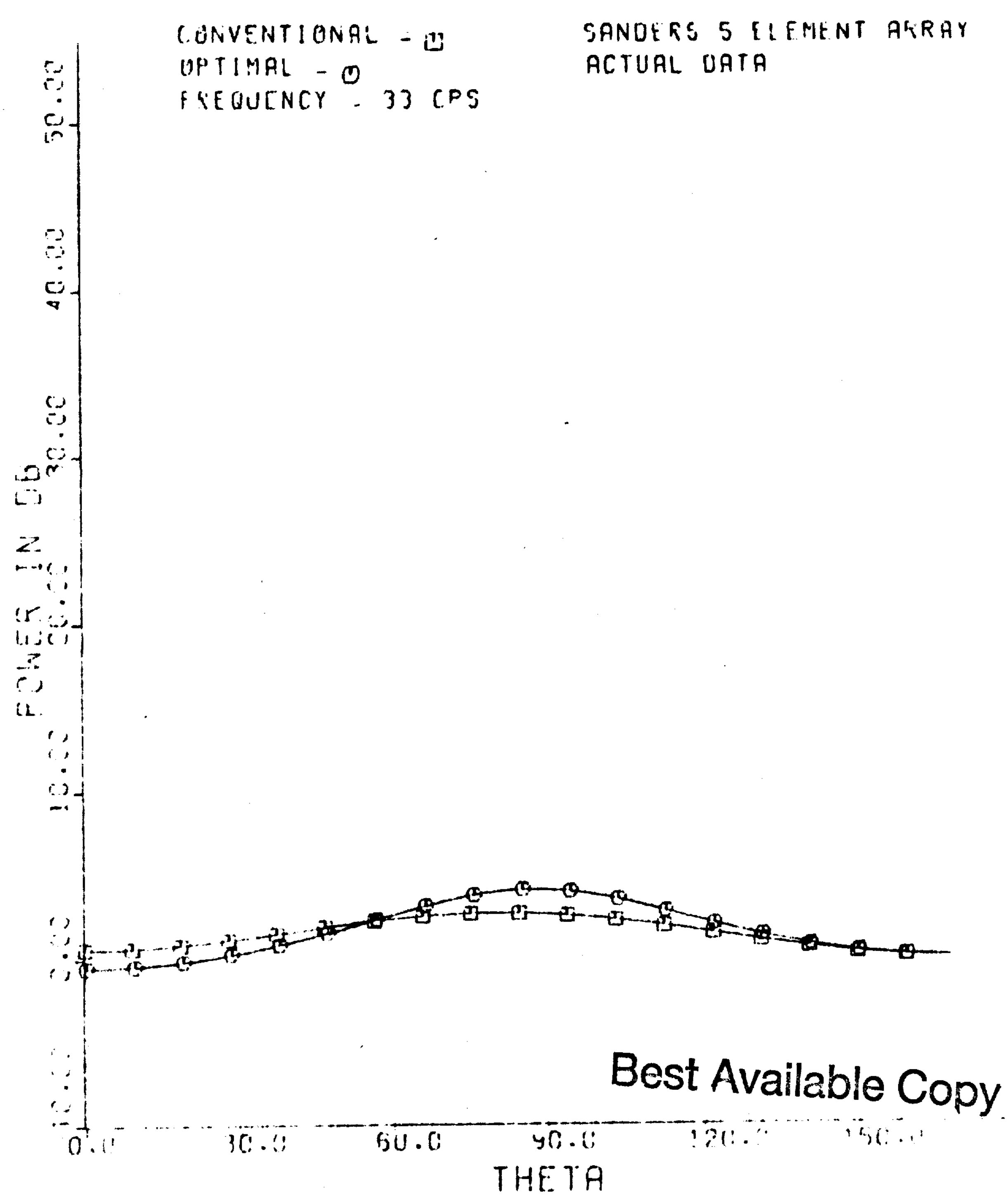

(U) Figure A2. BR – actual data – 33 cps.

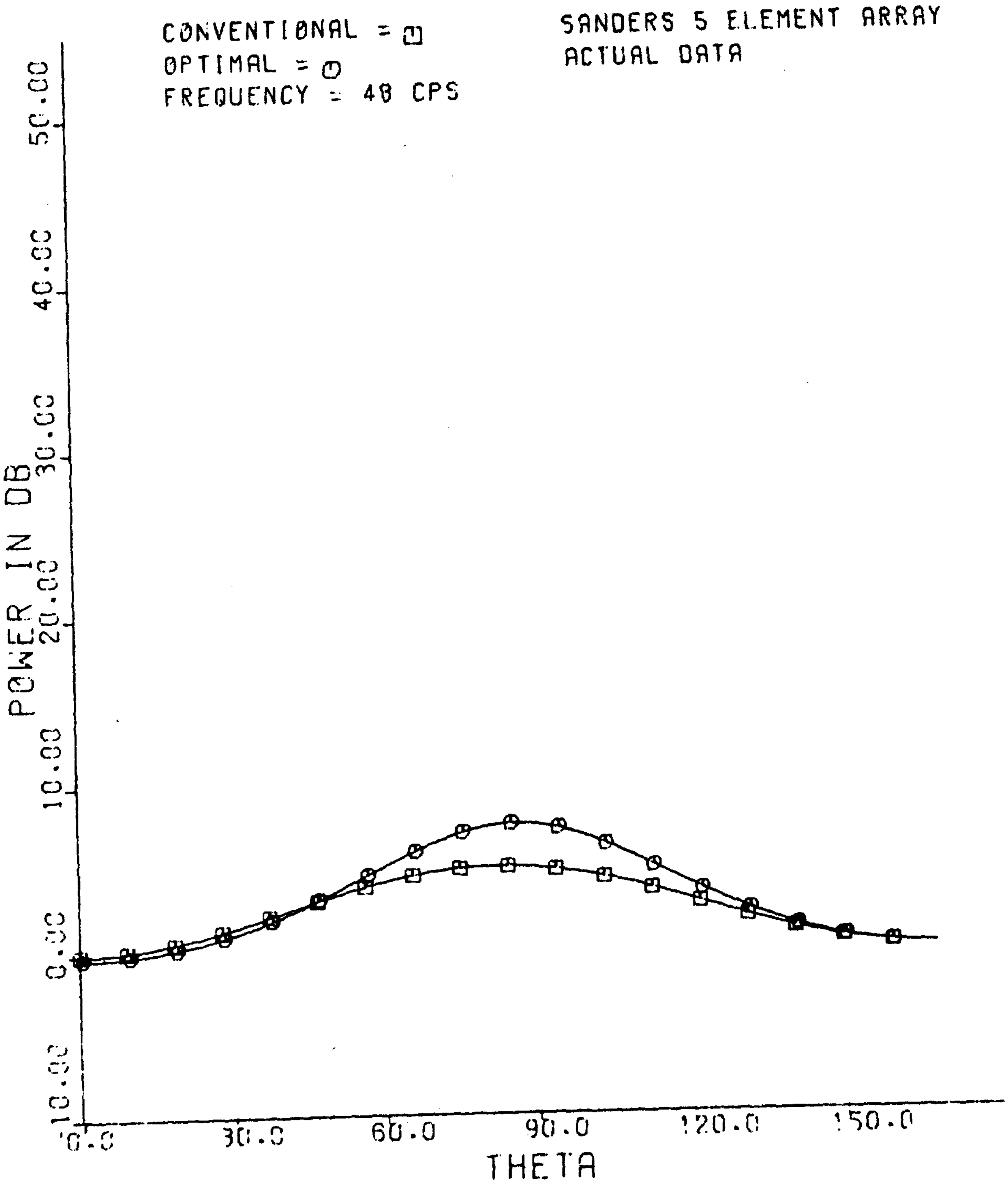

(U) Figure A3. BR – actual data – 48 cps.

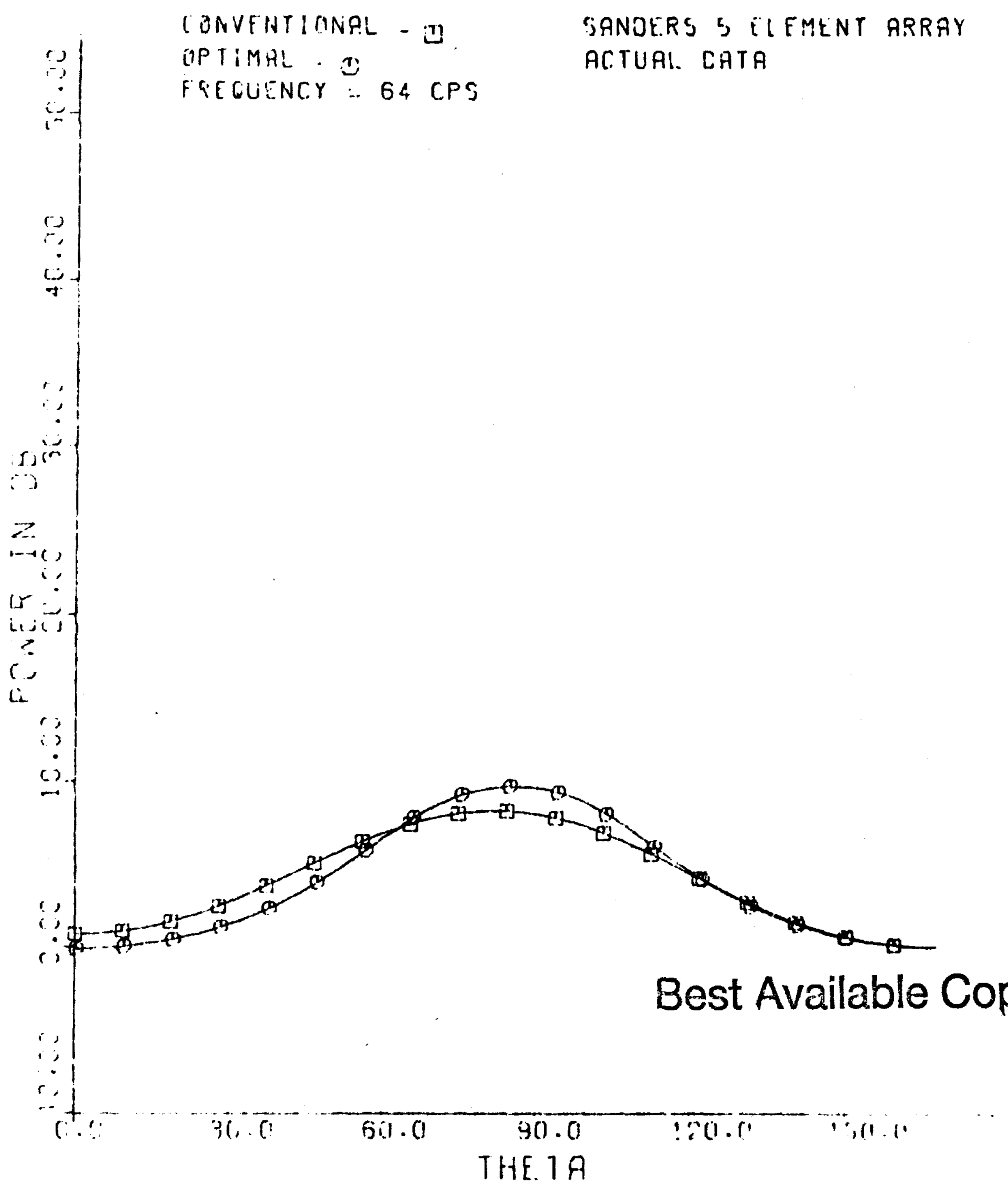

Best Available Copy

(U) Figure A4. BR – actual data – 64 cps.

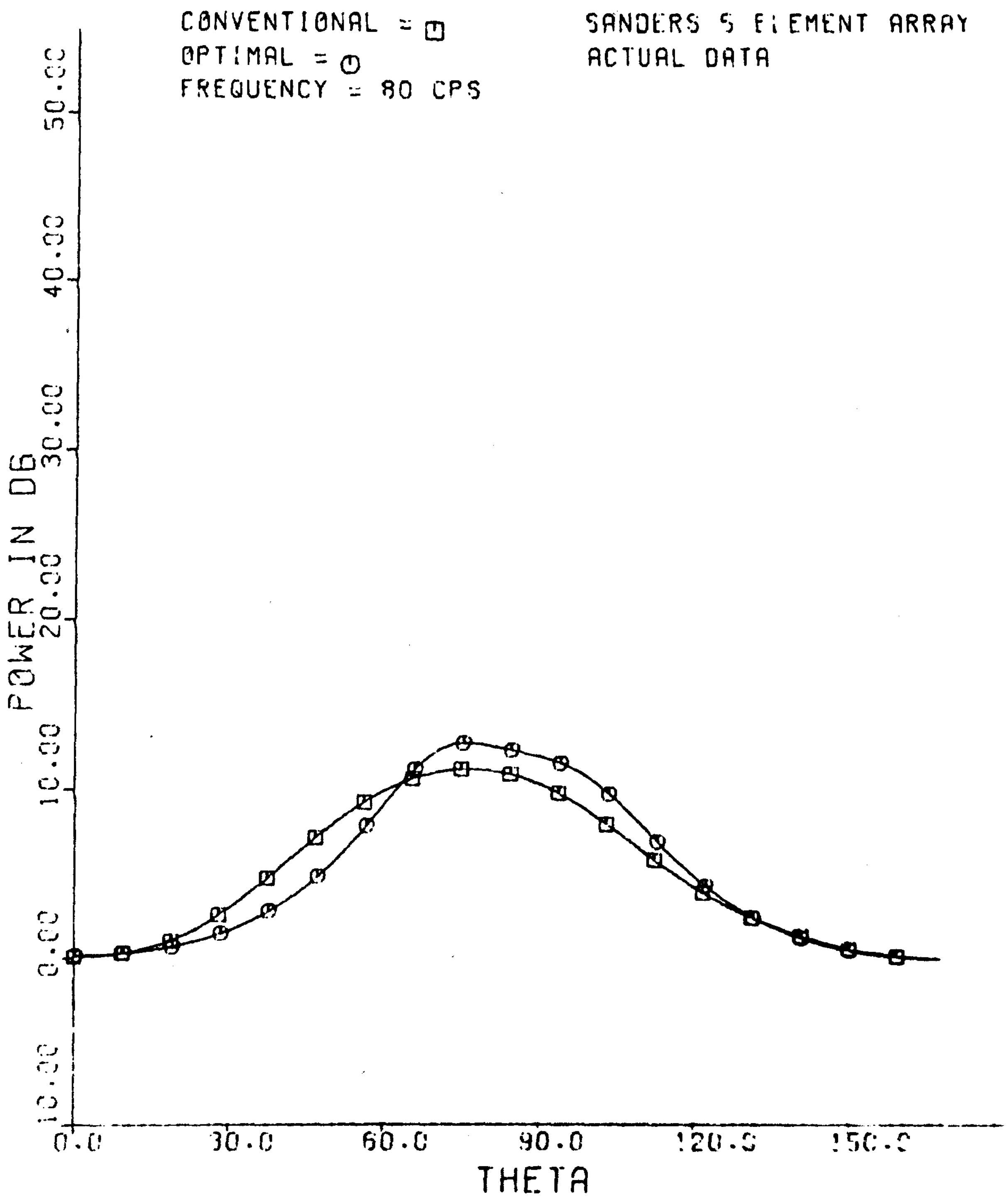

(U) Figure A5. BR – actual data – 80 cps.

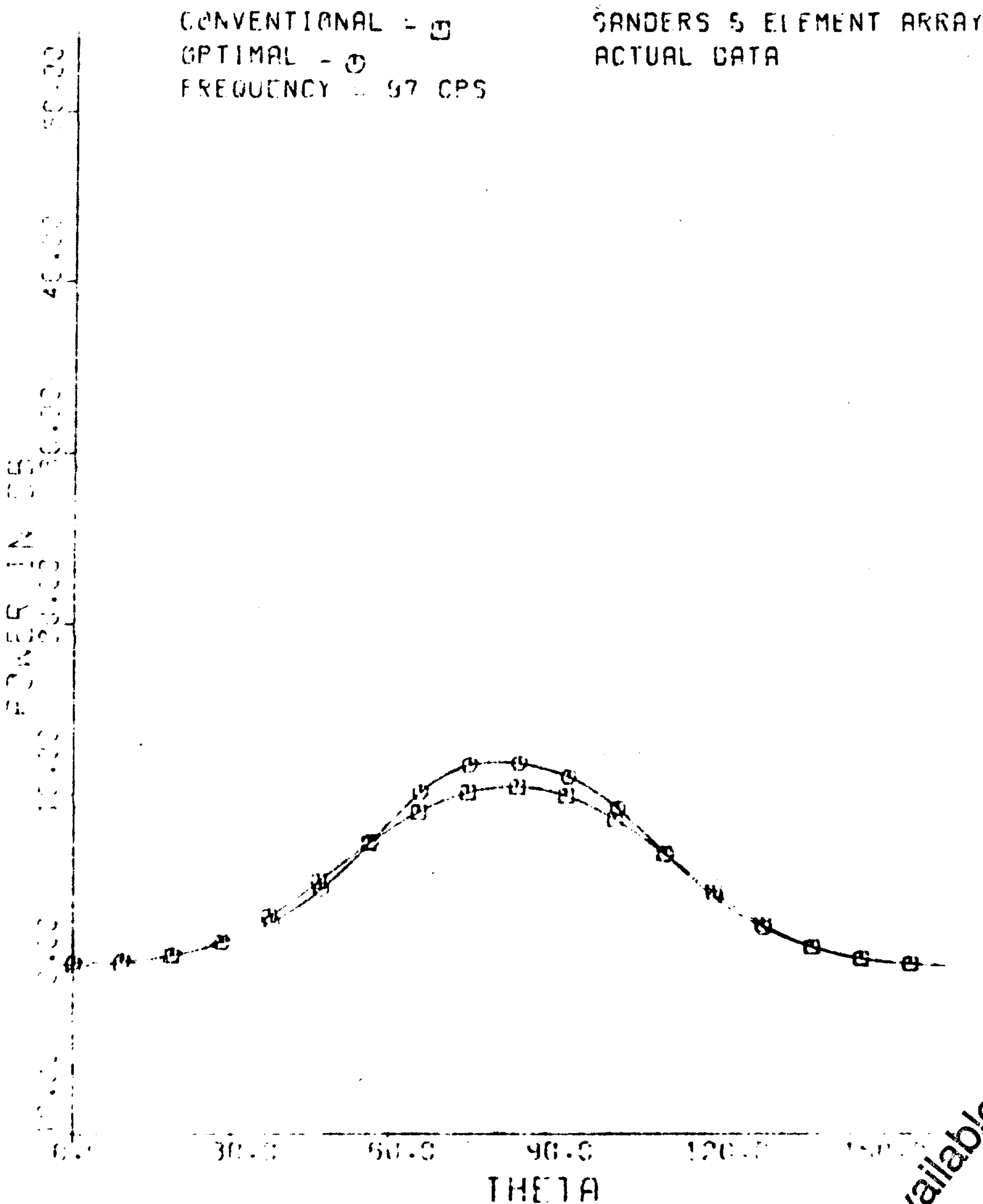

(U) Figure A6. BR actual data 97 cps.

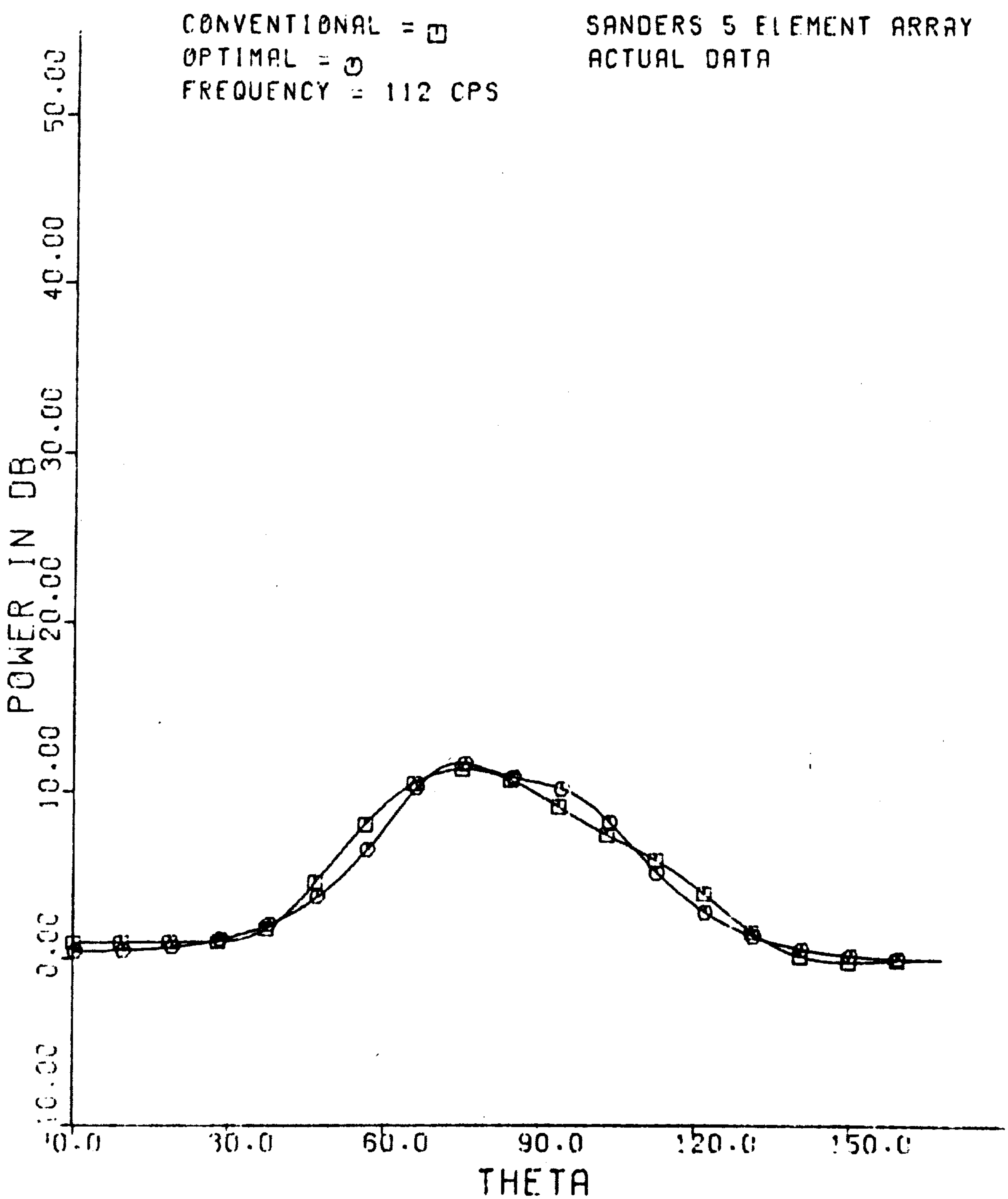

(U) Figure A7. BR – actual data – 112 cps.

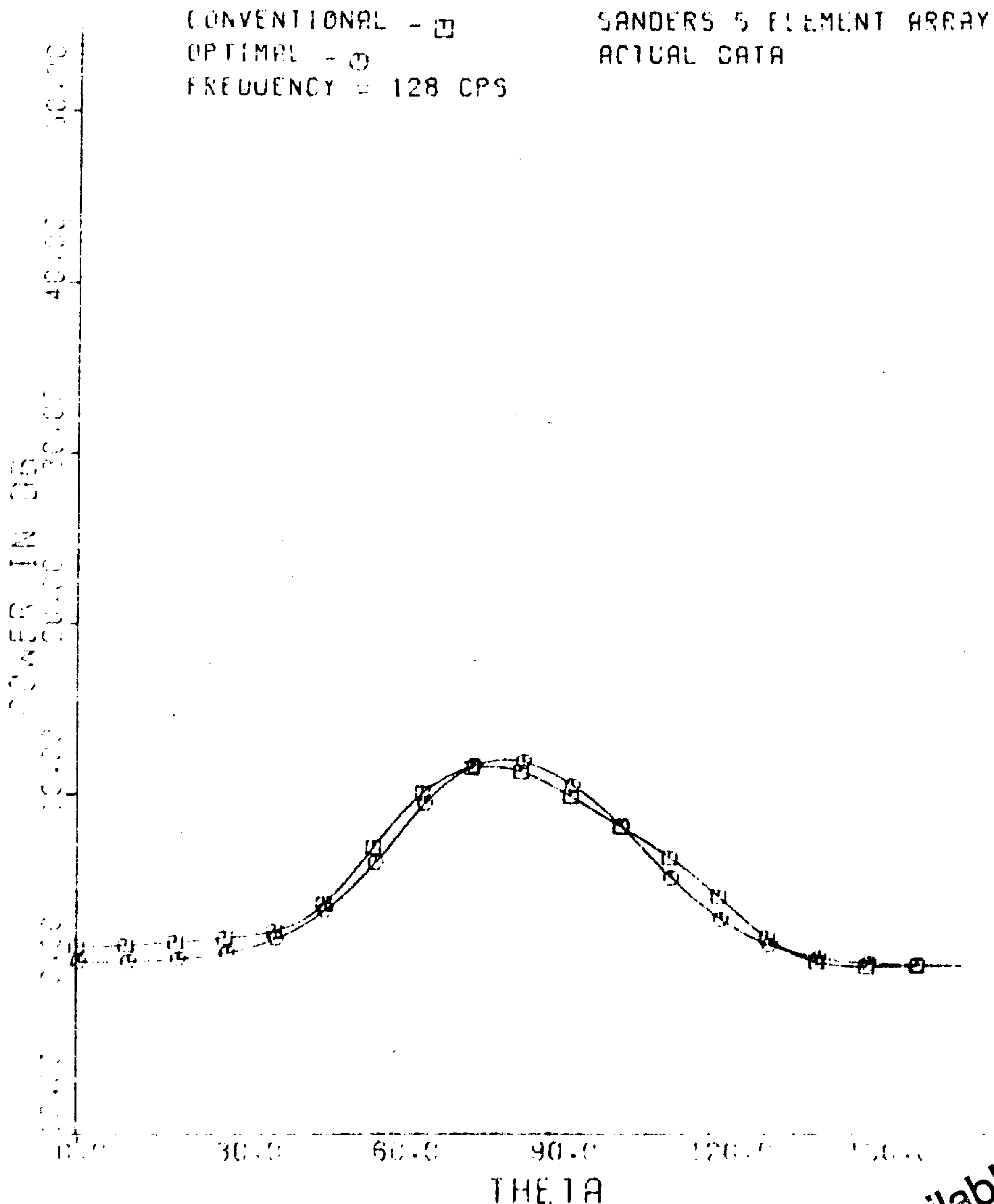

(U) Figure A8. BR actual data 128 cps.

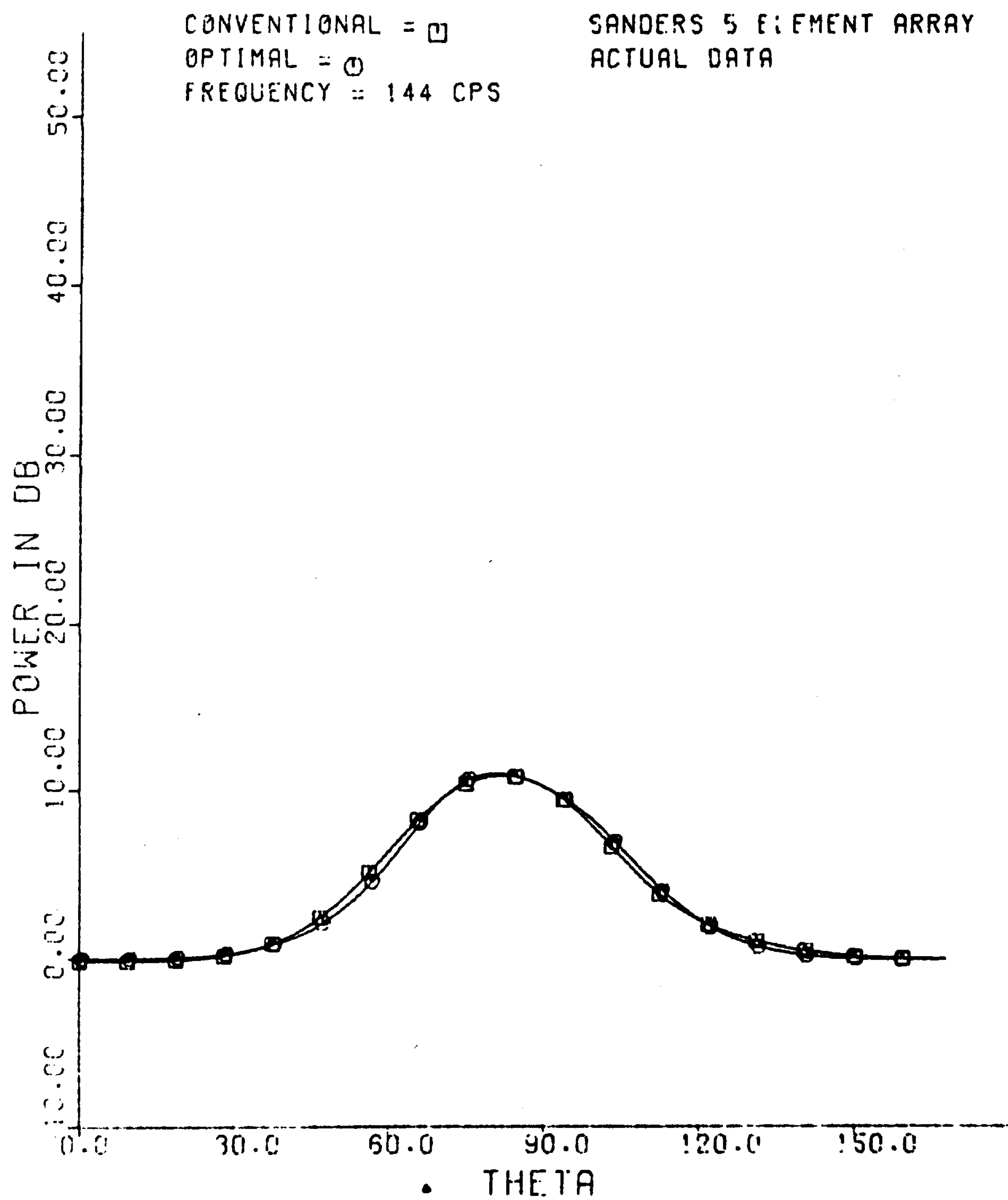

(U) Figure A9. BR – actual data – 144 cps.

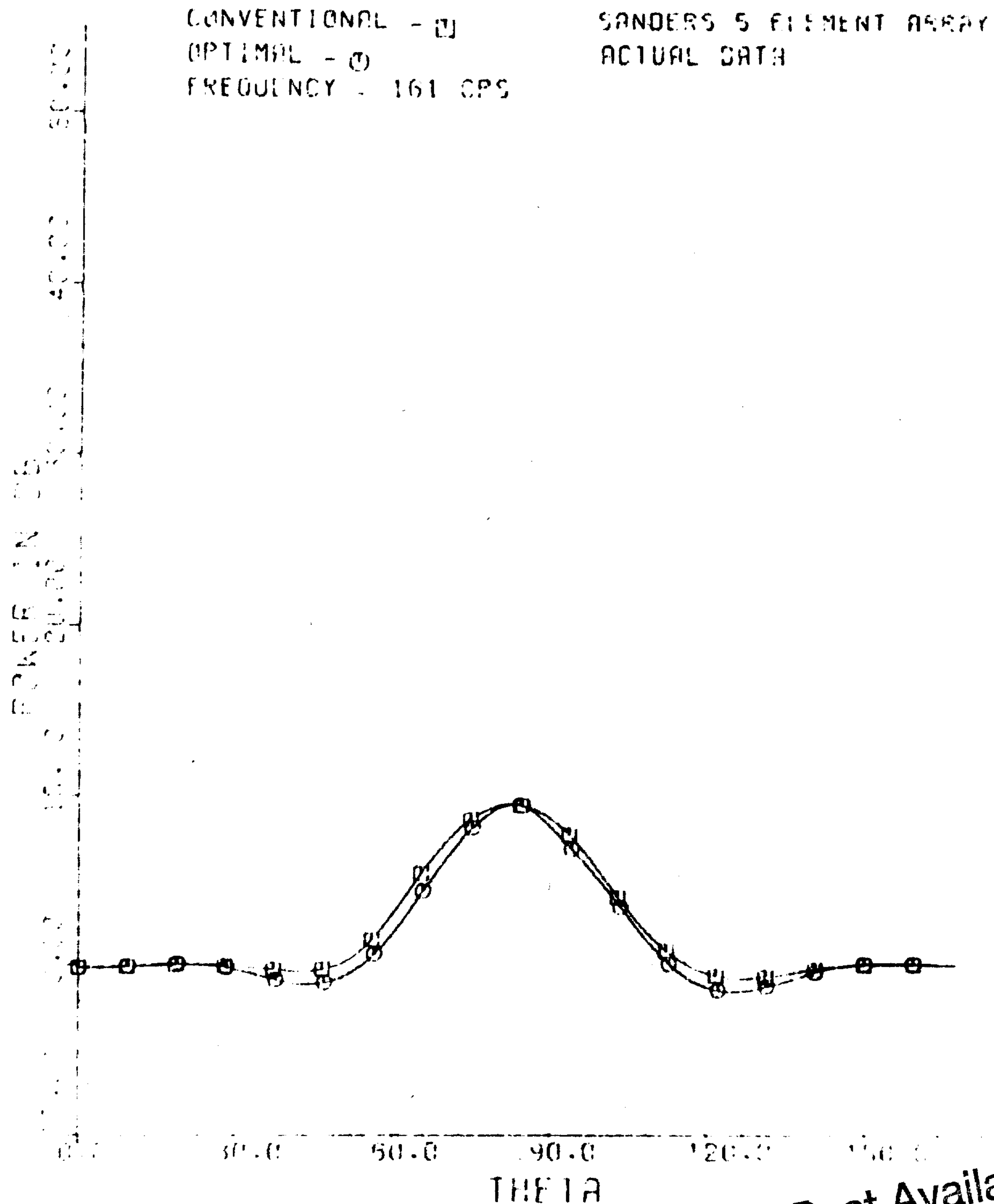

(U) Figure A10. BR actual data 161 cps.

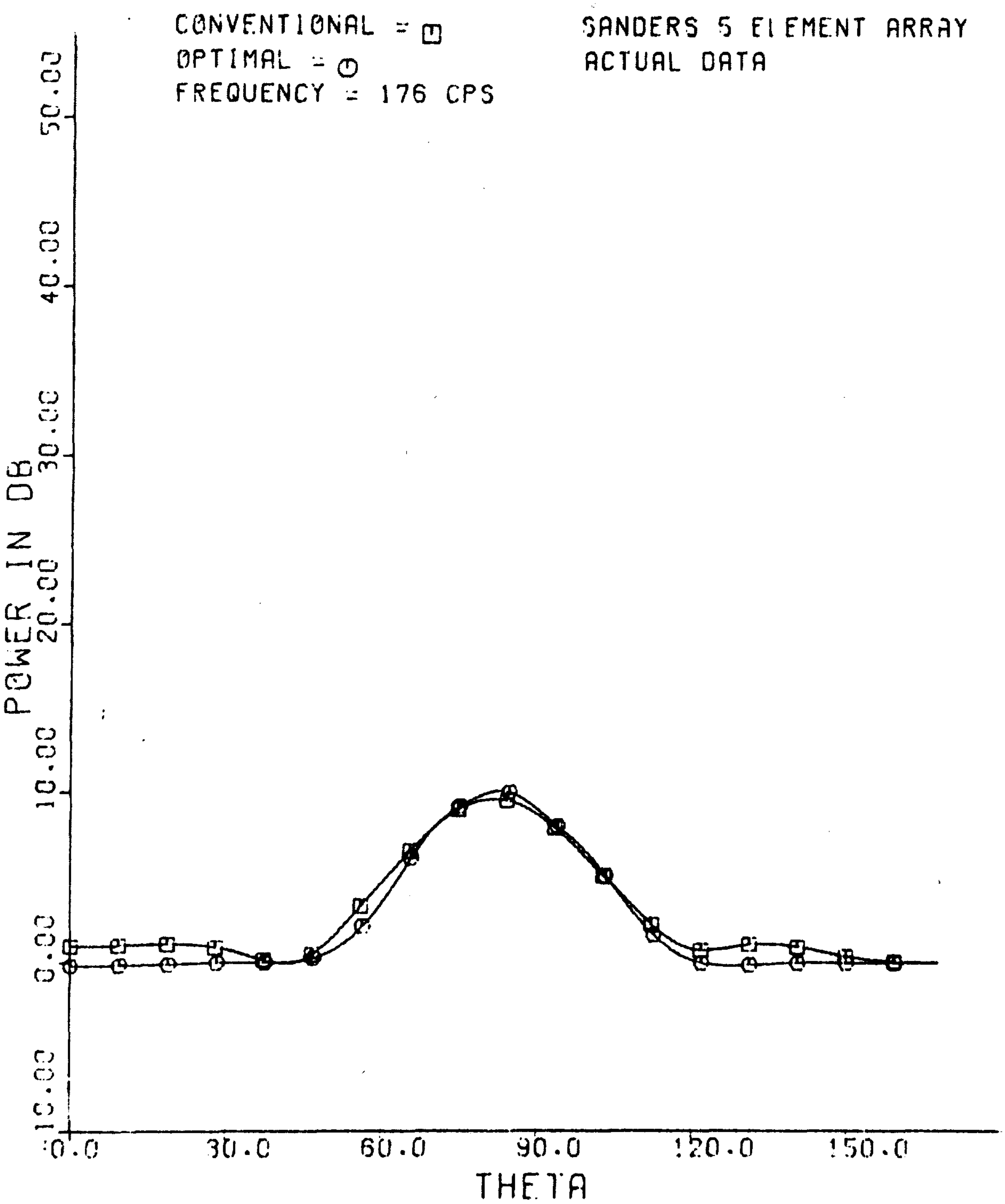

(U) Figure A11. BR -- actual data -- 176 cps.

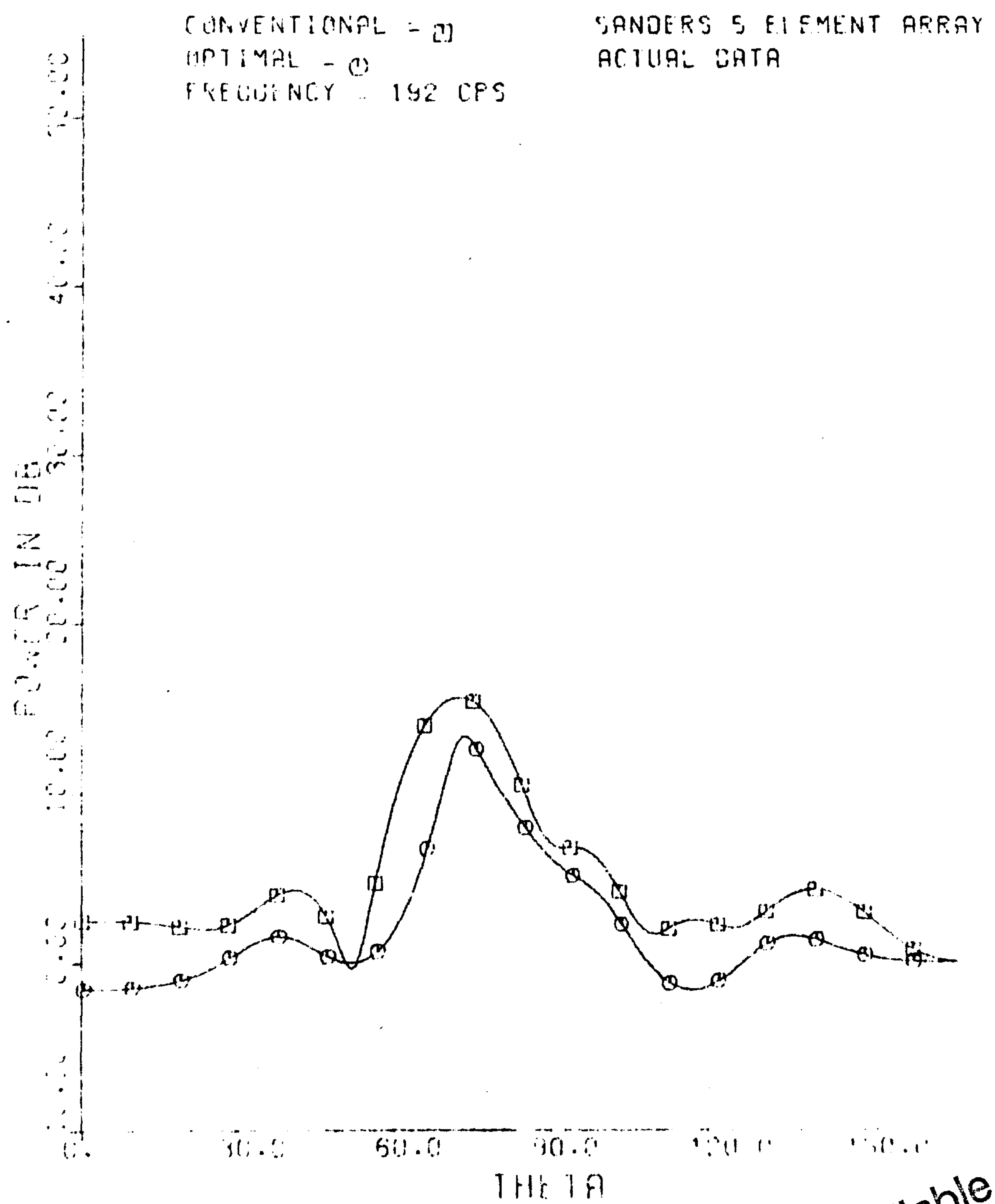

(U) Figure A12. BR – actual data – 192 cps.

PRECEDING PAGE BLANK - NOT FILMED

APPENDIX B

SIMULATED DATA RESULTS

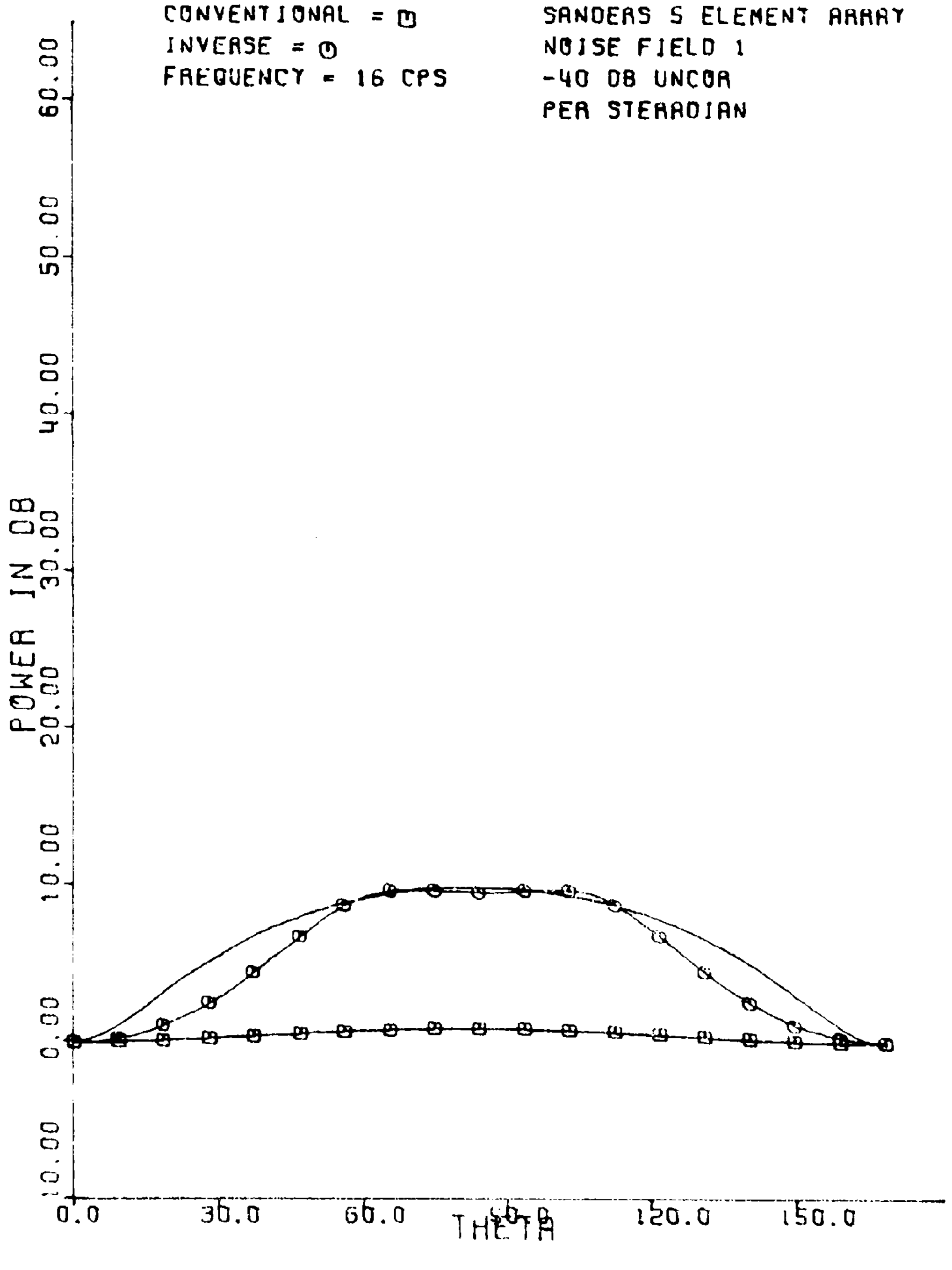

(U) Figure B1. BR noise field 1 16 cps. "Inverse" appears in figures B1 through B72 and has the same meaning as "adaptive."

UNCLASSIFIED

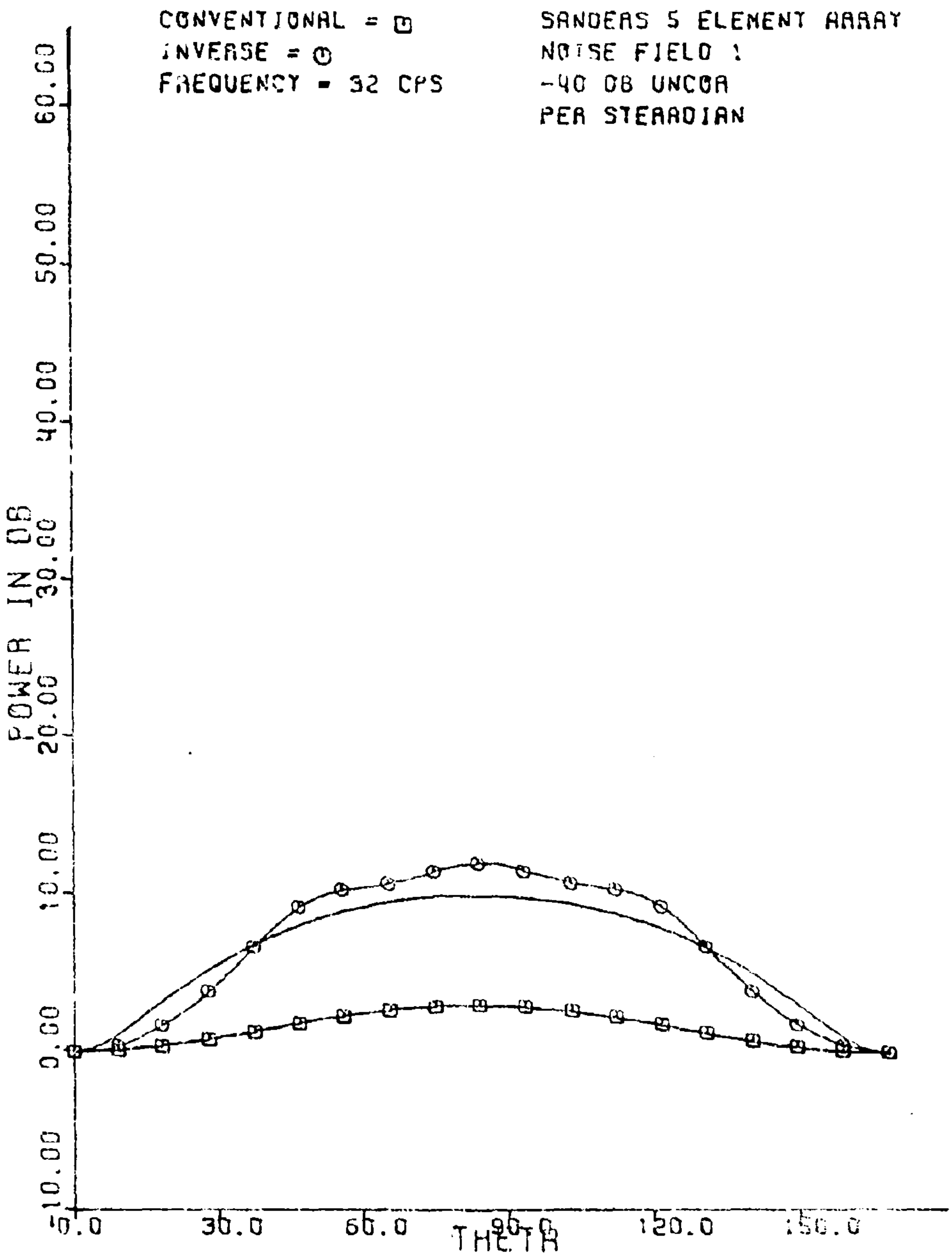

(U) Figure B2 BR noise field 1 32 cps.

UNCLASSIFIED

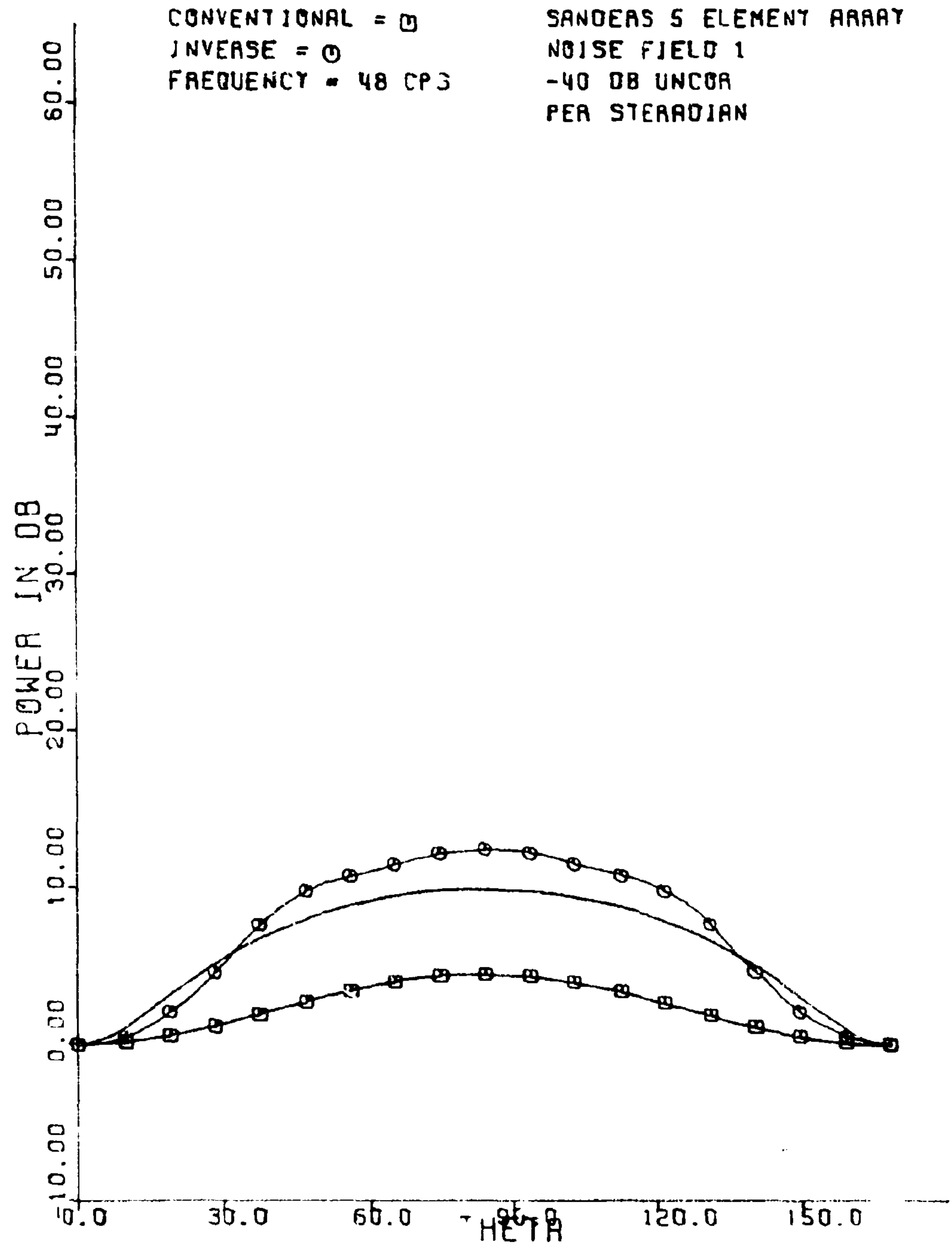

(U) Figure B3. BR noise field 1 - 48 cps.

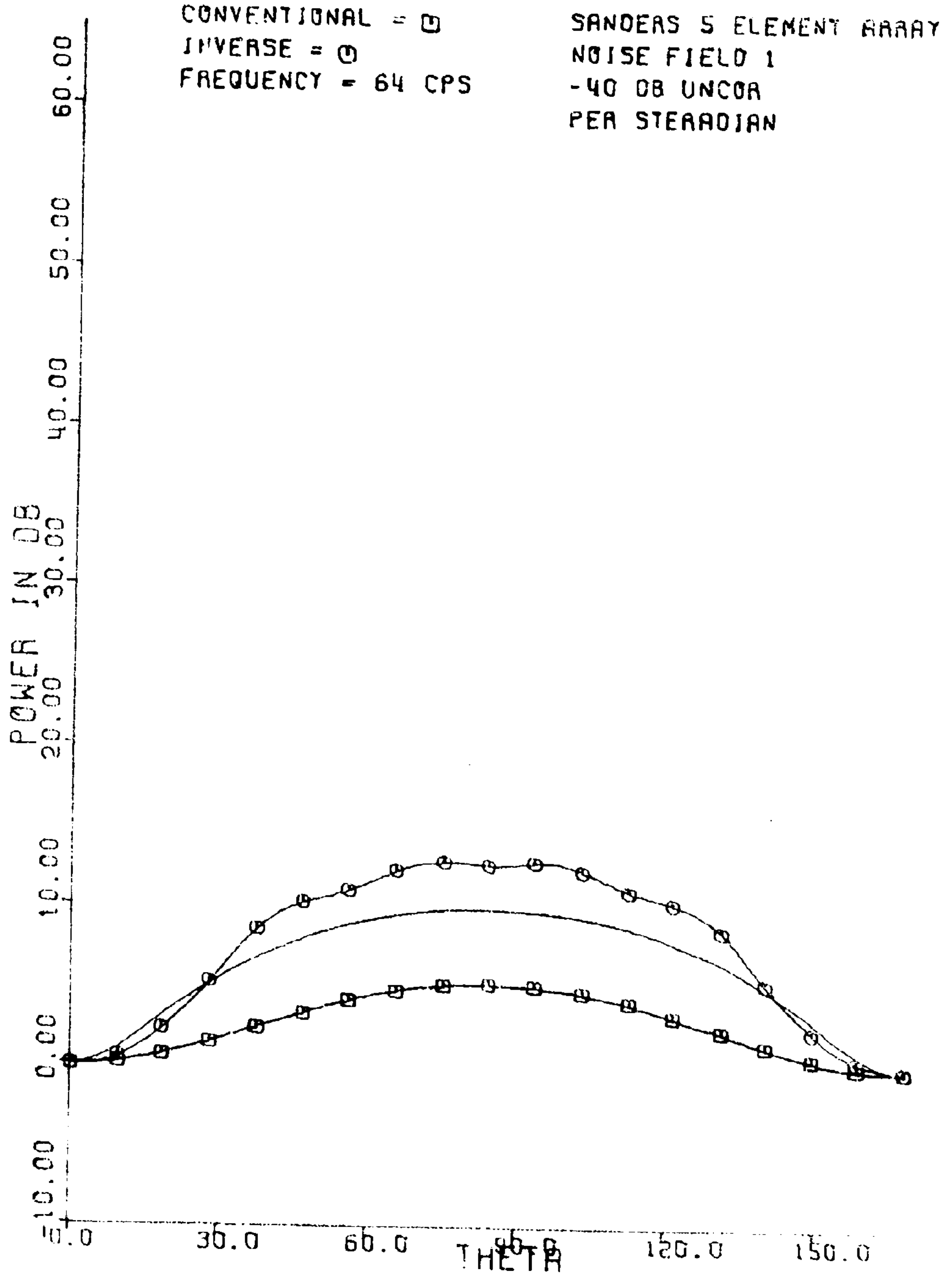

(U) Figure B4. BR noise field 1 64 cps.

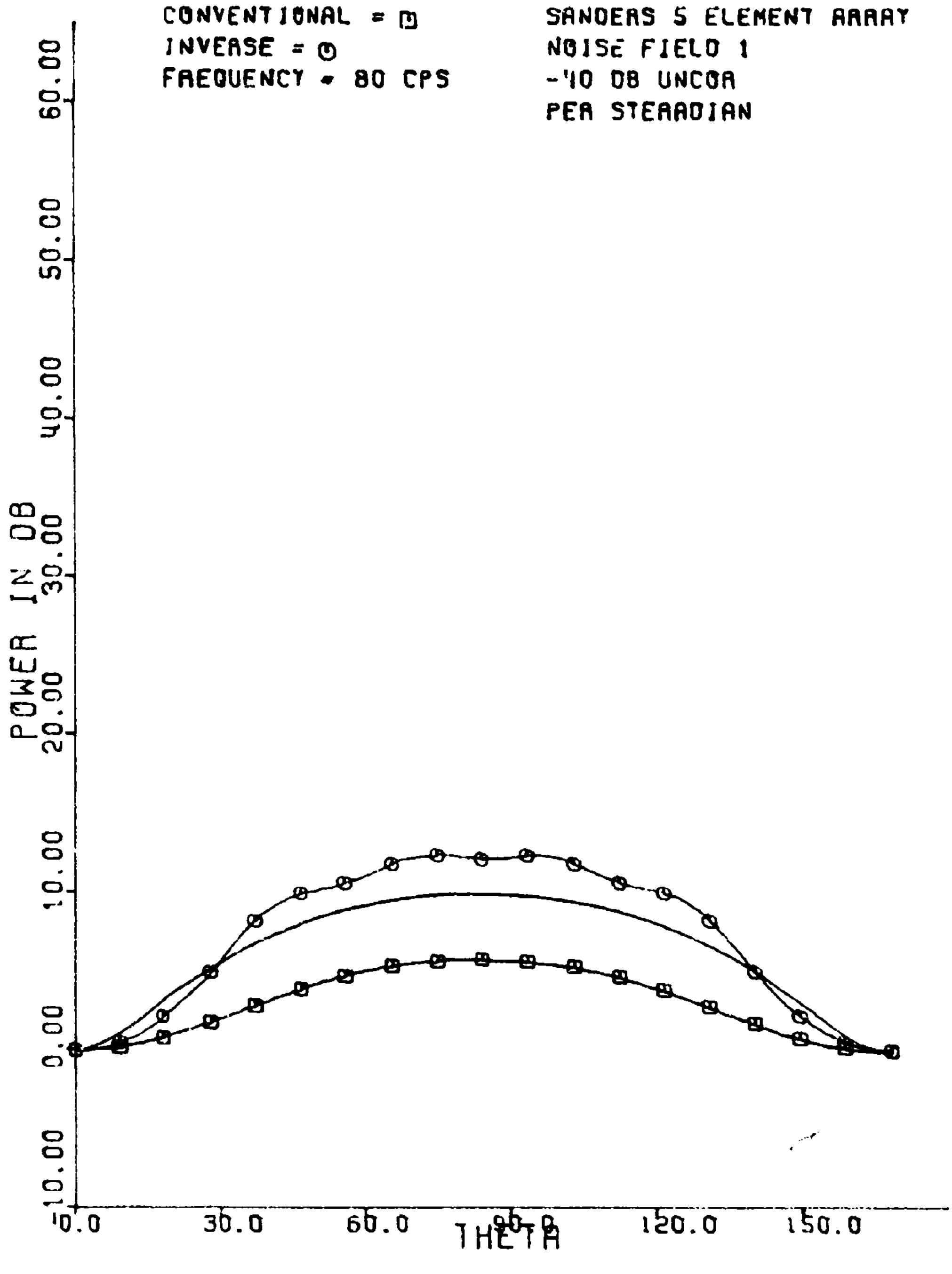

(U) Figure B5. BR noise field 1 - 80 cps.

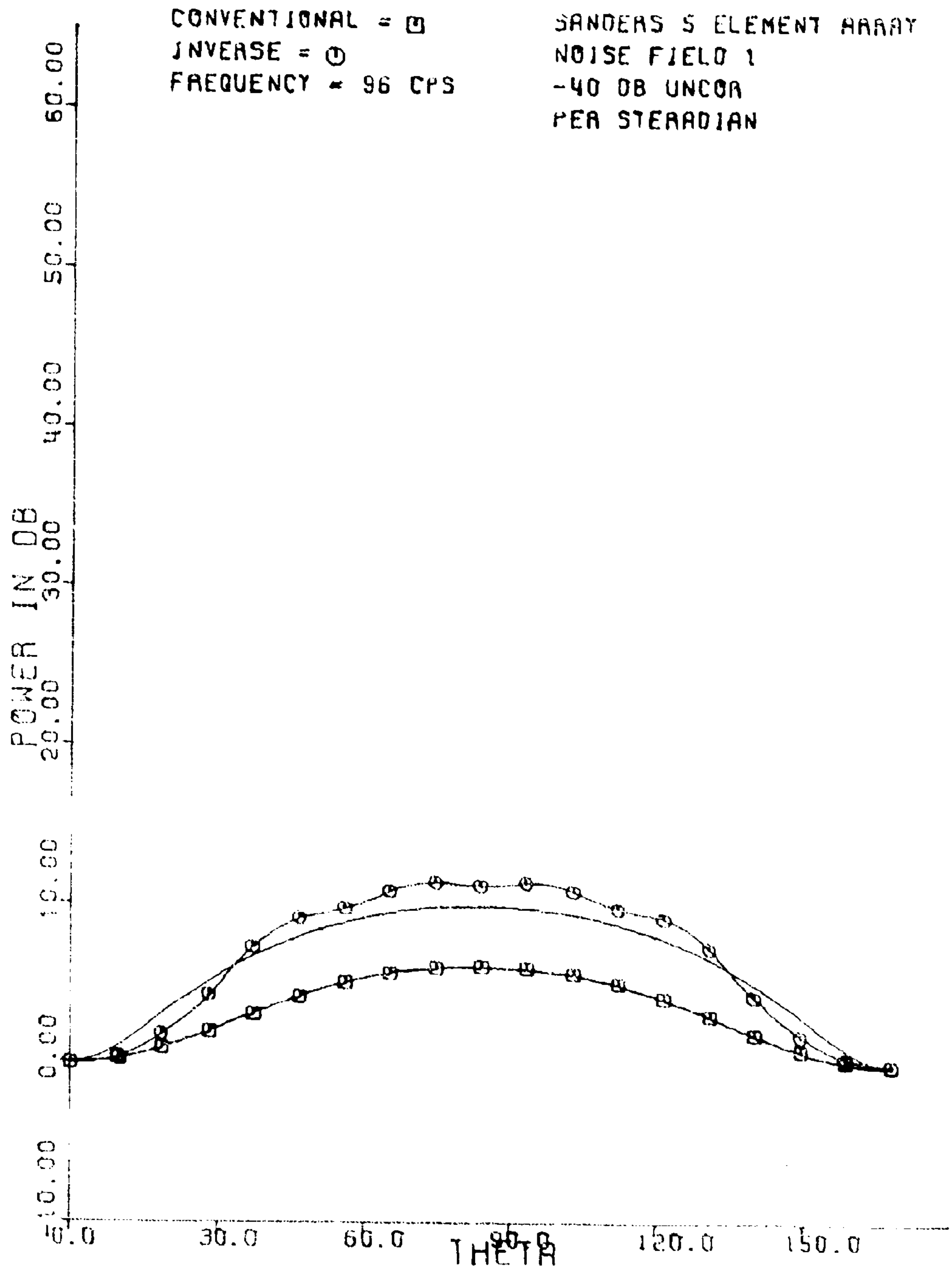

(U) Figure B6. BR noise field 1 96 cps.

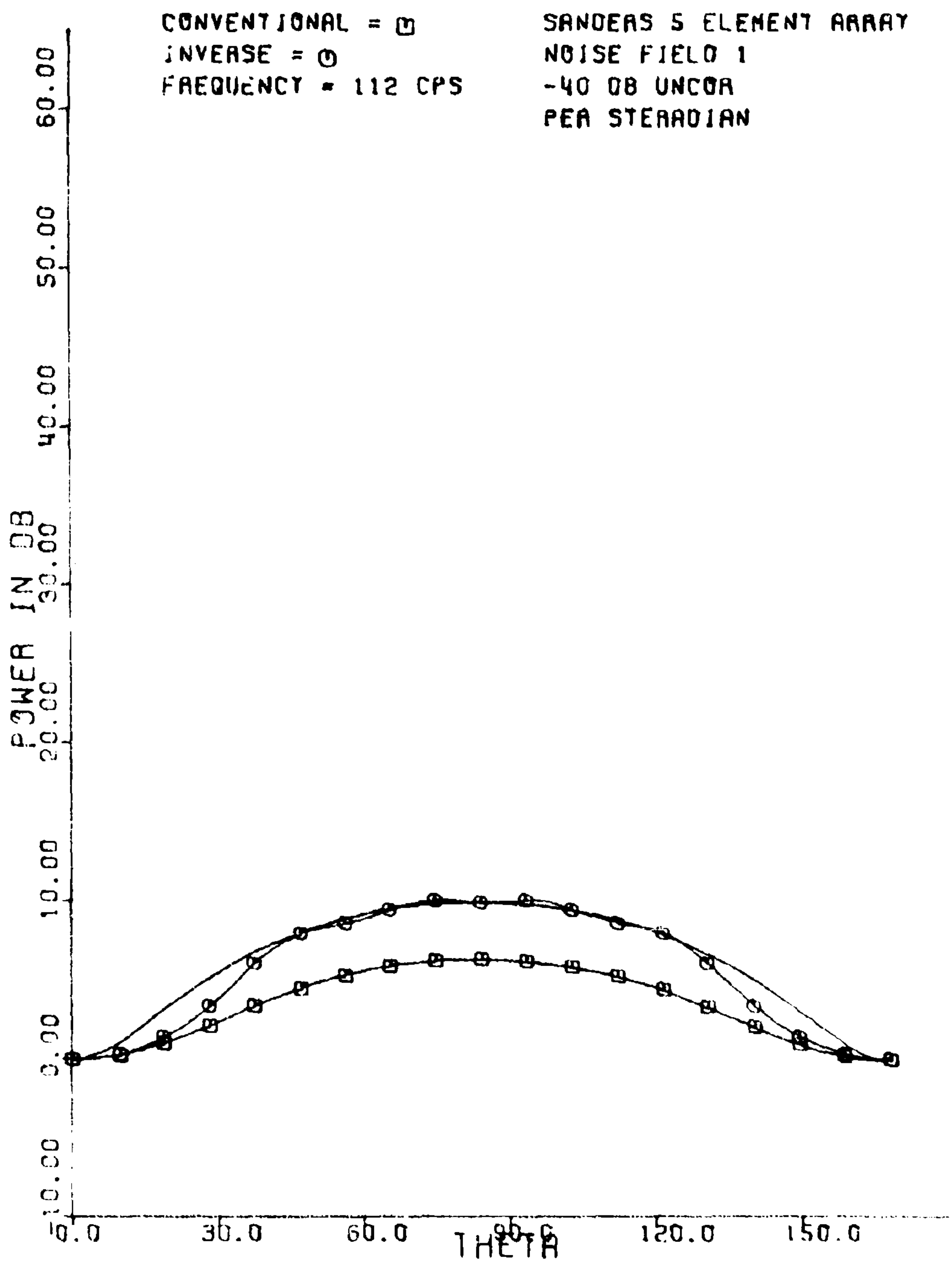

(U) Figure B7. BR noise field 1 112 cps.

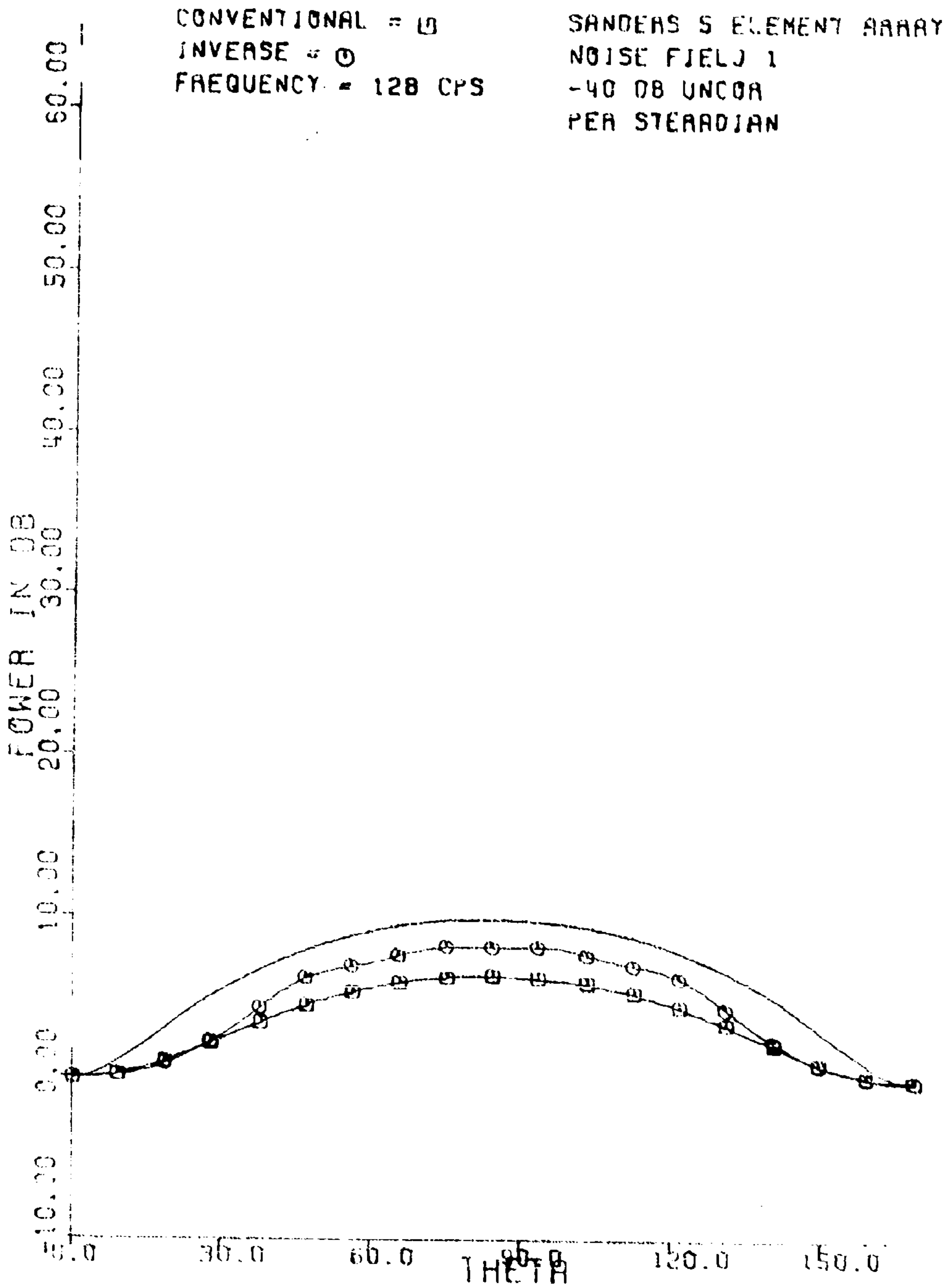

(U) Figure B8 BR noise field 1 128 cps.

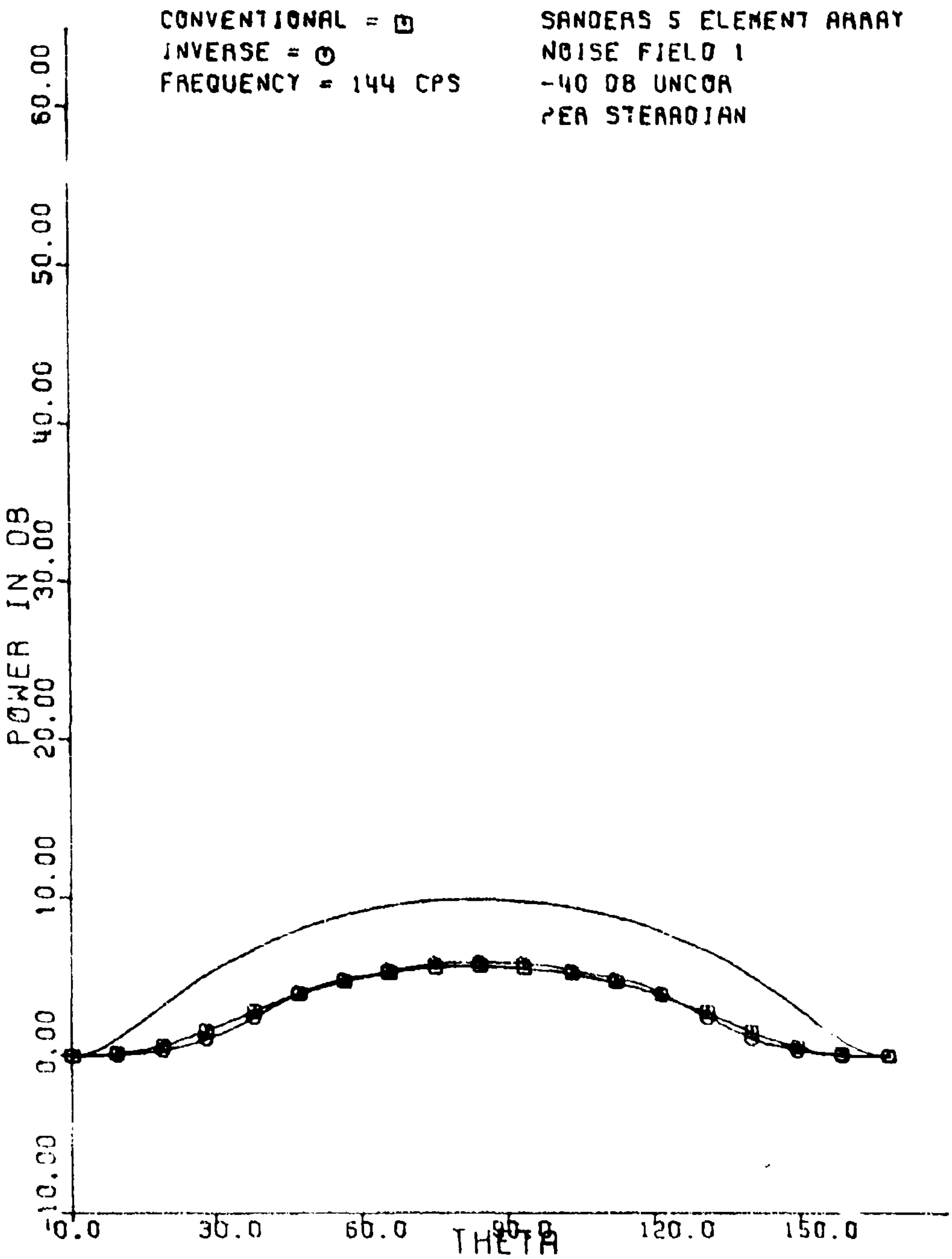

(U) Figure B9. BR noise field 1 144 cps.

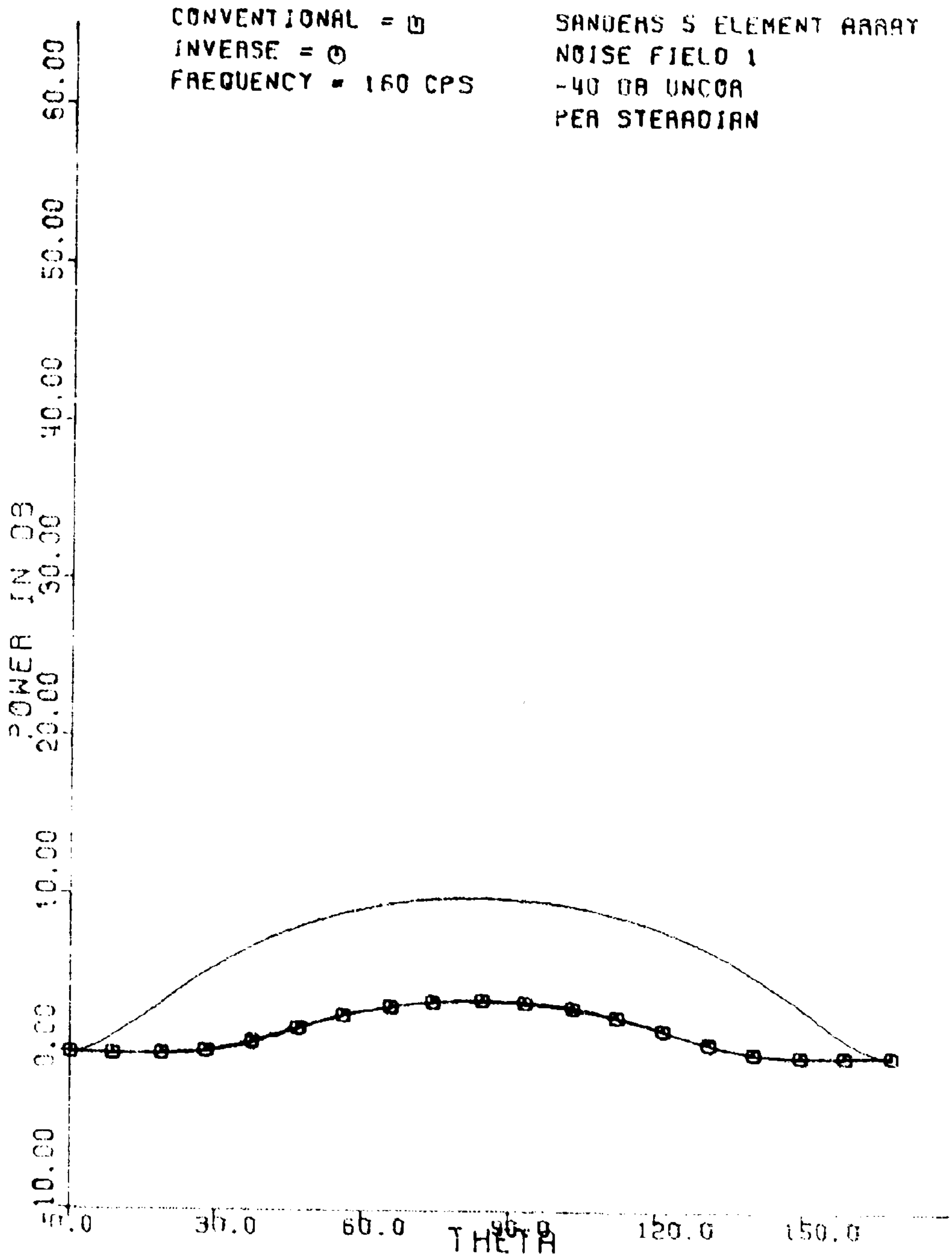

(U) Figure B10 BR noise field 1 160 cps.

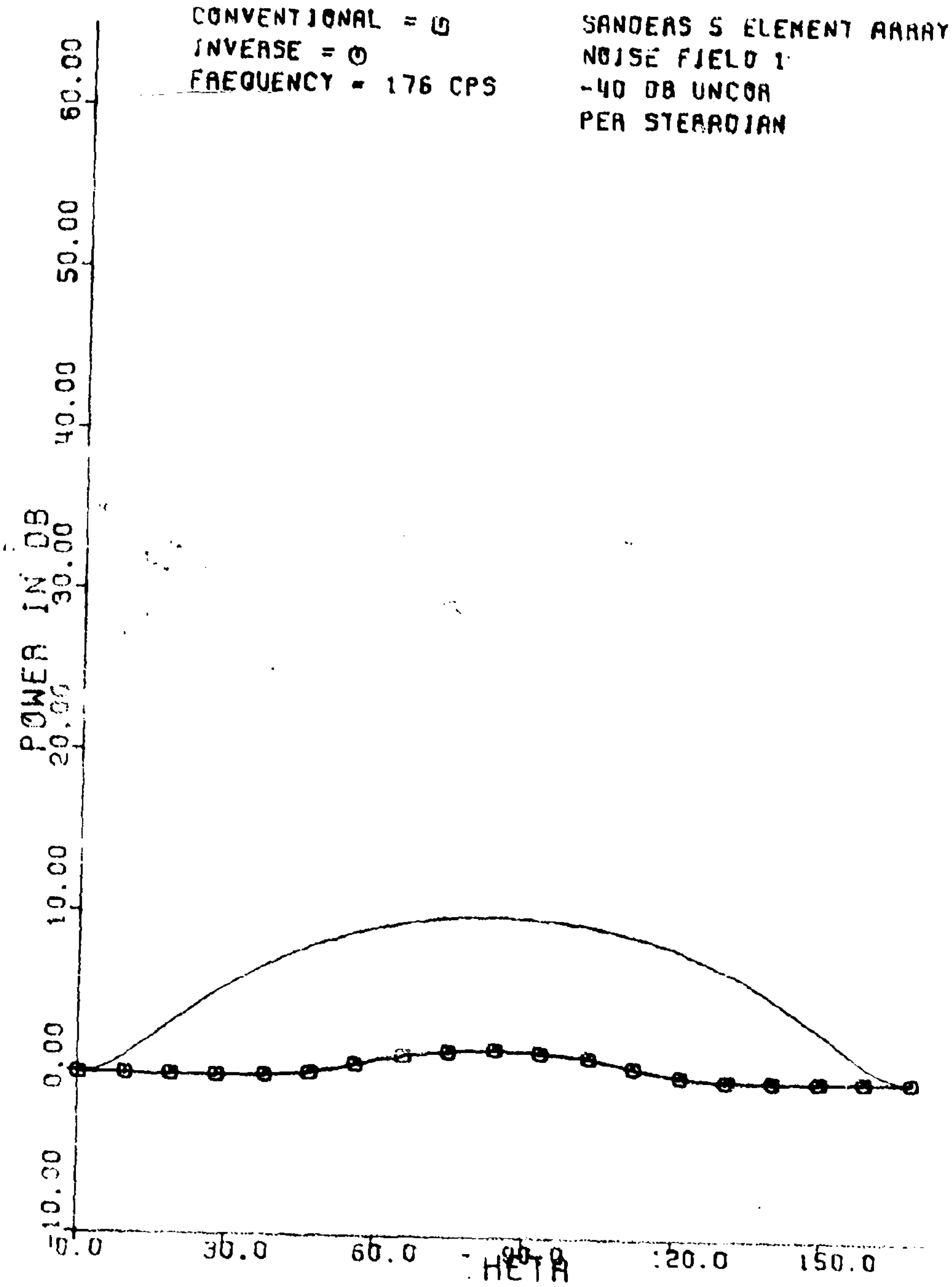

(U) Figure B11. BR noise field 1 176 cps.

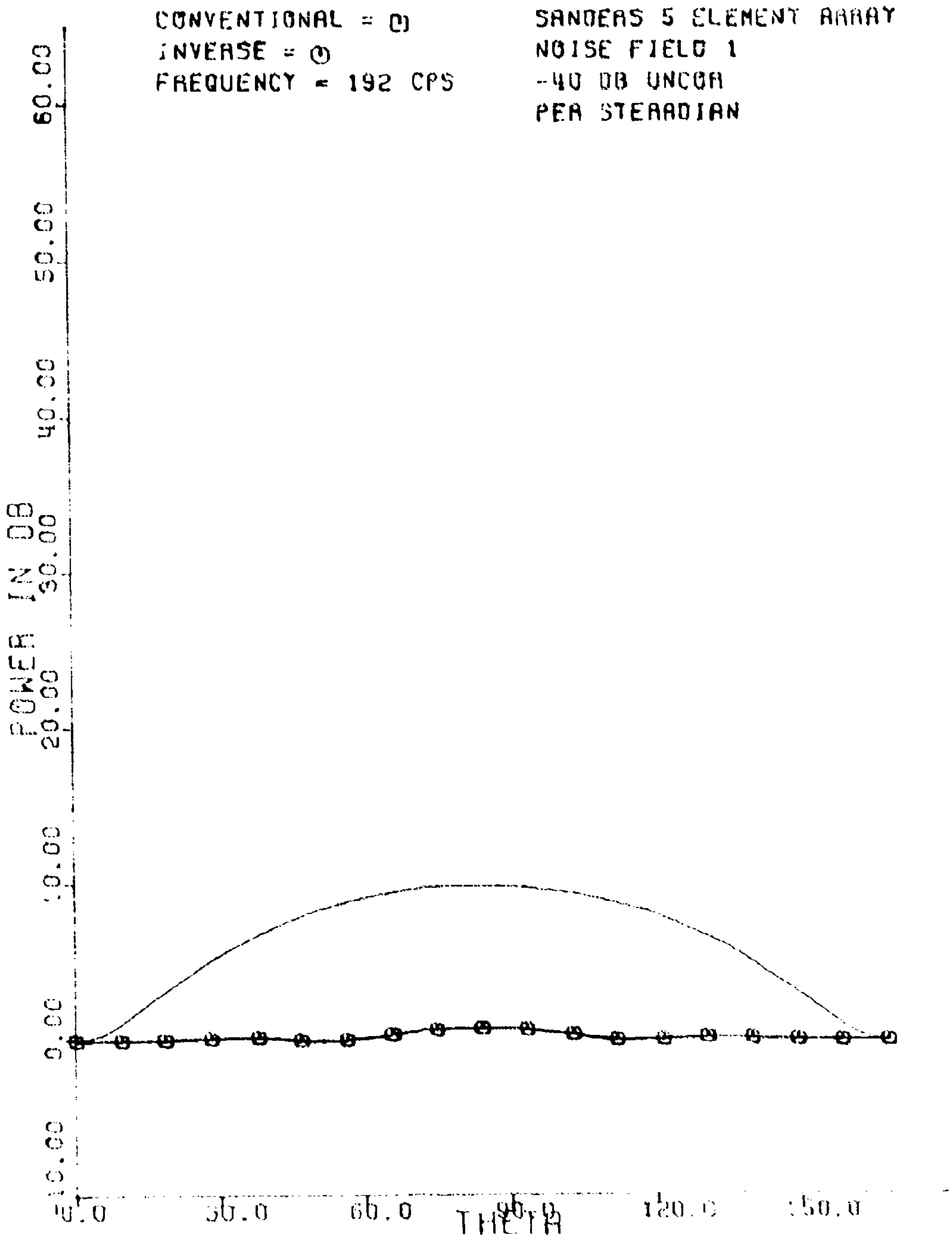

(U) Figure B12. BR — noise field 1 — 192 cps.

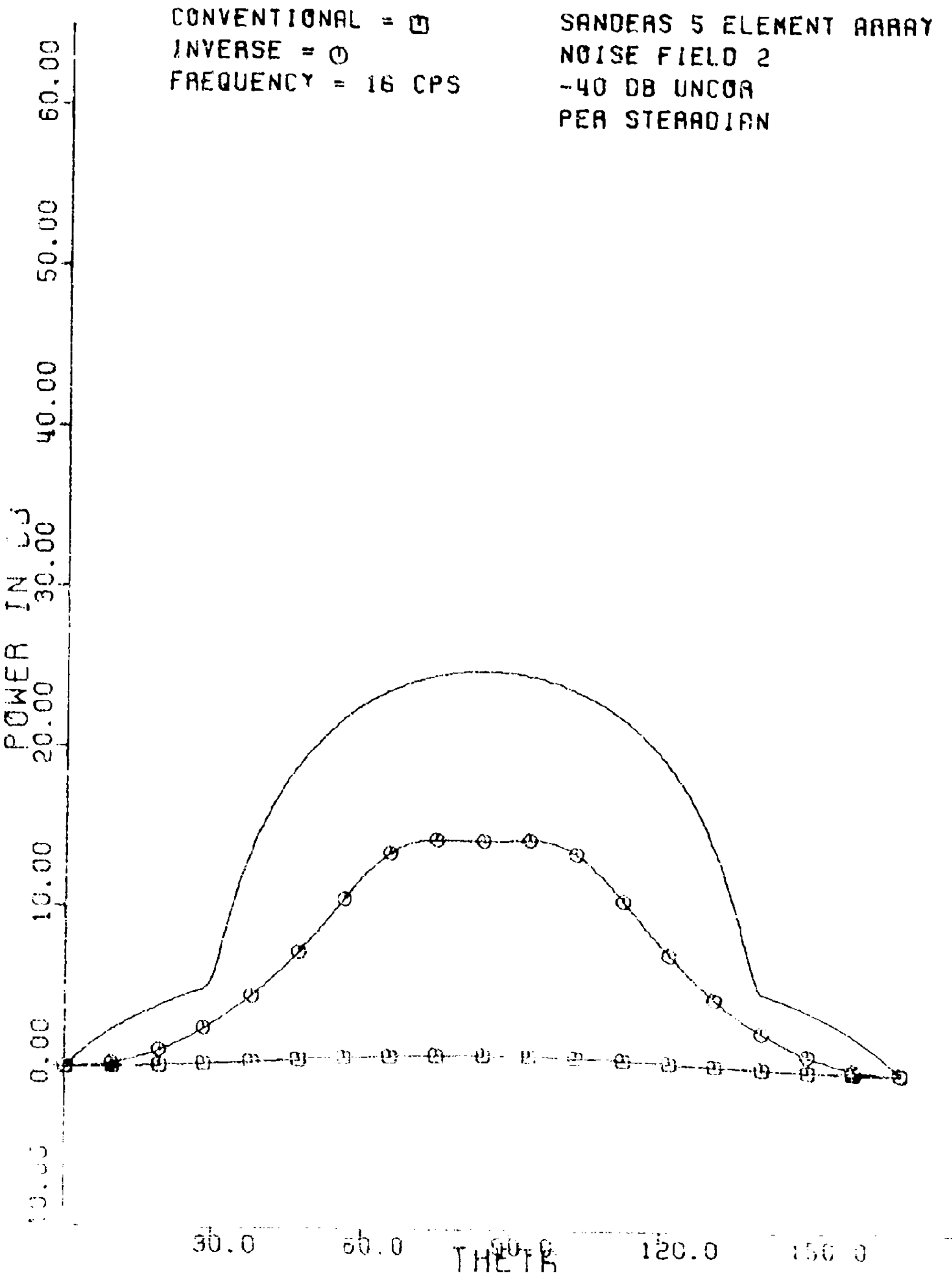

(U) Figure 81 [illegible] BR [illegible] noise field 2 [illegible] 16 cps

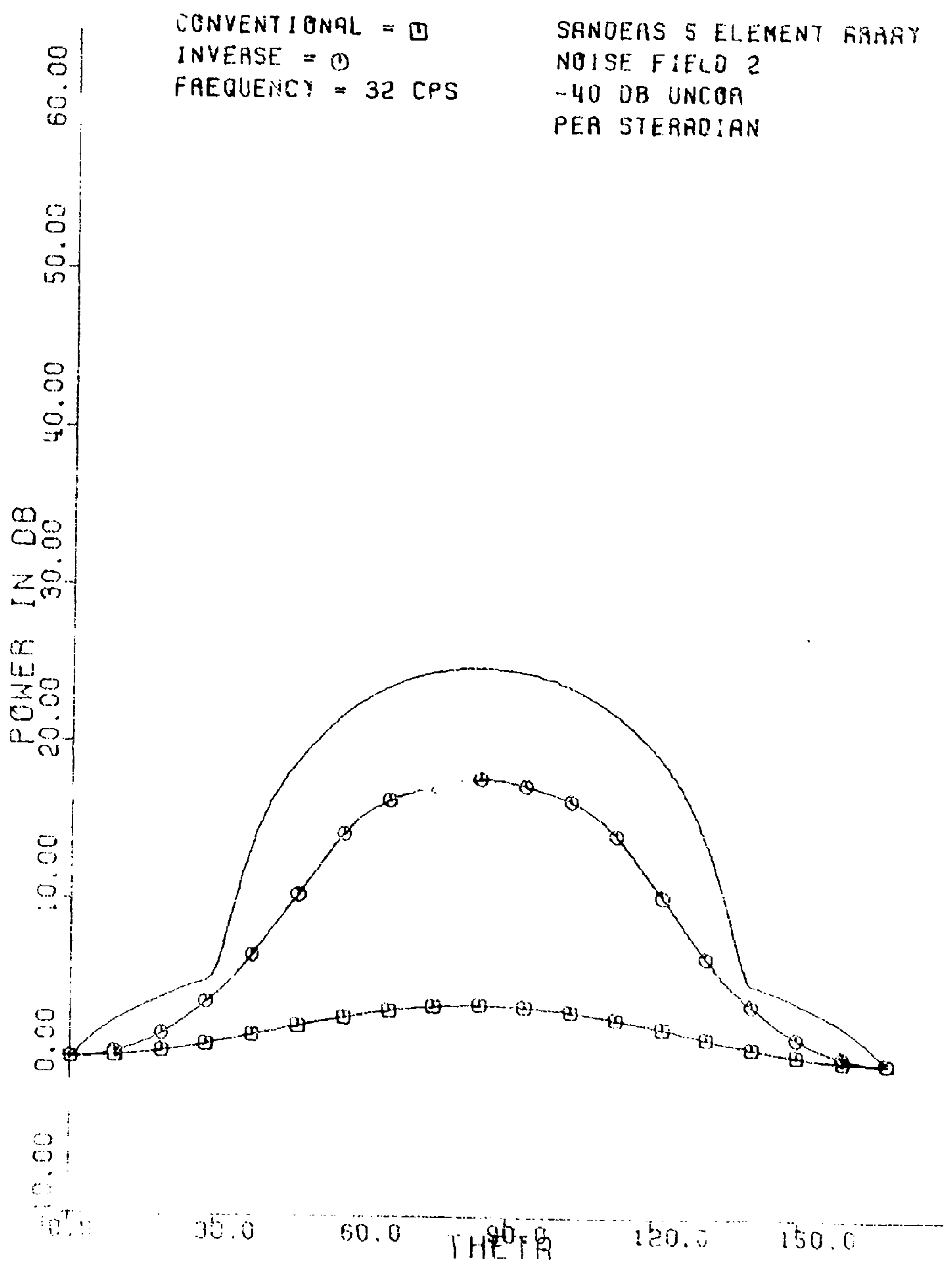

(U) Figure [illegible] noise field 2 [illegible] 32 cps

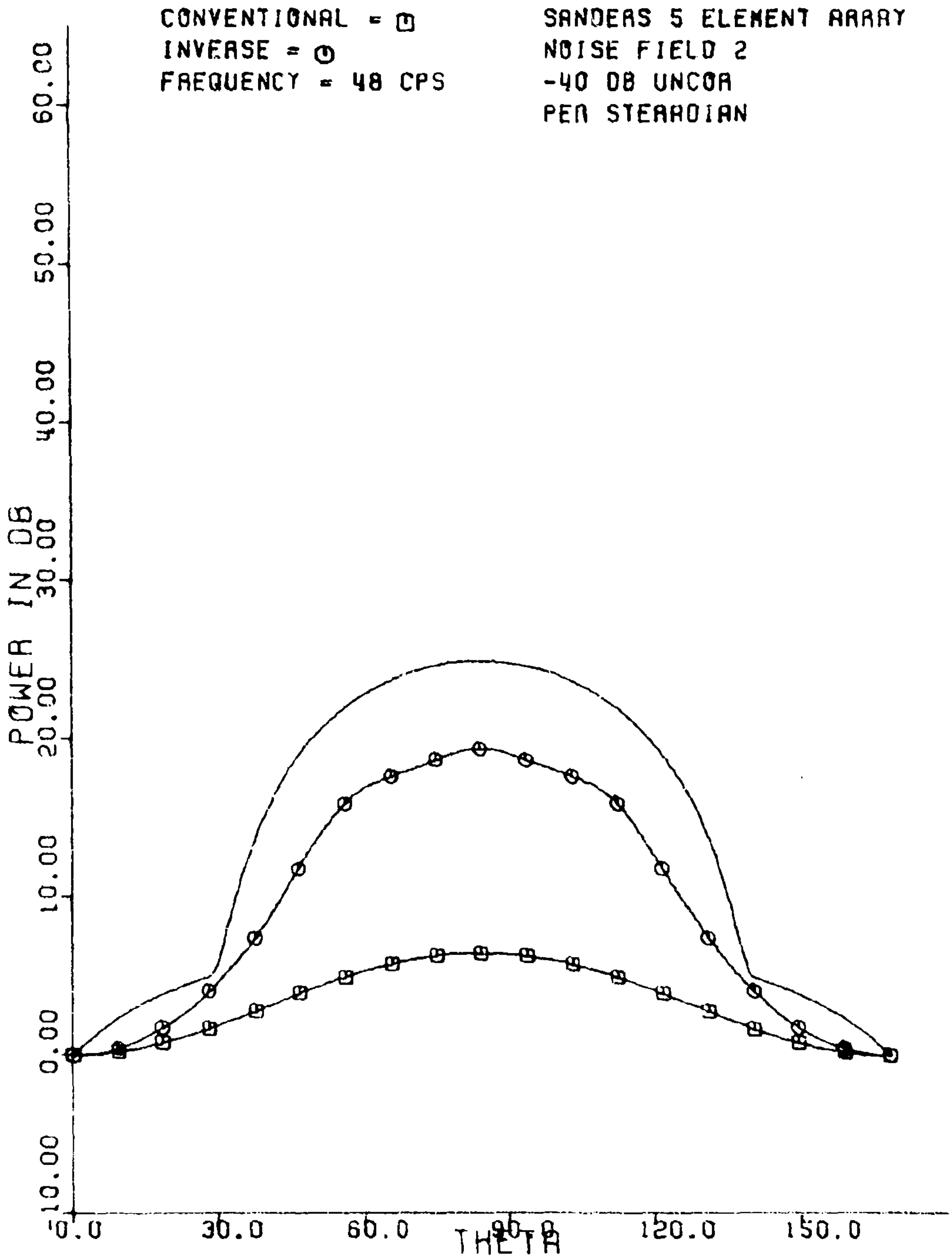

(U) Figure B15. BR noise field 2 48 cps.

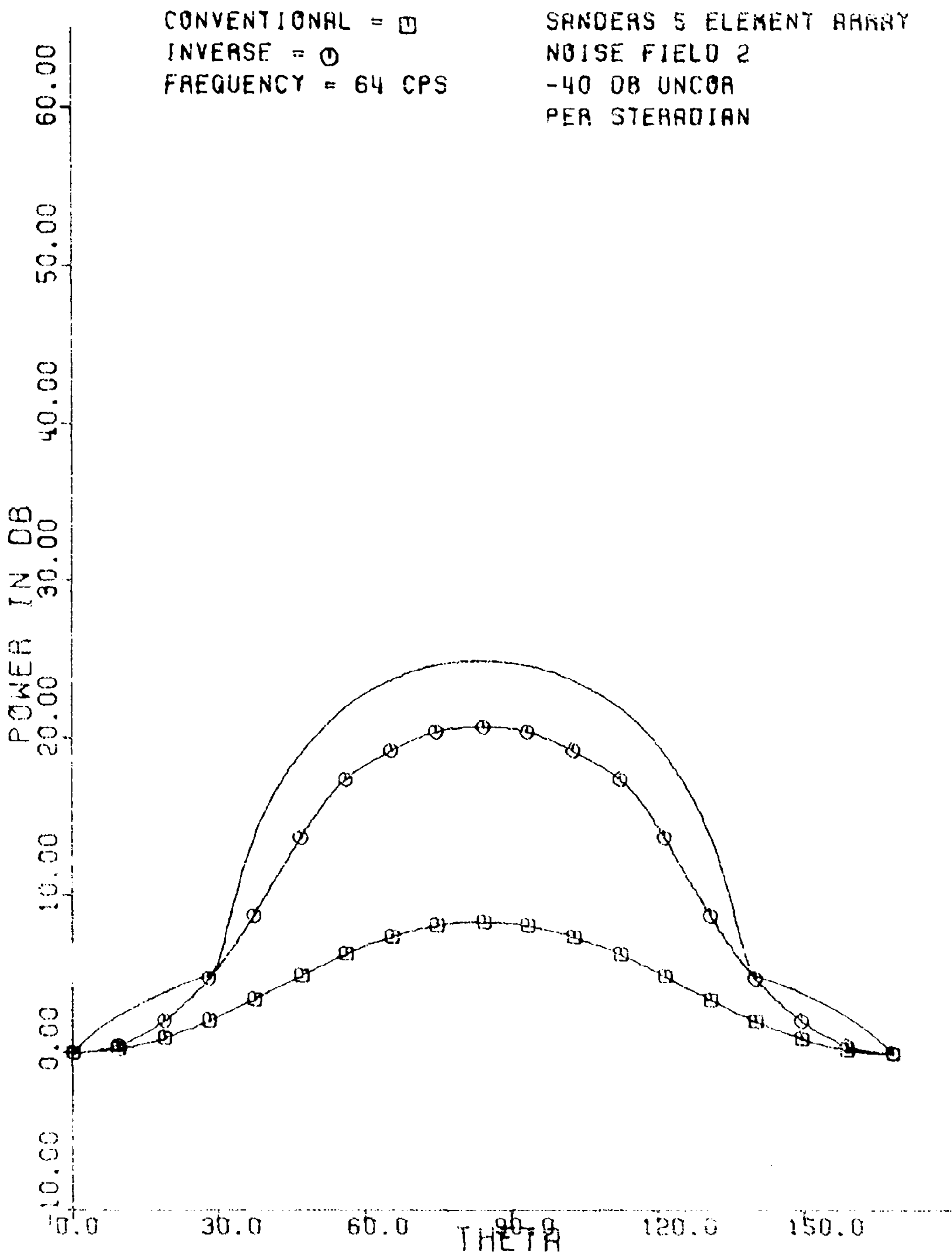

(U) Figure B16 BR noise field 2 64 cps.

UNCLASSIFIED

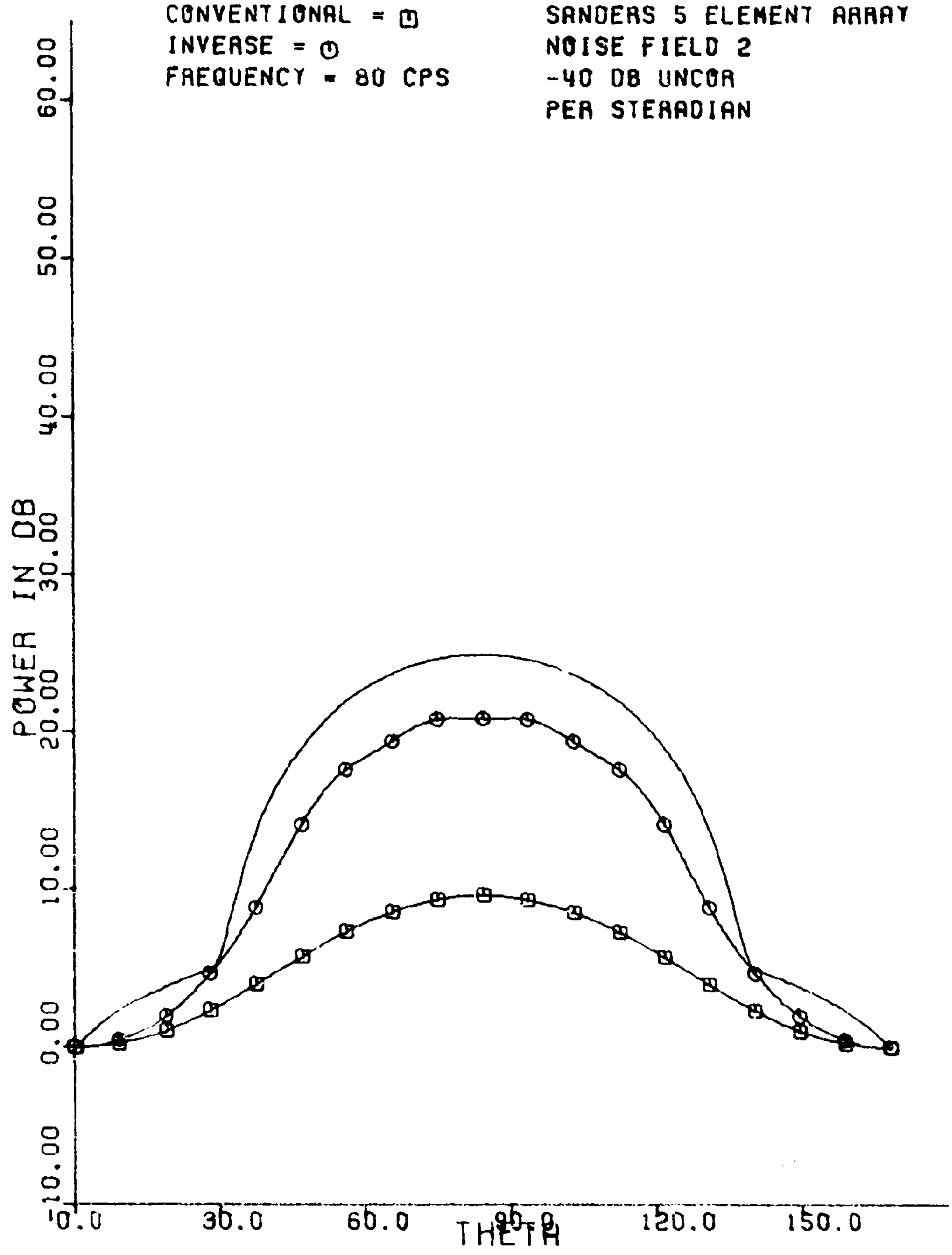

(U) Figure B17. BR noise field 2 80 cps.

UNCLASSIFIED

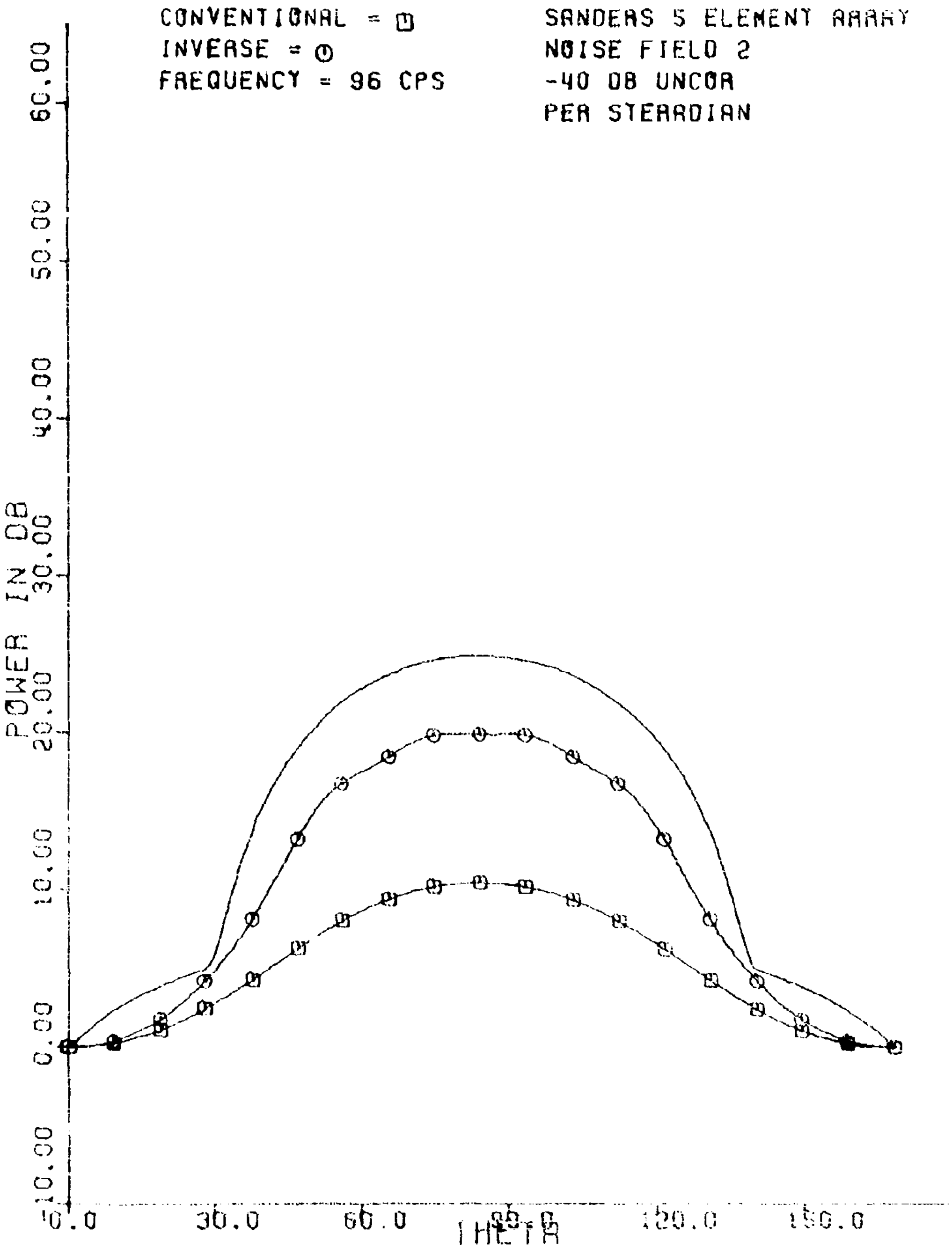

(U) Figure B18. BR — noise field 2 — 96 cps.

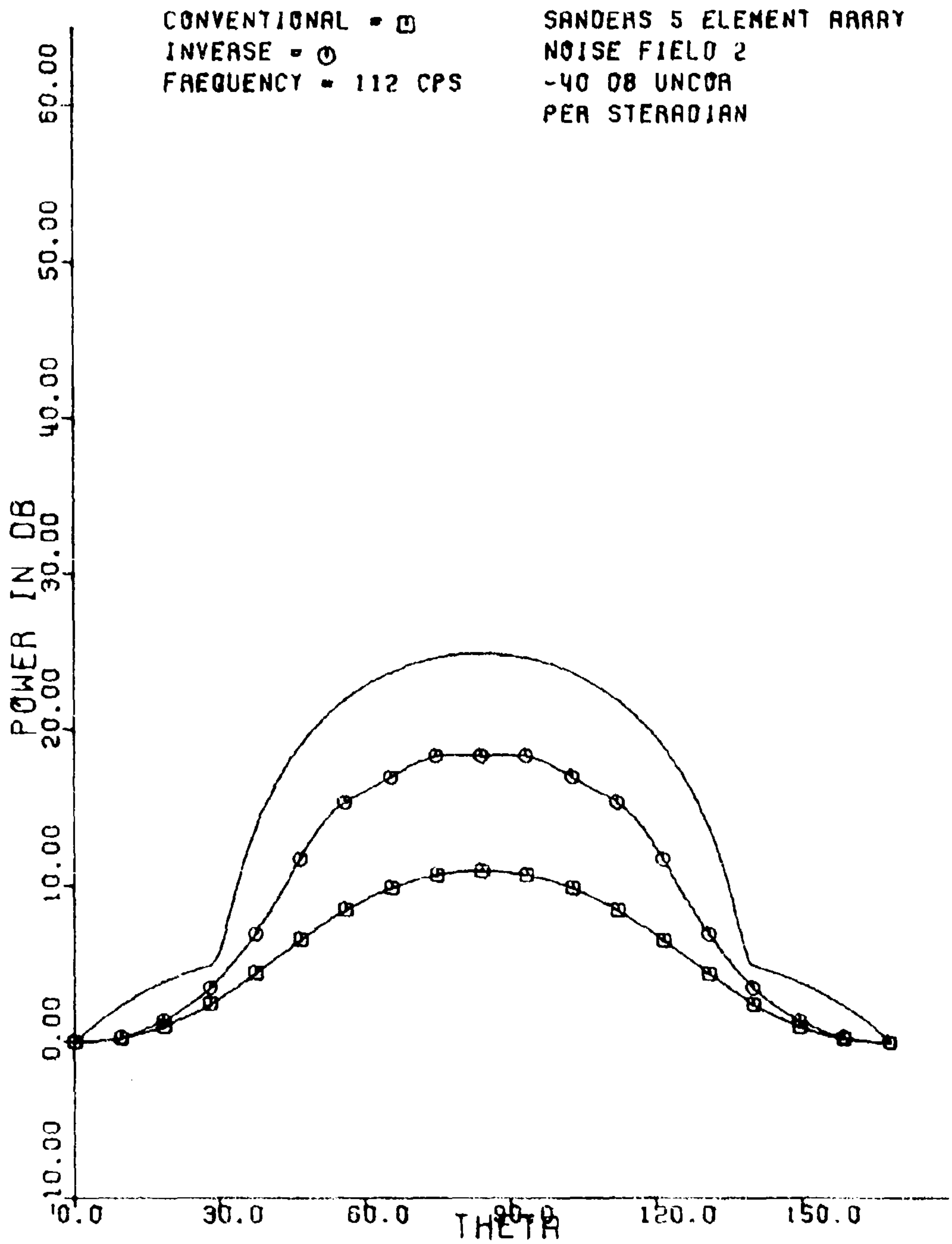

(U) Figure B19. BR noise field 2 – 112 cps.

UNCLASSIFIED

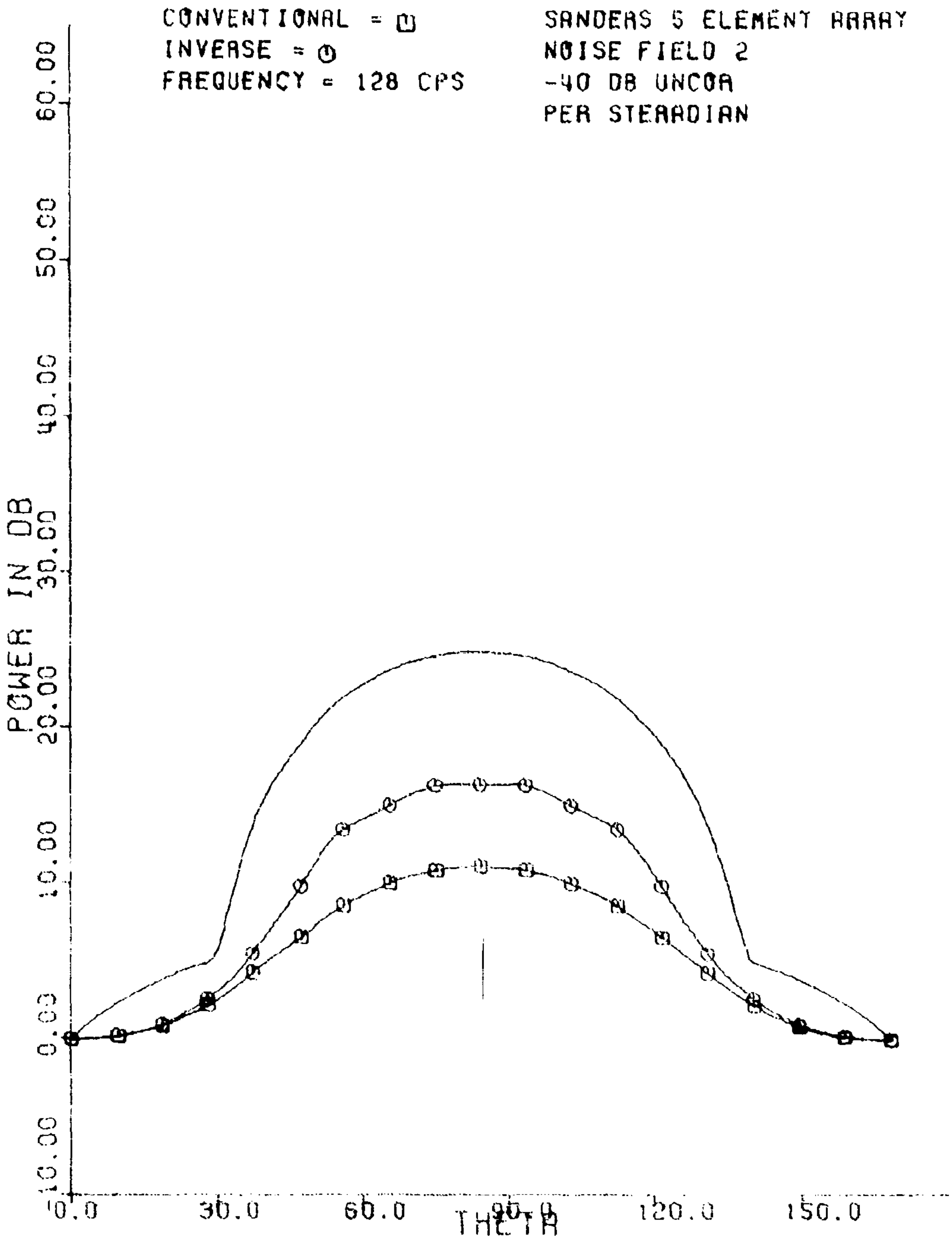

(U) Figure B20 BR noise field 2 128 cps.

UNCLASSIFIED

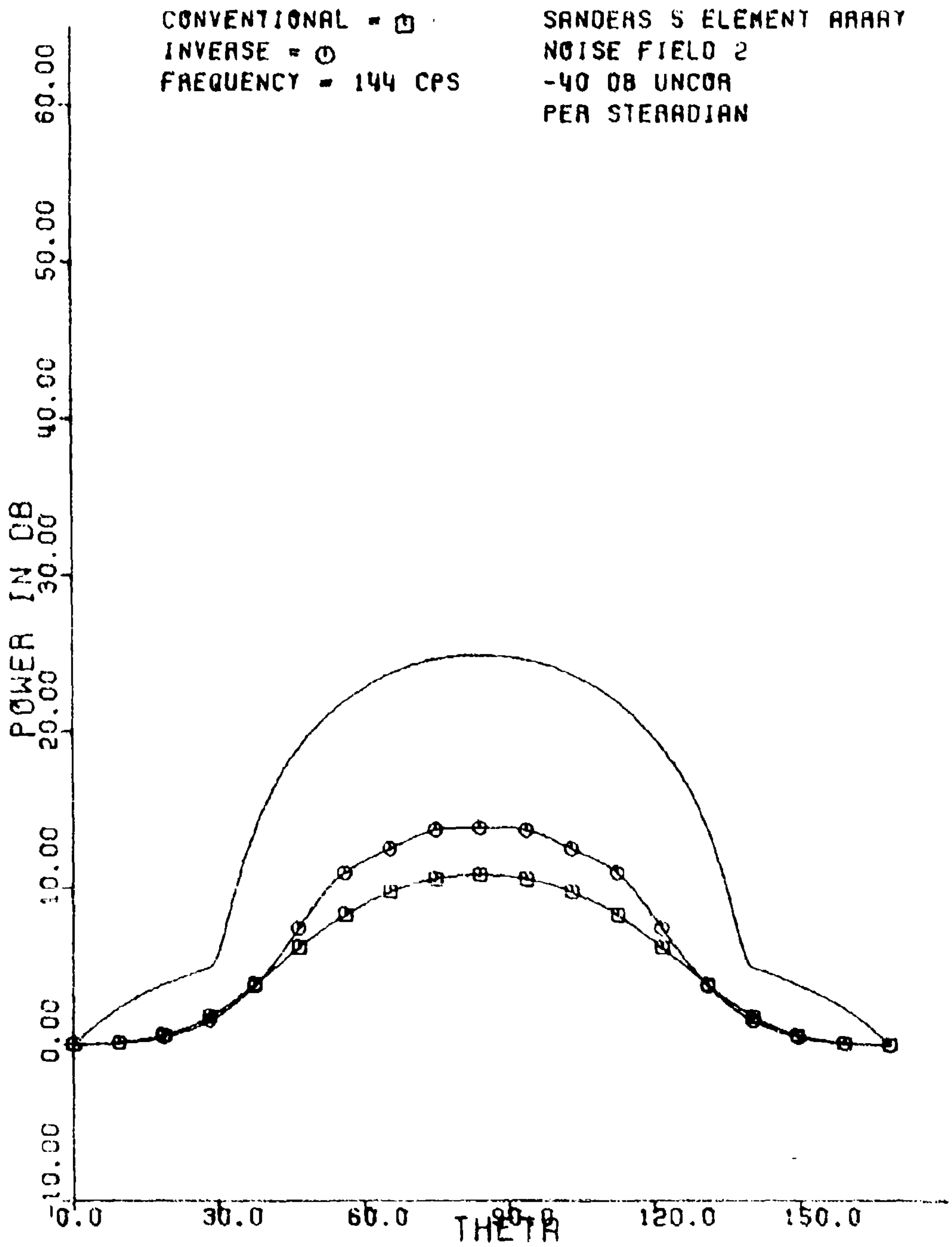

(U) Figure B21. BR noise field 2 144 cps.

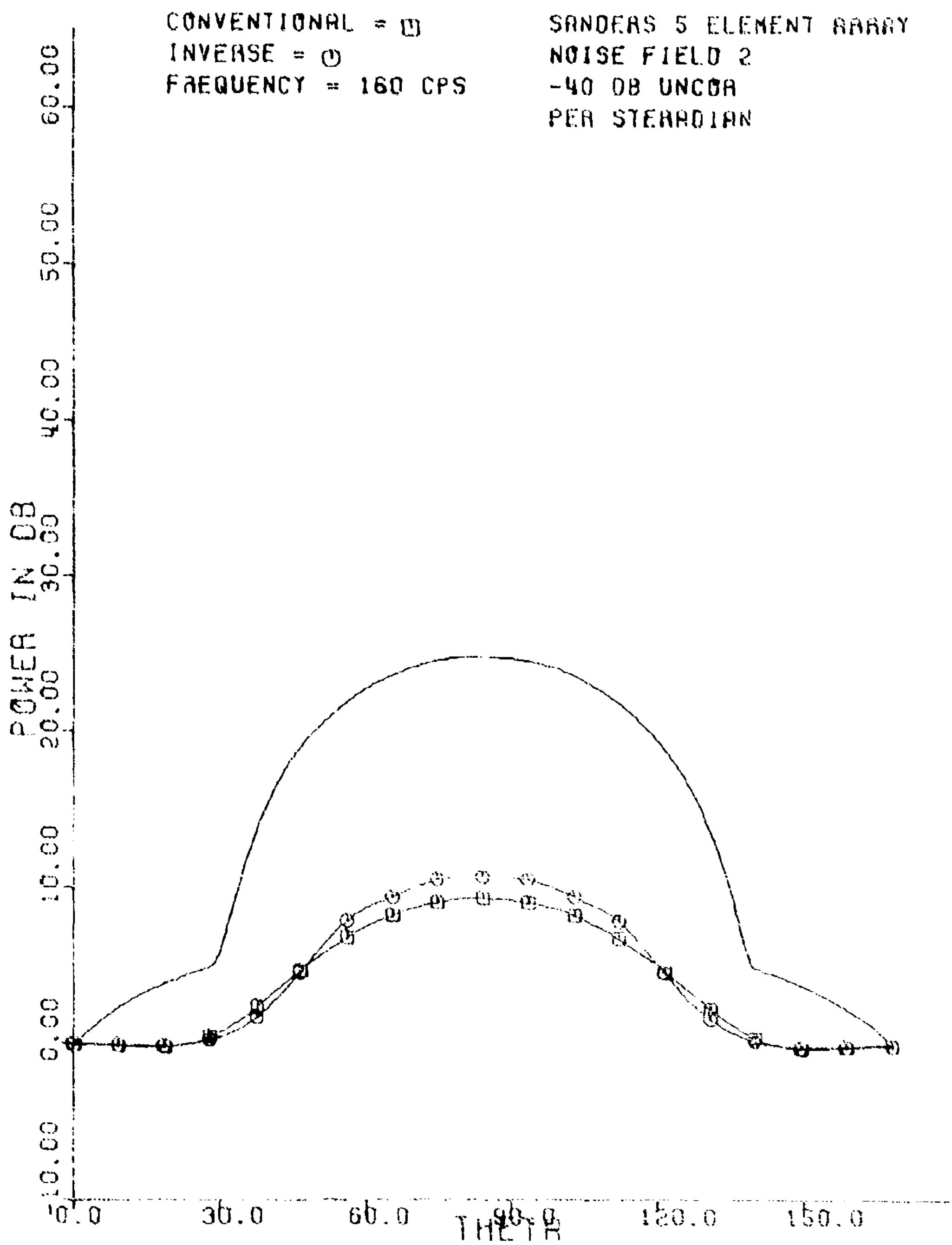

(U) Figure B22. BR noise field 2 160 cps

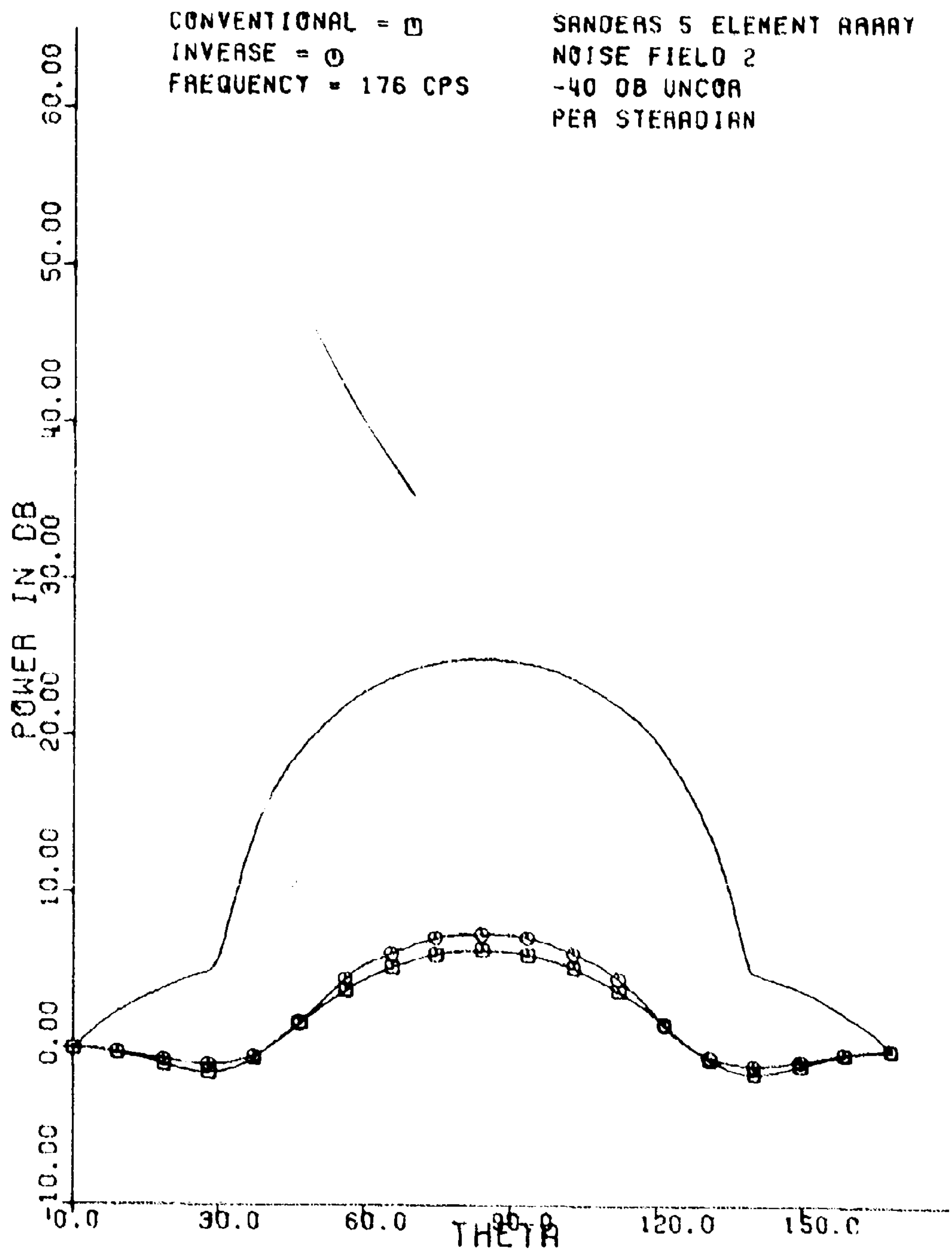

(U) Figure B23. BR noise field 2 176 cps.

UNCLASSIFIED

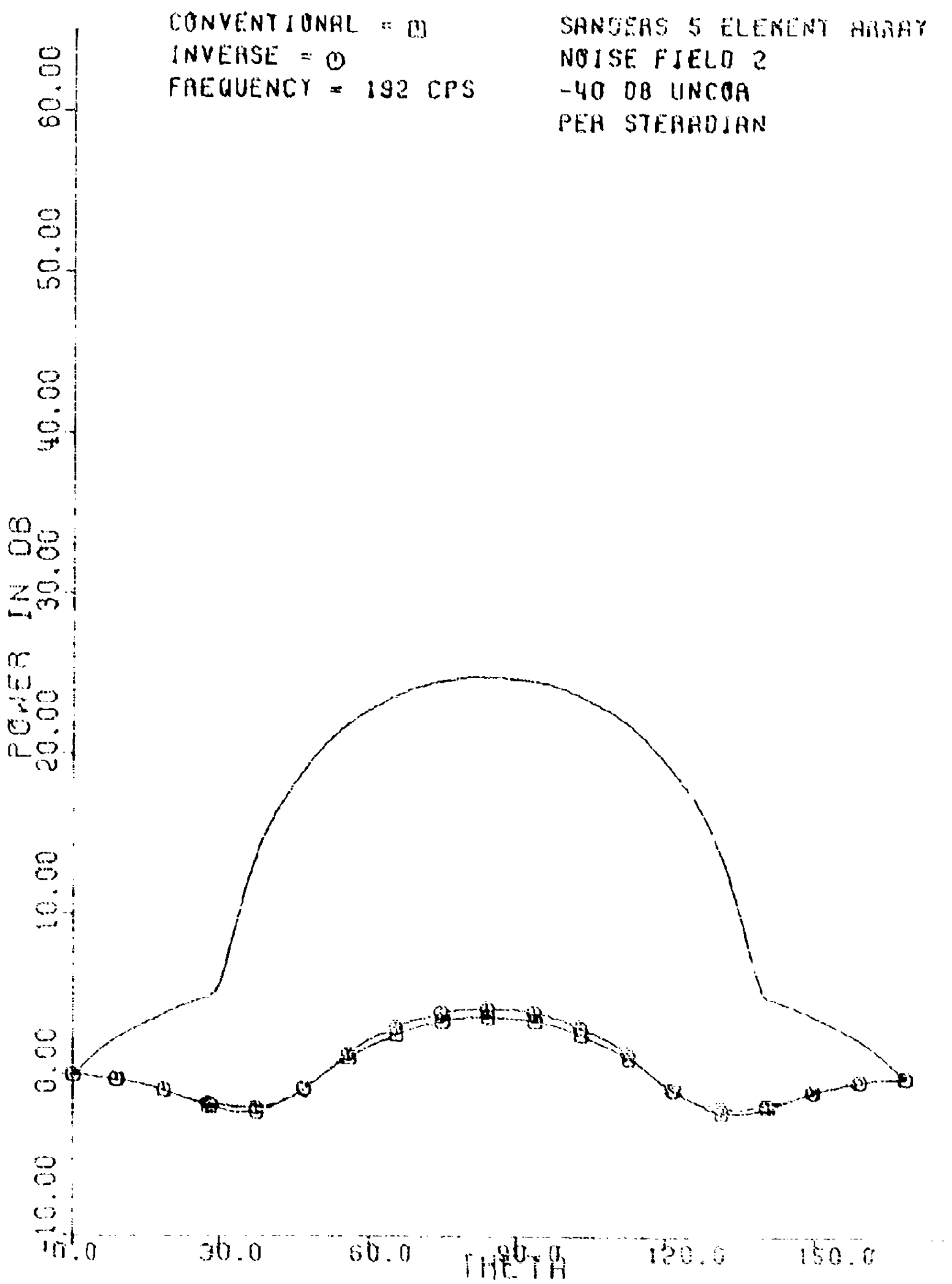

(U) Figure B24. ER noise field 2 192 cps

UNCLASSIFIED

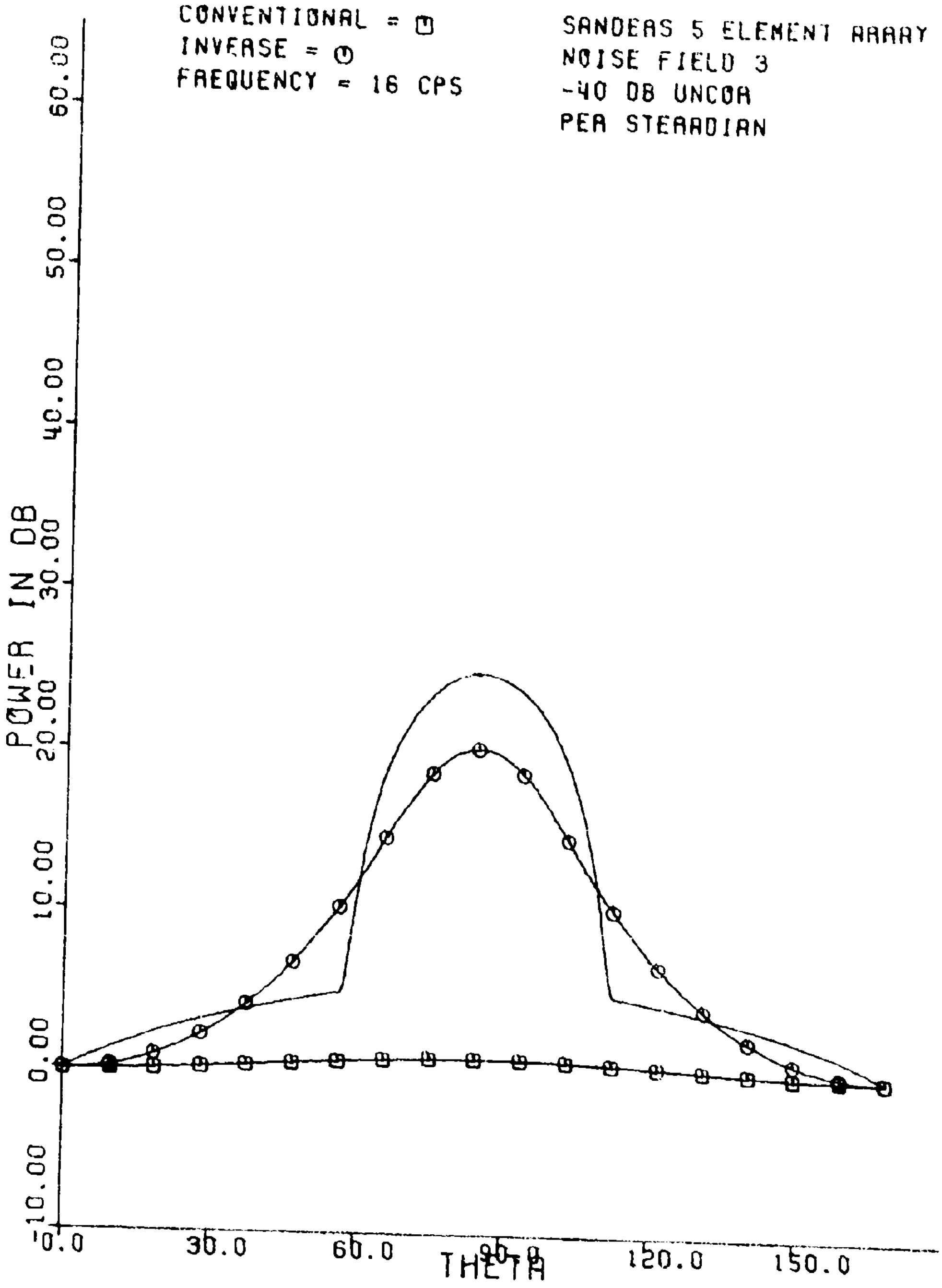

(U) Figure B25. BR - noise field 3 - 16 cps.

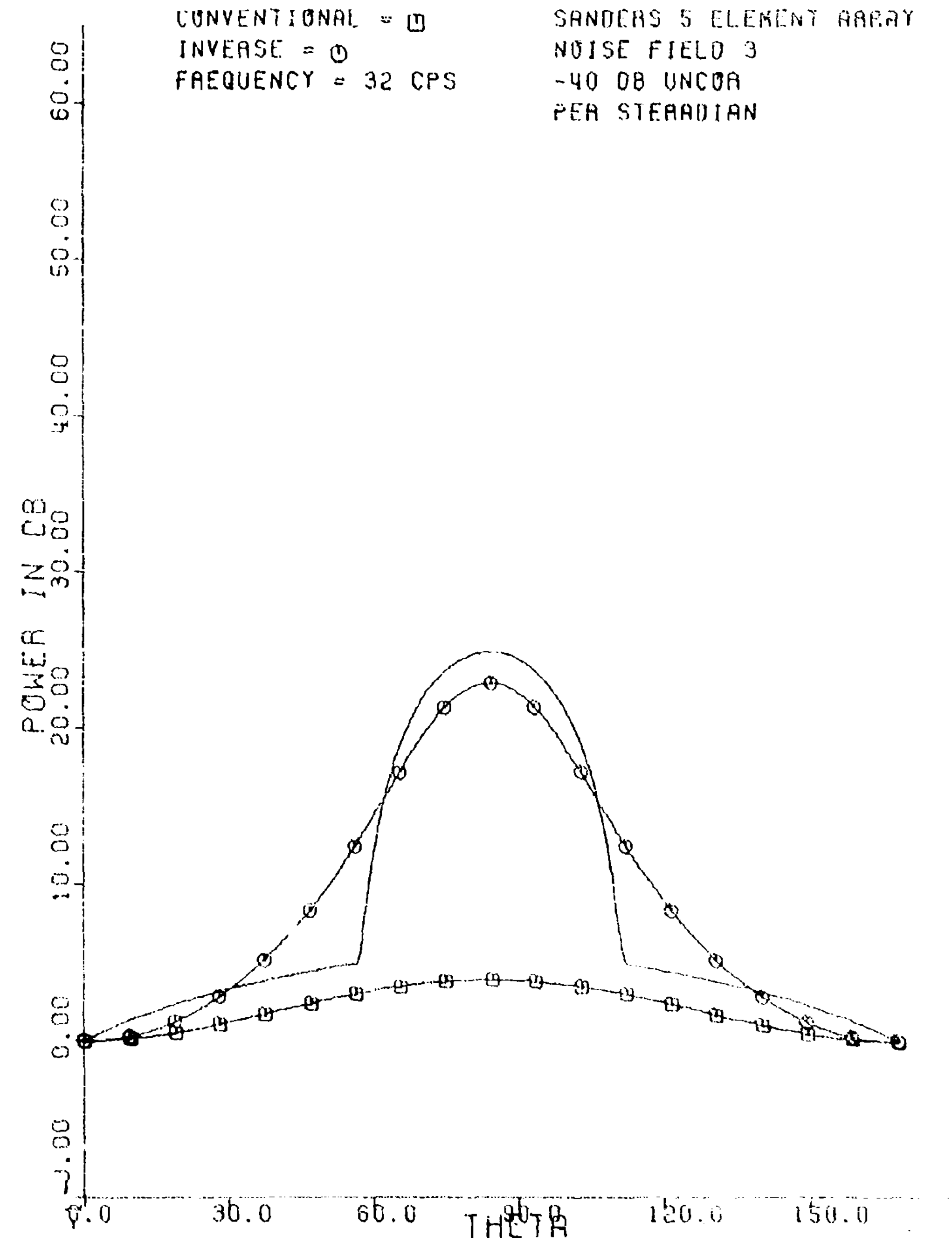

(U) Figure B26. BR noise field 3 32 cps.

UNCLASSIFIED

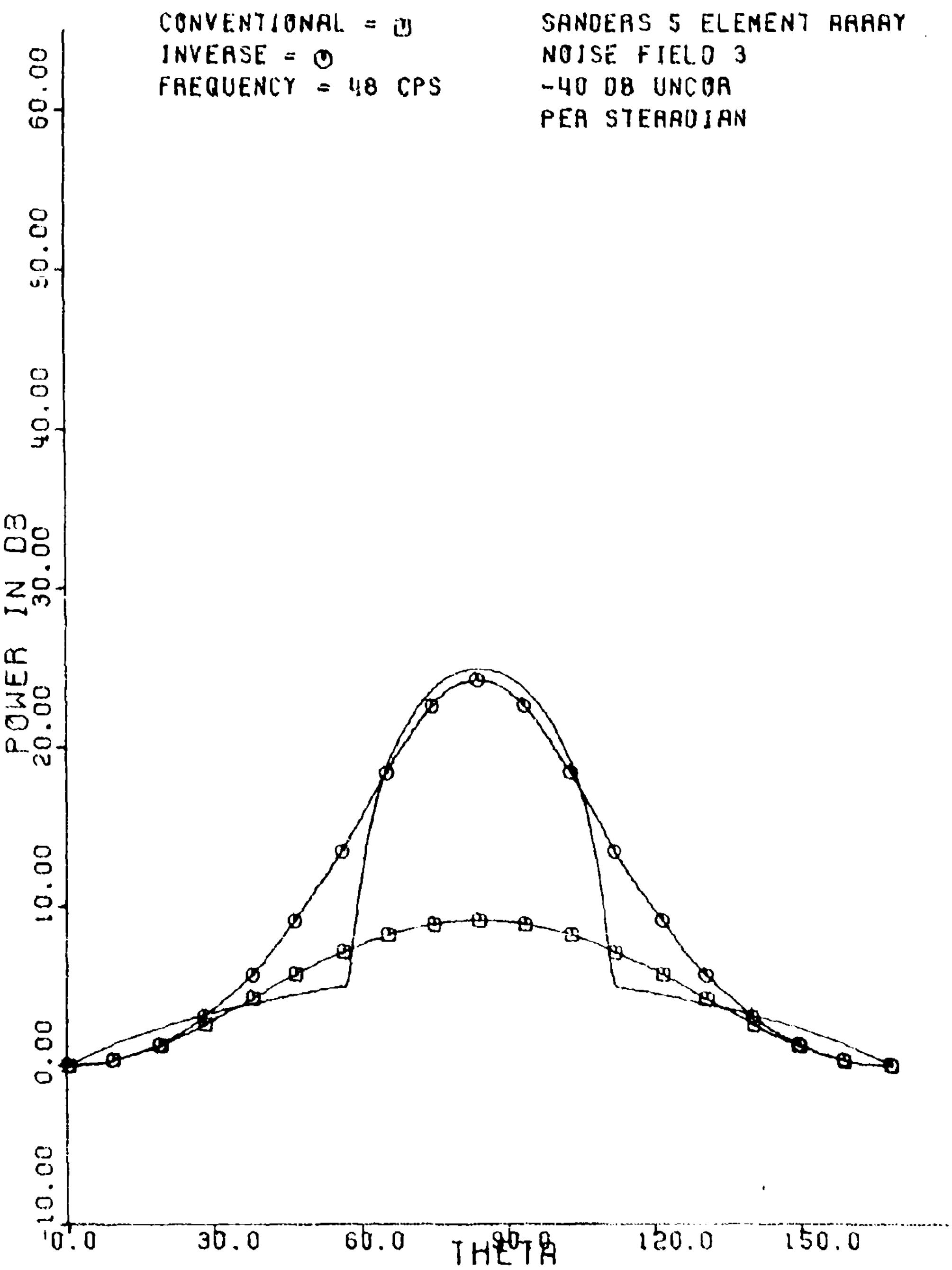

(U) Figure B27. BR noise field 3 48 cps.

UNCLASSIFIED

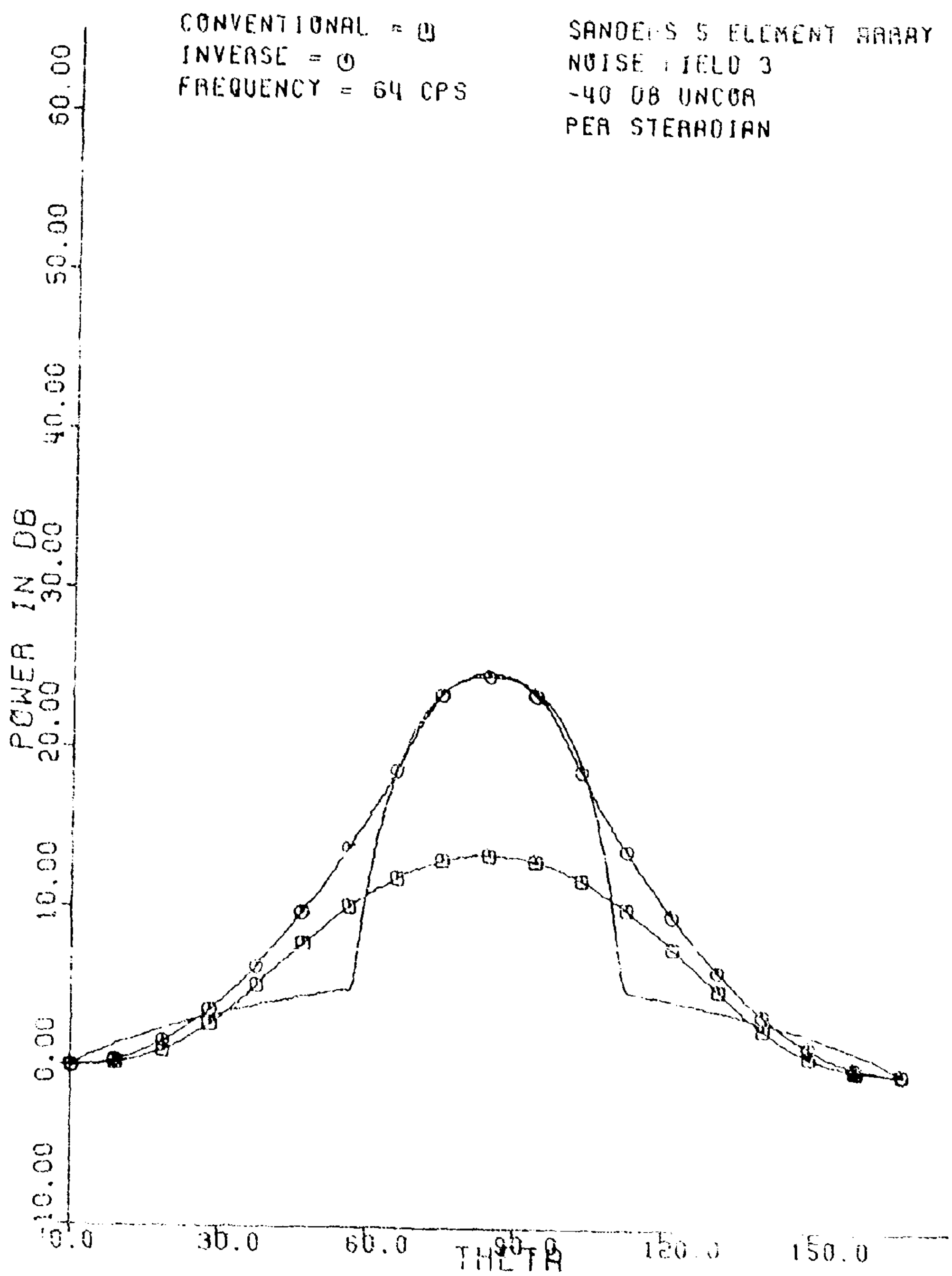

(U) Figure B28. BR — noise field 3 — 64 cps

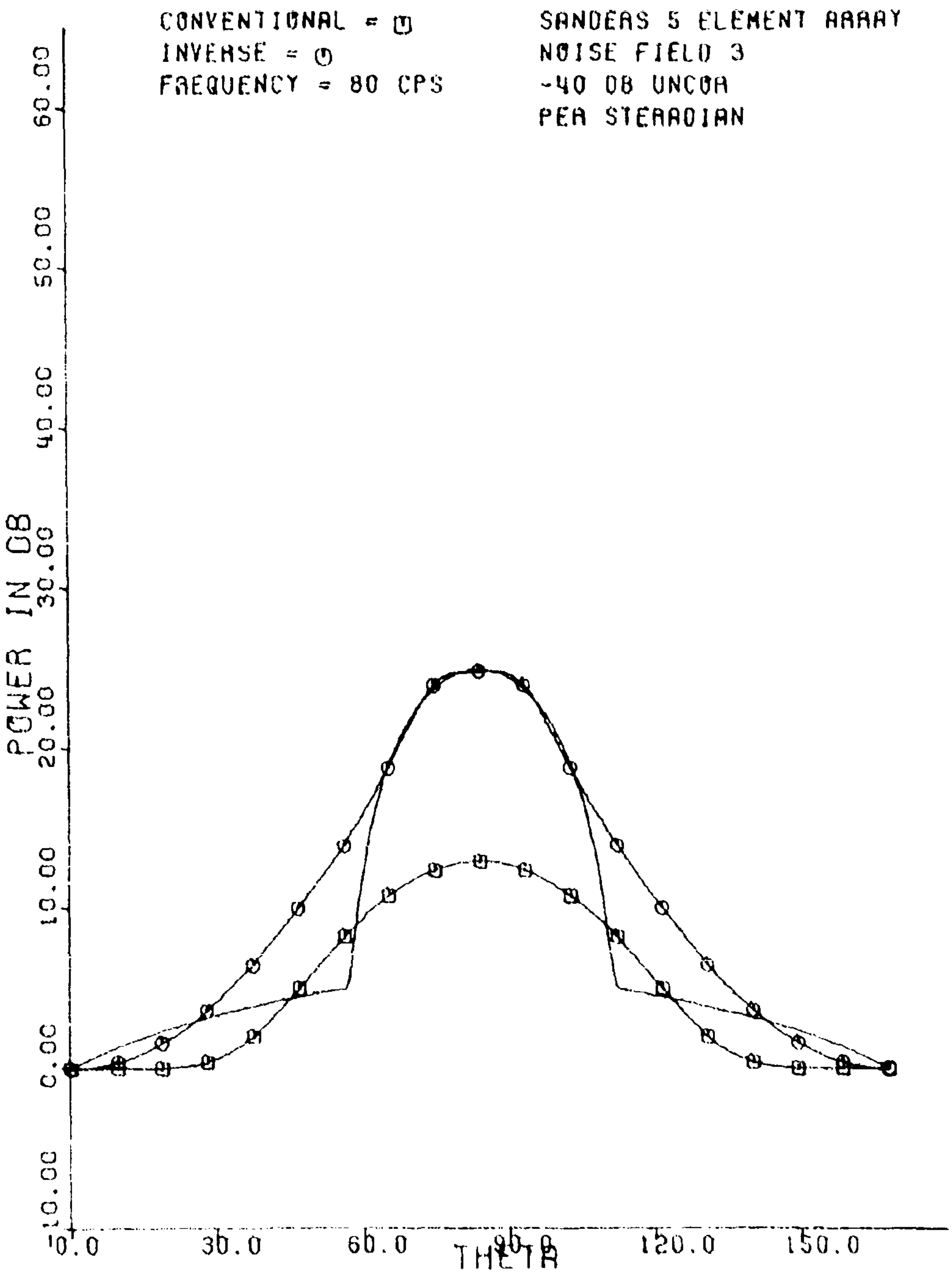

(U) Figure B29. BR noise field 3 80 cps

UNCLASSIFIED

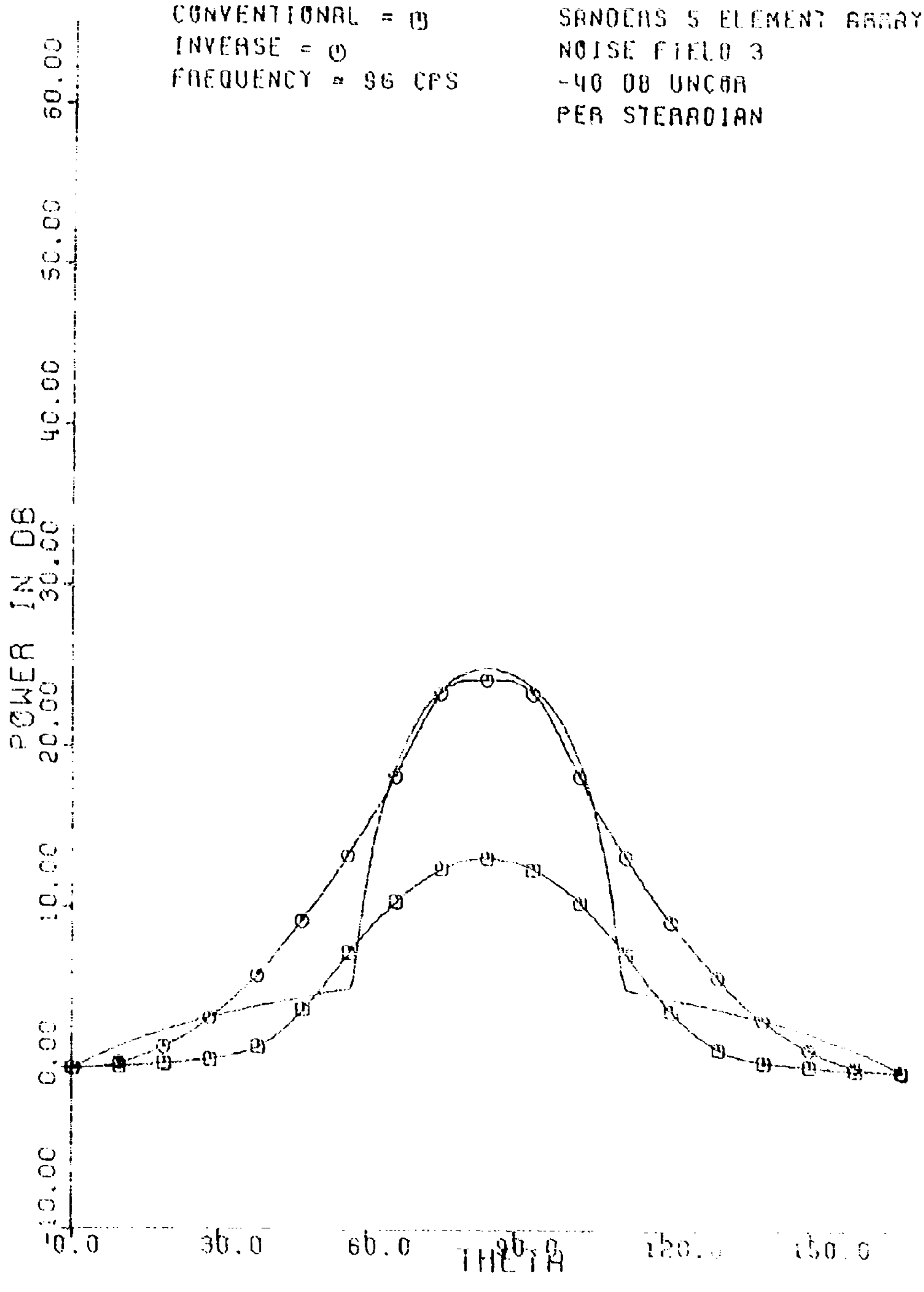

(U) Figure B30 BR noise field 3 96 cps

UNCLASSIFIED

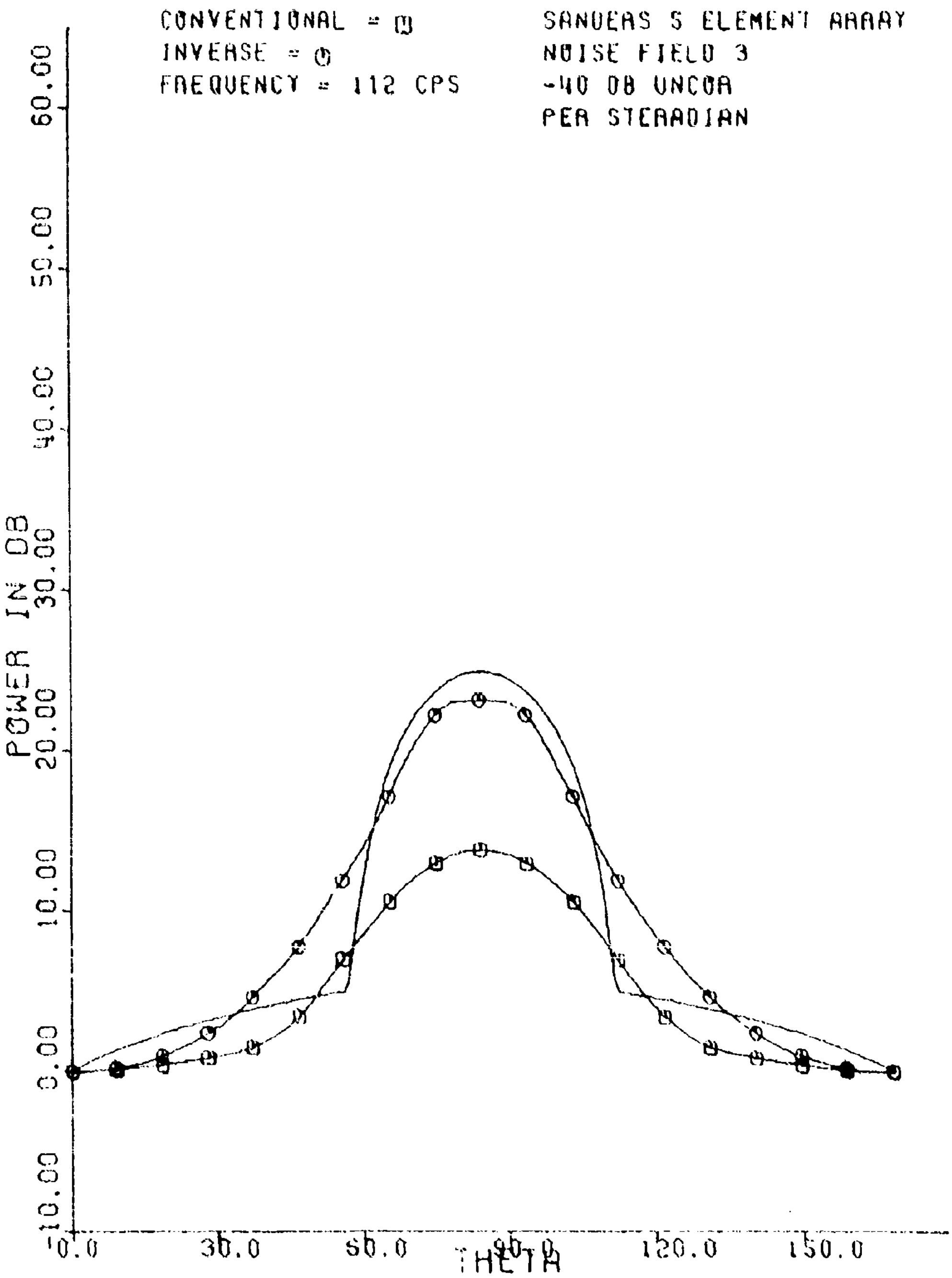

(U) Figure B31 BR noise field 3 112 cps

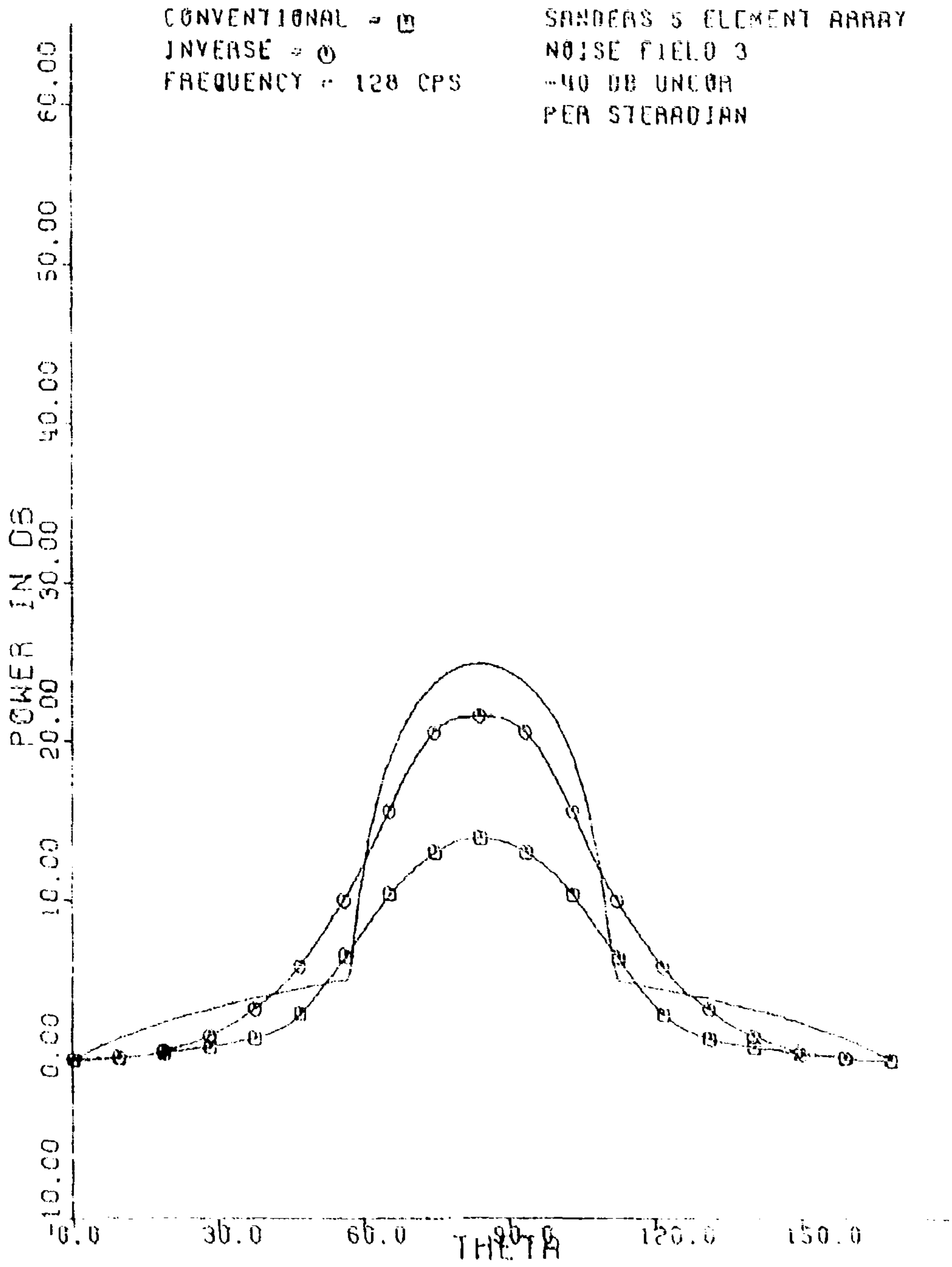

(U) Figure B32 BR – noise field 3 – 128 cps

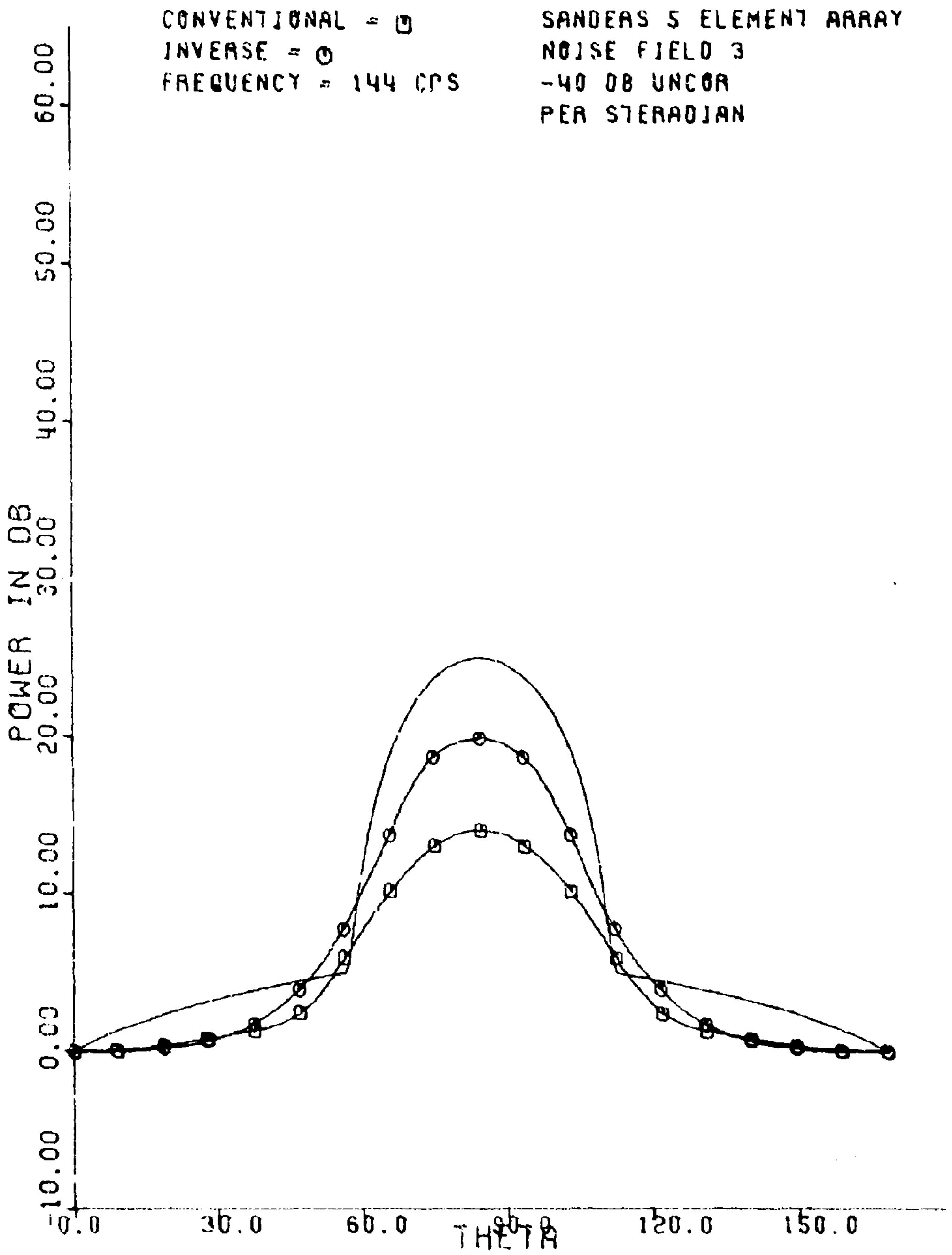

(U) Figure B33. BR noise field 3 144 cps.

UNCLASSIFIED

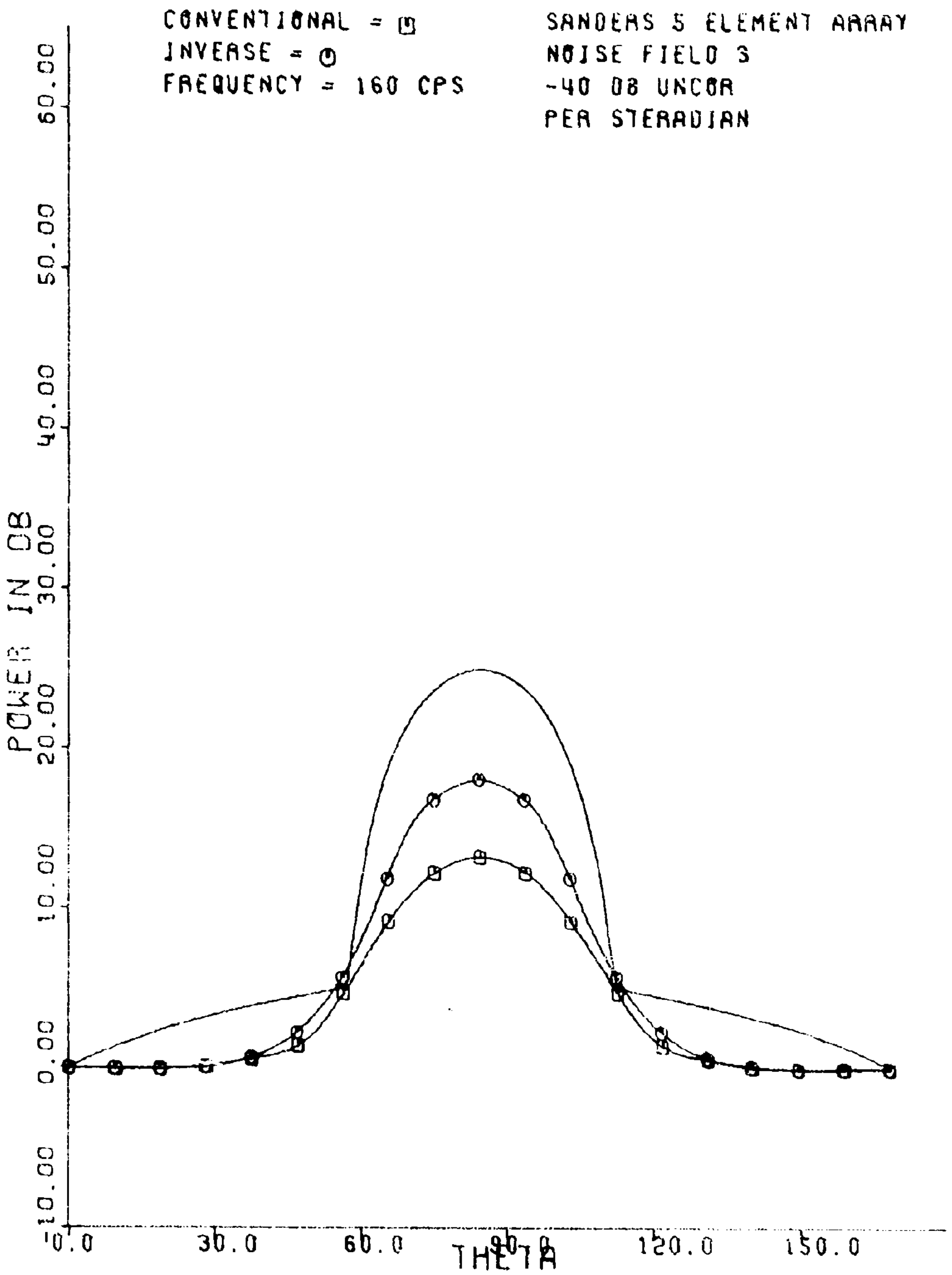

(U) Figure B34. BR noise field 3 160 cps.

UNCLASSIFIED

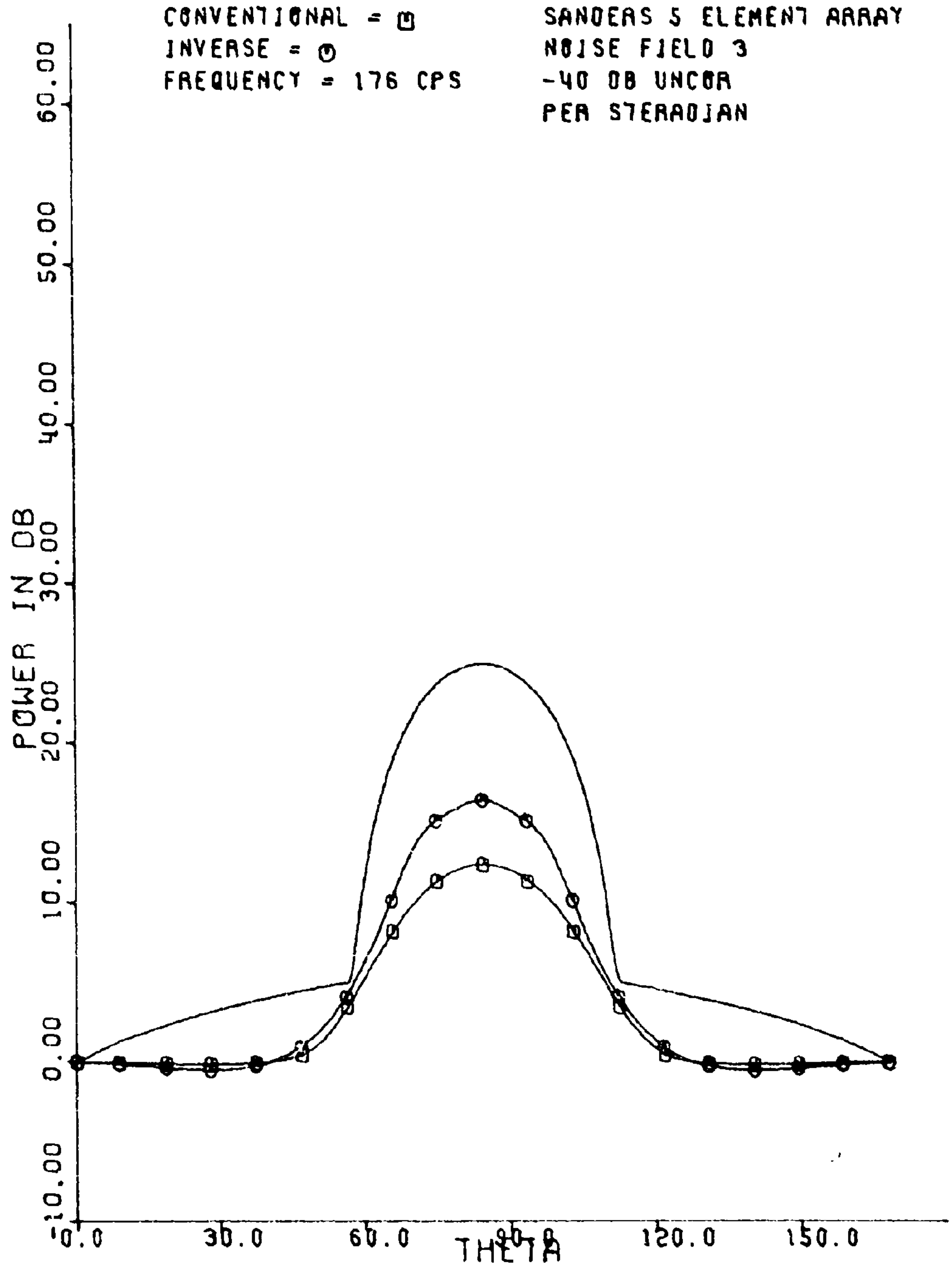

(U) Figure B35. BR noise field 3 176 cps.

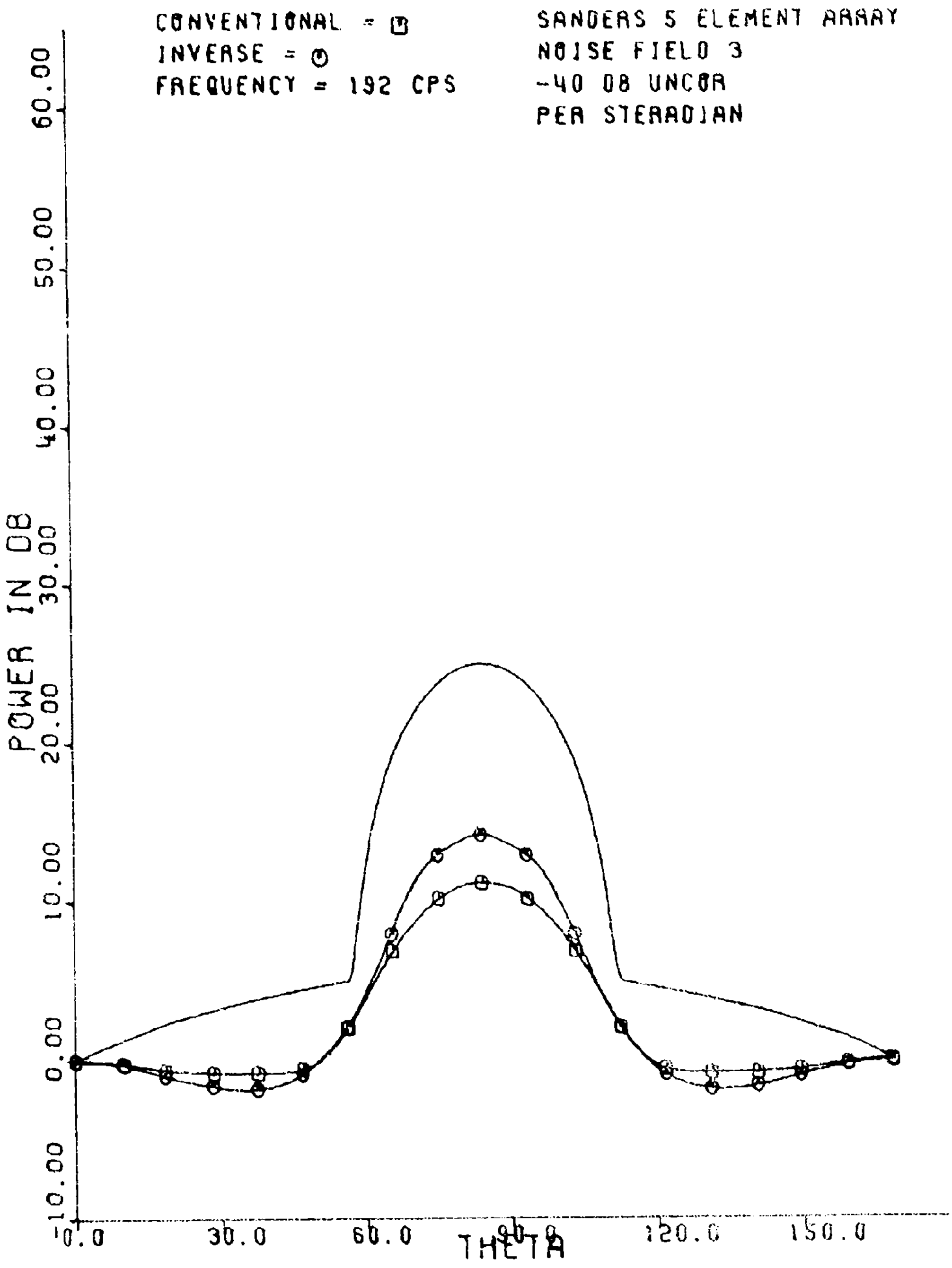

(U) Figure B36. BR noise field 3 192 cps.

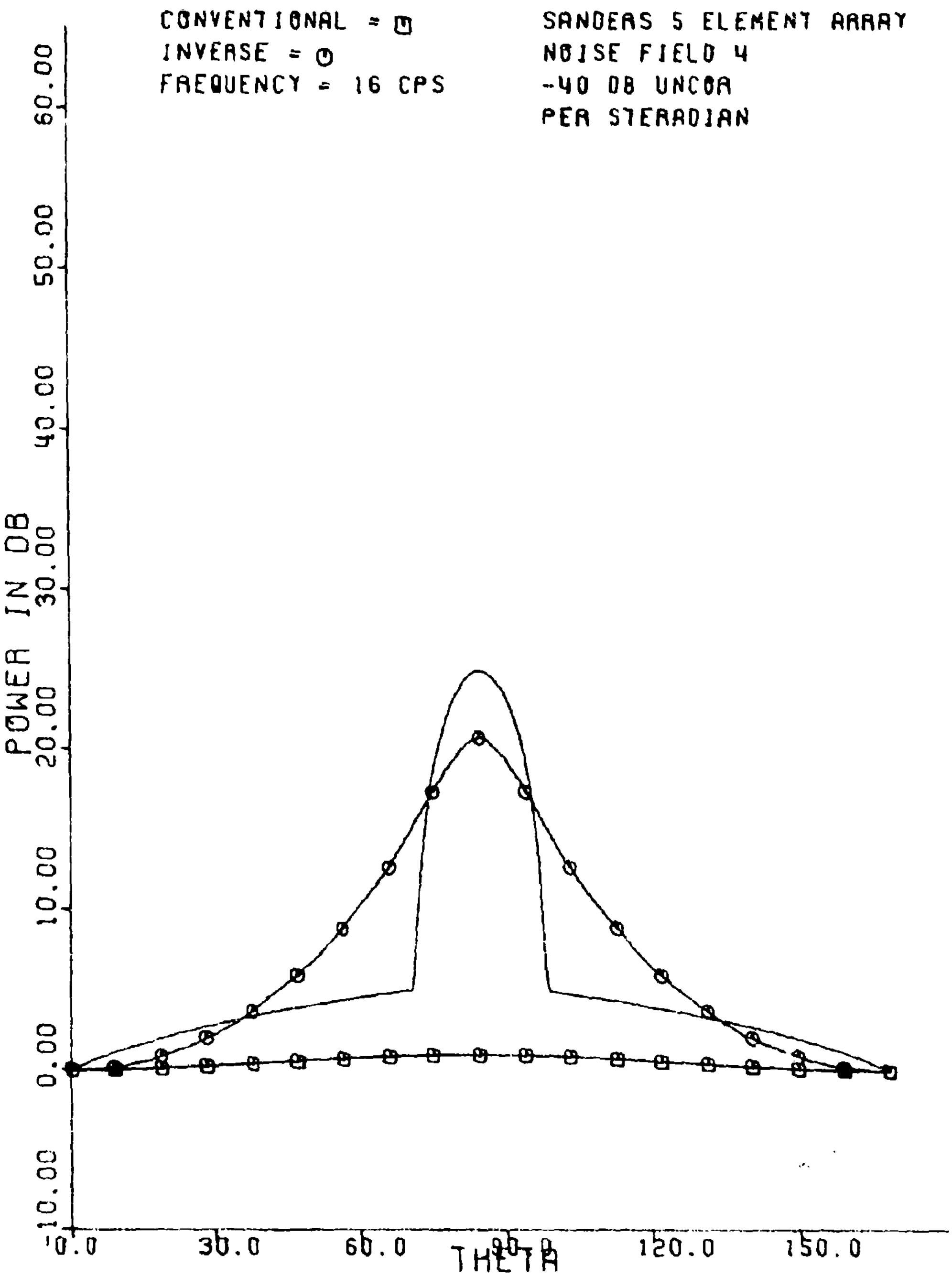

(U) Figure B37. BR noise field 4 - 16 cps.

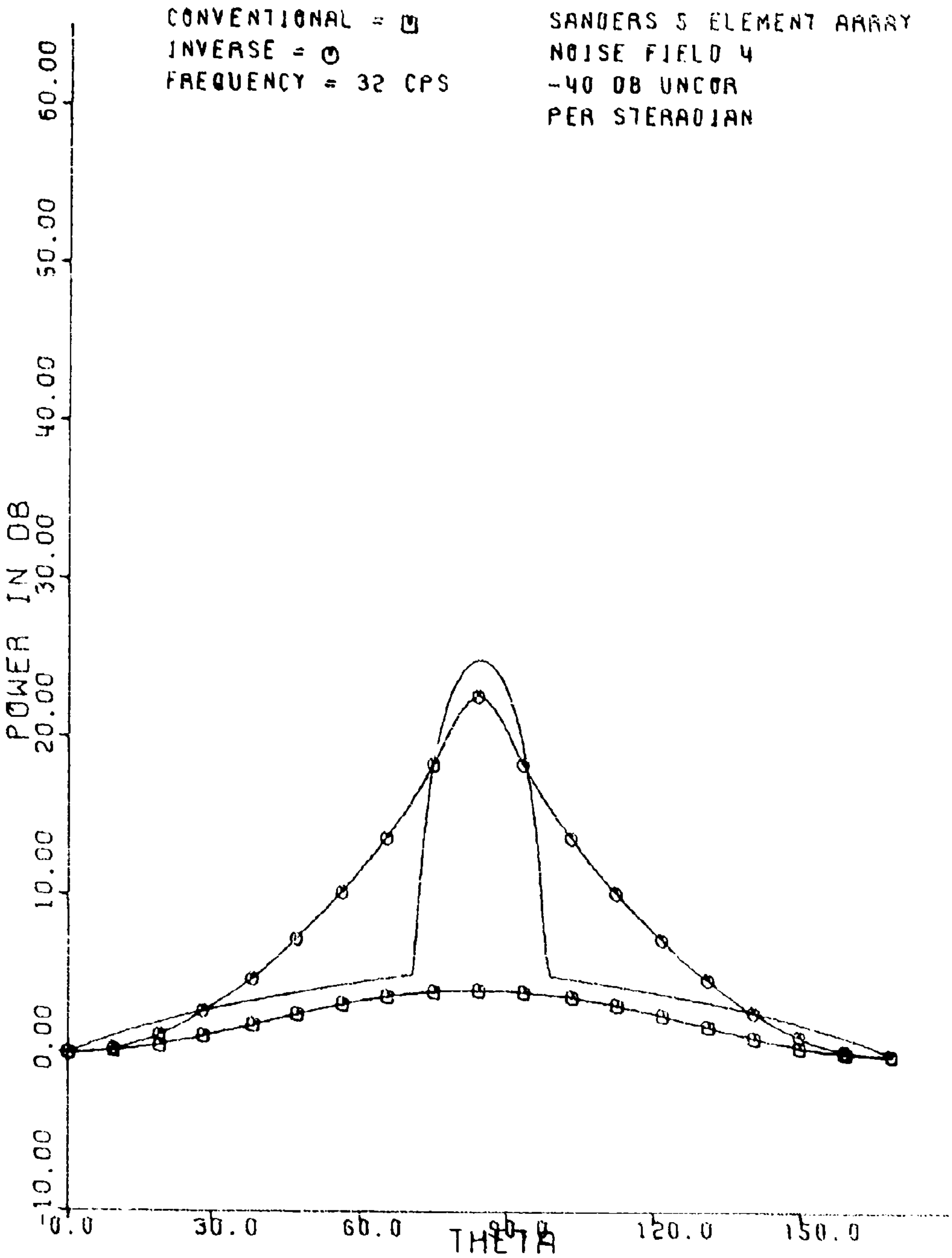

(U) Figure B38. BR noise field 4 32 cps.

UNCLASSIFIED

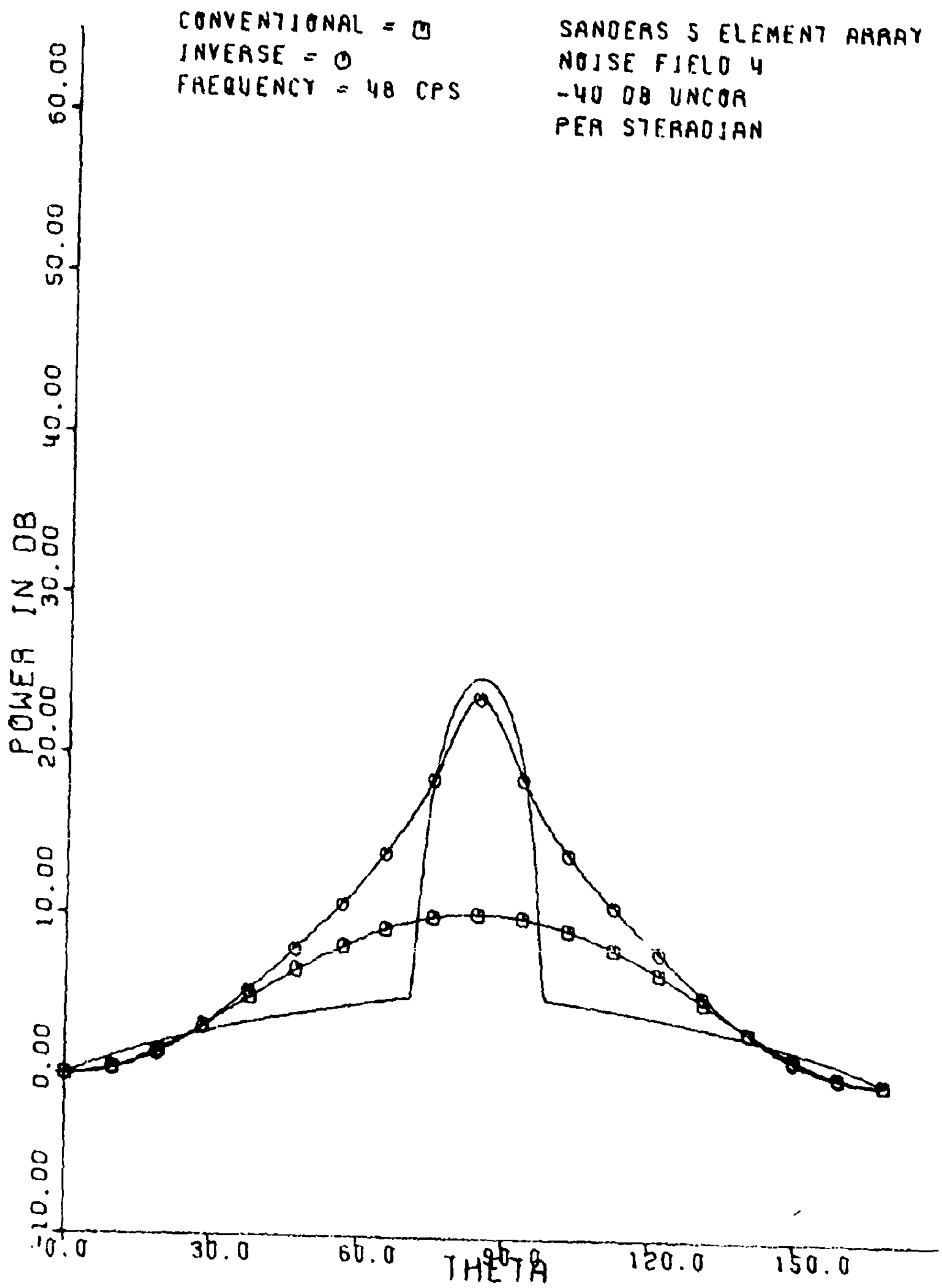

(U) Figure B39. BR noise field 4 - 48 cps.

UNCLASSIFIED

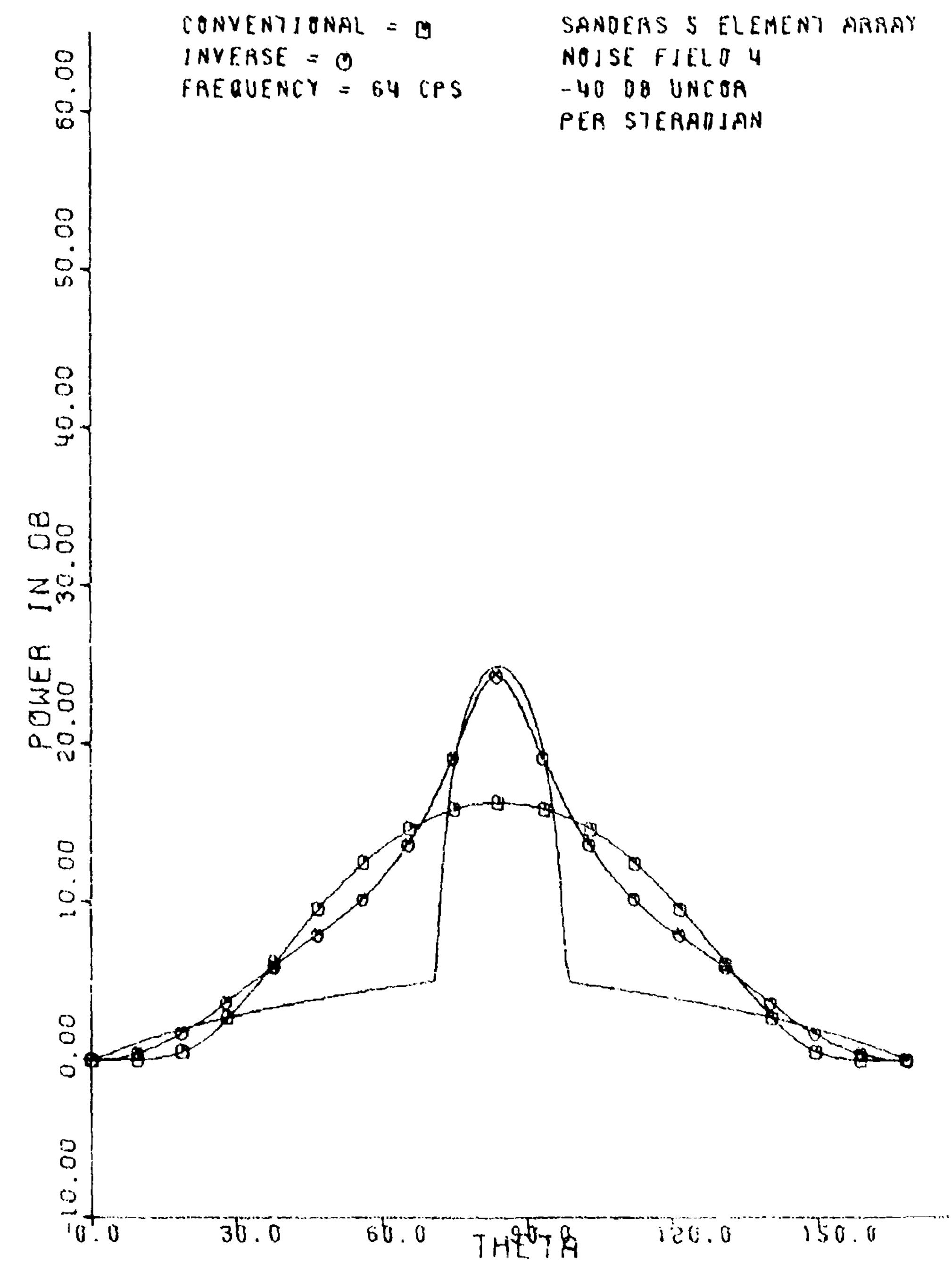

(U) Figure B40. BR noise field 4 64 cps.

UNCLASSIFIED

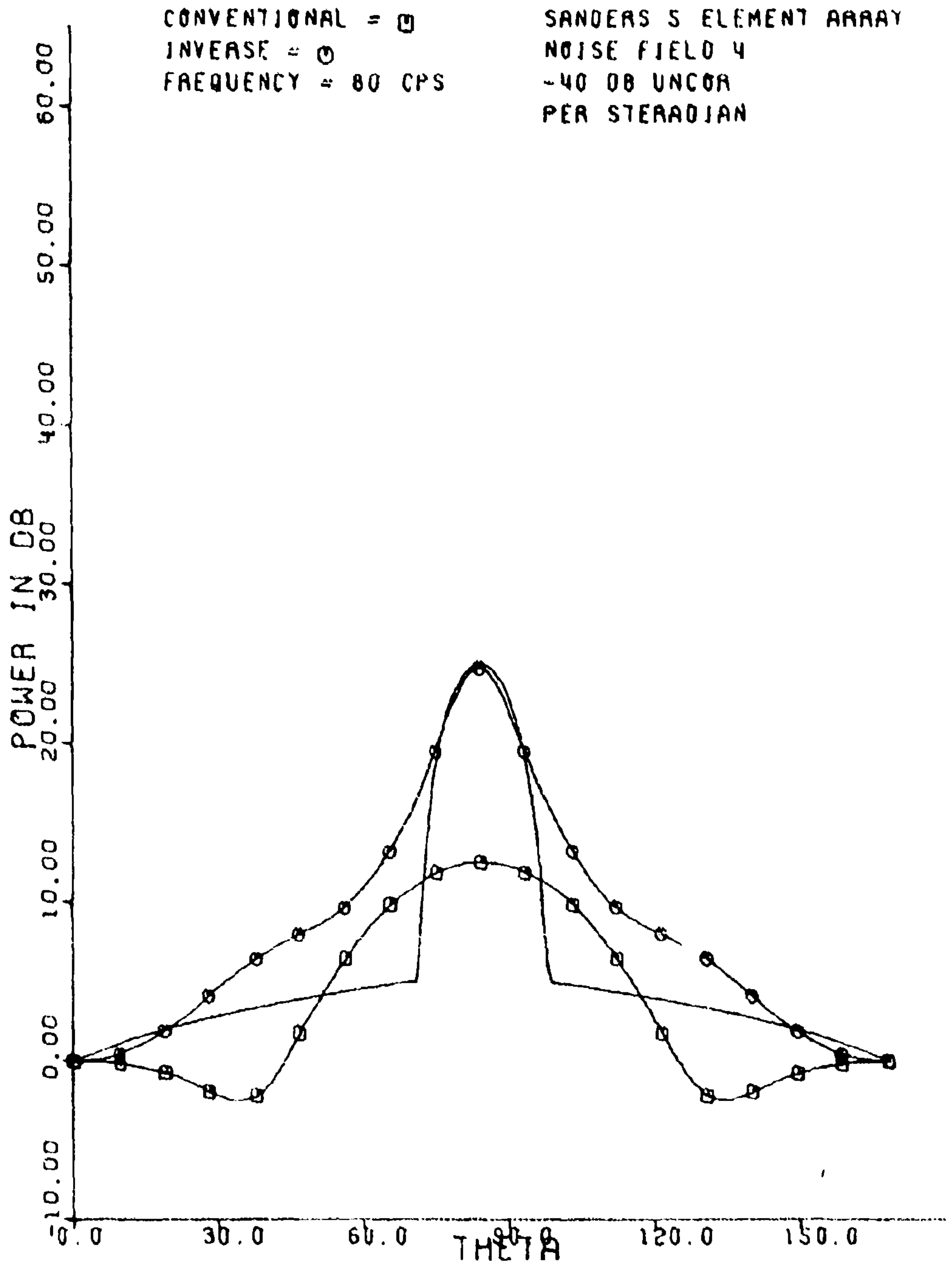

(U) Figure B41. BR noise field 4 80 cps.

UNCLASSIFIED

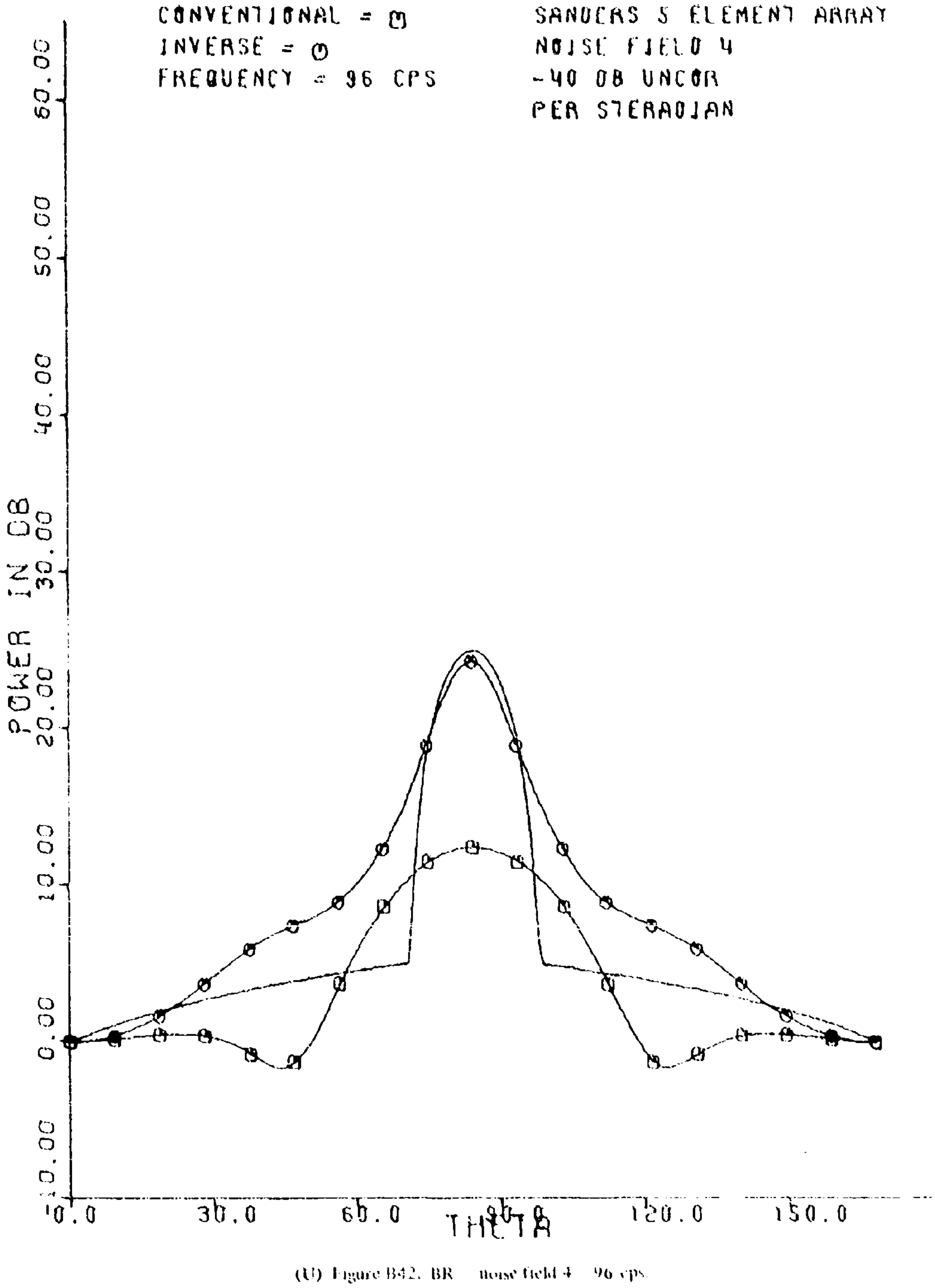

(U) Figure B42. BR noise field 4 96 cps

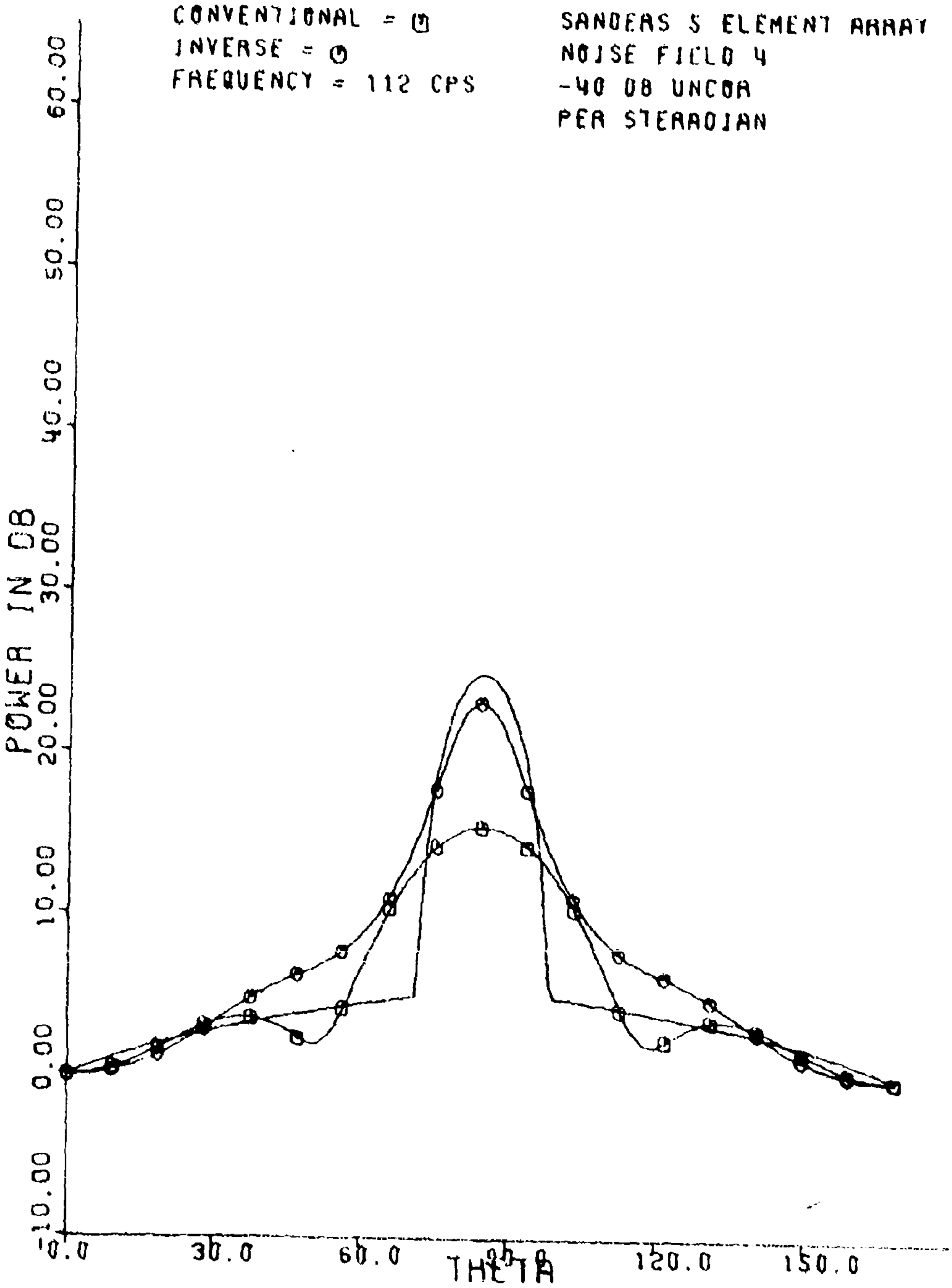

(U) Figure B43. BR noise field 4 112 cps.

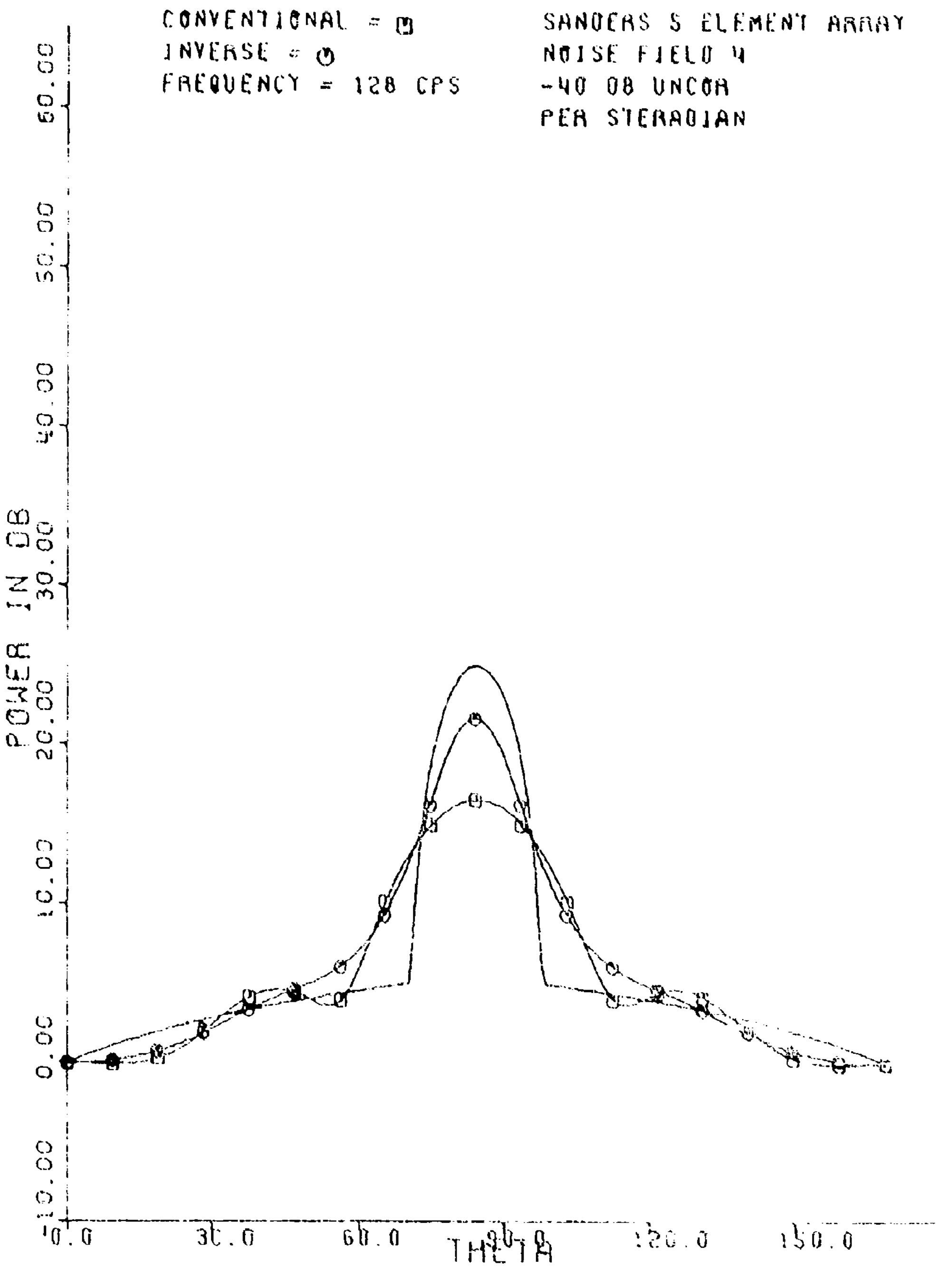

(U) Figure B44 BF noise field 4 128 cps

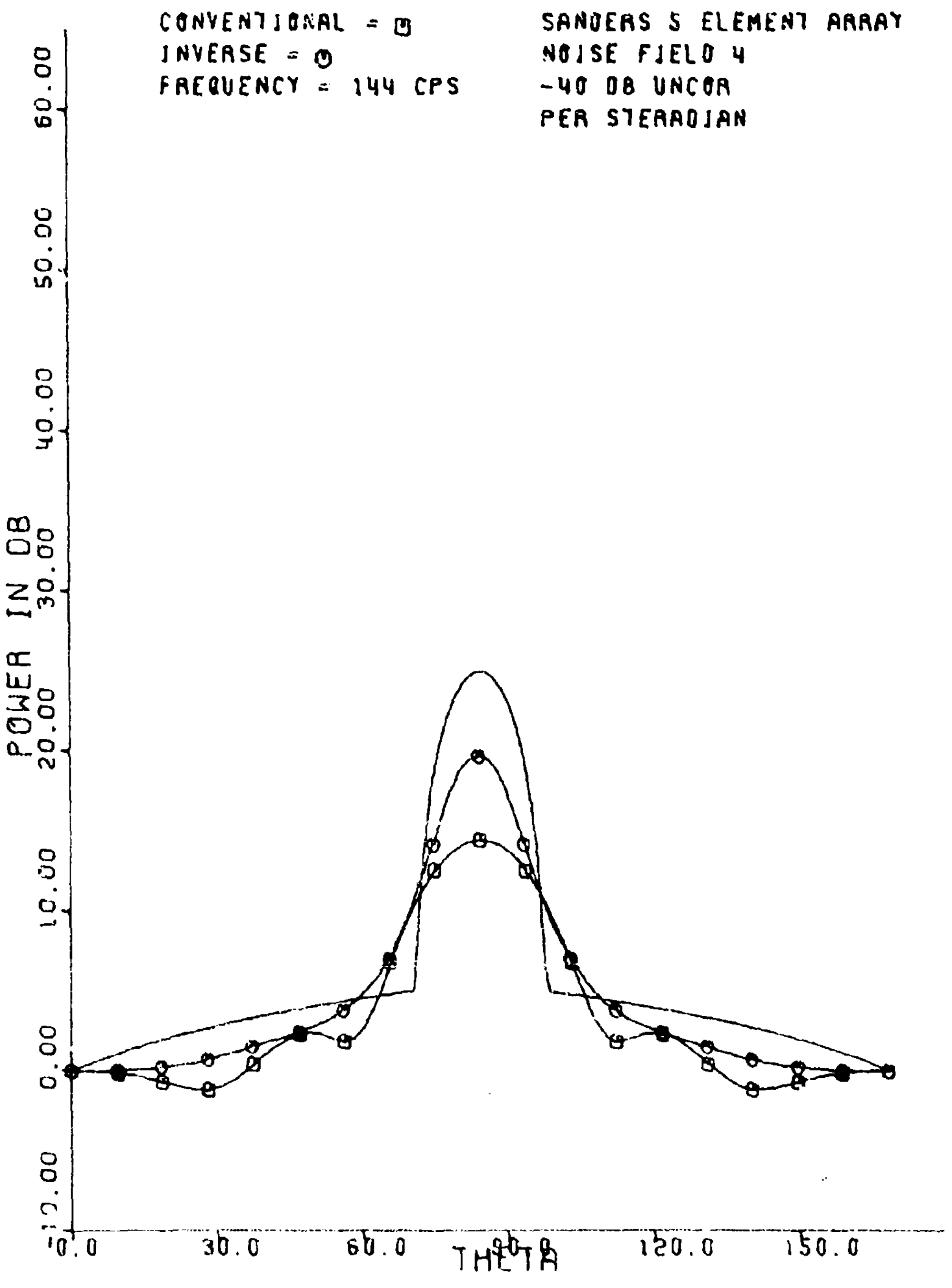

(U) Figure B45. BR noise field 4 144 cps.

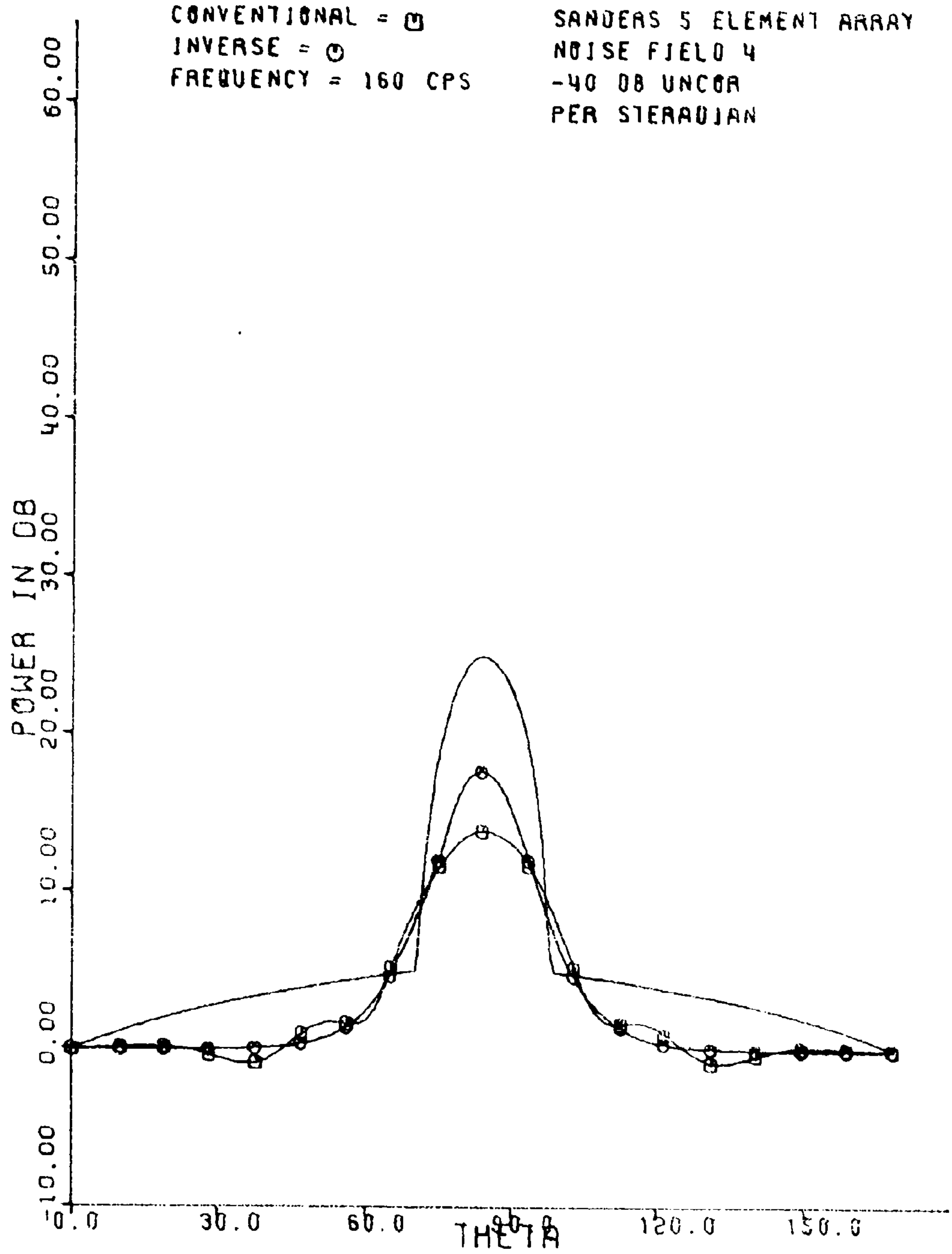

(U) Figure B46. BK noise field 4 160 cps.

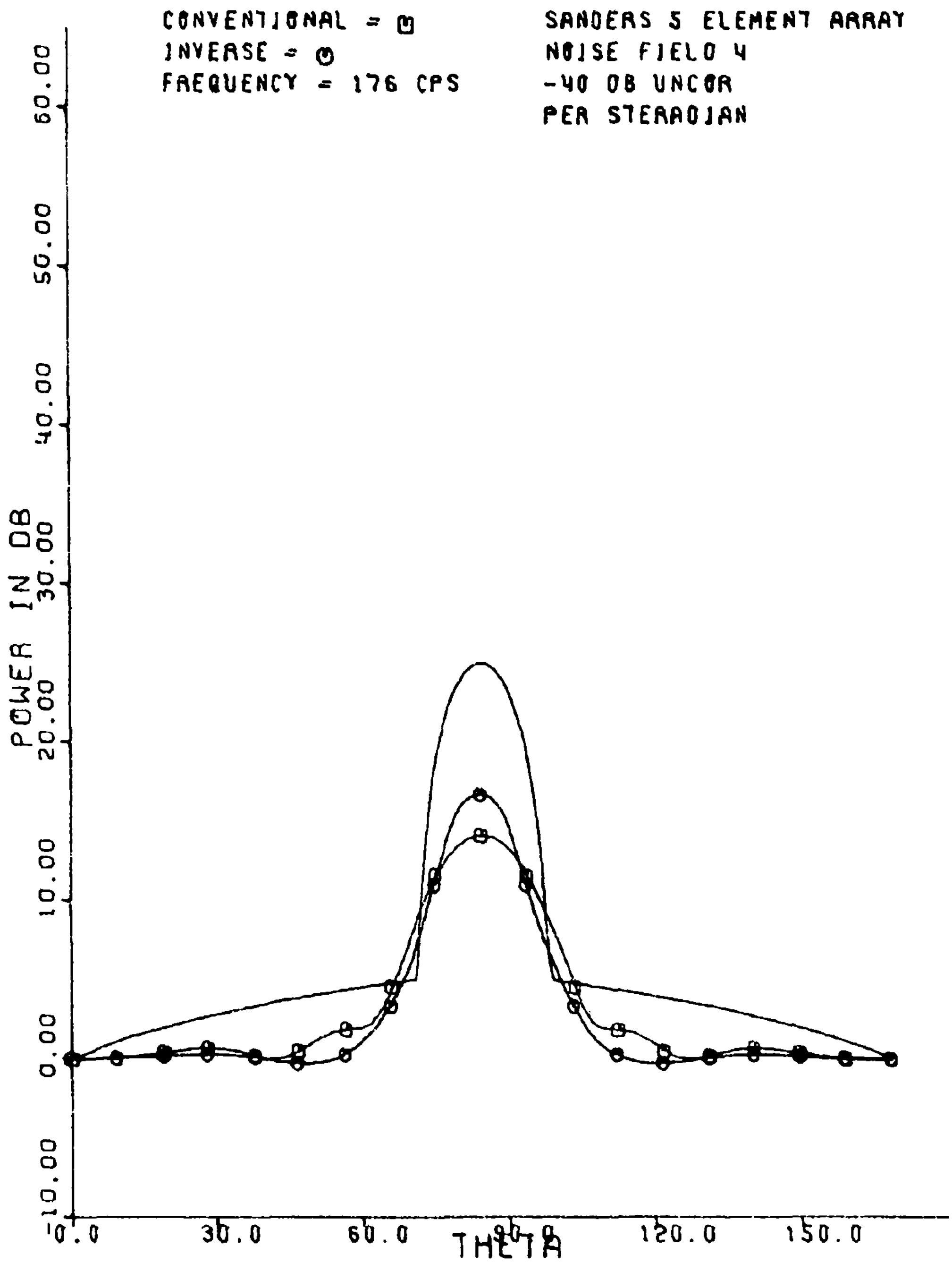

(U) Figure B47. BR – noise field 4 – 176 cps.

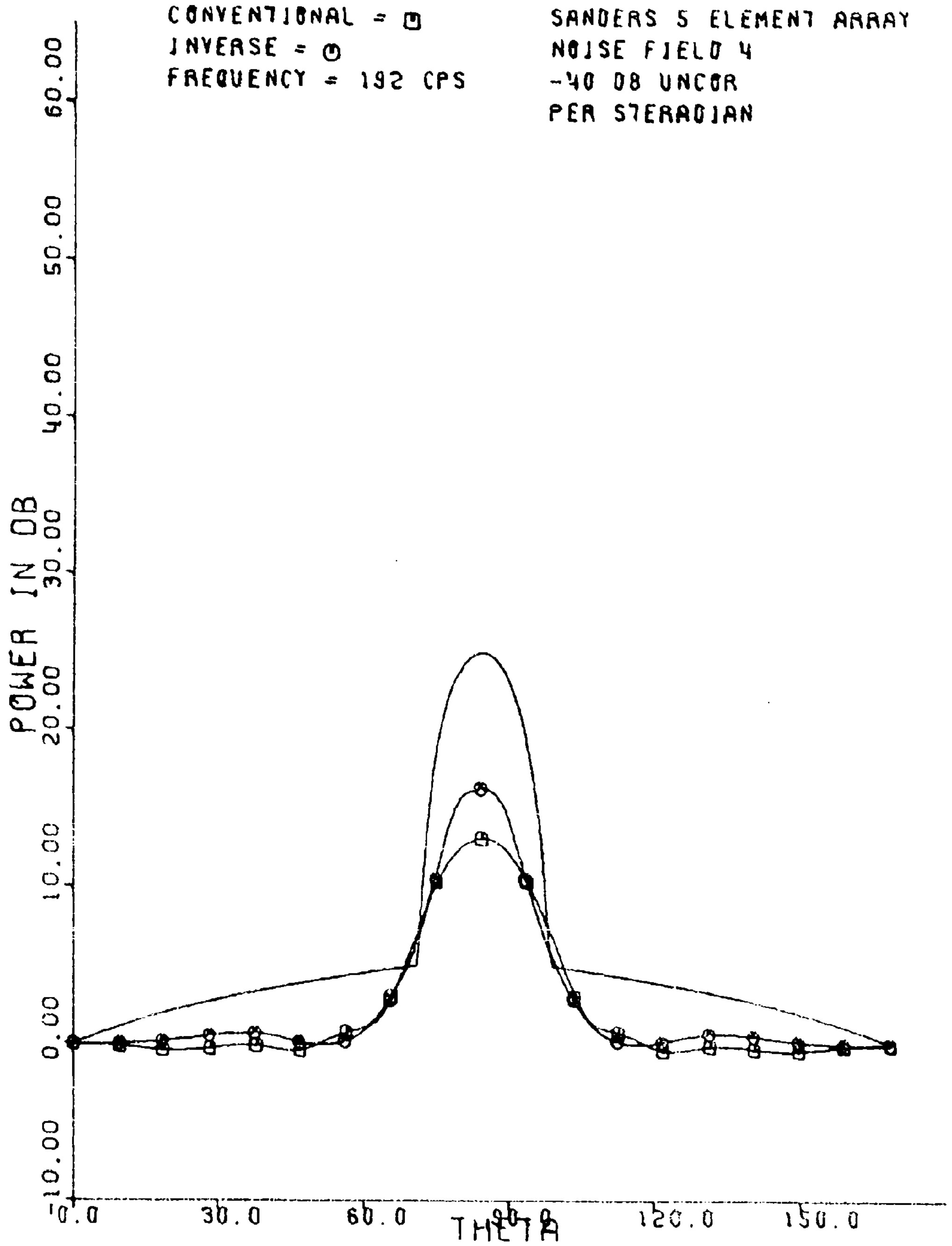

(U) Figure B48. BR noise field 4 192 cps.

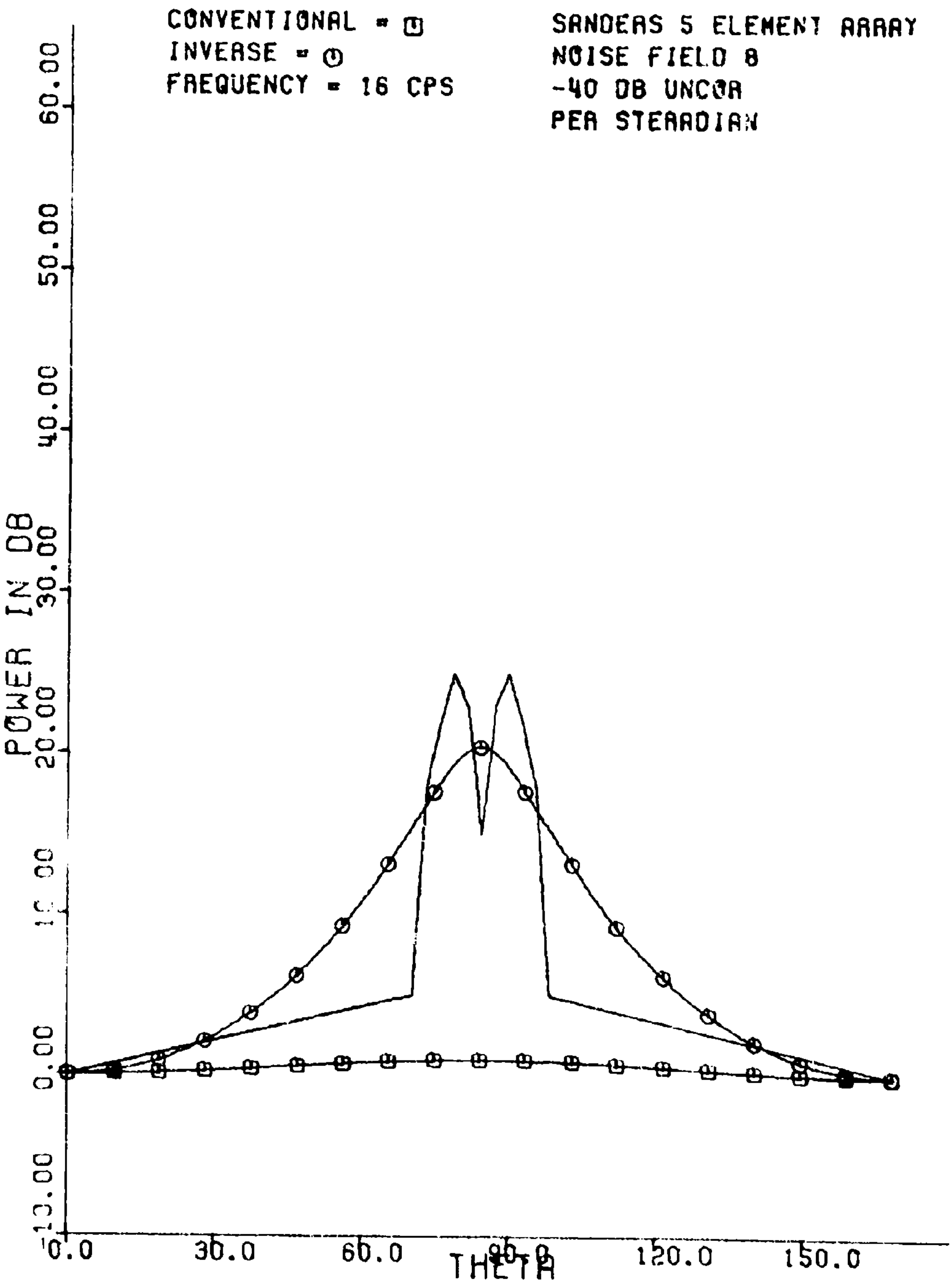

(U) Figure B49. BR noise field 8 – 16 cps.

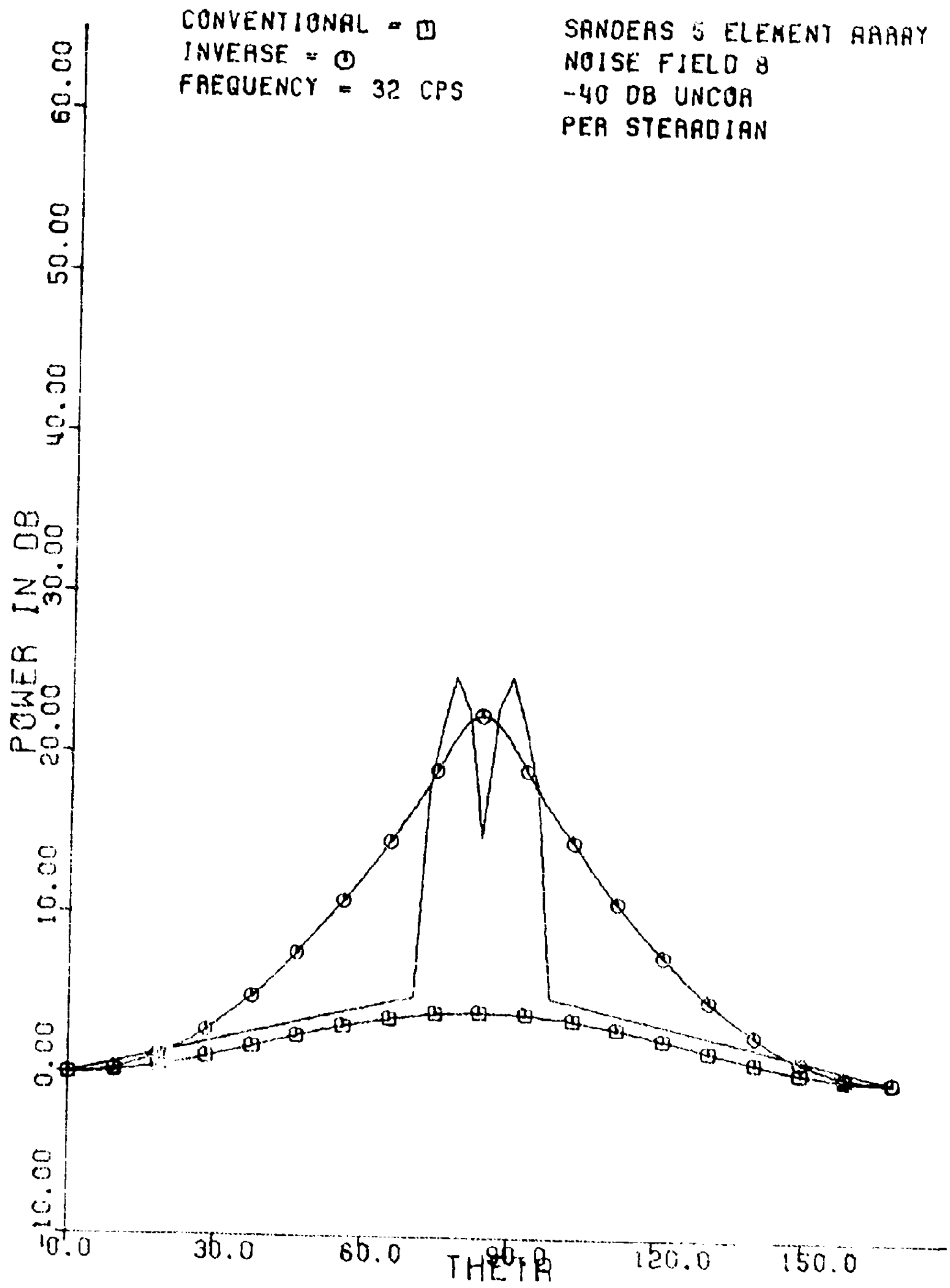

(U) Figure B50. BR noise field 8 32 cps.

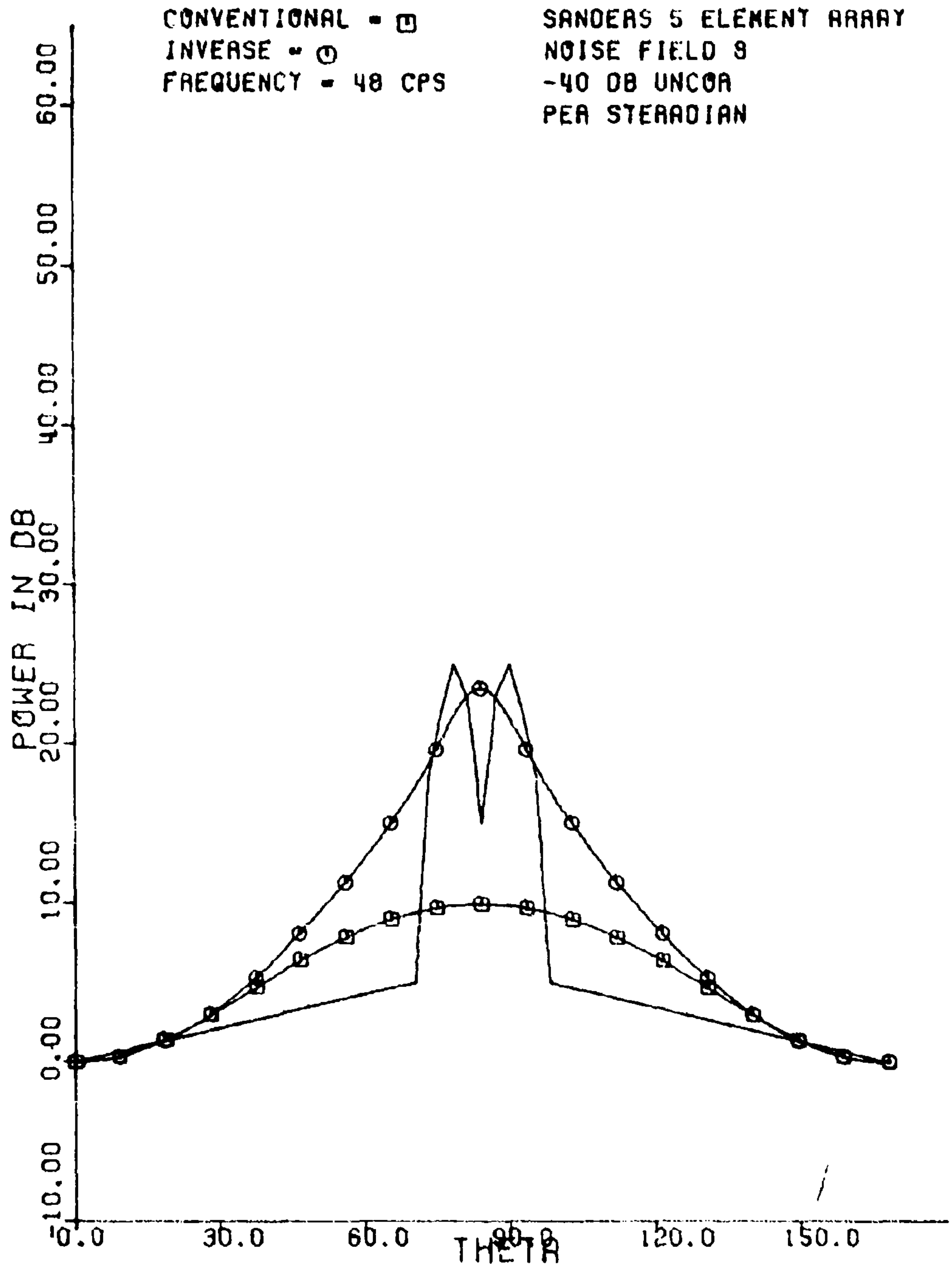

(U) Figure B51. BR – noise field 8 – 48 cps.

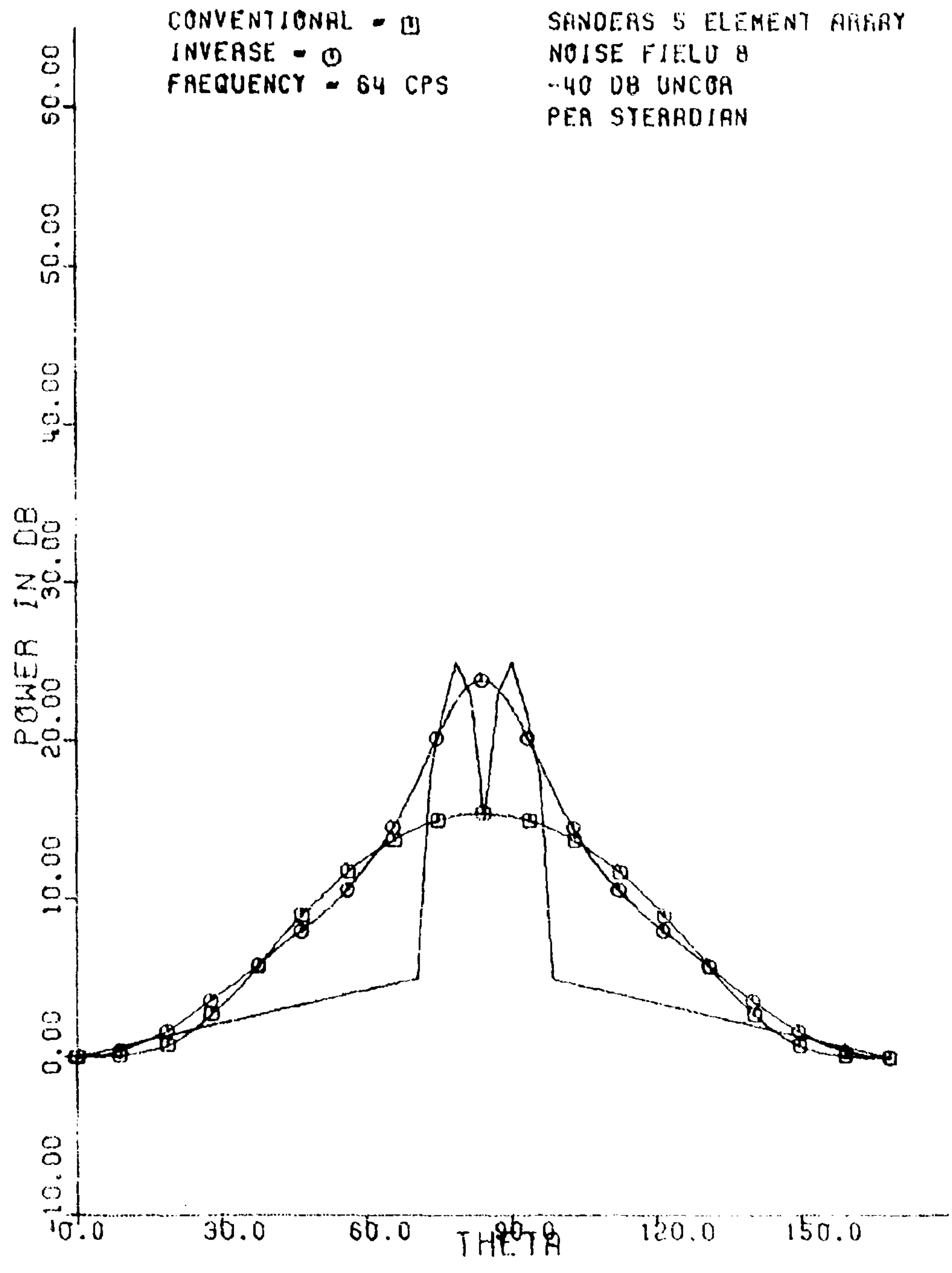

(U) Figure B52. BR noise field 8 64 cps.

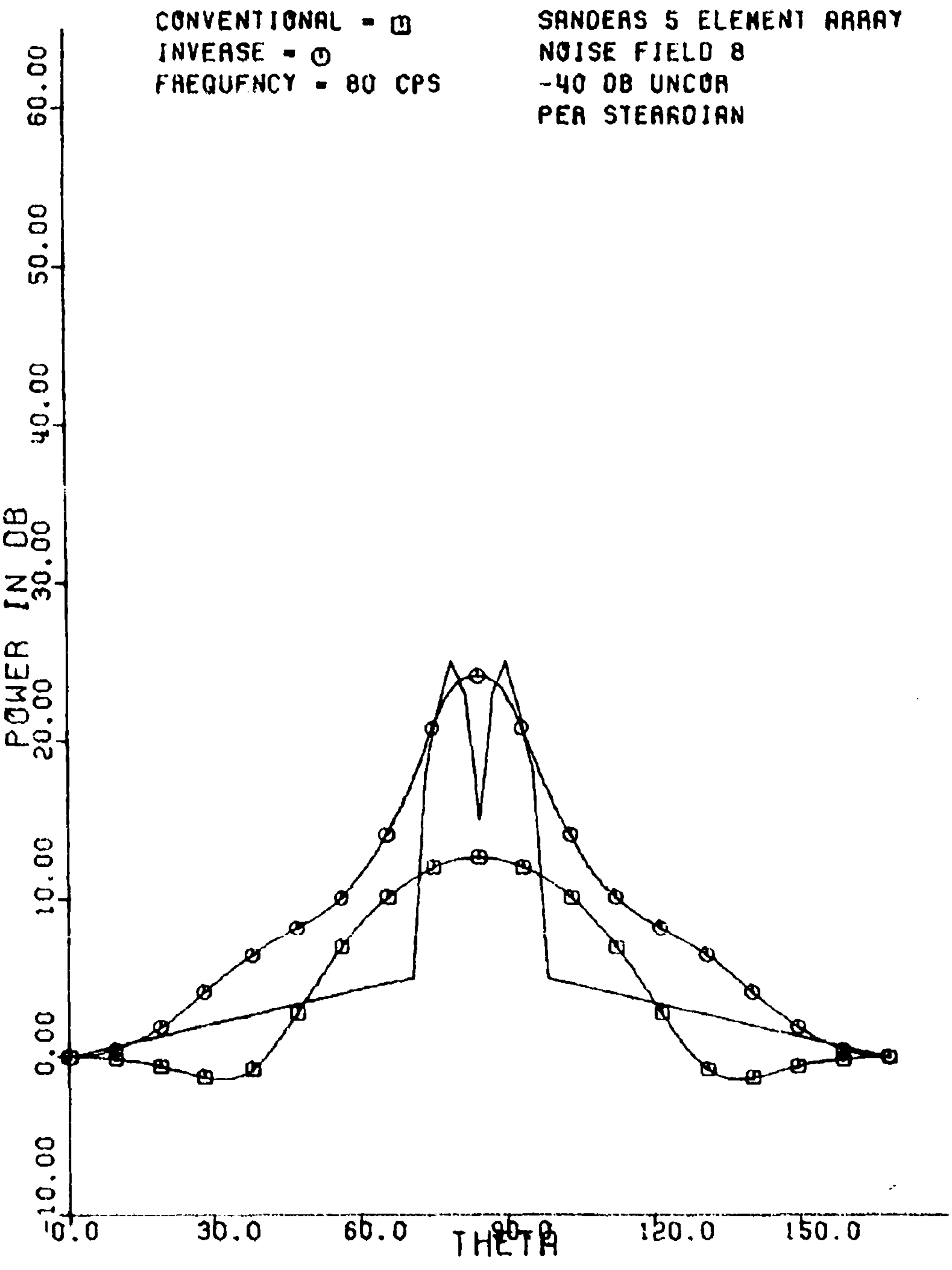

(U) Figure B53. BR – noise field 8 – 80 cps.

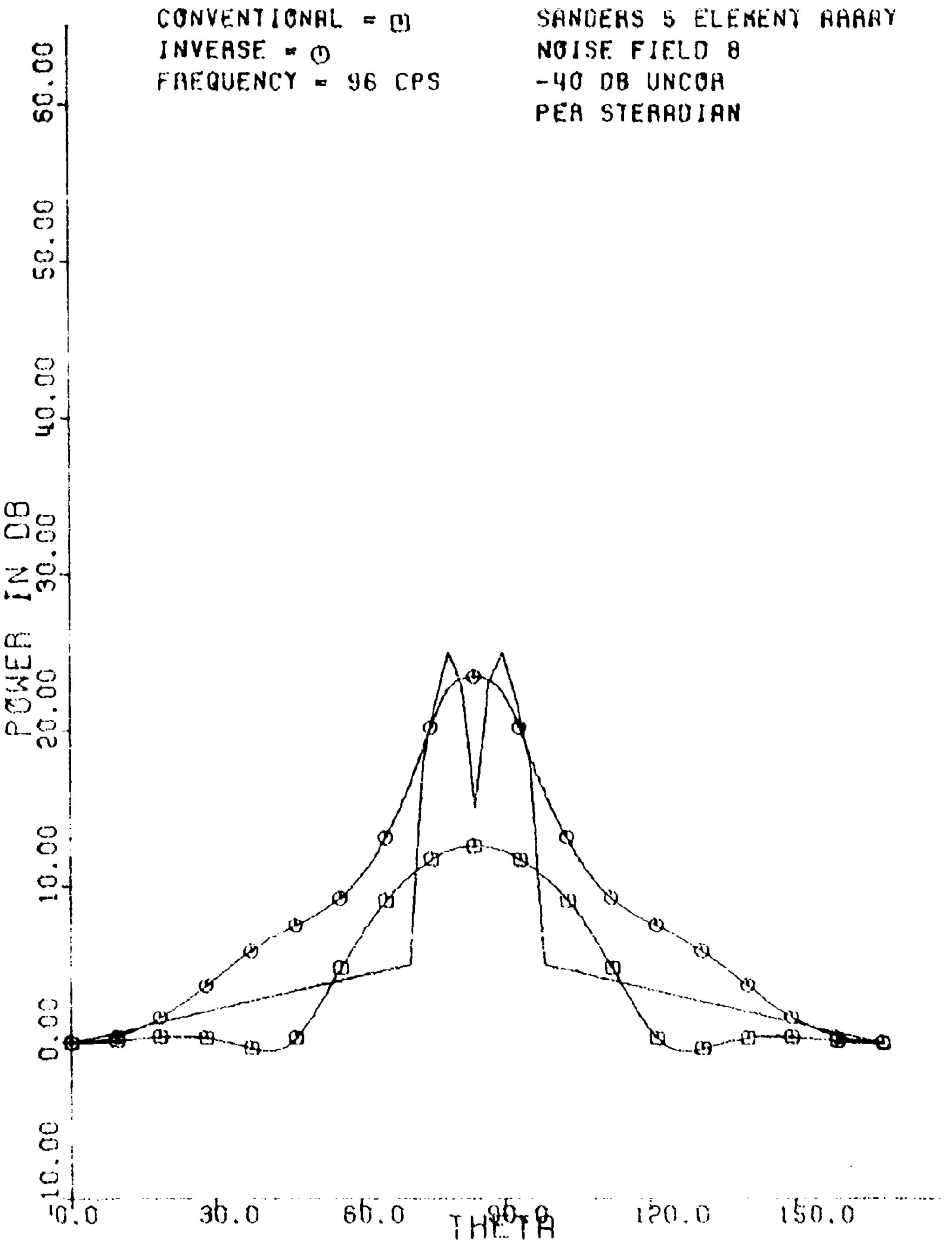

(U) Figure B54. BR noise field 8 96 cps.

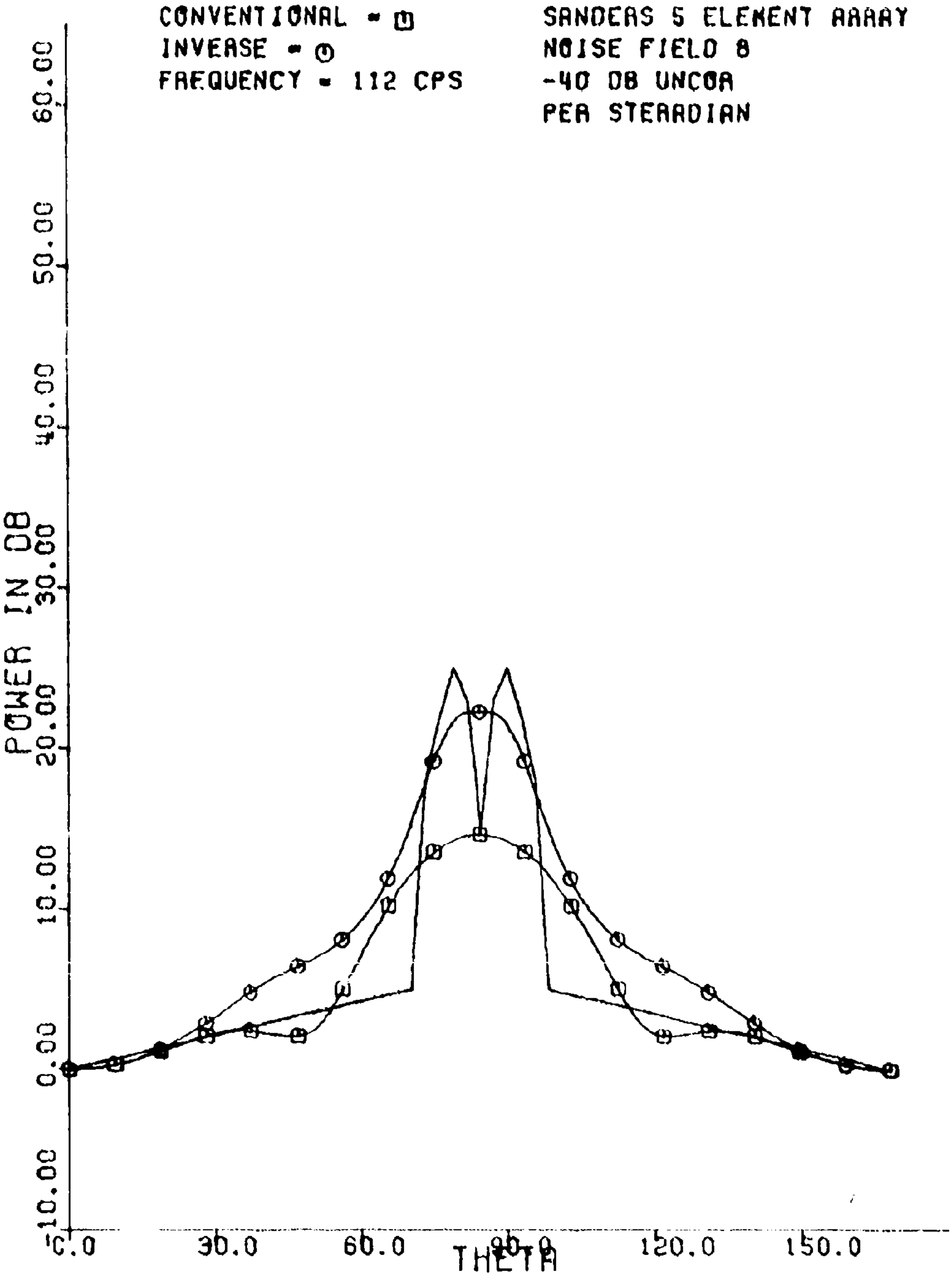

(U) Figure B55. BR noise field 8 112 cps.

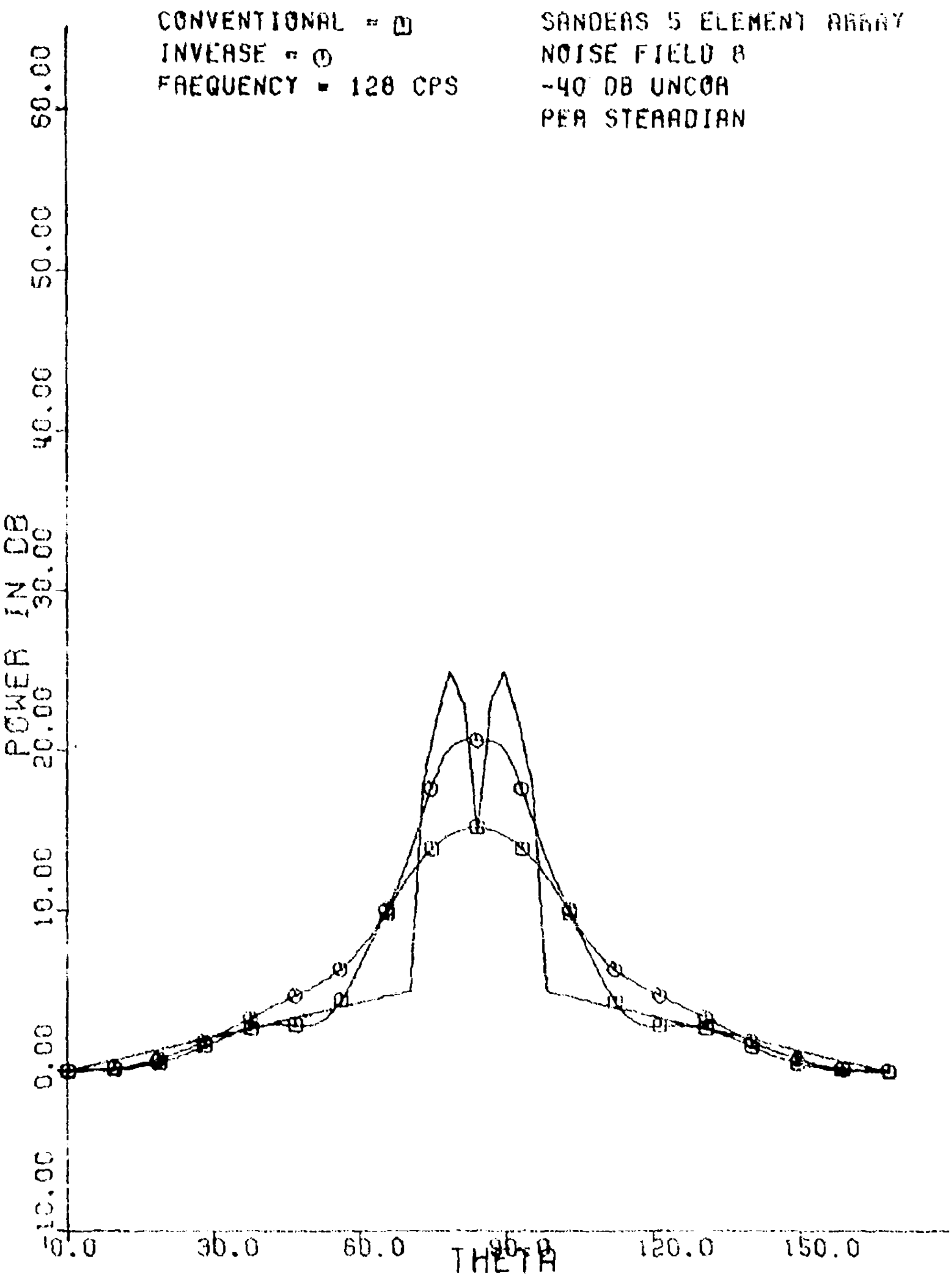

(U) Figure B56. BR noise field 8 128 cps

UNCLASSIFIED

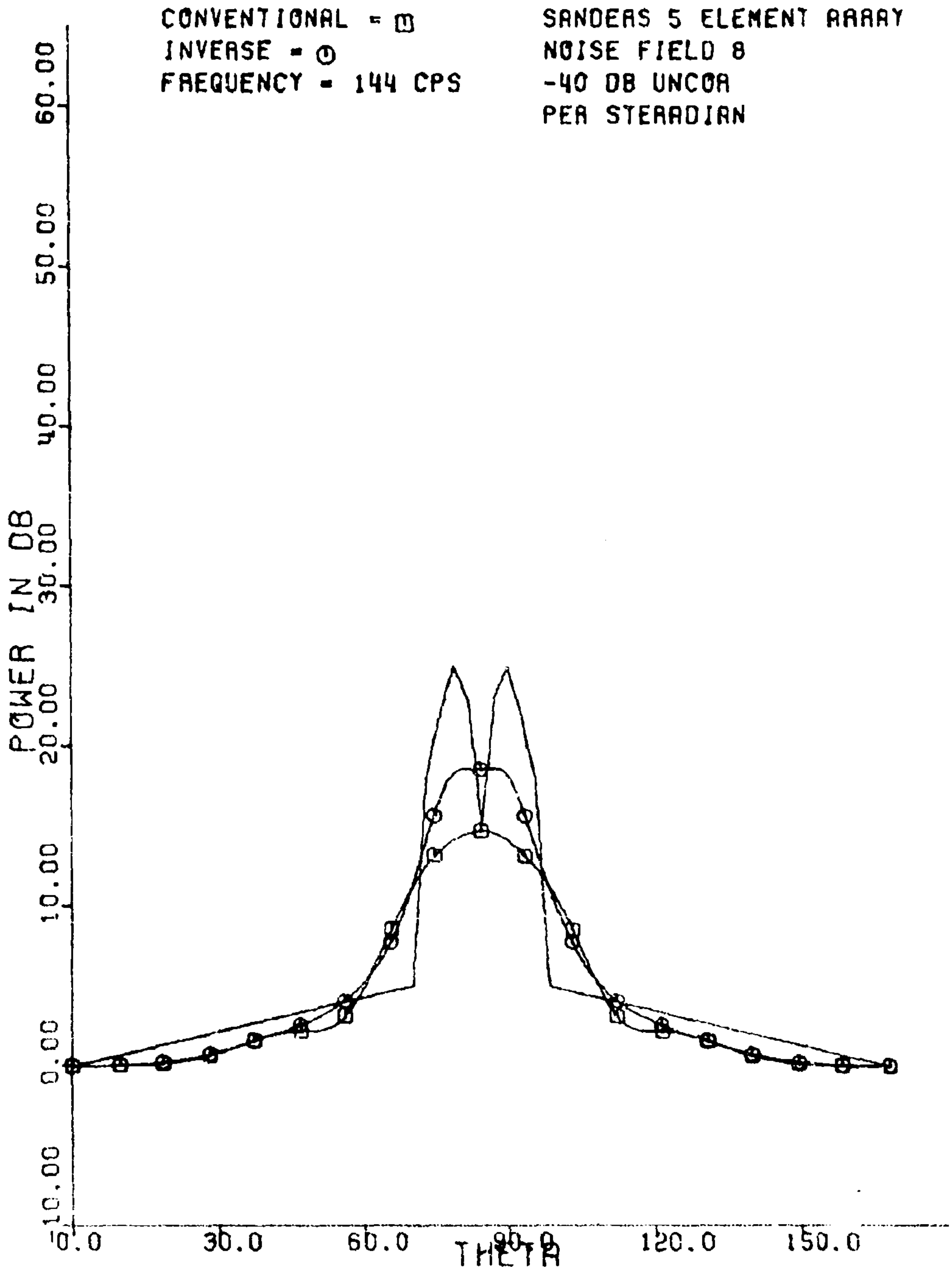

(U) Figure B57. BR noise field 8 144 cps.

UNCLASSIFIED

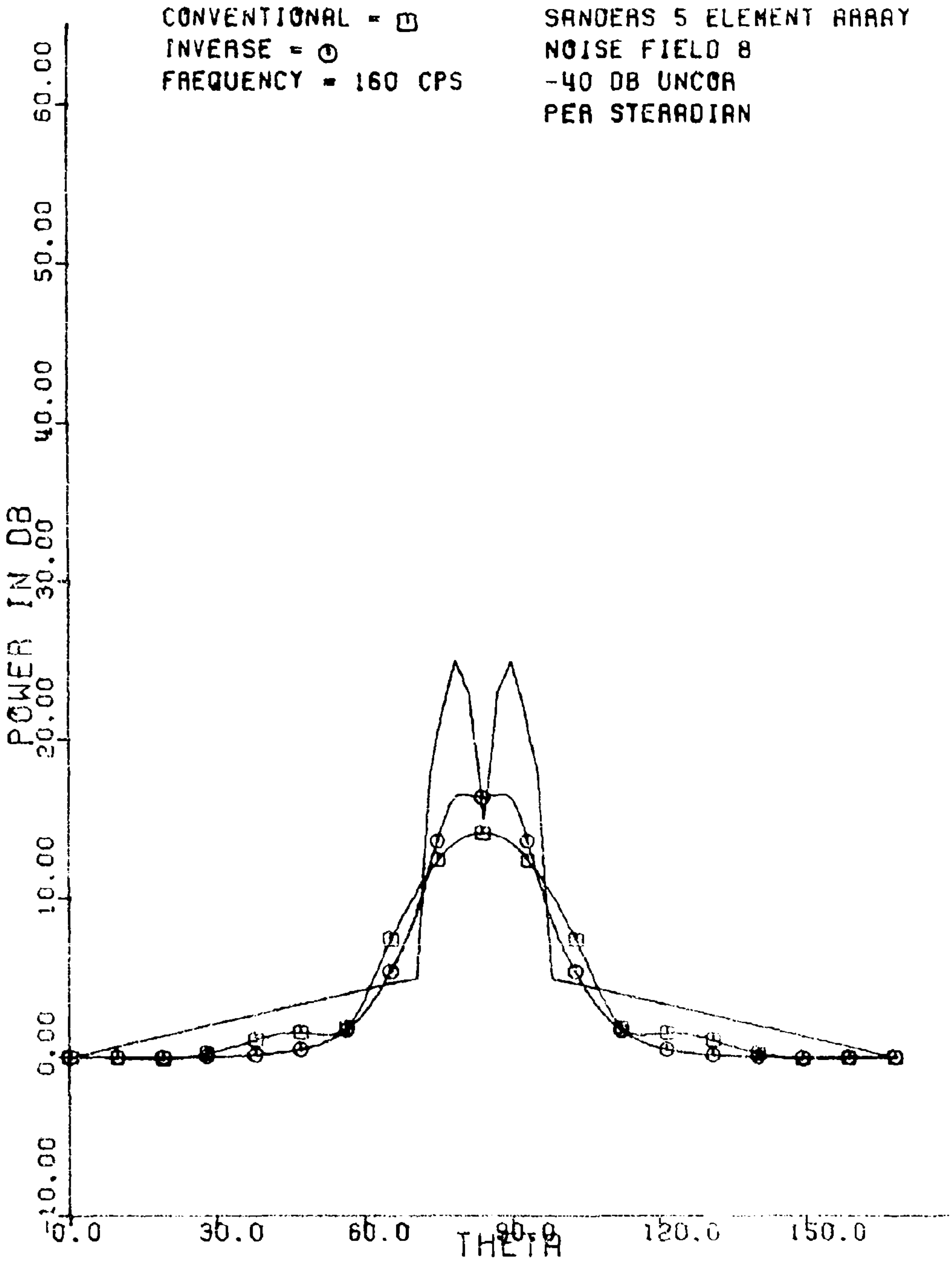

(U) Figure B58. BR noise field 8 160 cps.

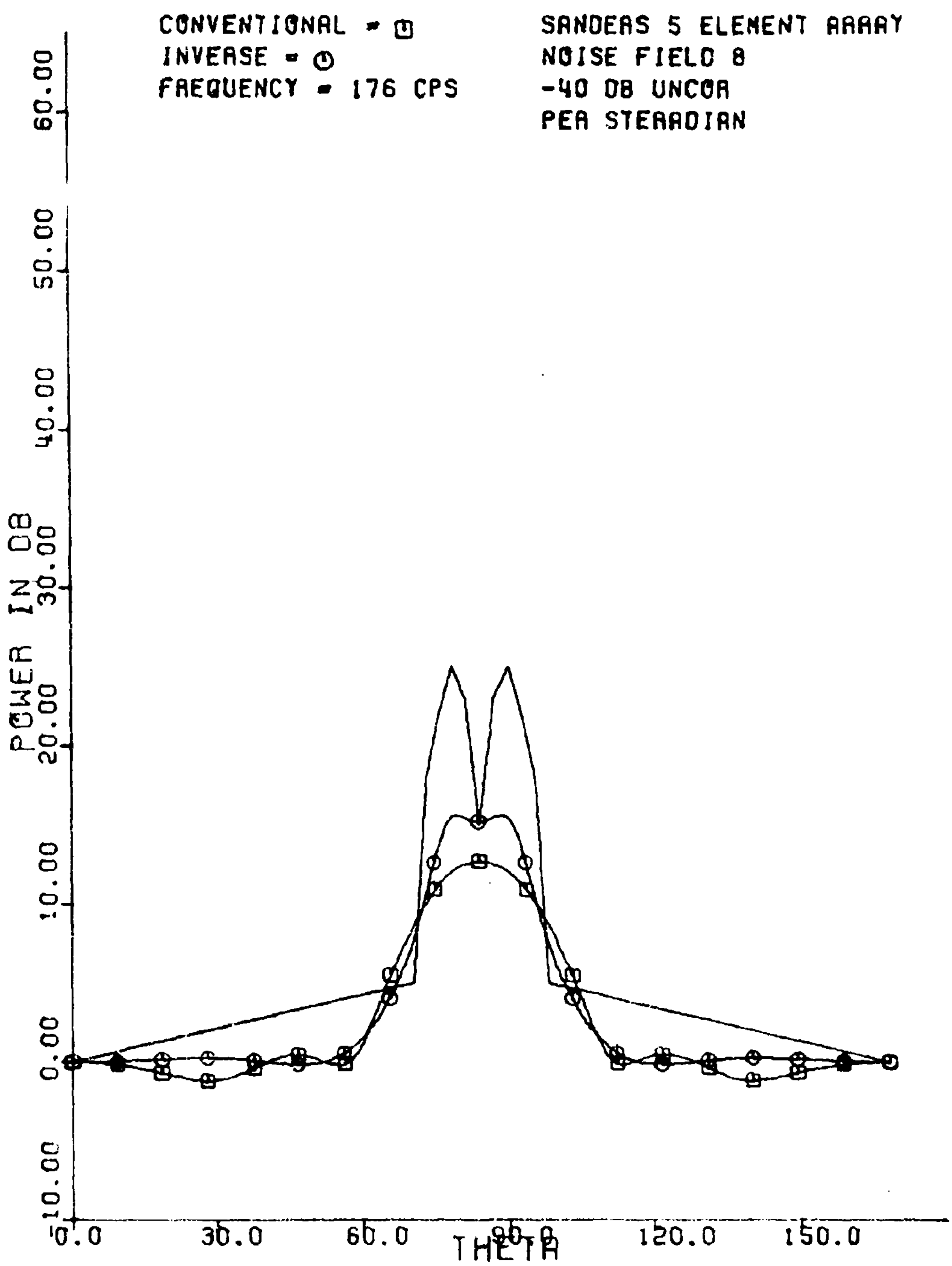

(U) Figure B59. BR noise field 8 176 cps.

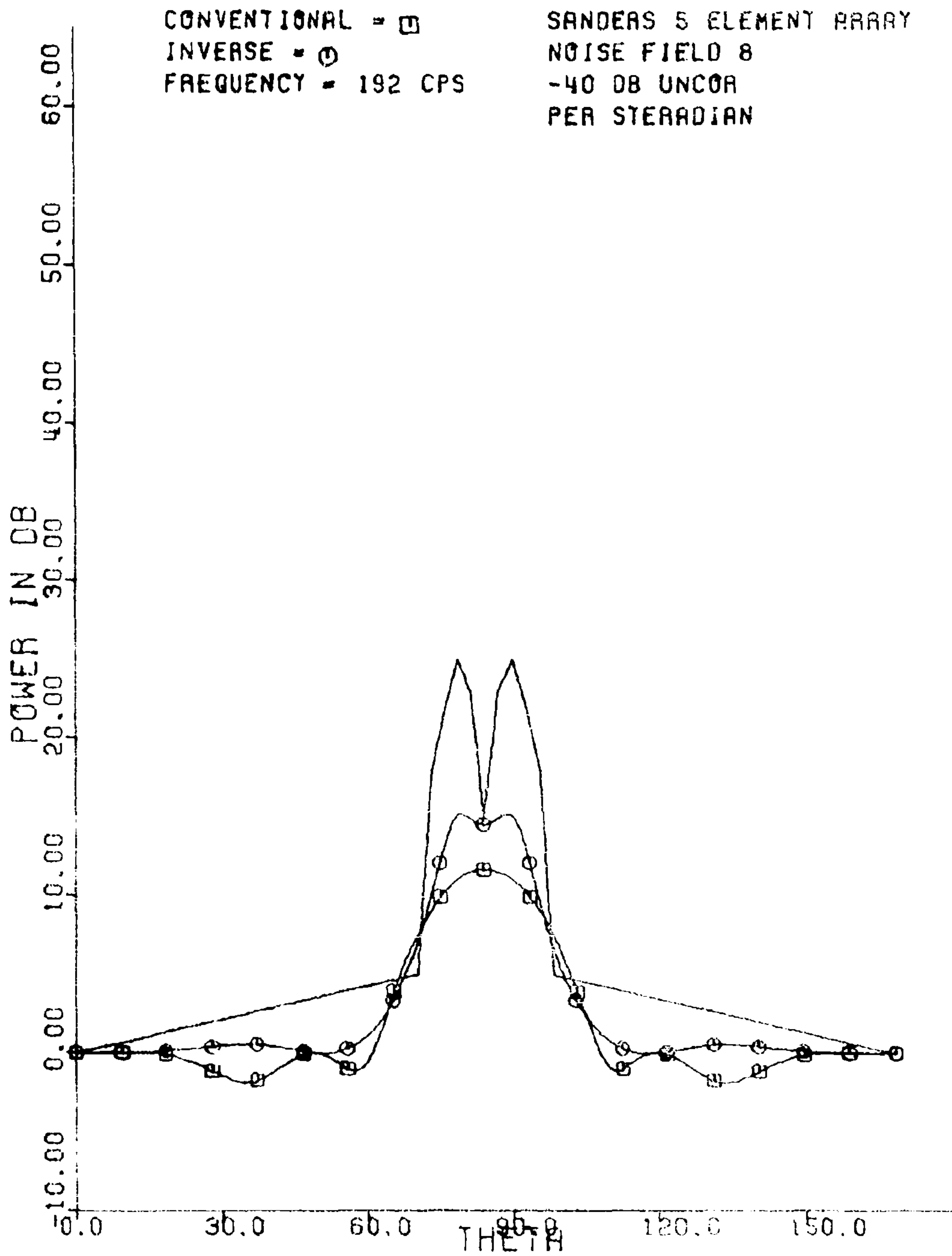

(U) Figure B60. BR noise field 8 192 cps

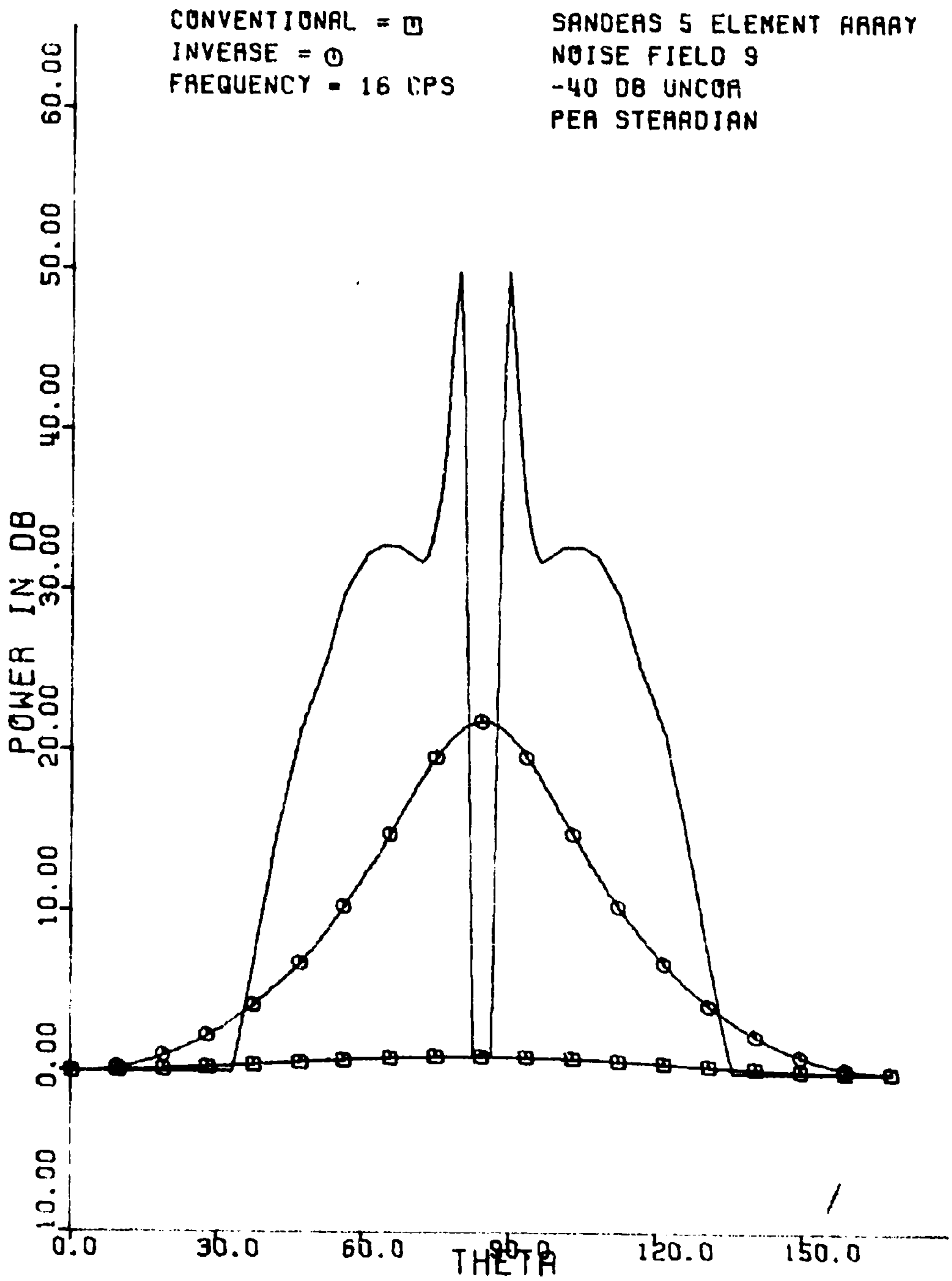

(U) Figure B61. BR - noise field 9 16 cps.

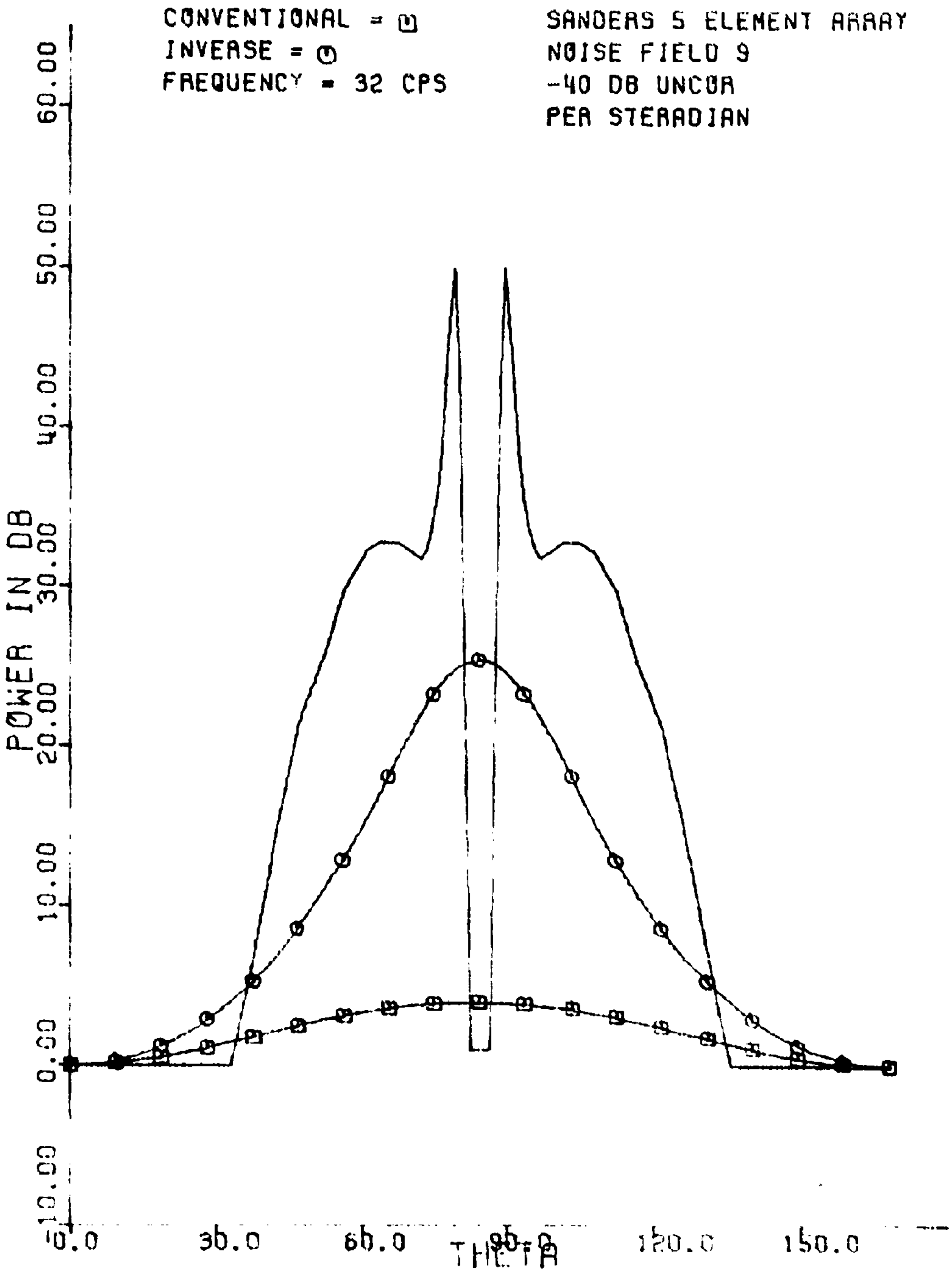

(U) Figure B62. BR noise field 9 32 cps.

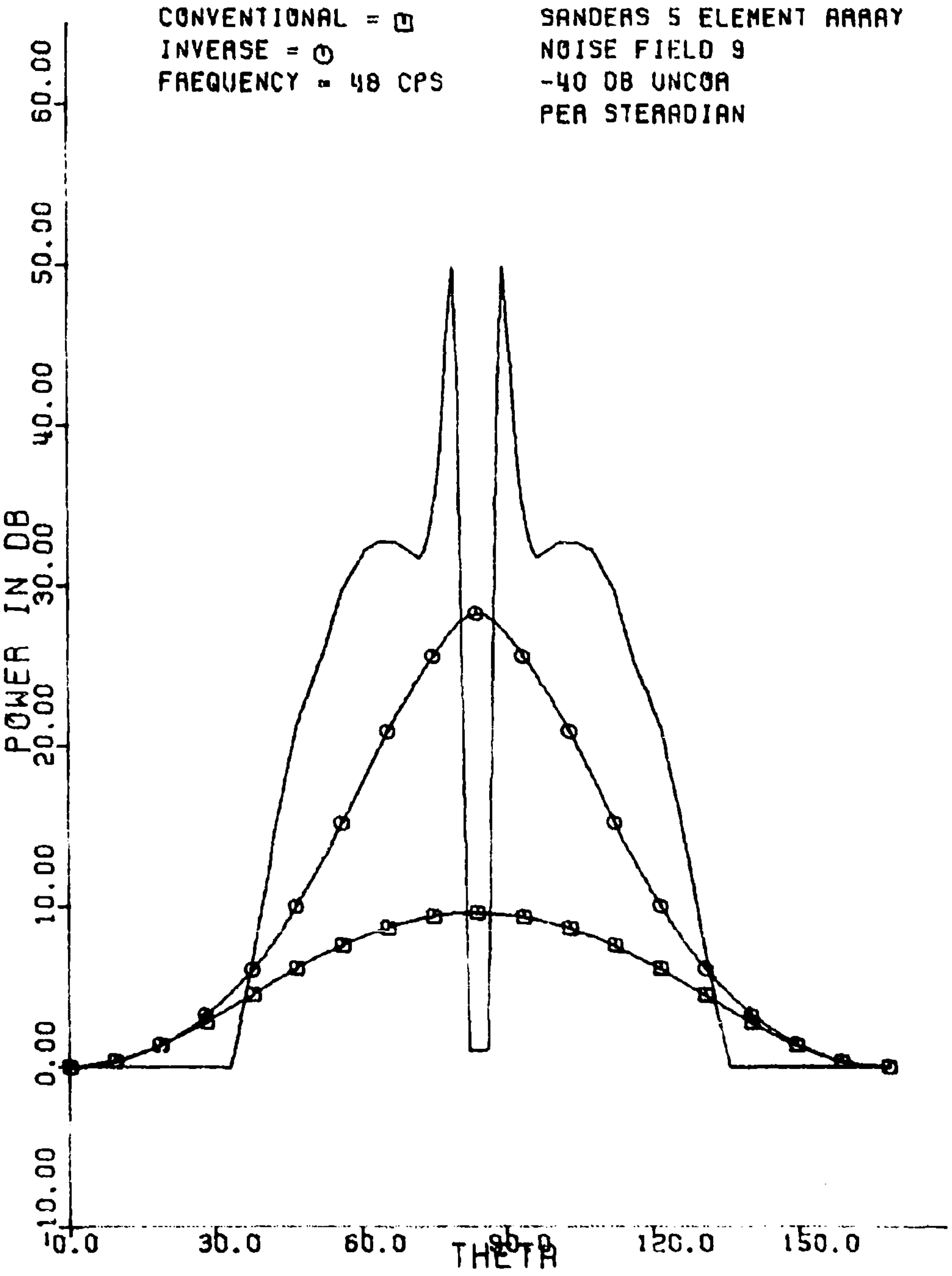

(U) Figure B63. BR noise field 9 48 cps.

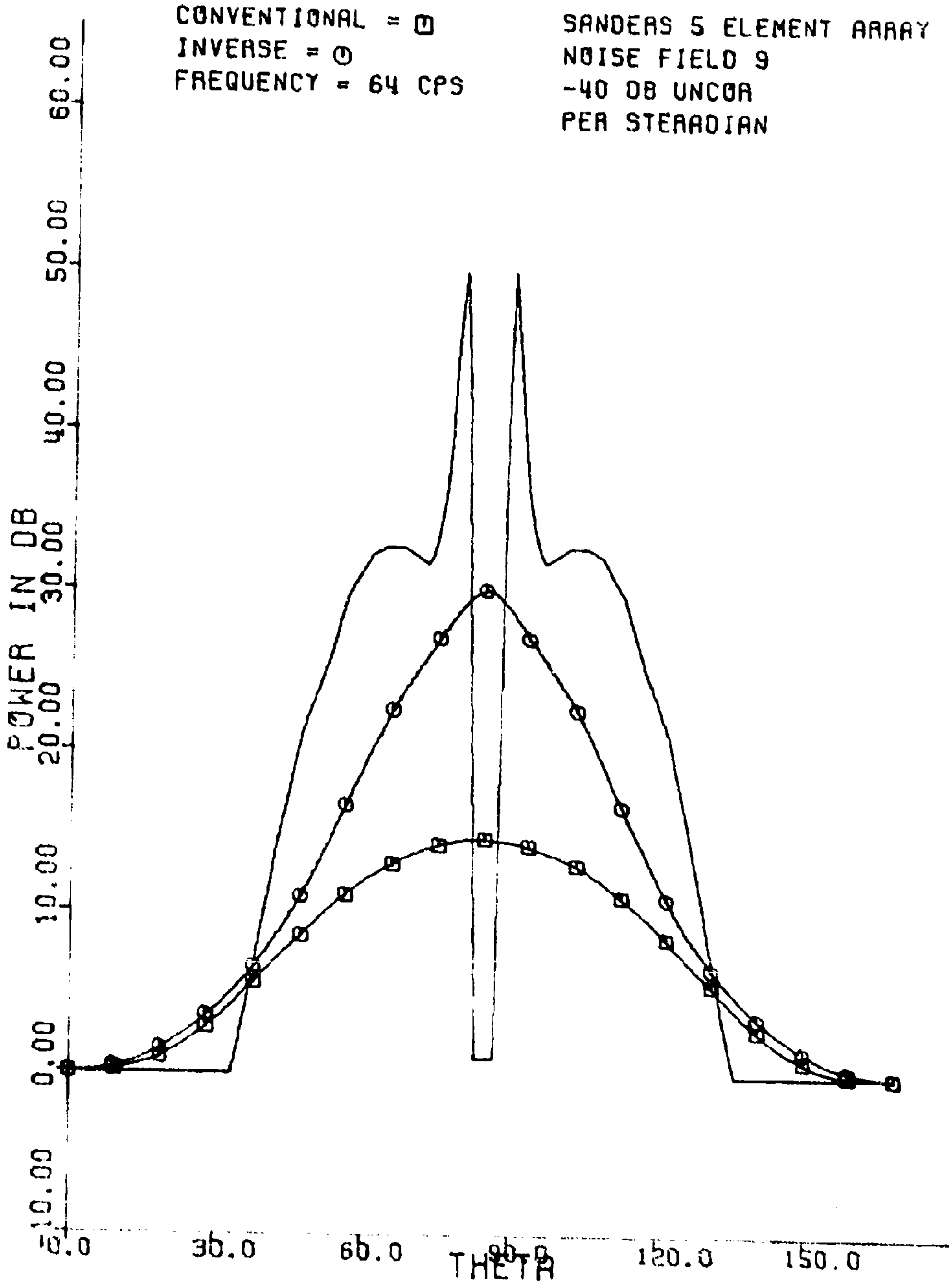

(U) Figure B64. BR noise field 9 64 cps.

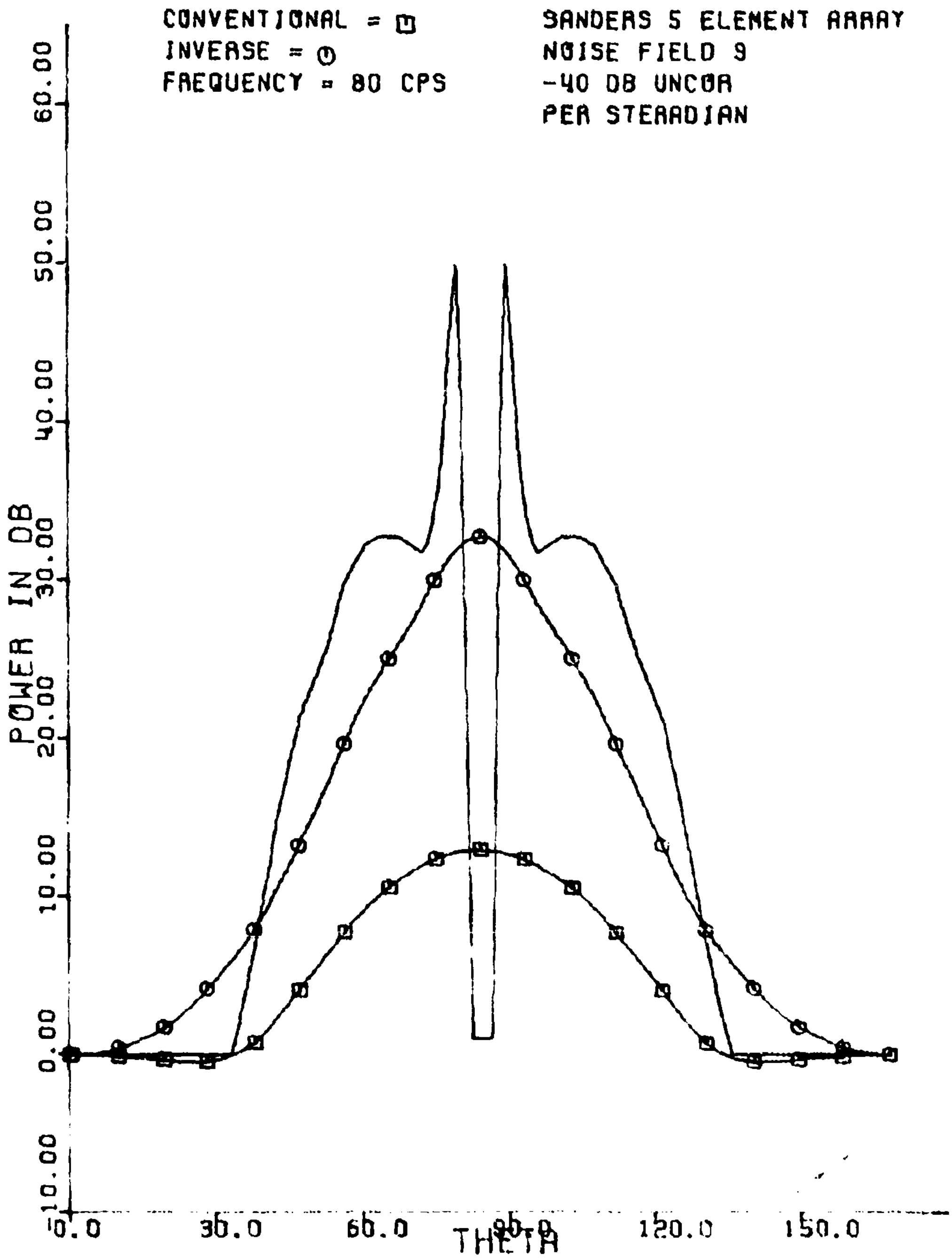

(U) Figure B65. BR noise field 9 80 cps.

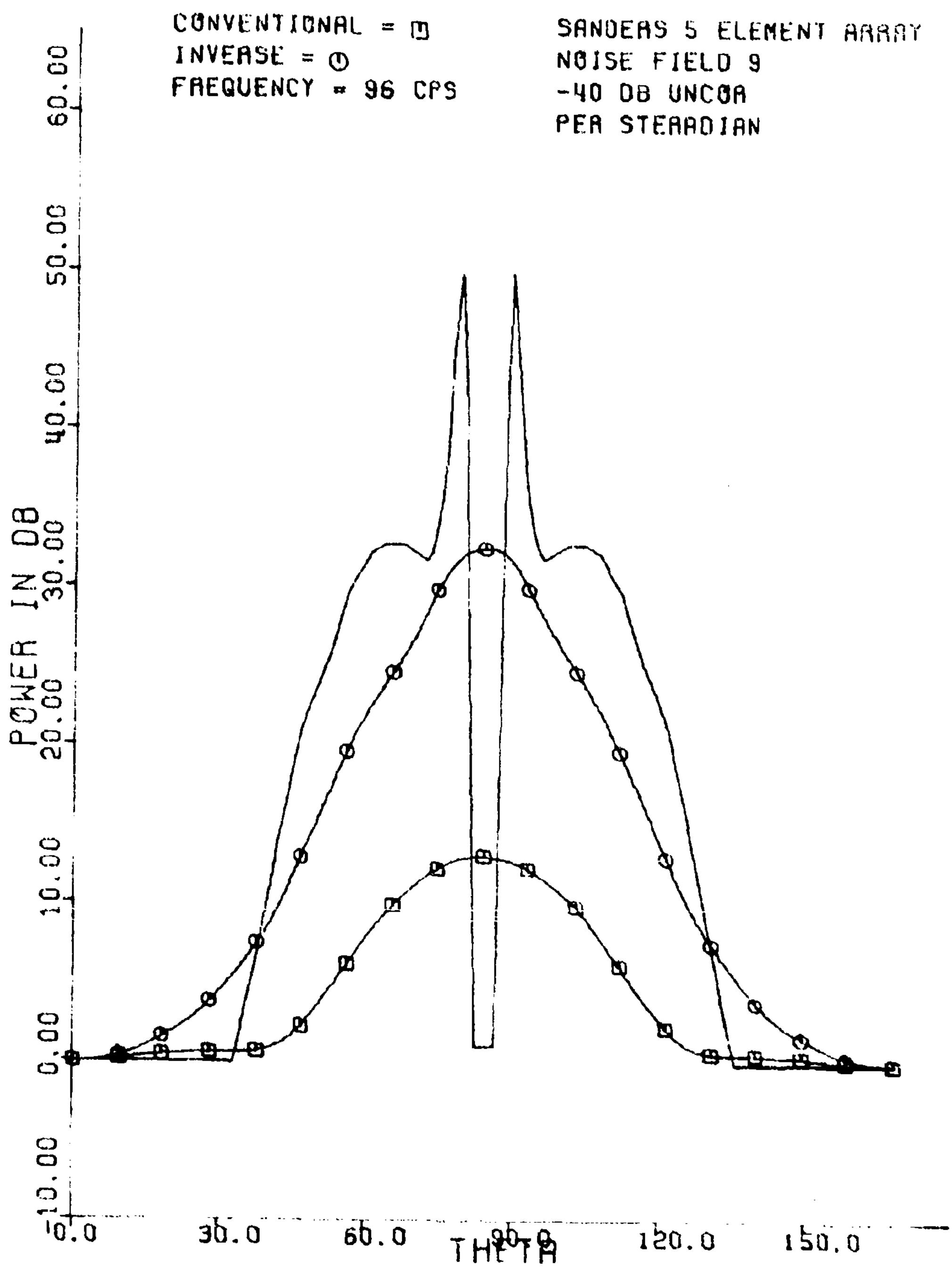

(U) Figure B66. BR noise field 9 96 cps.

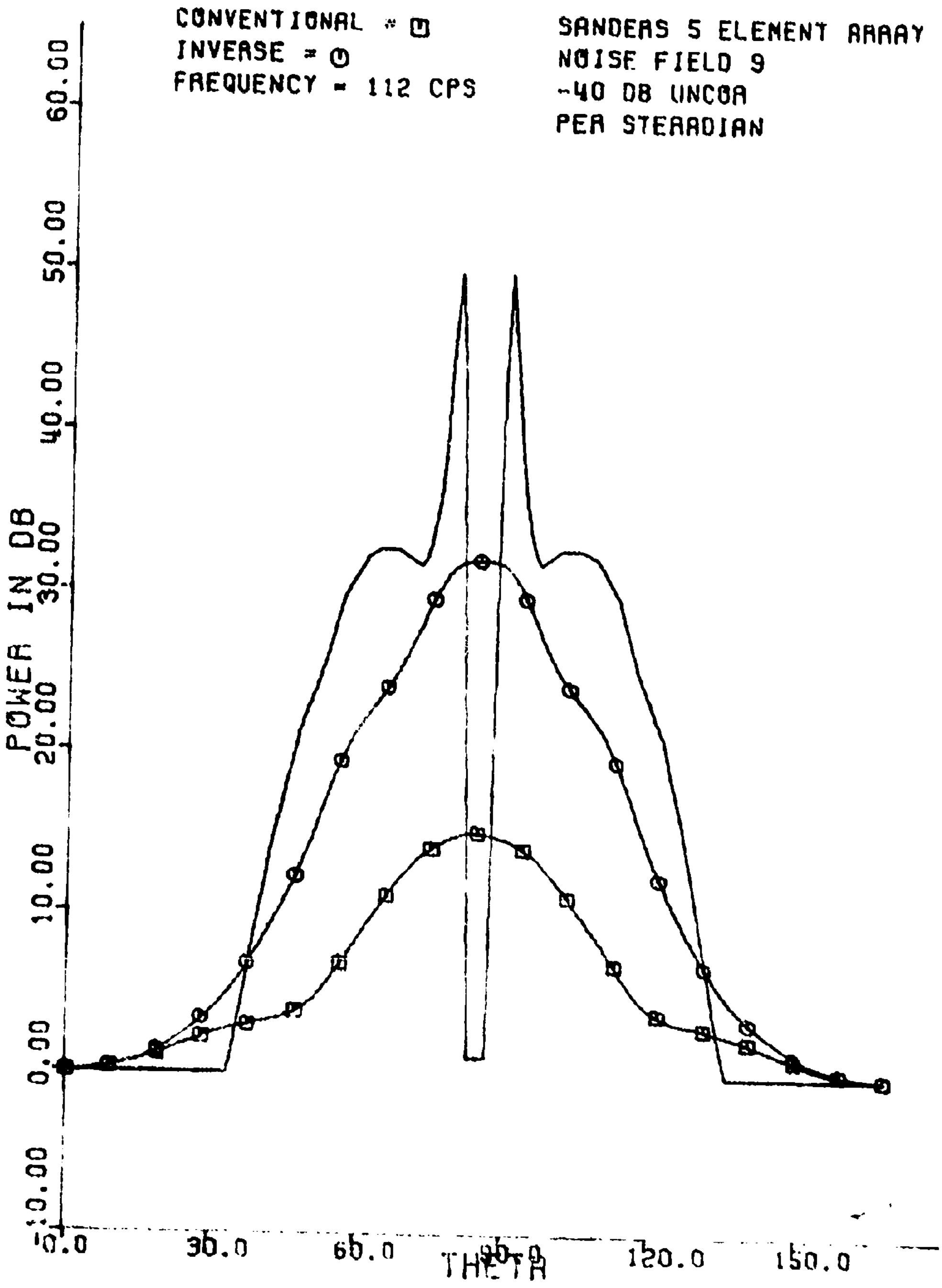

(U) Figure B67. BR noise field 9 – 112 cps.

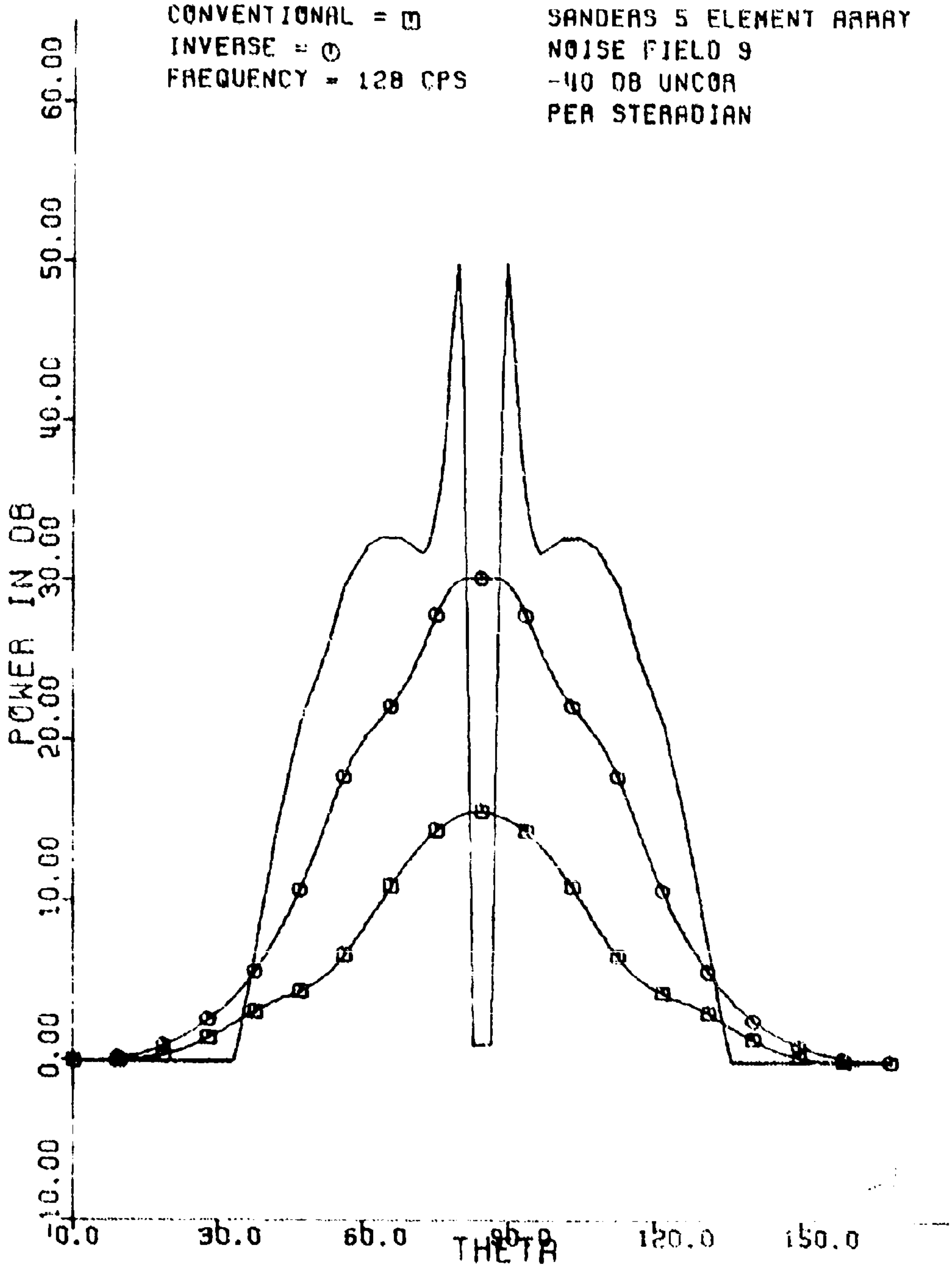

(U) Figure B68. BR noise field 9 128 cps

UNCLASSIFIED

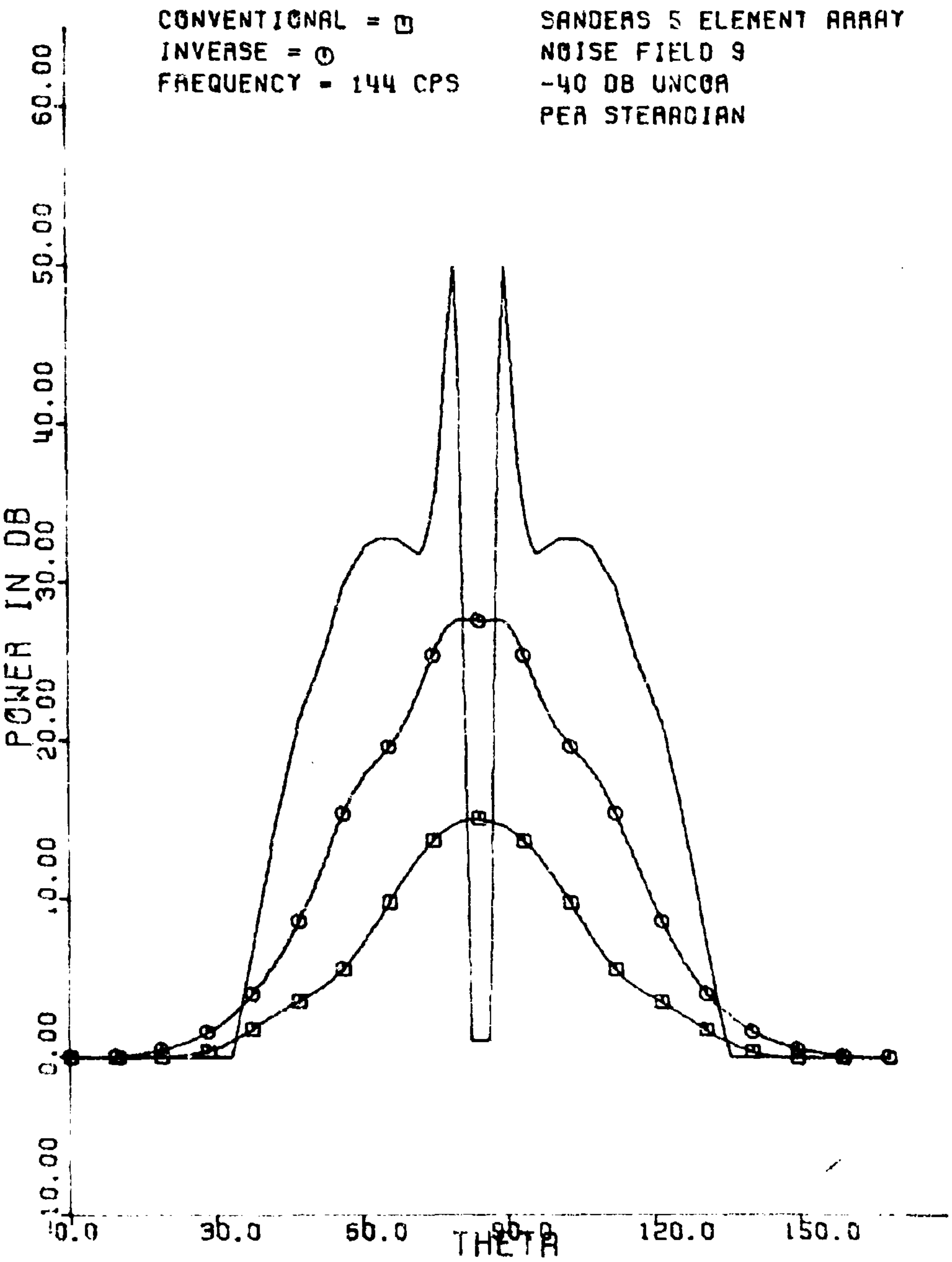

(U) Figure B69. BR noise field 9 144 cps.

UNCLASSIFIED

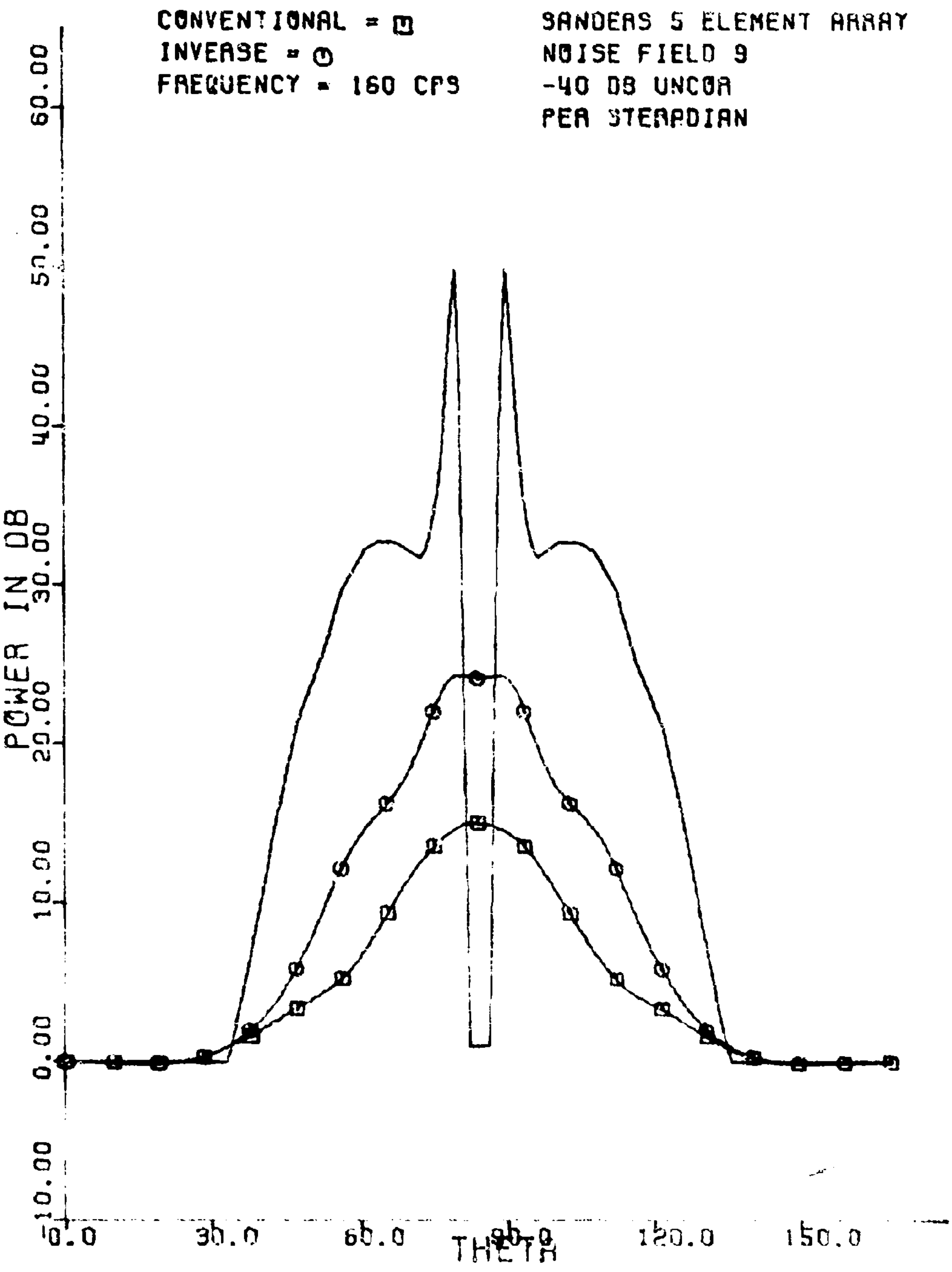

(U) Figure B70. BR noise field 9 160 cps.

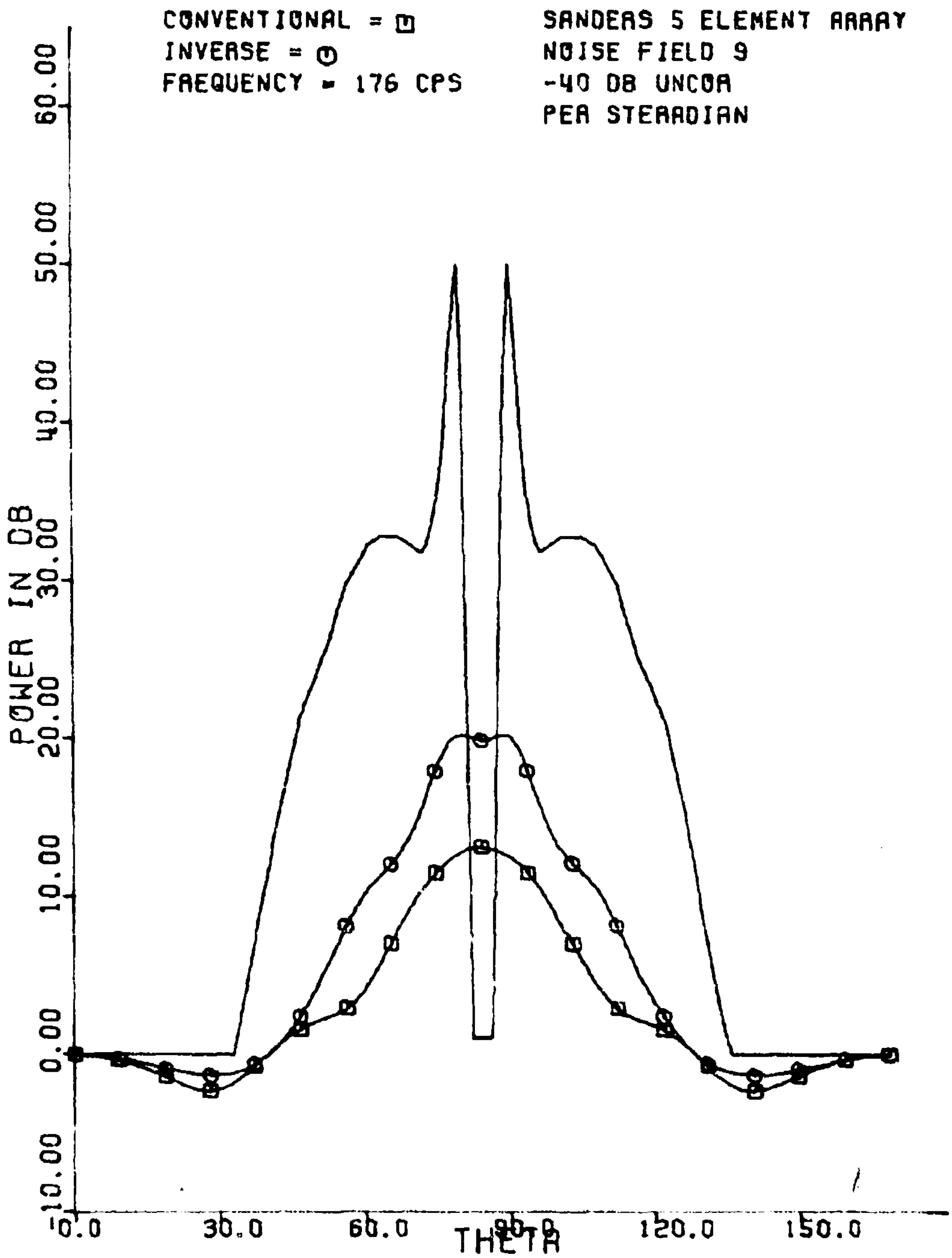

(U) Figure B71. BR — noise field 9 — 176 cps.

UNCLASSIFIED

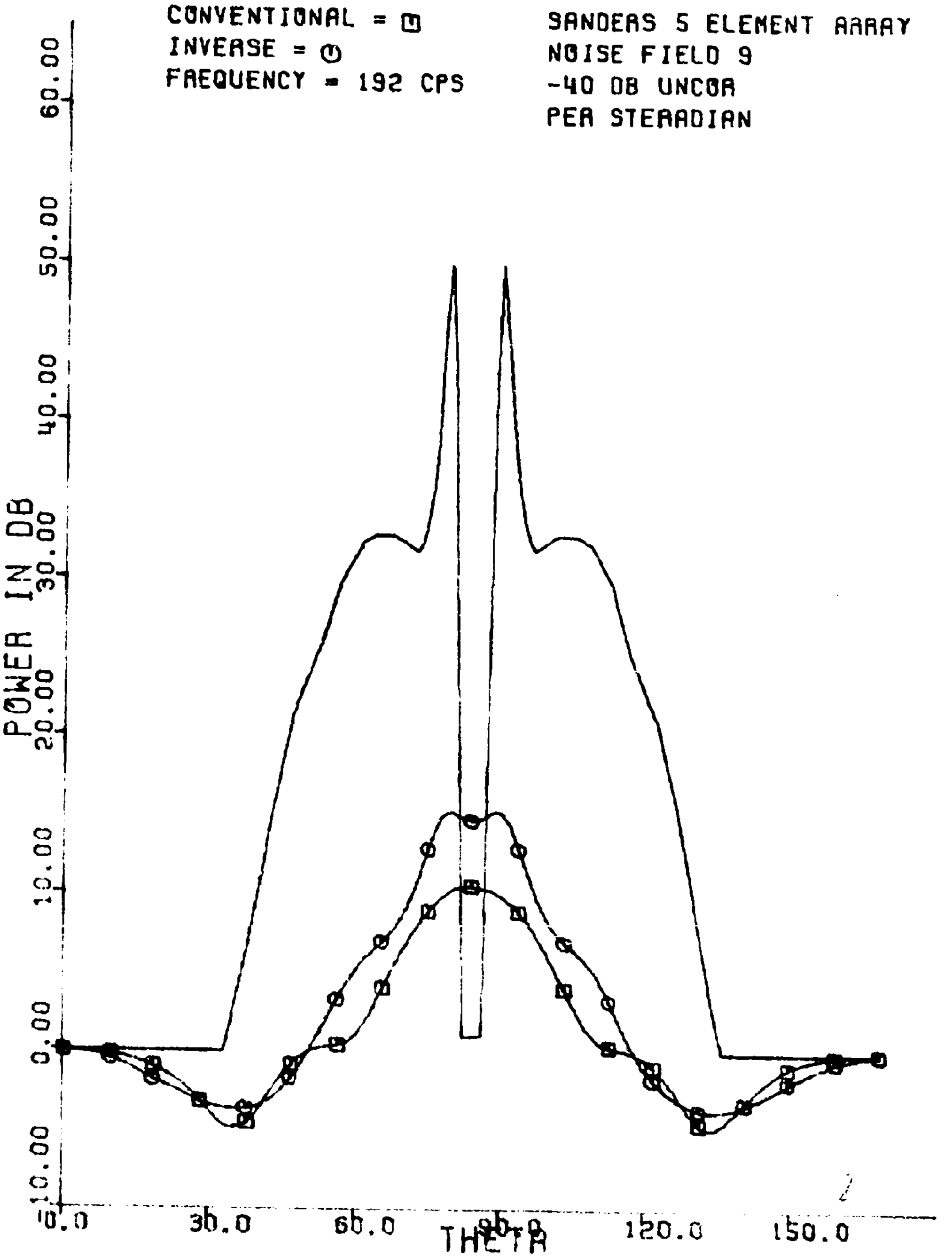

(U) Figure B72. BR noise field 9 192 cps.

UNCLASSIFIED

APPENDIX C

ARRAY GAIN FOR ACTUAL DATA

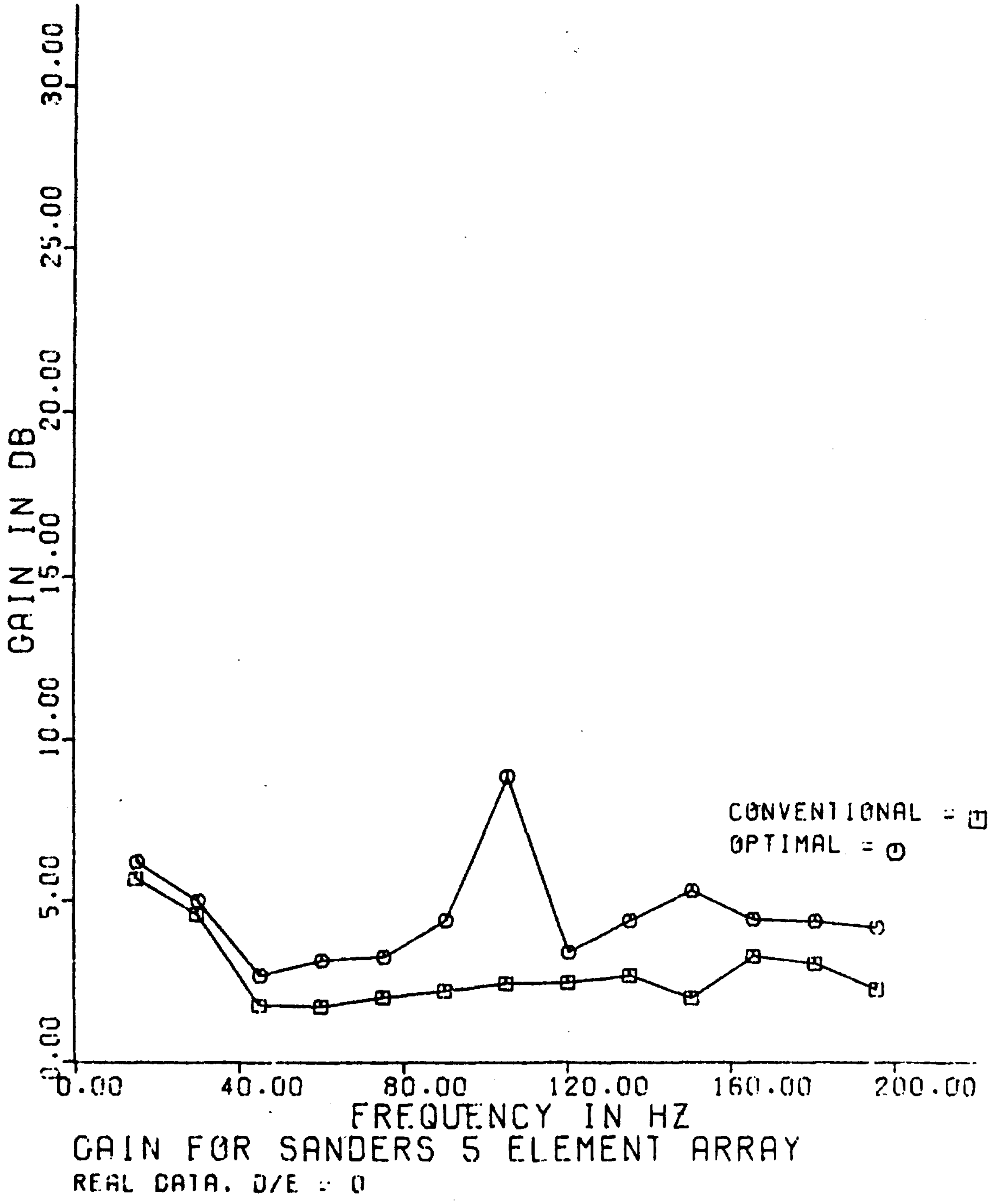

(C) **Figure C1. Array gain – actual data – D/E = 0. "Optimal" appears in figures C1-C7 and has the same meaning as "adaptive."**

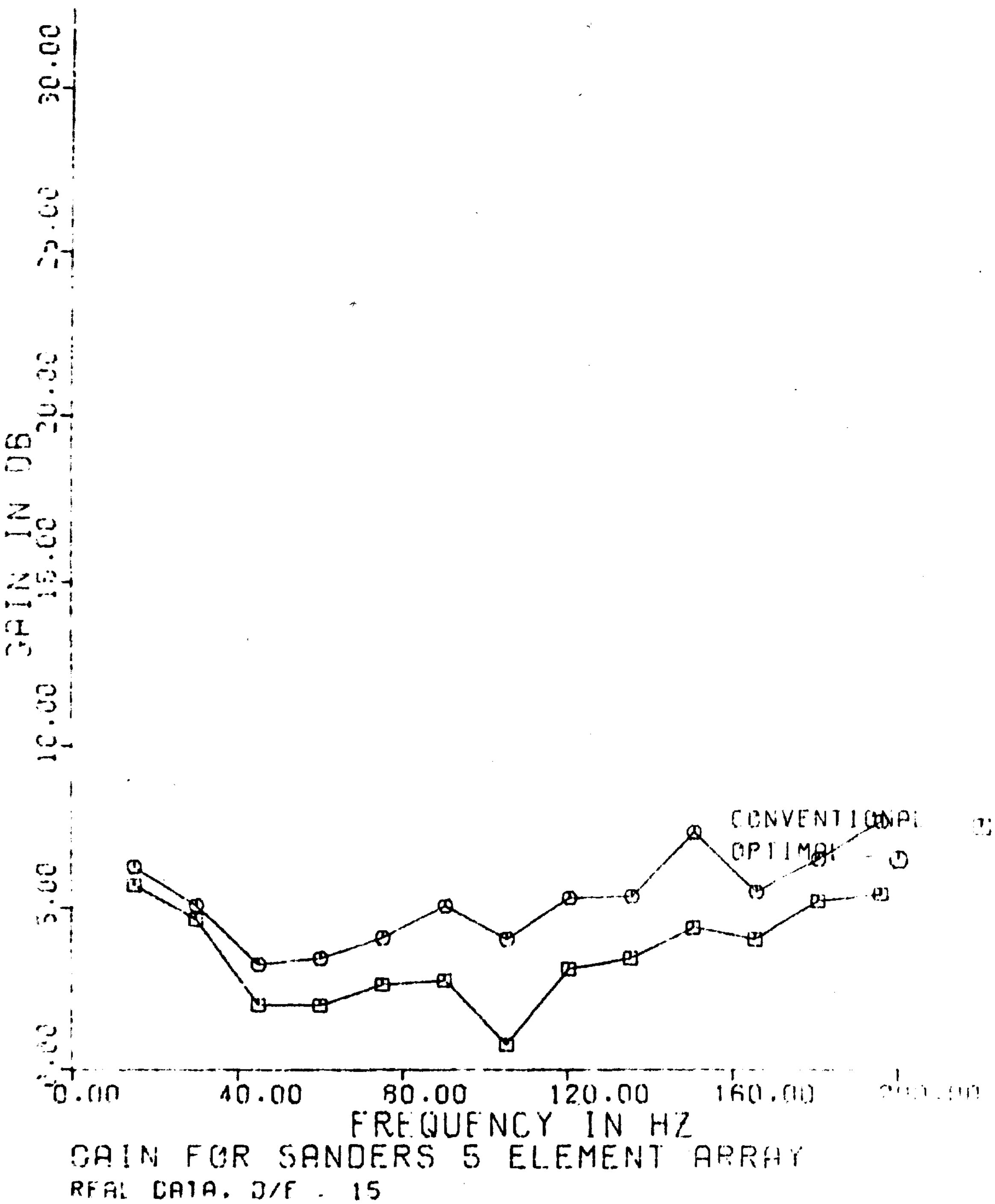

(C) Figure C2. Array gain -- actual data -- D/E = 15.

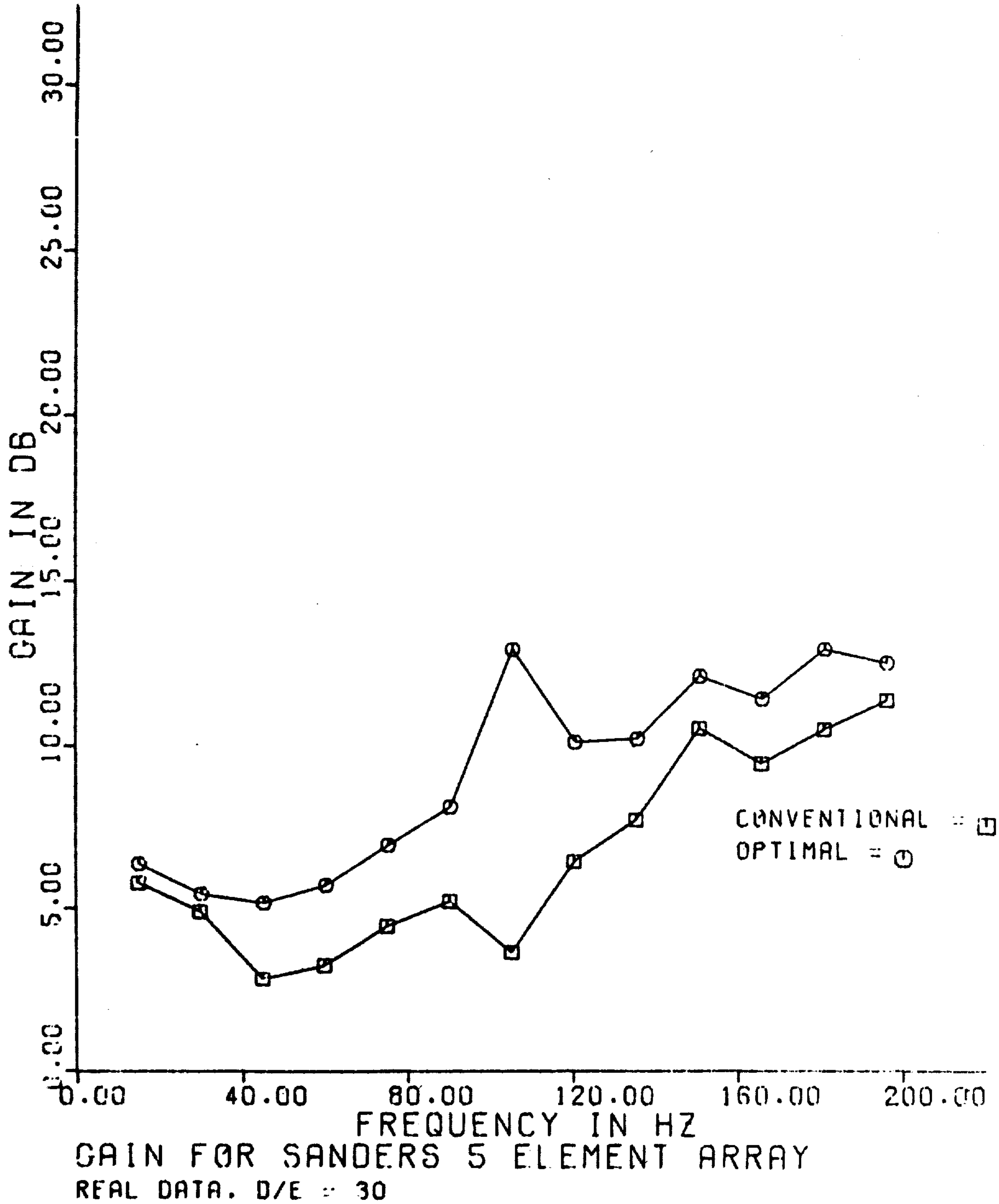

(C) Figure C3. Array gain – actual data – D/E = 30.

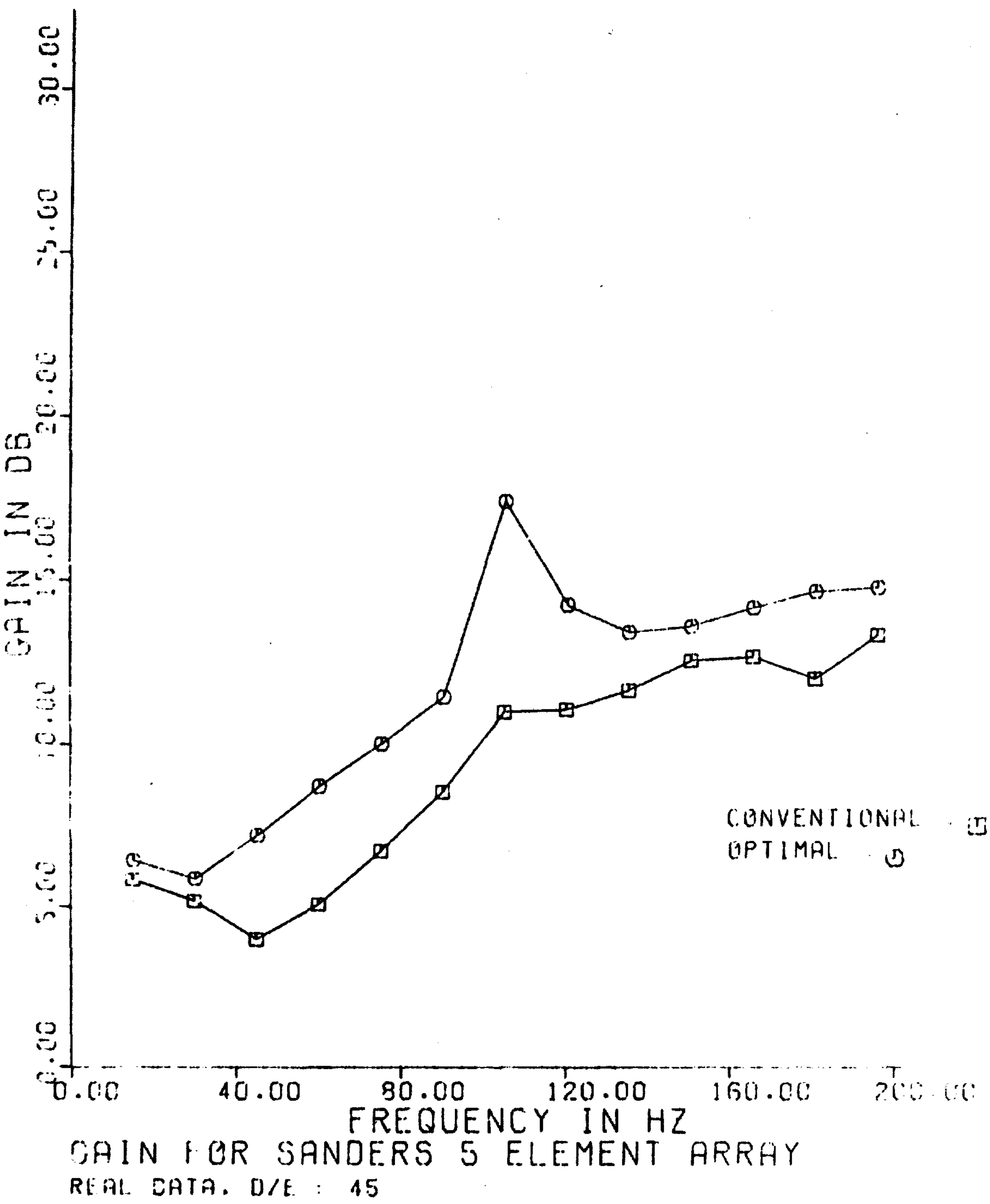

(C) **Figure C4. Array gain -- actual data -- D/E = 45.**

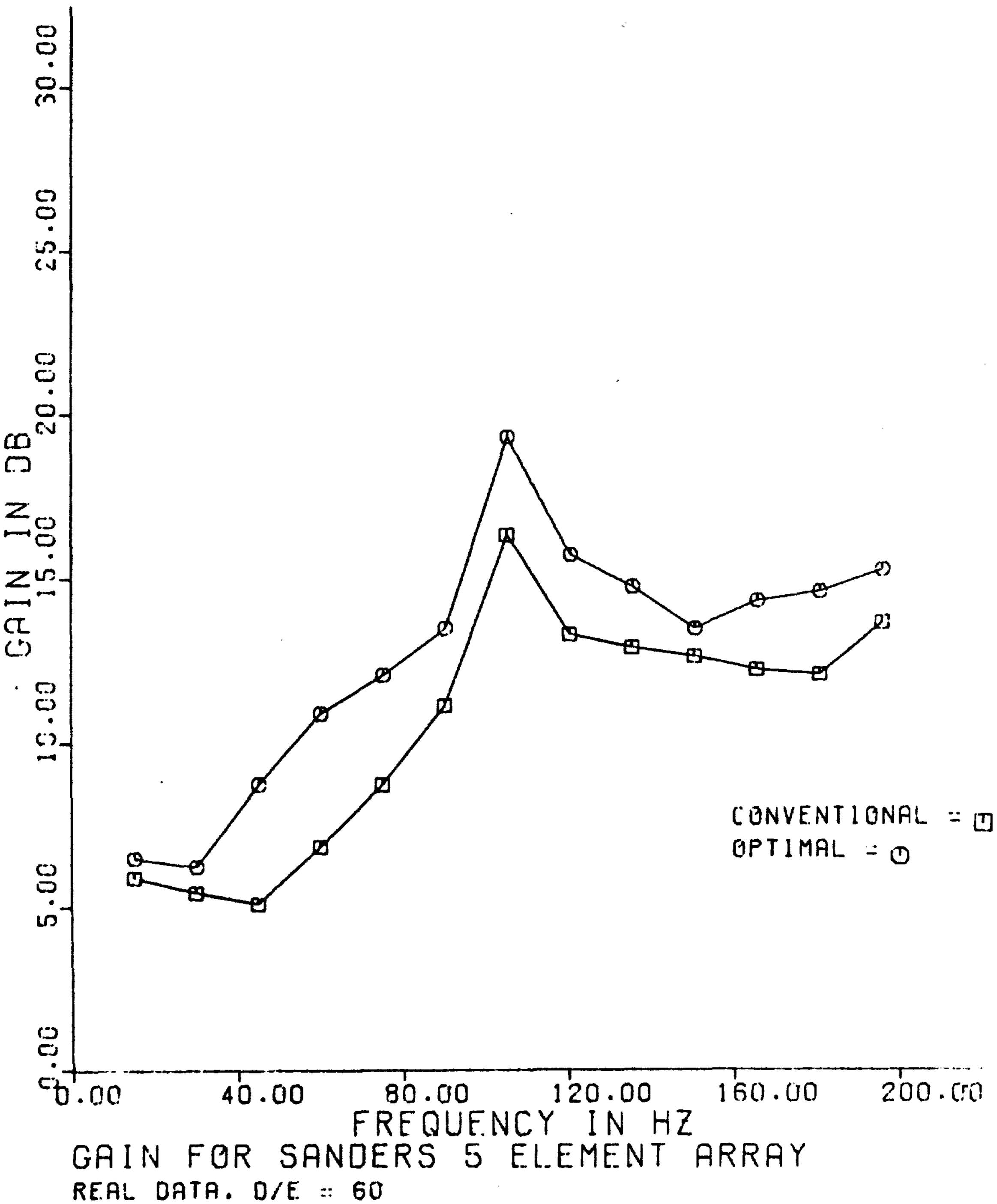

(C) Figure C5. Array gain – actual data – D/E = 60.

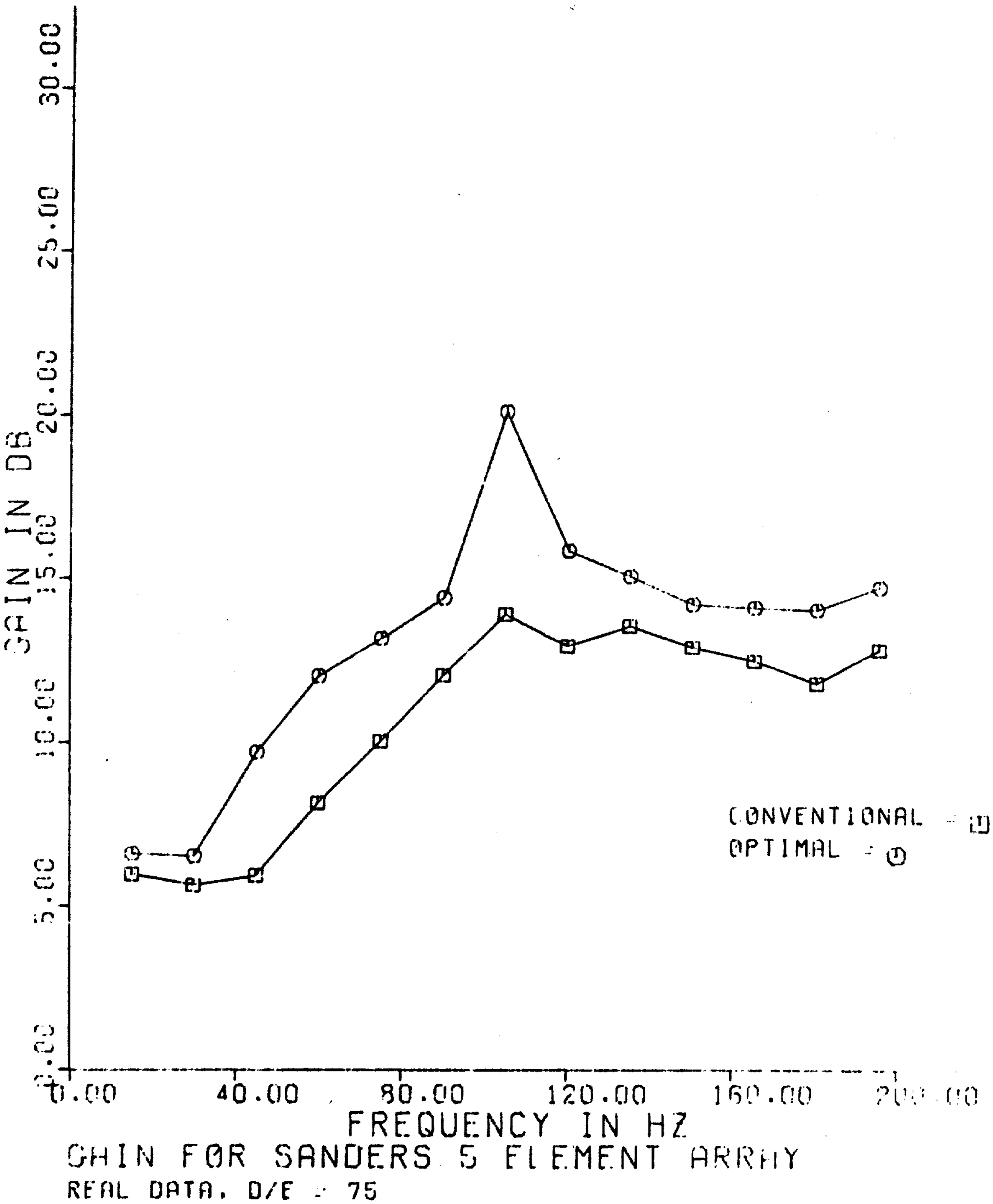

(C) Figure C6. Array gain -- actual data -- D/E = 75.

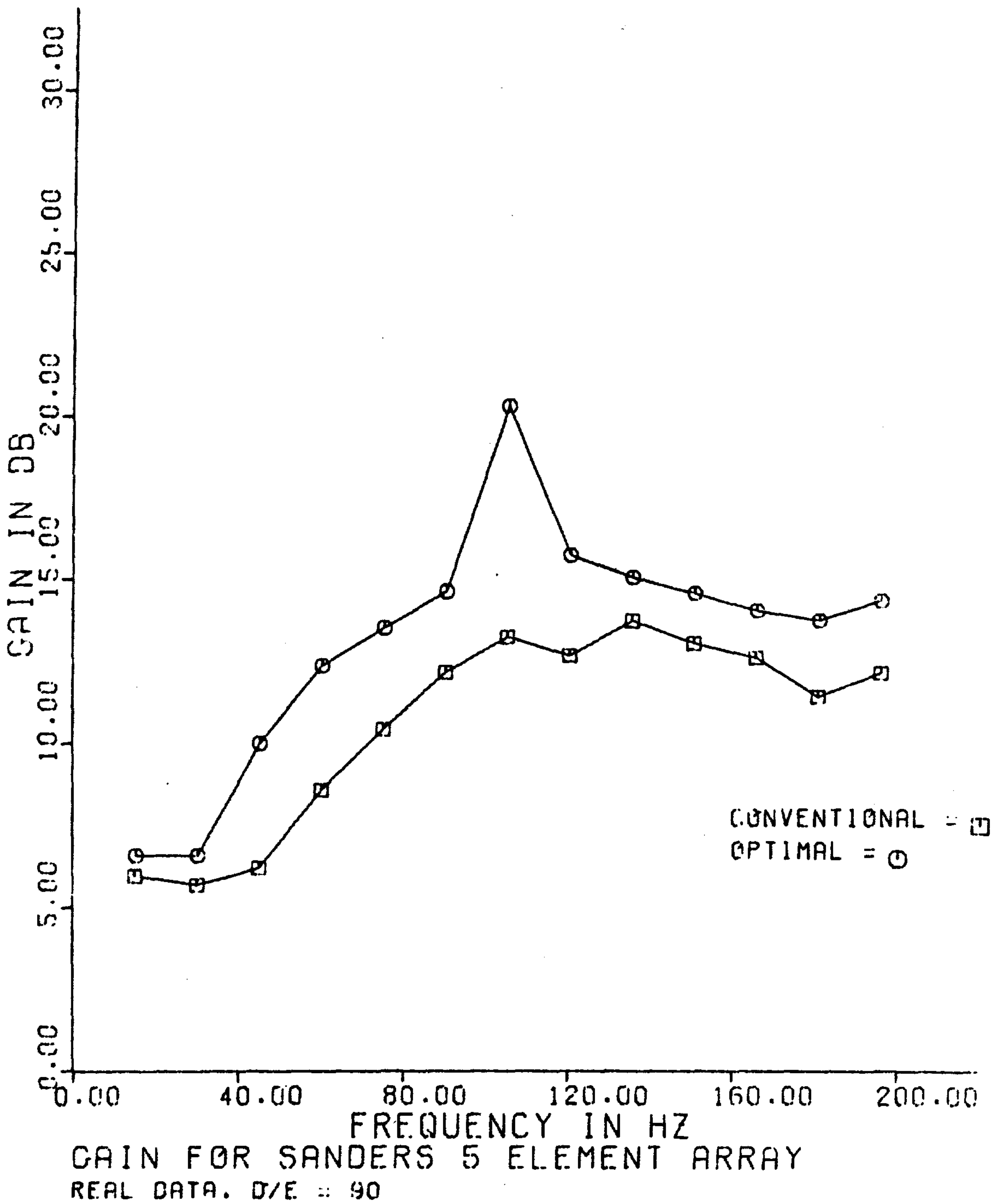

(C) Figure C7. Array gain - actual data – D/E = 90.

APPENDIX D

ARRAY GAINS FOR SIMULATED NOISE FIELDS

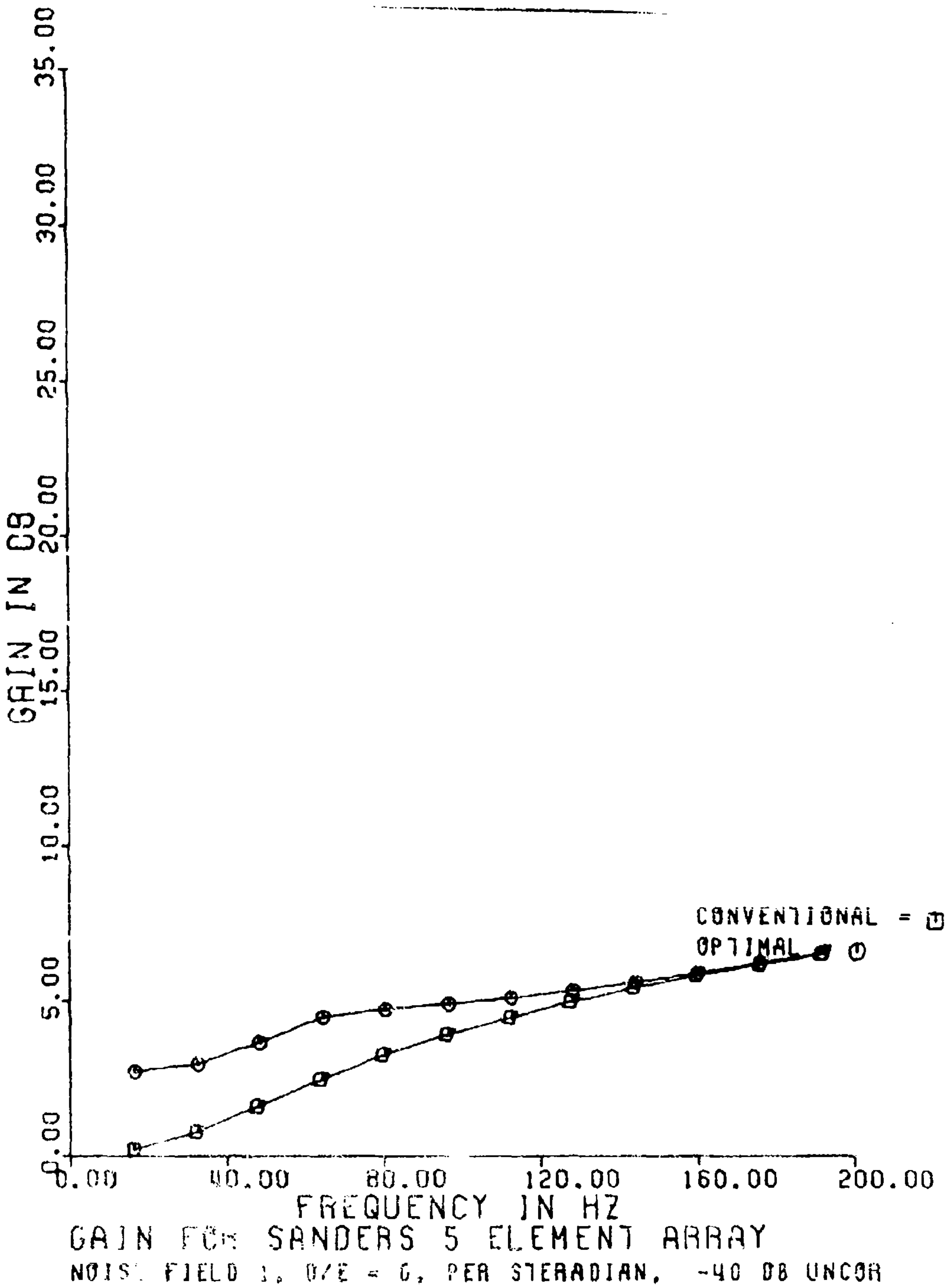

Figure D1. Array gain [illegible] noise field 1 [illegible] D/E = 0. "Optimal" appears in figures D1-D42 and has the same meaning as "adaptive."

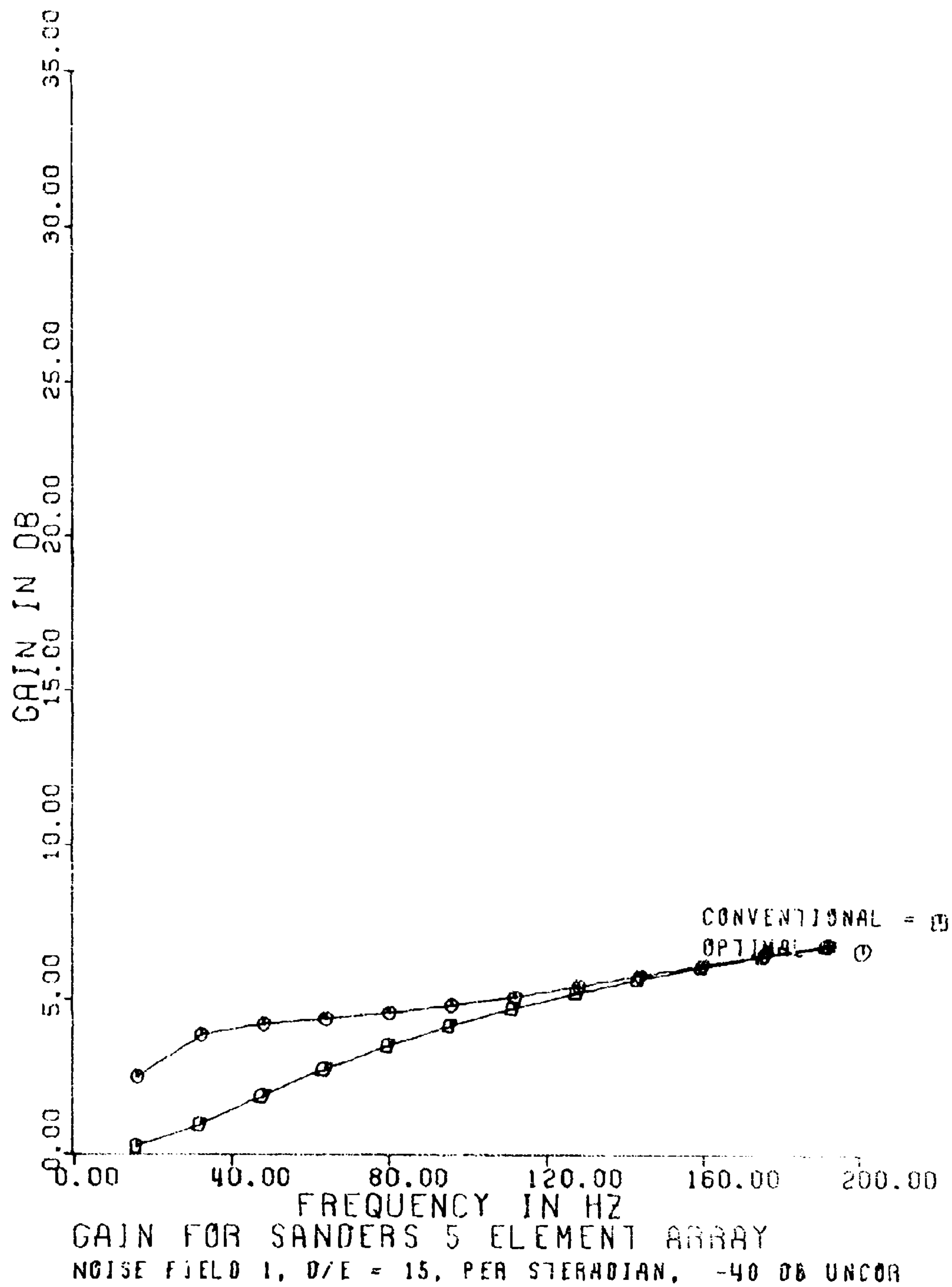

(U) Figure D2. Array gain – noise field 1 – D/E = 15.

UNCLASSIFIED

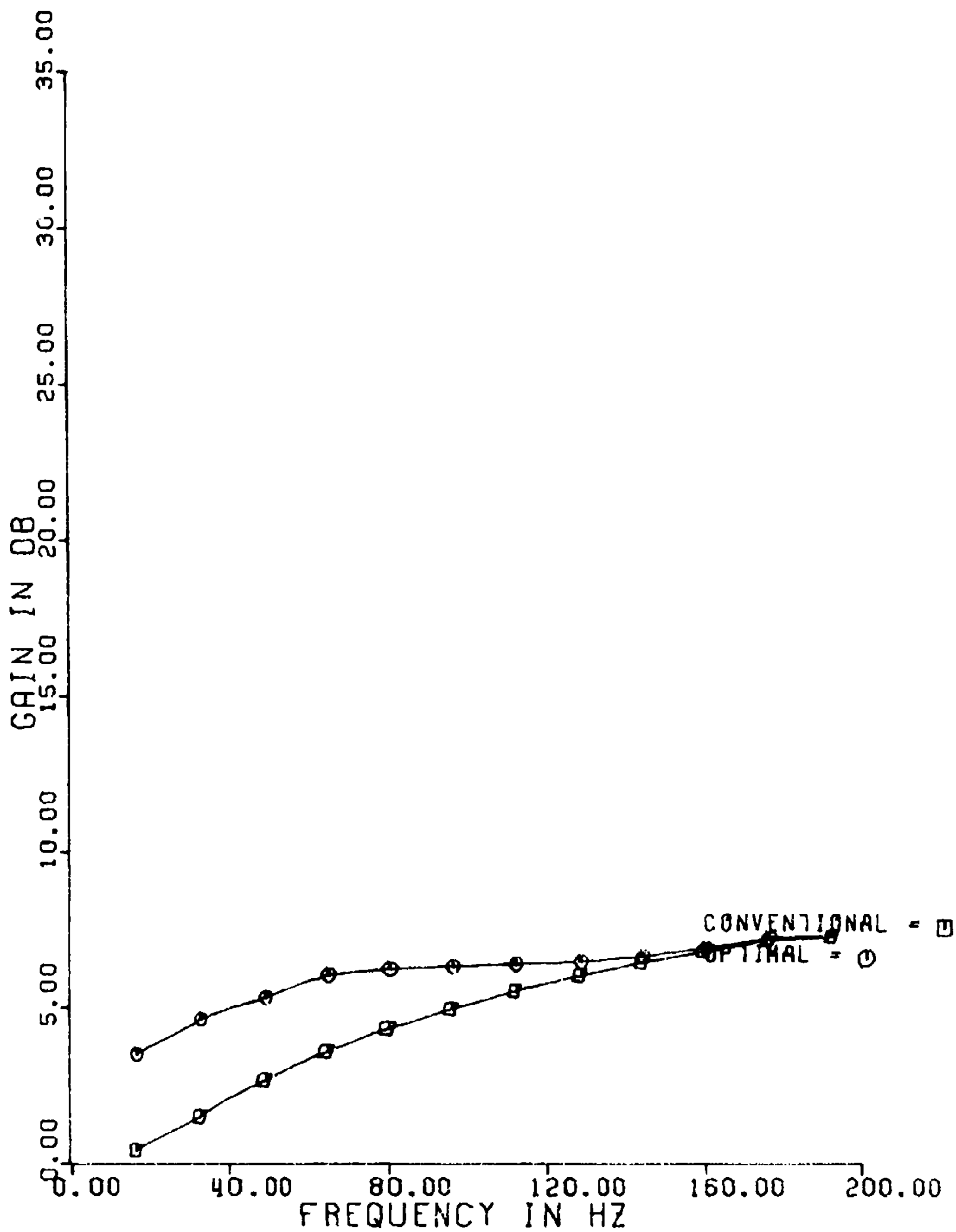

GAIN FOR SANDERS 5 ELEMENT ARRAY

NOISE FIELD 1, D/E = 30, PER STERADIAN, -40 DB UNCOR

(U) Figure D3. Array gain - noise field 1 D/E = 30.

UNCLASSIFIED

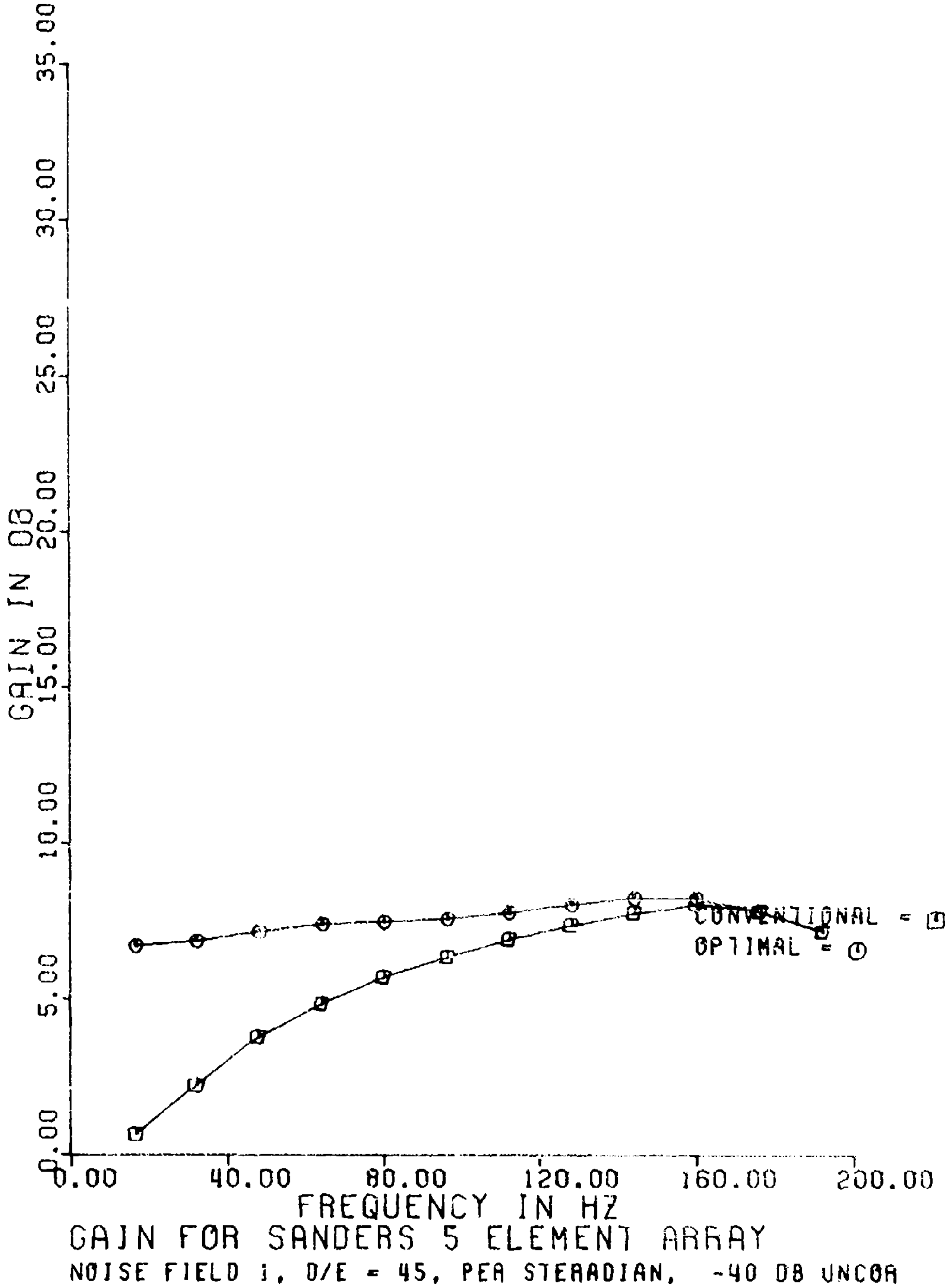

(U) Figure D4. Array gain – noise field 1 – D/E = 45.

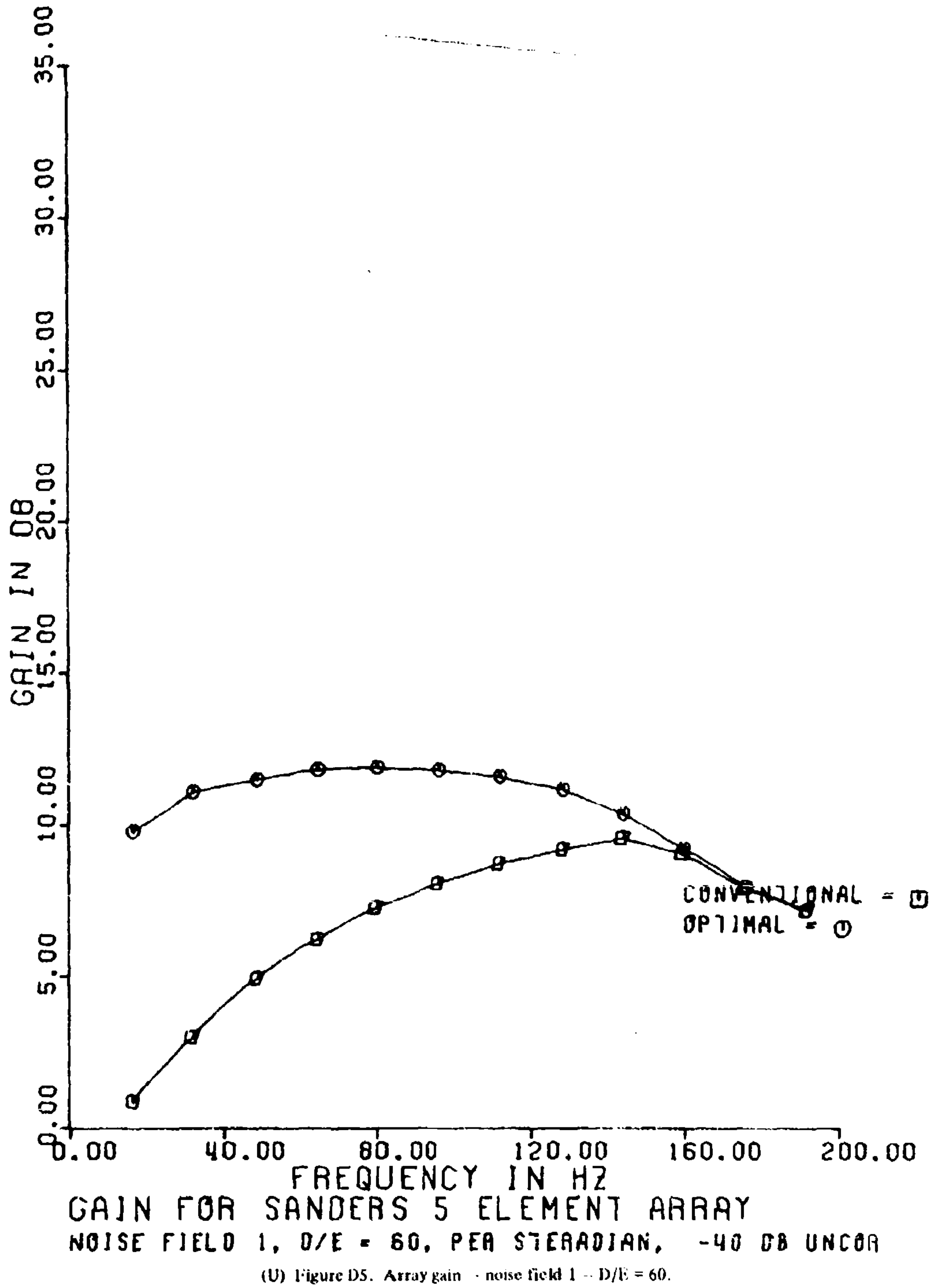

(U) Figure D5. Array gain – noise field 1 – D/E = 60.

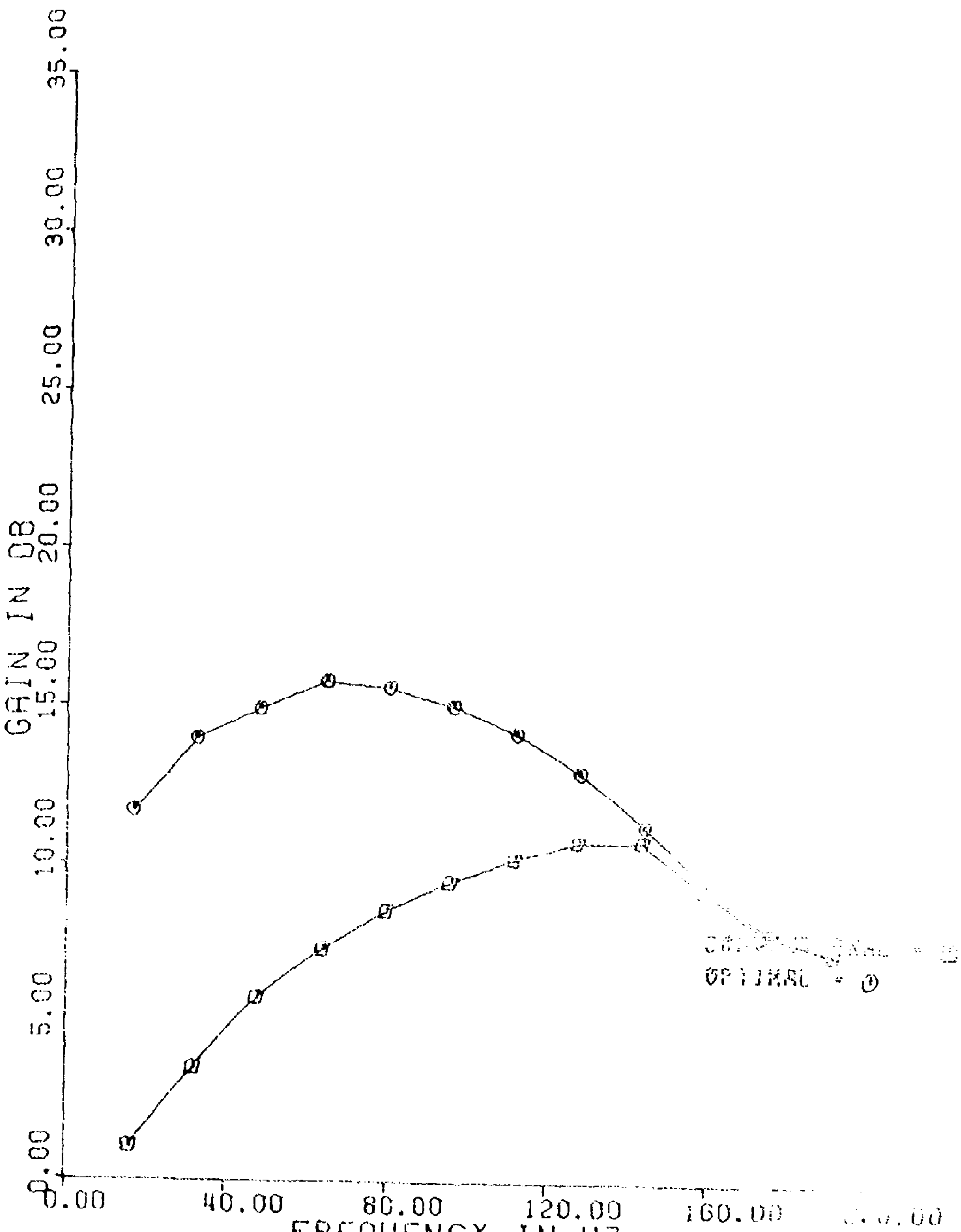

GAIN FOR SANDERS 5 ELEMENT ARRAY
NOISE FIELD 1, D/E = 75, PER STERADIAN, -40 DB UNCOR

(U) Figure D6. Array gain — noise field 1 — D/E = 75.

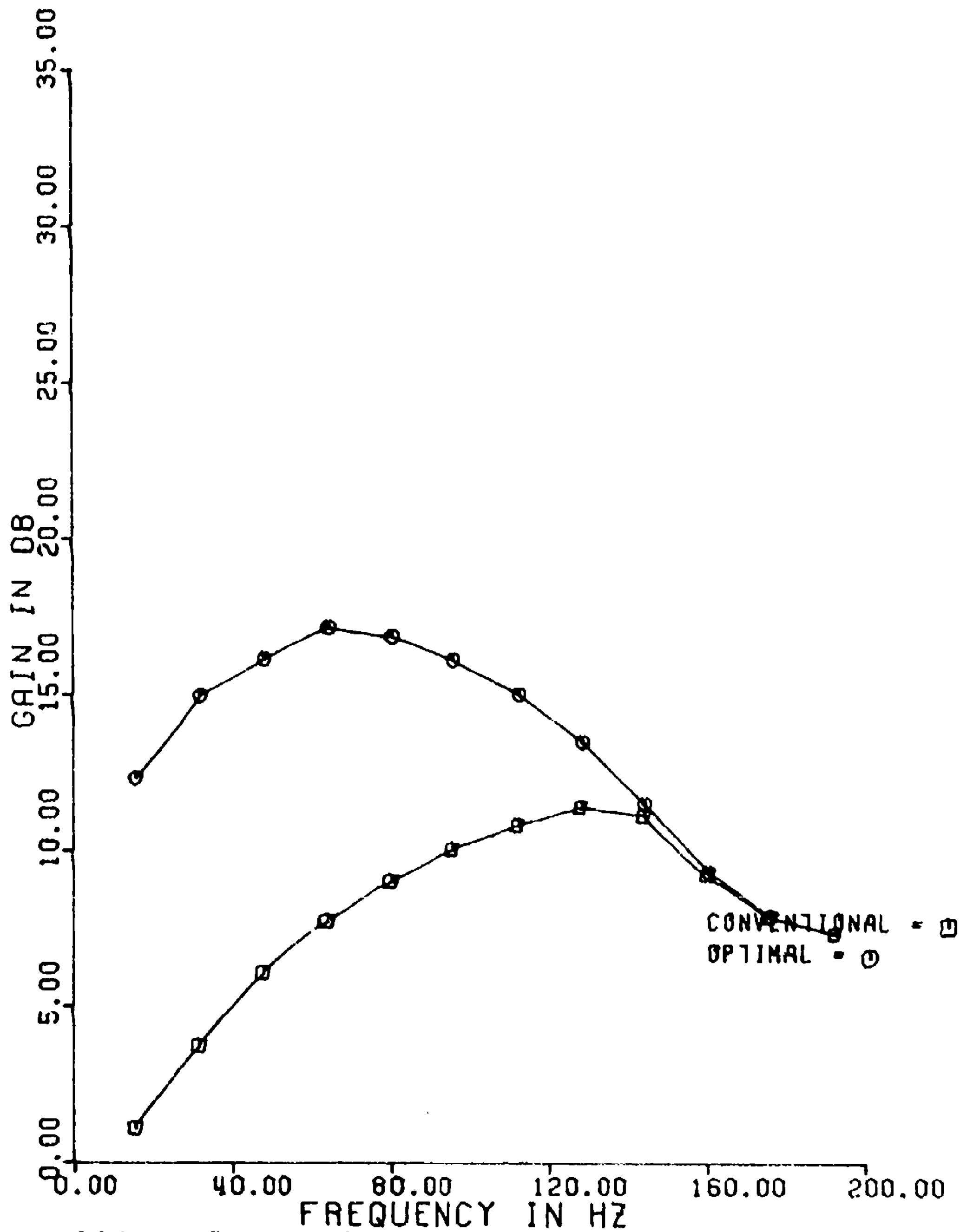

GAIN FOR SANDERS 5 ELEMENT ARRAY

NOISE FIELD 1, D/E = 90, PER STERADIAN, -40 DB UNCOR

(U) Figure D7. Array gain - noise field 1 - D/E = 90.

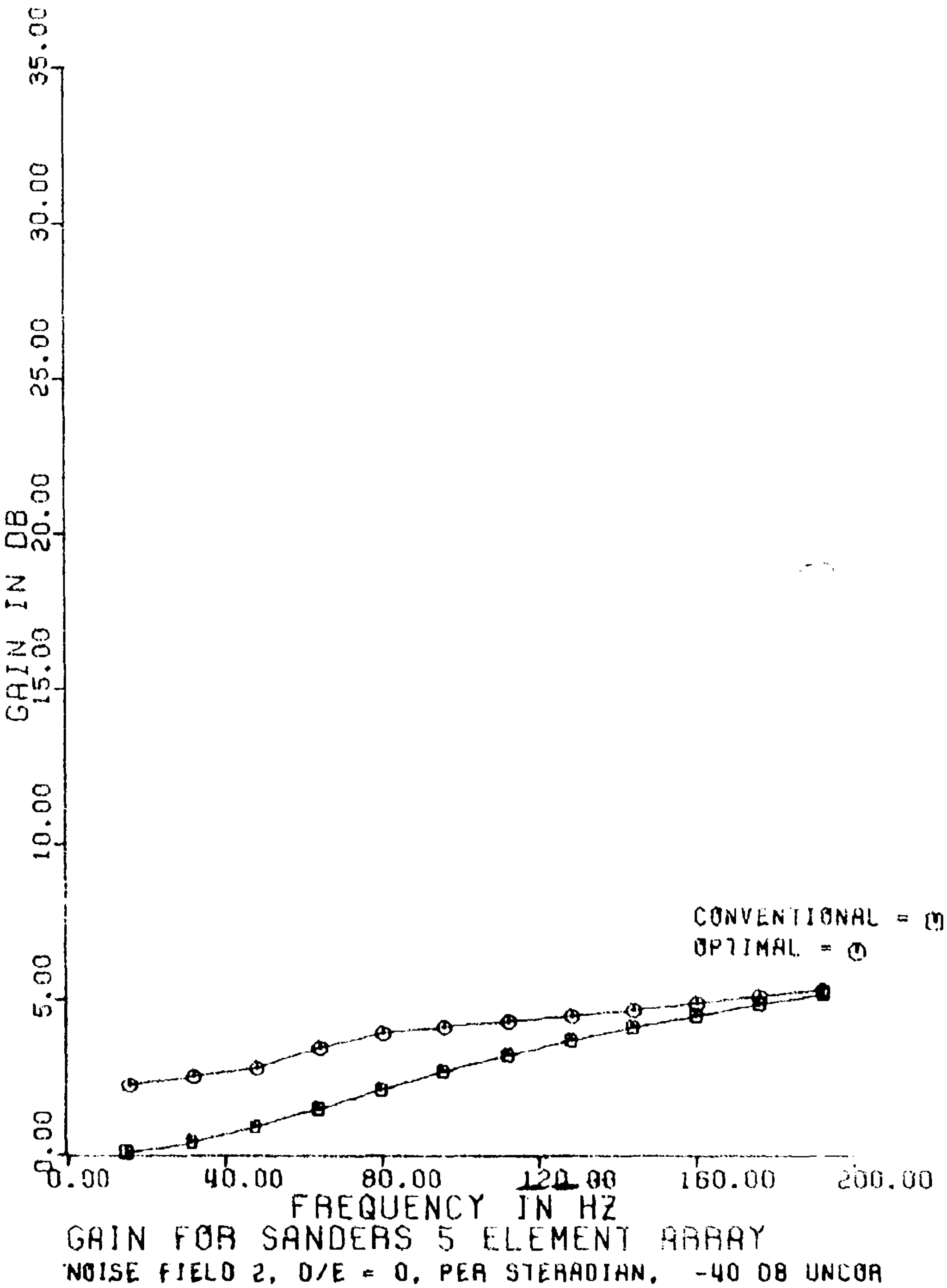

(U) Figure D8. Array gain noise field 2 D/E = 0.

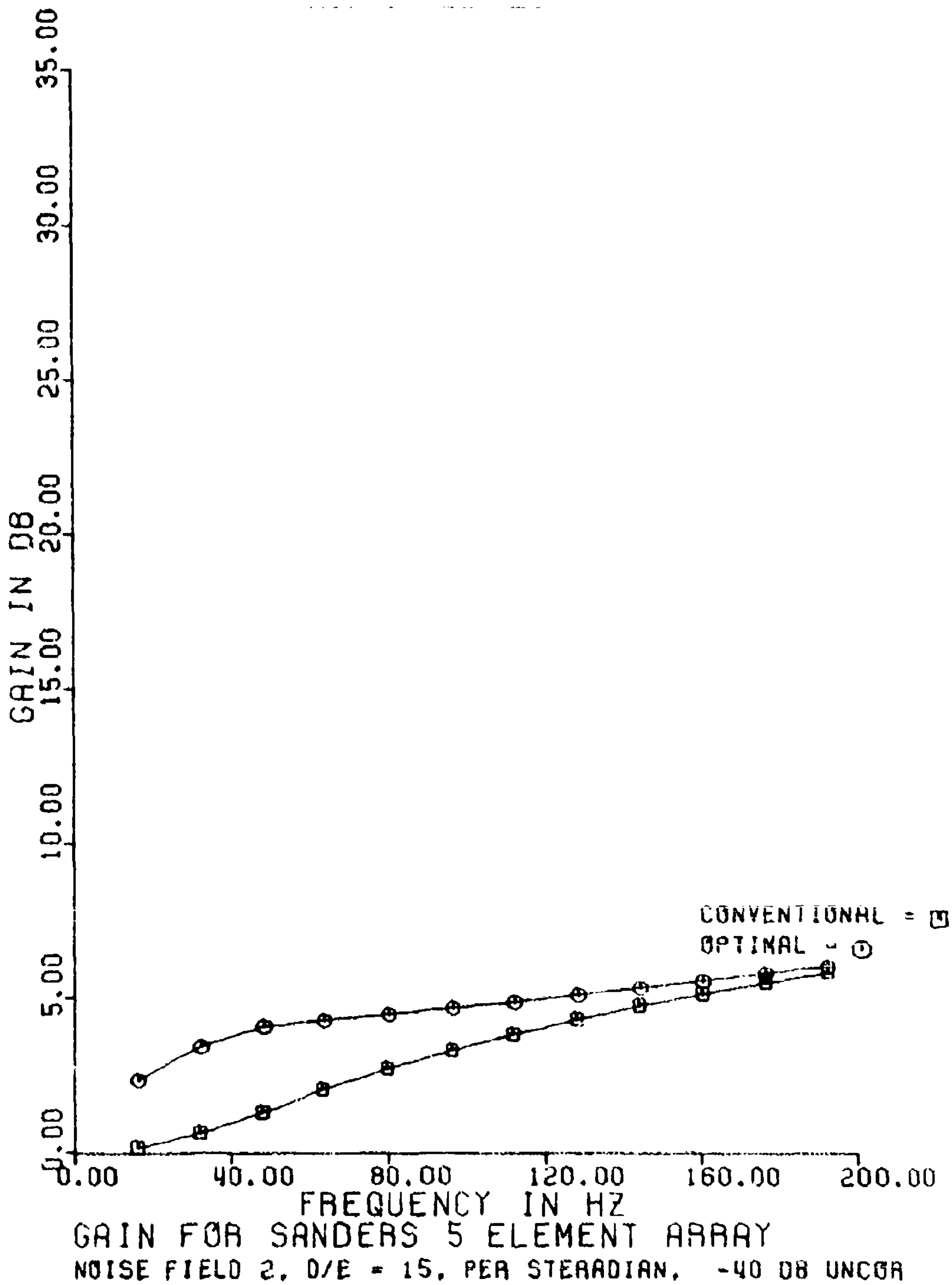

(U) Figure D9. Array gain – noise field 2 – D/E = 15.

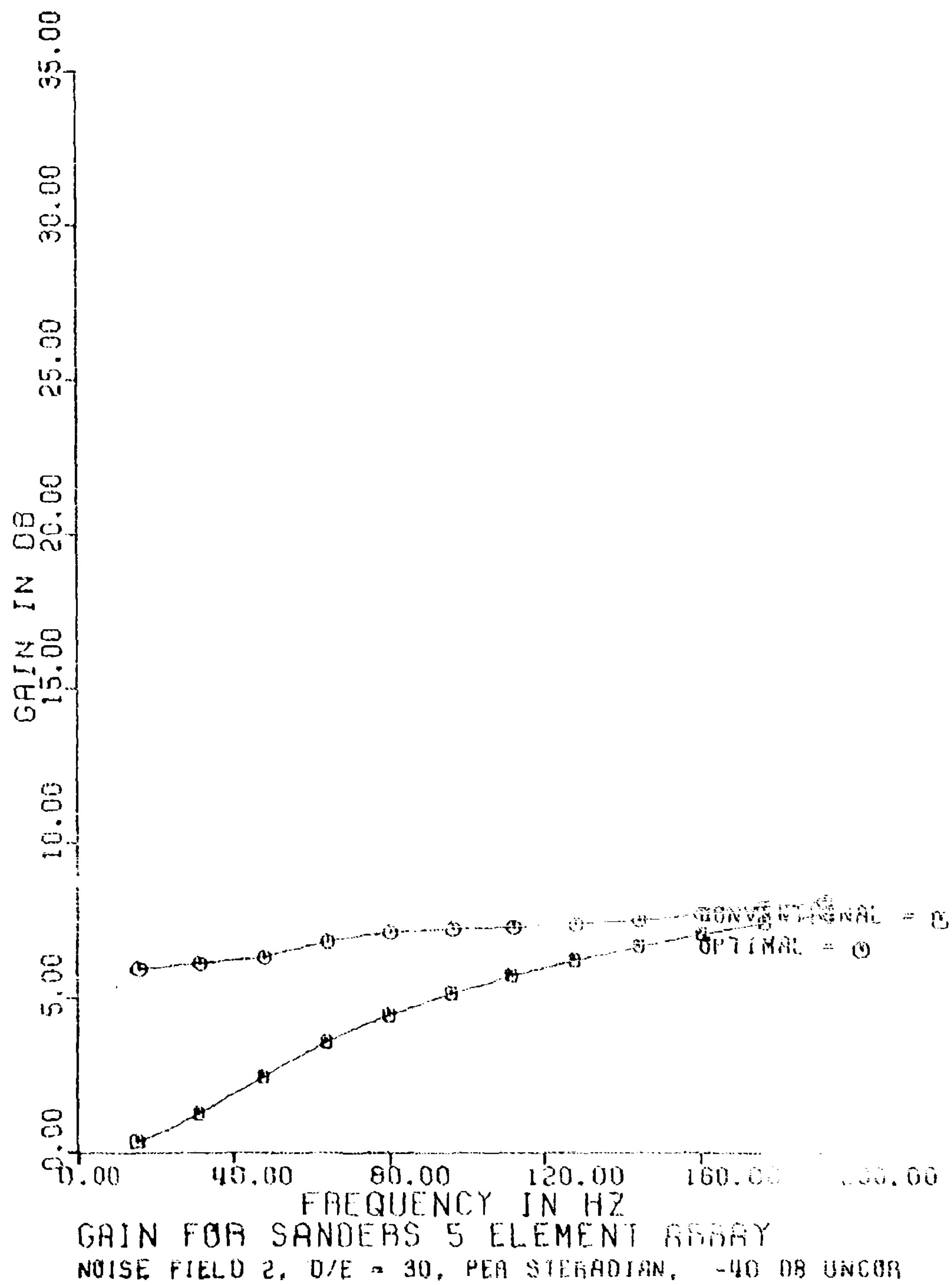

(U) Figure D10 Array gain - noise field 2 D/E = 30

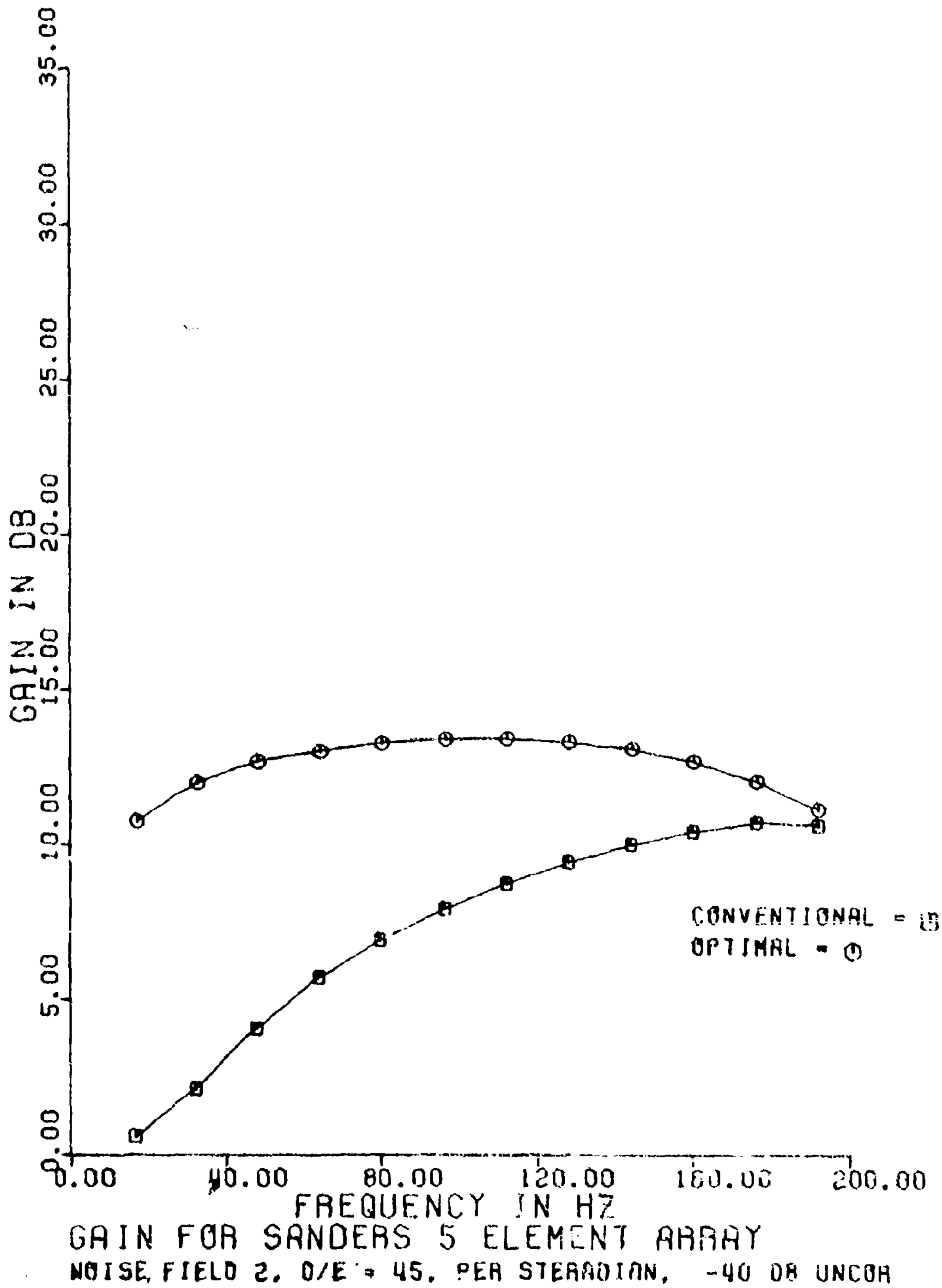

(U) Figure D11. Array gain – noise field 2 D/E = 45.

UNCLASSIFIED

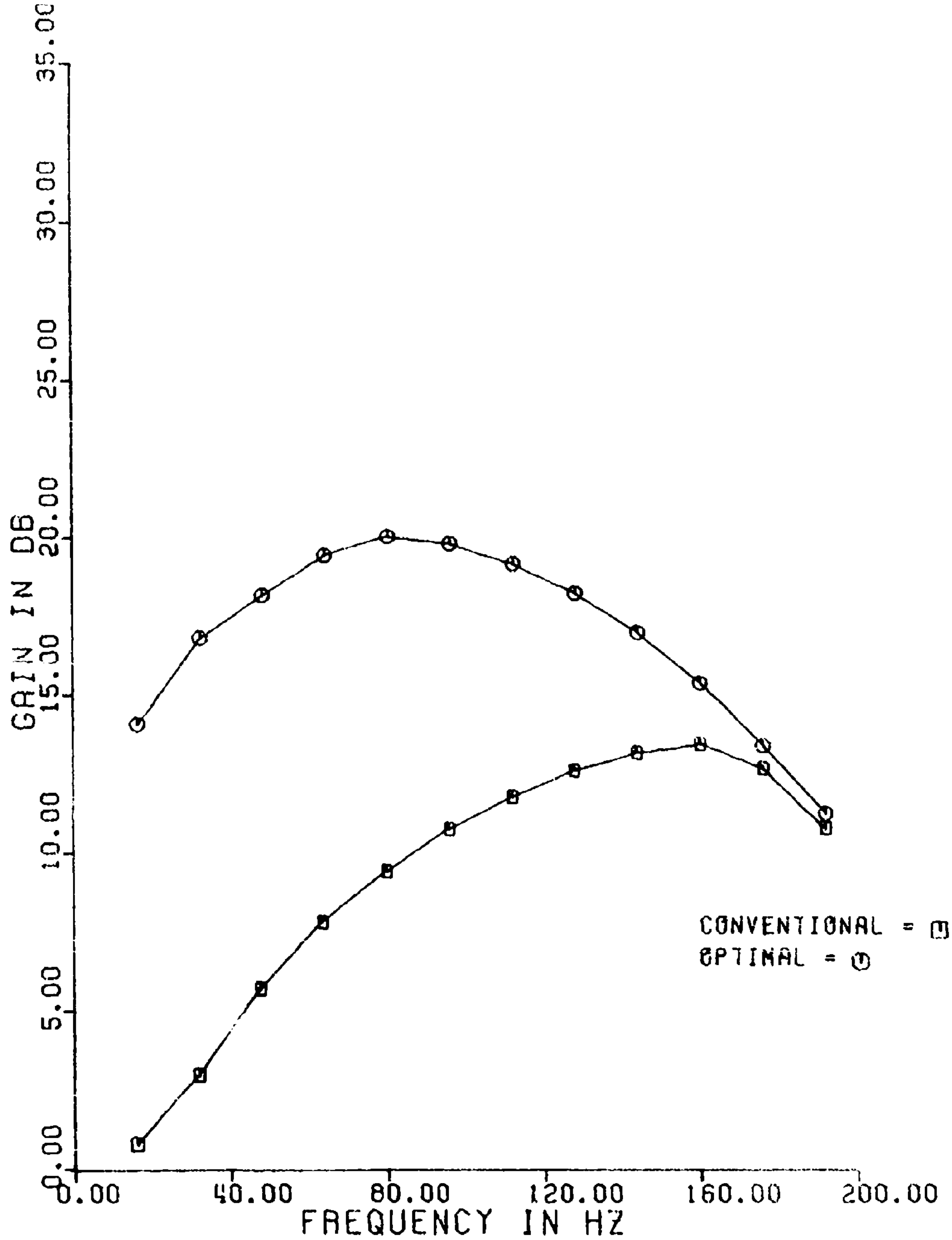

GAIN FOR SANDERS 5 ELEMENT ARRAY
NOISE FIELD 2, D/E = 60, PER STERADIAN, -40 DB UNCOR

(U) Figure D12. Array gain noise field 2 D/E = 60.

UNCLASSIFIED

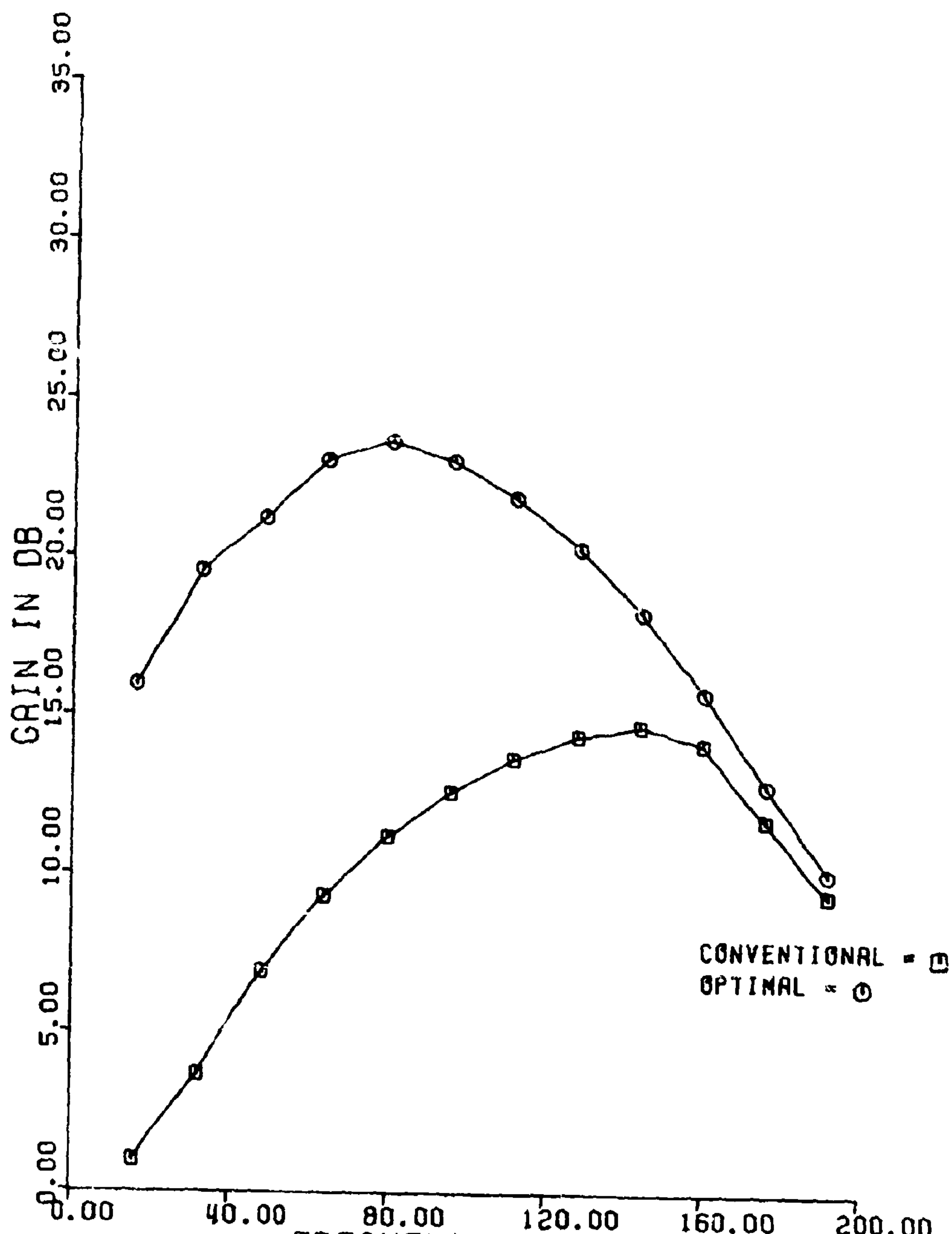

GAIN FOR SANDERS 5 ELEMENT ARRAY
NOISE FIELD 2, D/E = 75, PER STERADIAN, -40 DB UNCOR

(U) Figure D13. Array gain -- noise field 2 - D/E = 75.

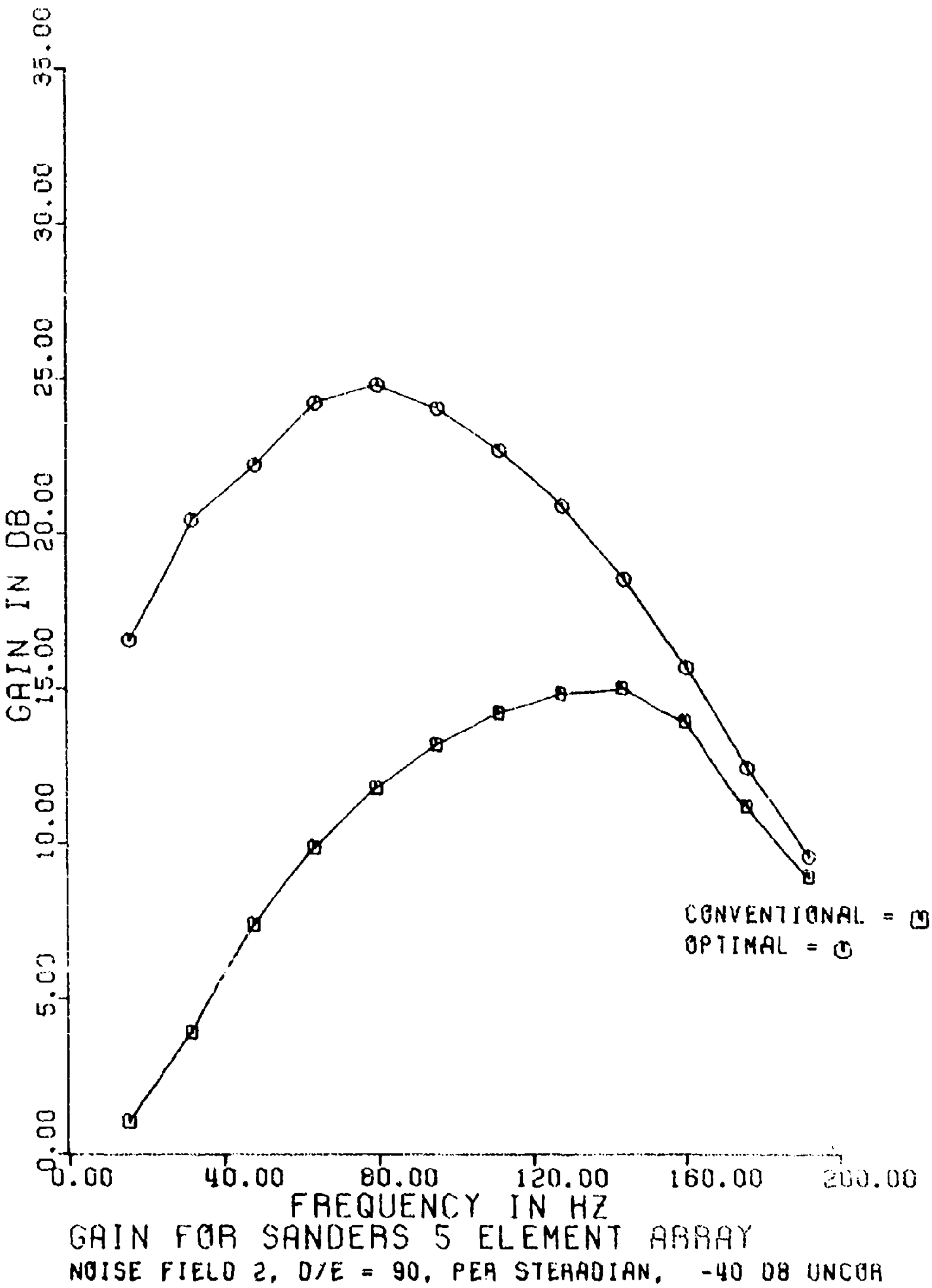

(U) Figure D14. Array gain – noise field 2 – D/E = 90.

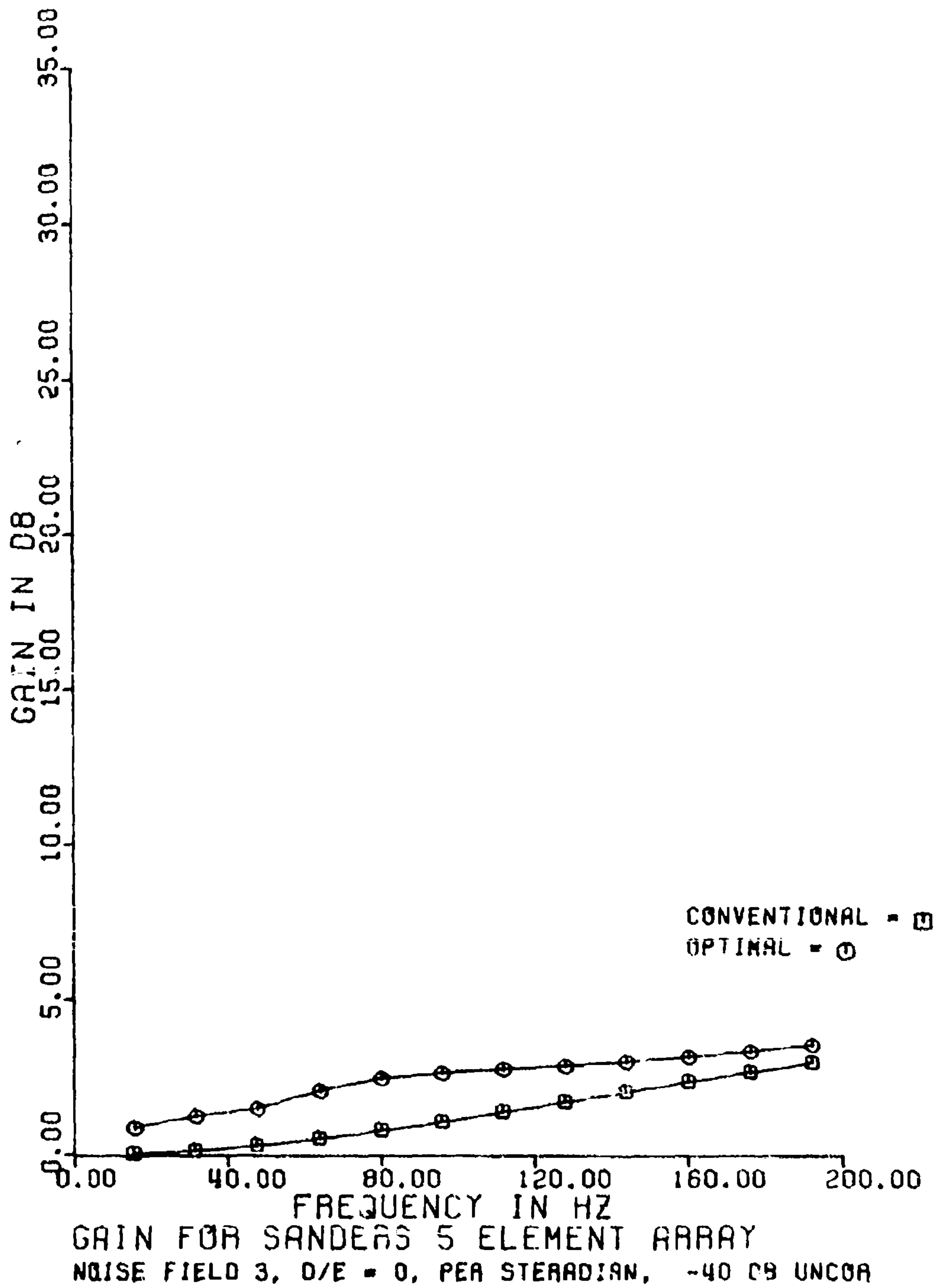

(U) Figure D15. Array gain noise field 3 D/E = 0.

UNCLASSIFIED

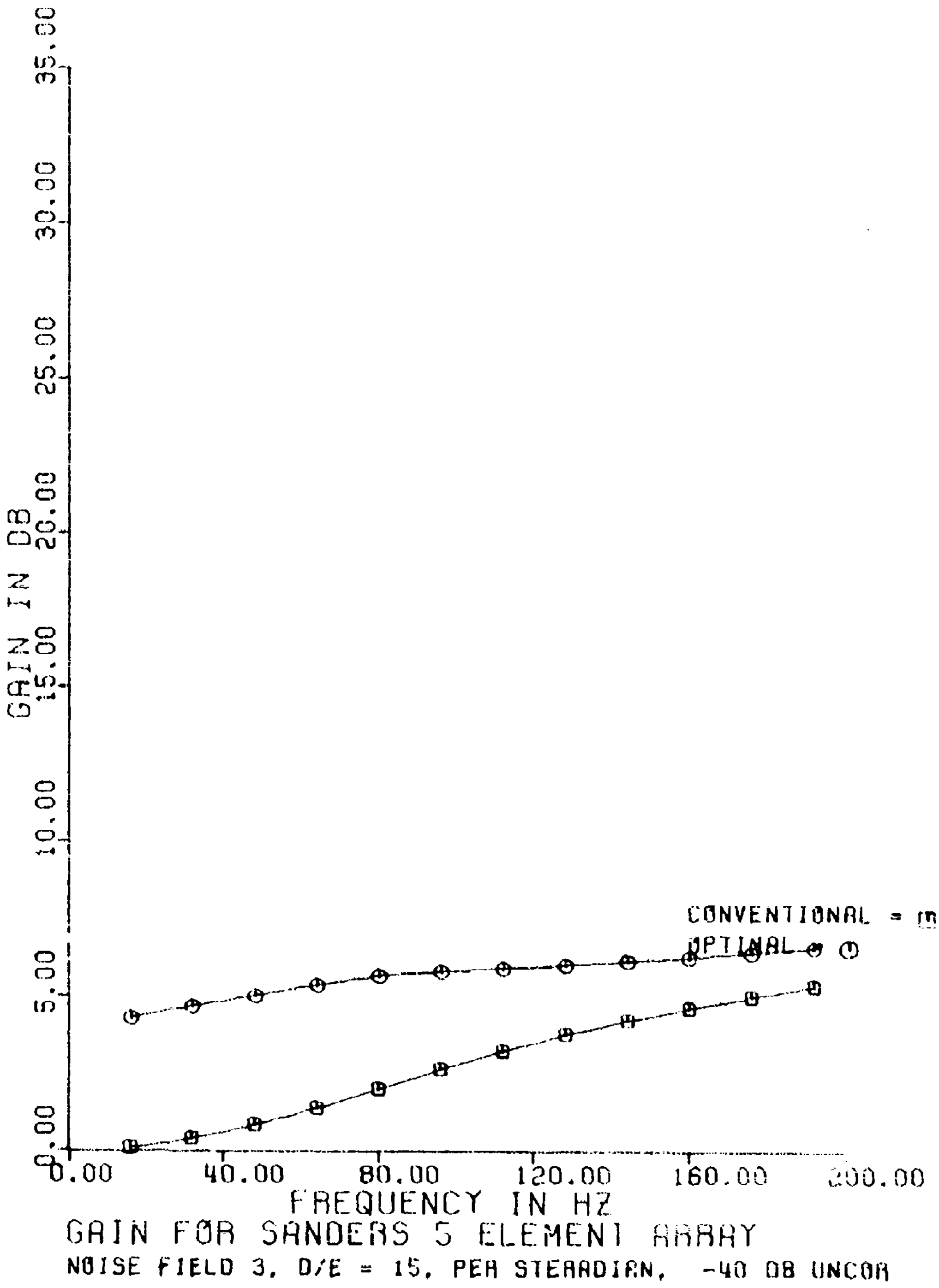

(U) Figure D16. Array gain noise field 3 D/E = 15.

UNCLASSIFIED

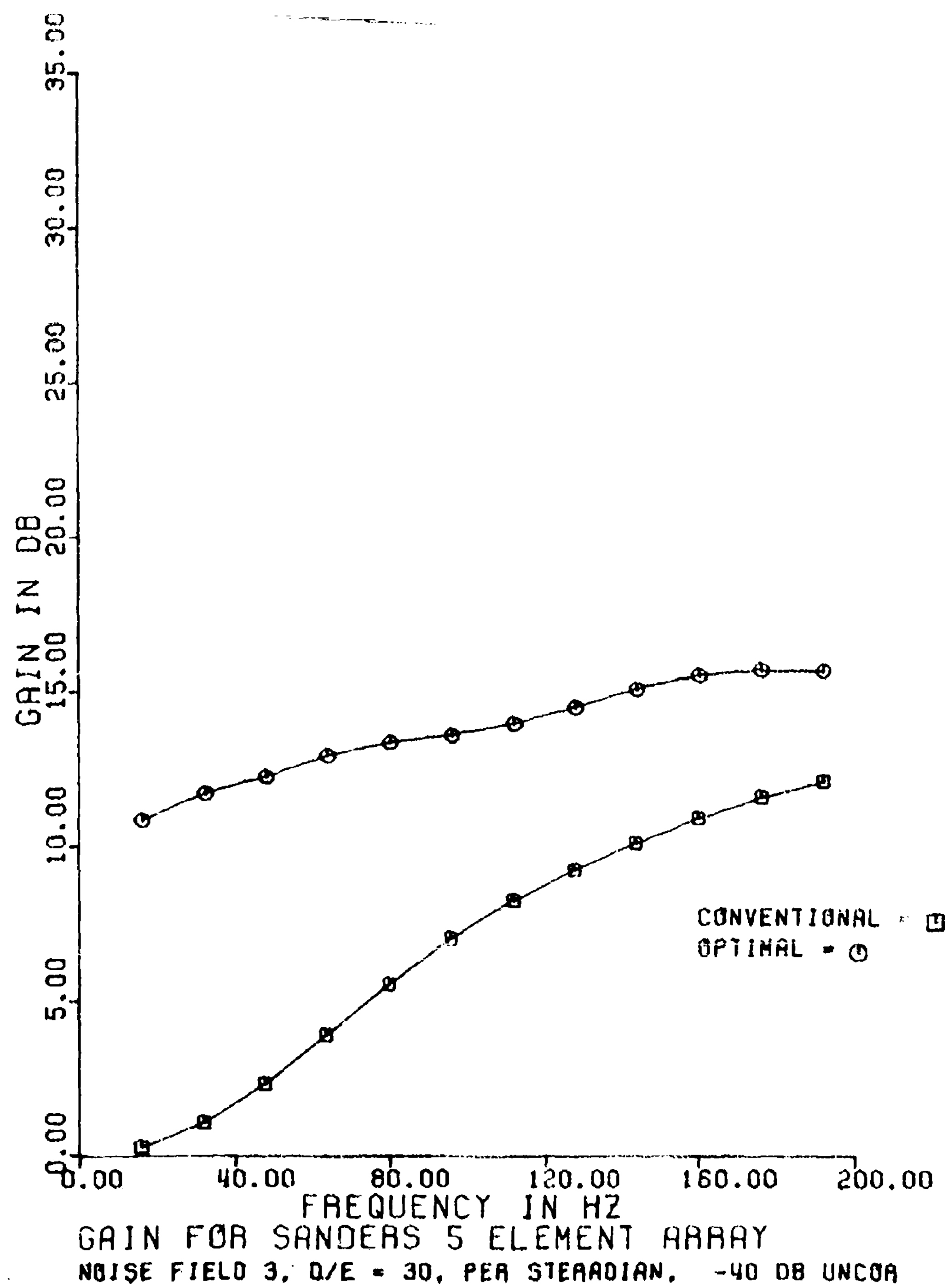

(U) Figure D17. Array gain noise field 3 D/E = 30.

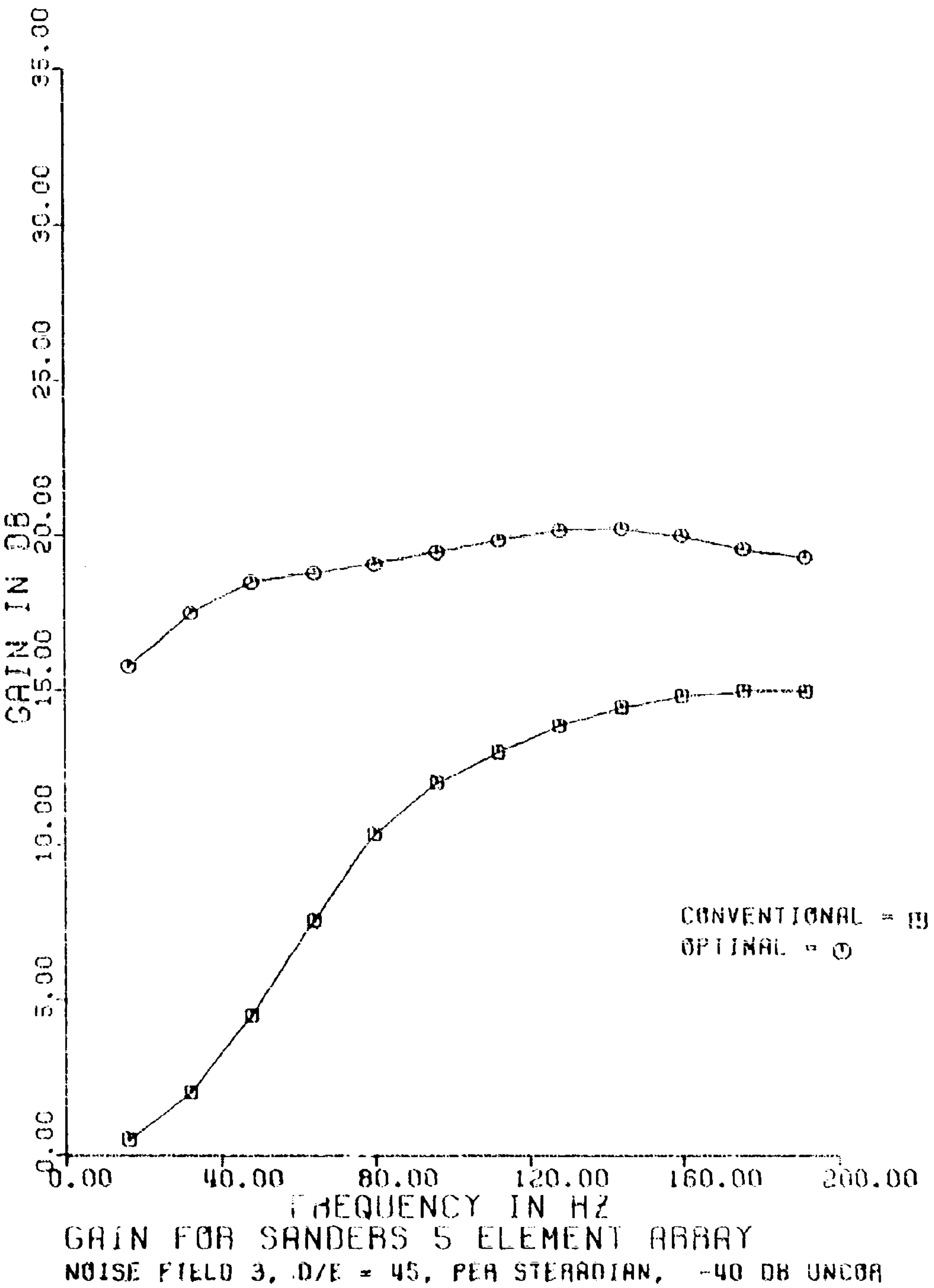

(U) Figure D18. Array gain – noise field 3 – D/L = 45.

UNCLASSIFIED

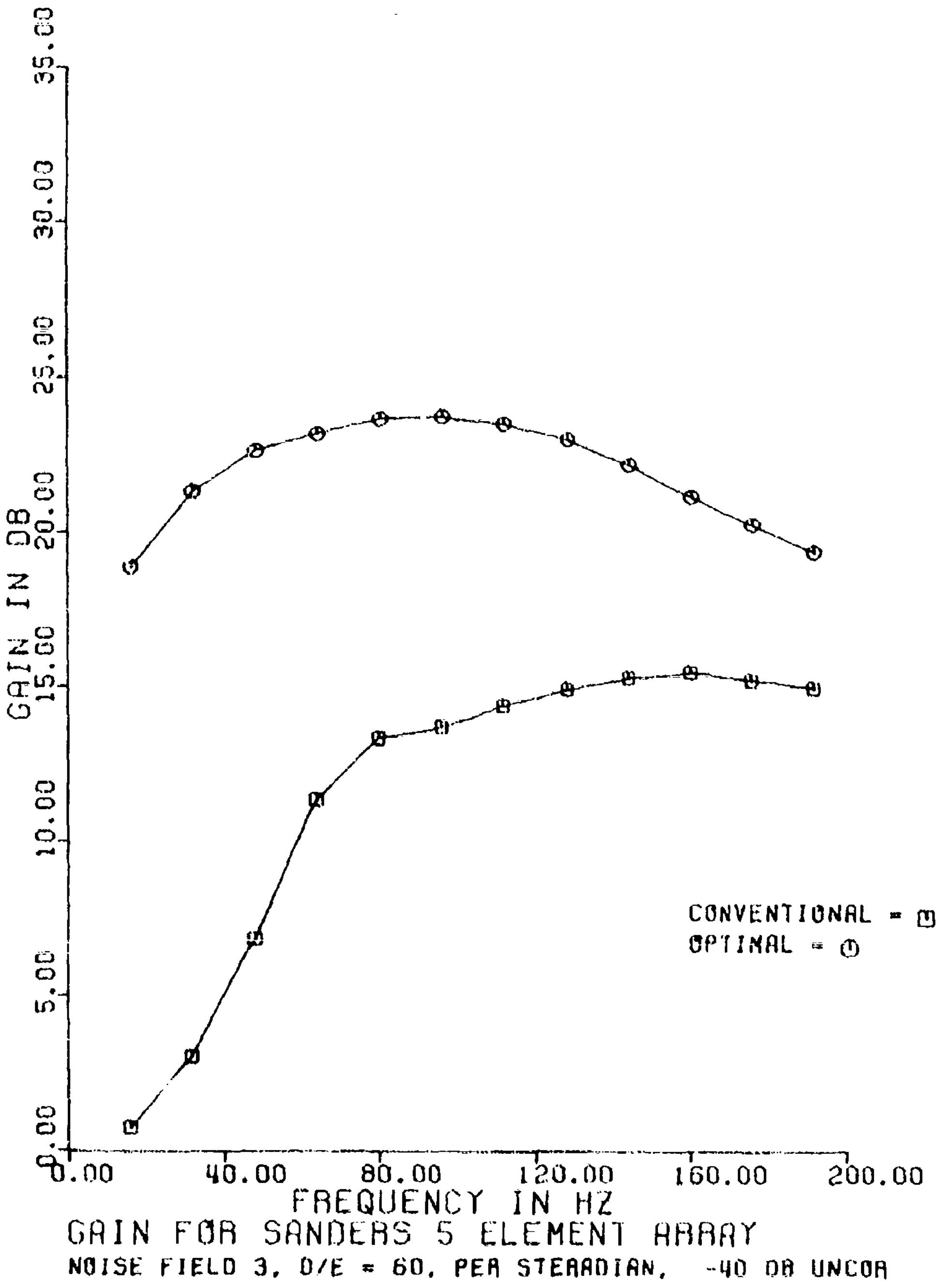

(U) Figure D19. Array gain noise field 3 D/E = 60.

UNCLASSIFIED

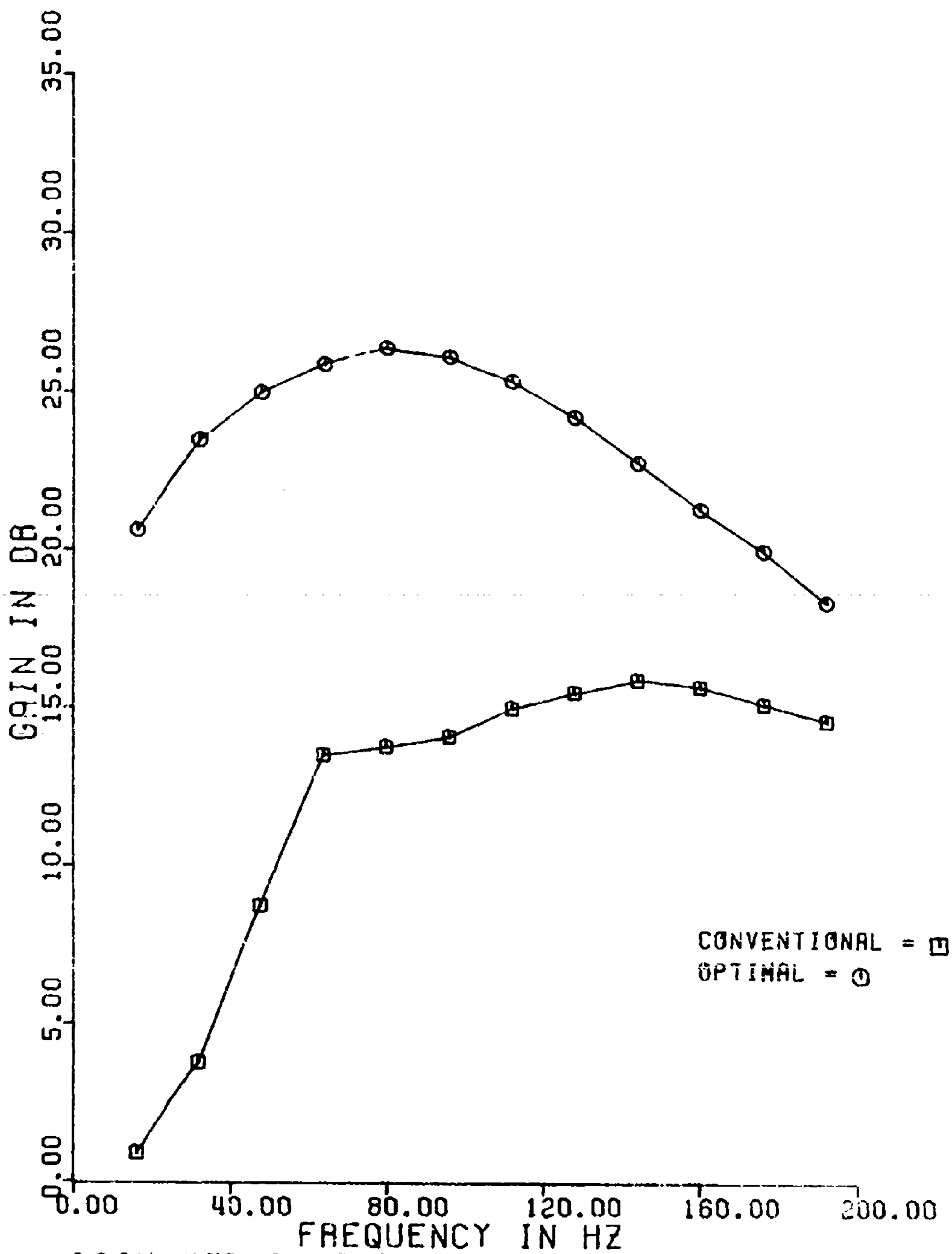

GAIN FOR SANDERS 5 ELEMENT ARRAY
NOISE FIELD 3, D/E = 75, PER STERADIAN, -40 DB UNCOR

(U) Figure D20. Array gain noise field 3 — D/E = 75.

UNCLASSIFIED

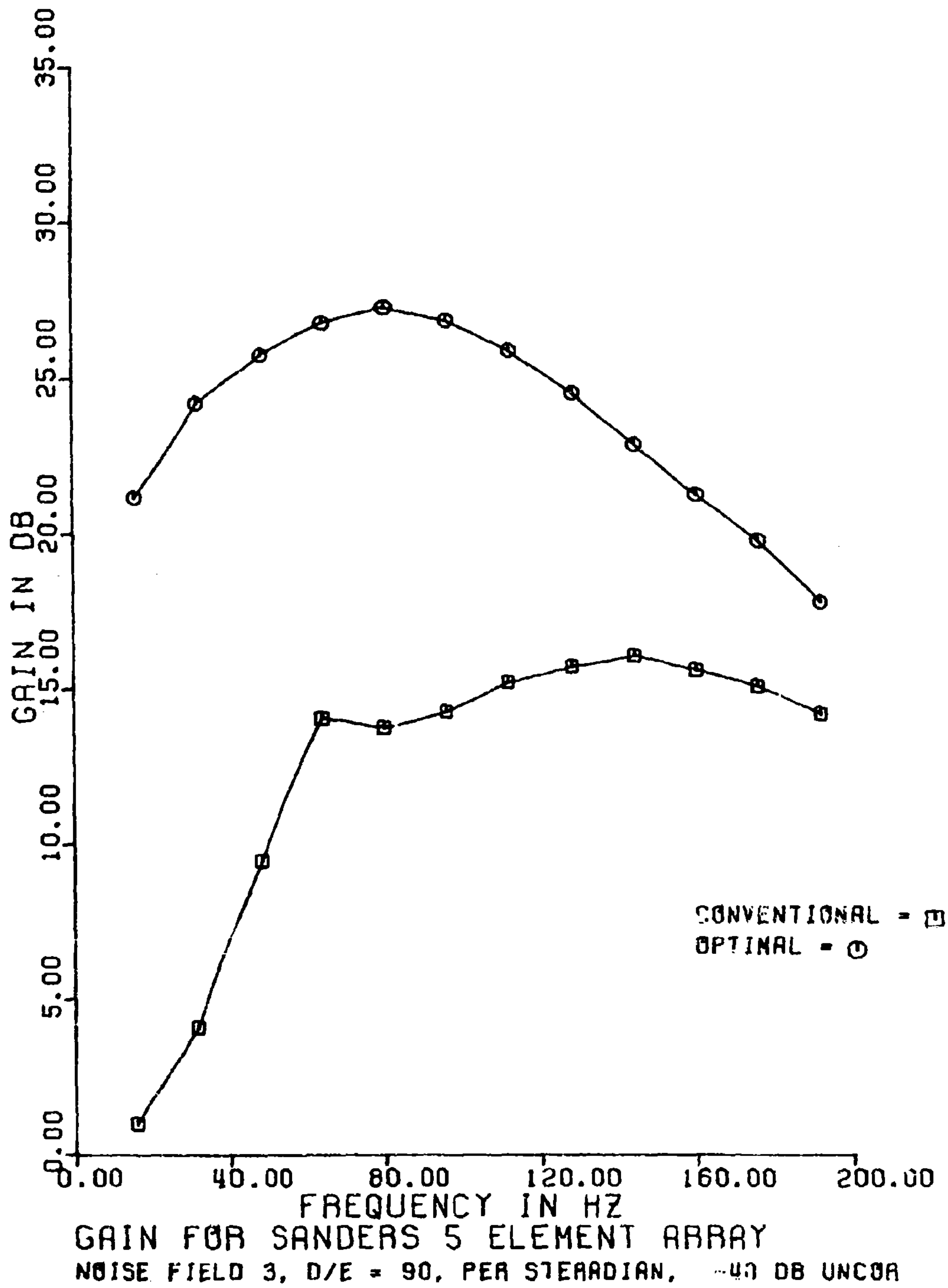

(U) Figure D21. Array gain – noise field 3 – D/E = 90.

UNCLASSIFIED

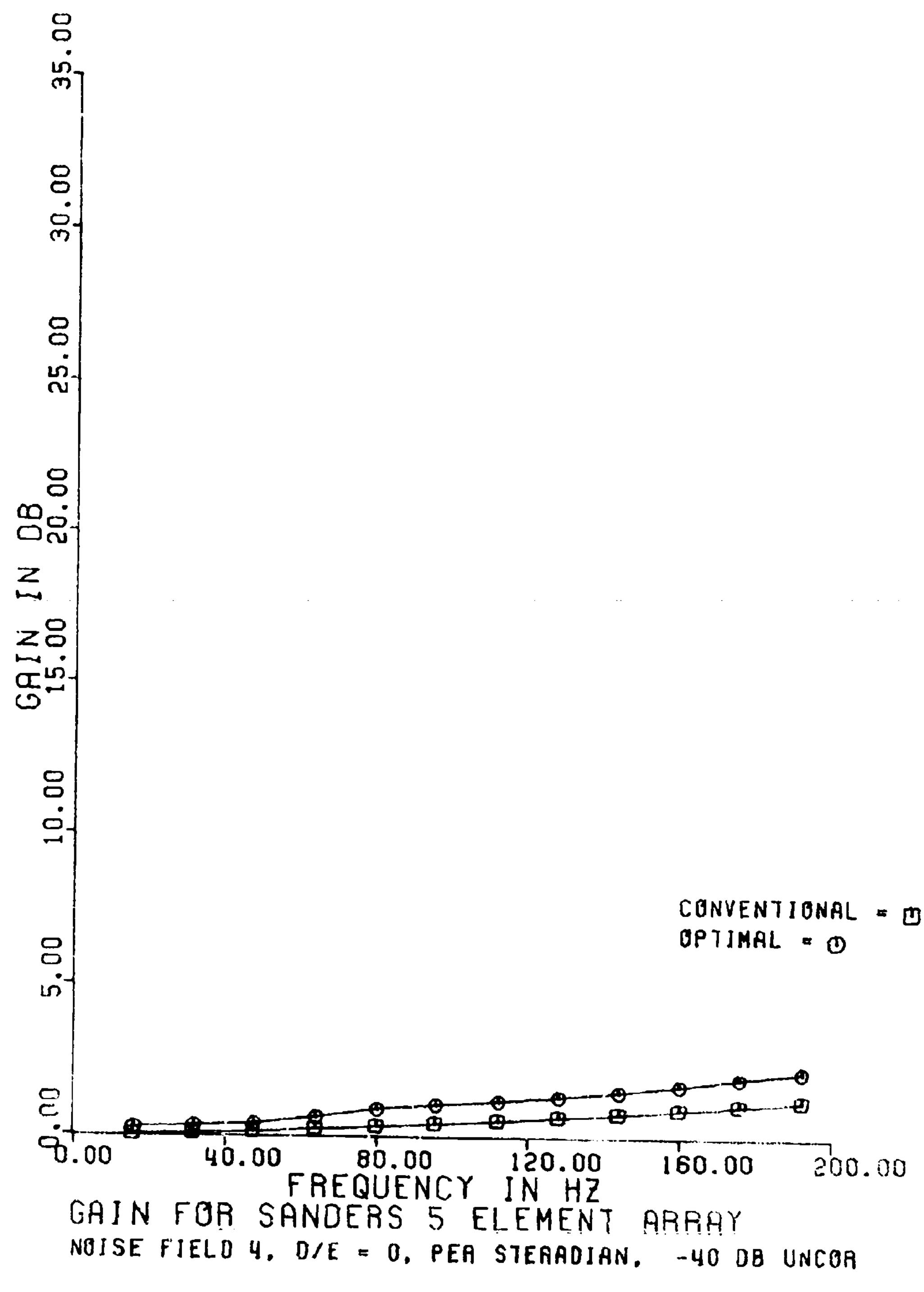

(U) Figure D22. Array gain – noise field 4 – D/E = 0.

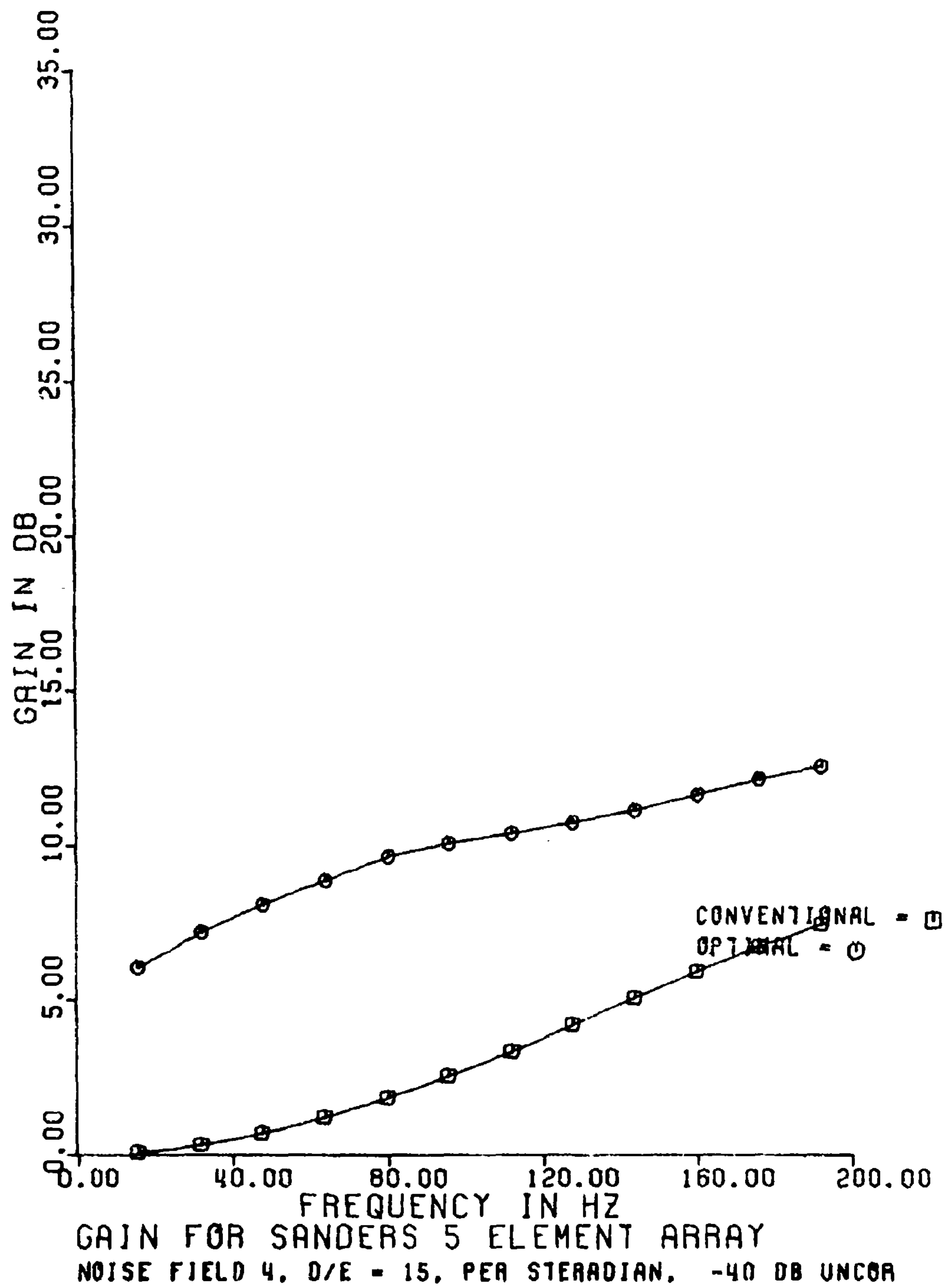

(U) Figure D23. Array gain – noise field 4 – D/E = 15.

UNCLASSIFIED

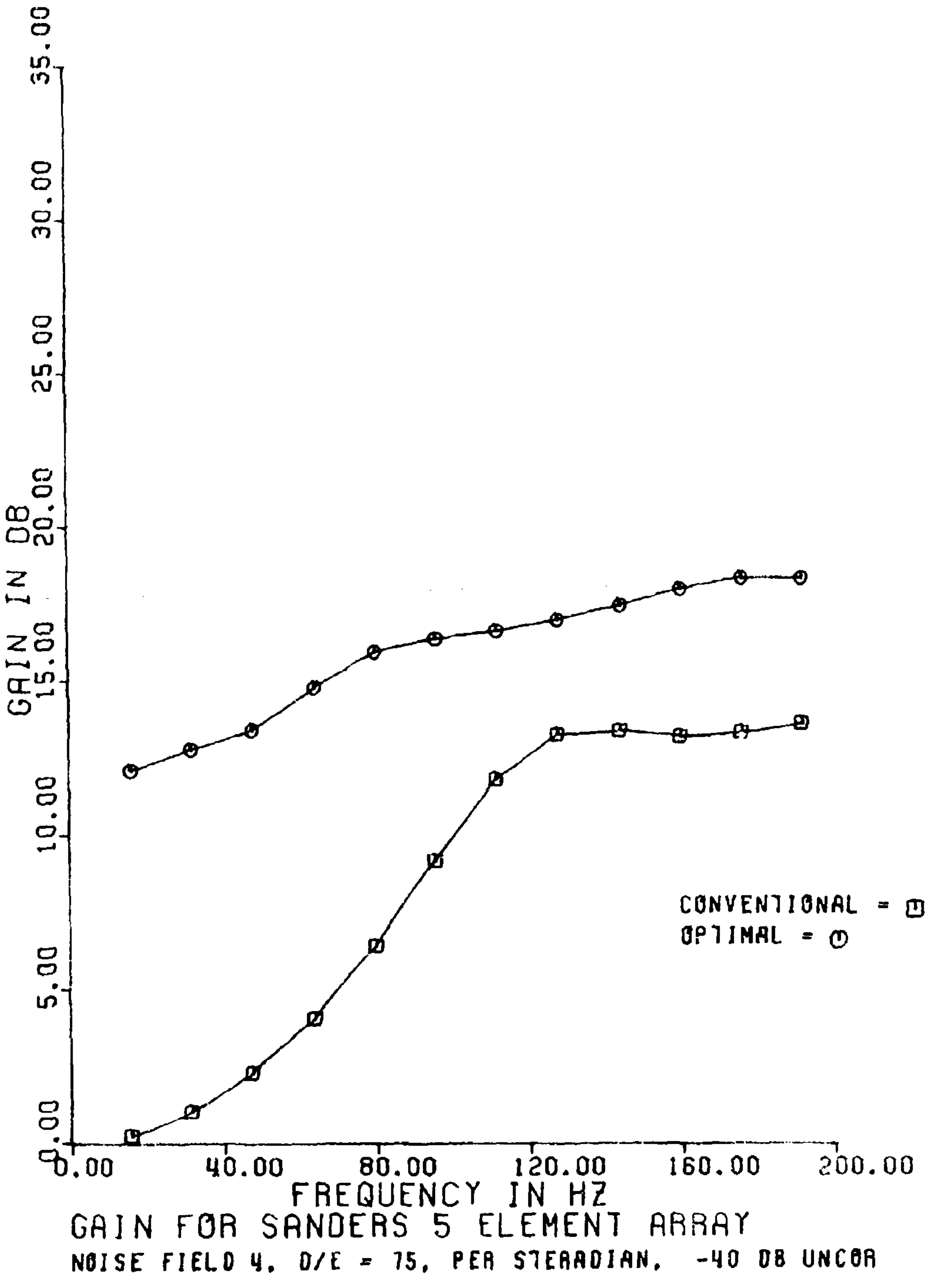

(U) Figure D24. Array gain - noise field 4 D/E = 30.

UNCLASSIFIED

UNCLASSIFIED

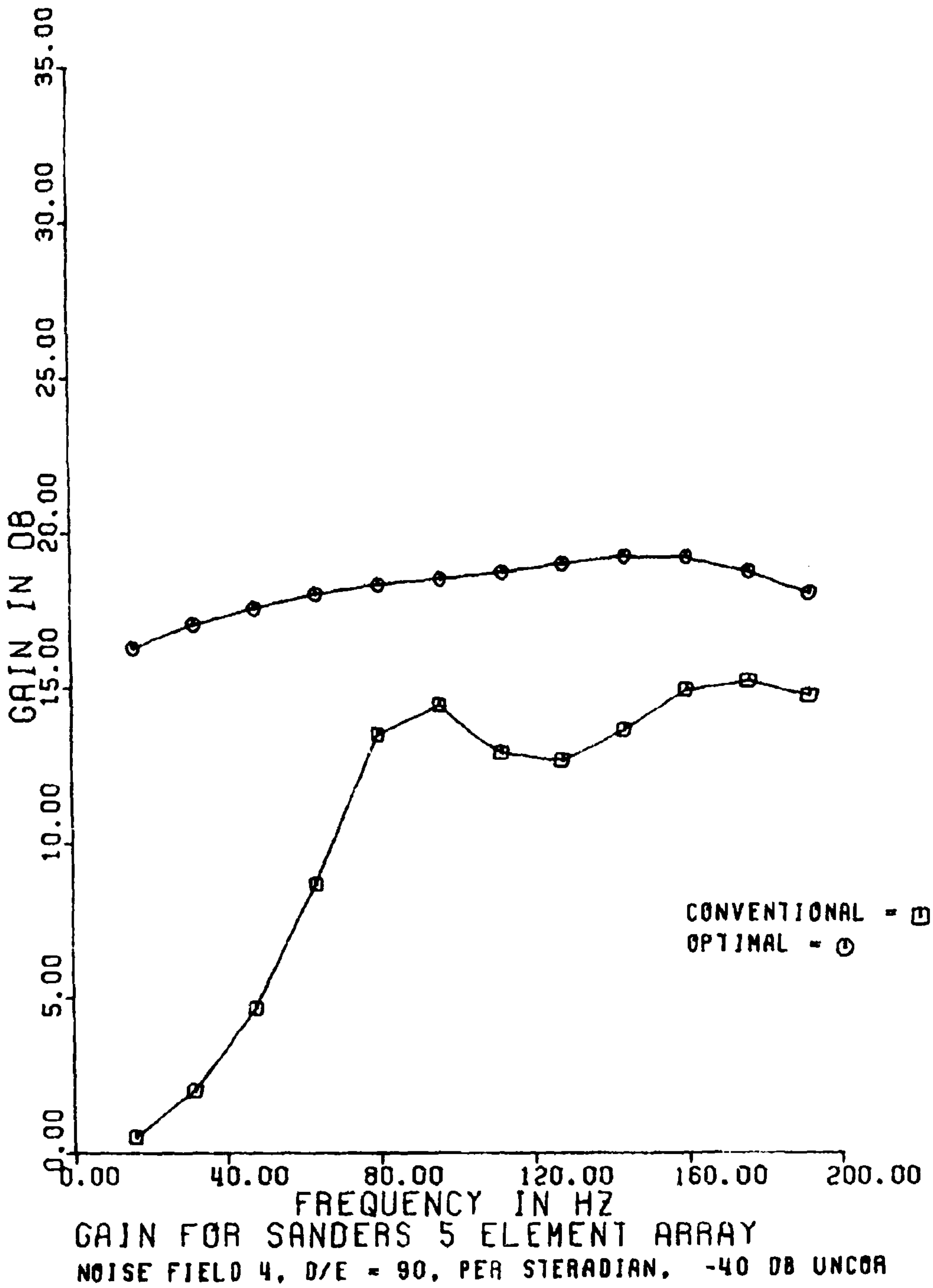

(U) Figure D25. Array gain -- noise field 4 -- D/E = 45.

UNCLASSIFIED

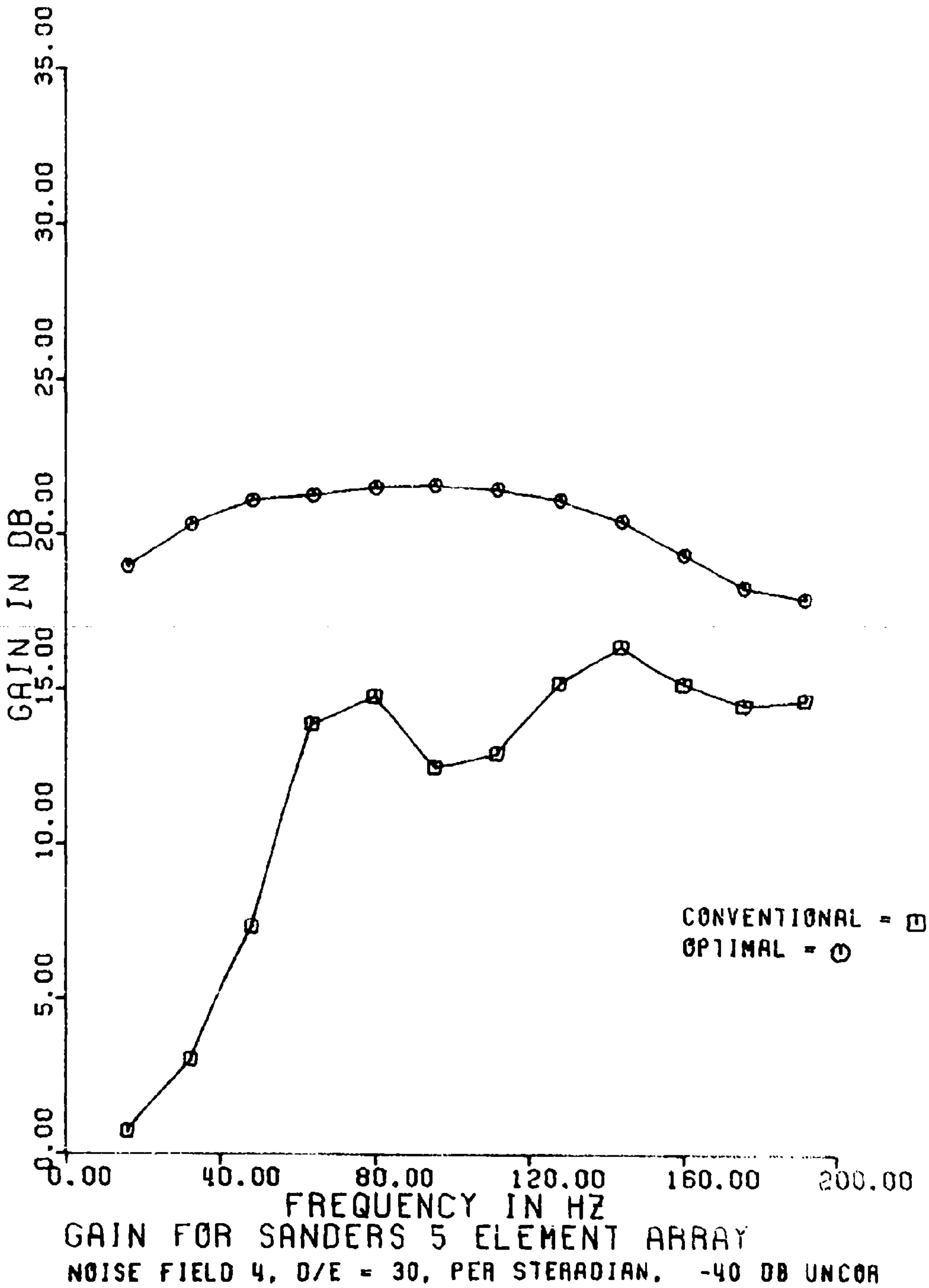

(U) Figure D26. Array gain – noise field 4 – D/E = 60.

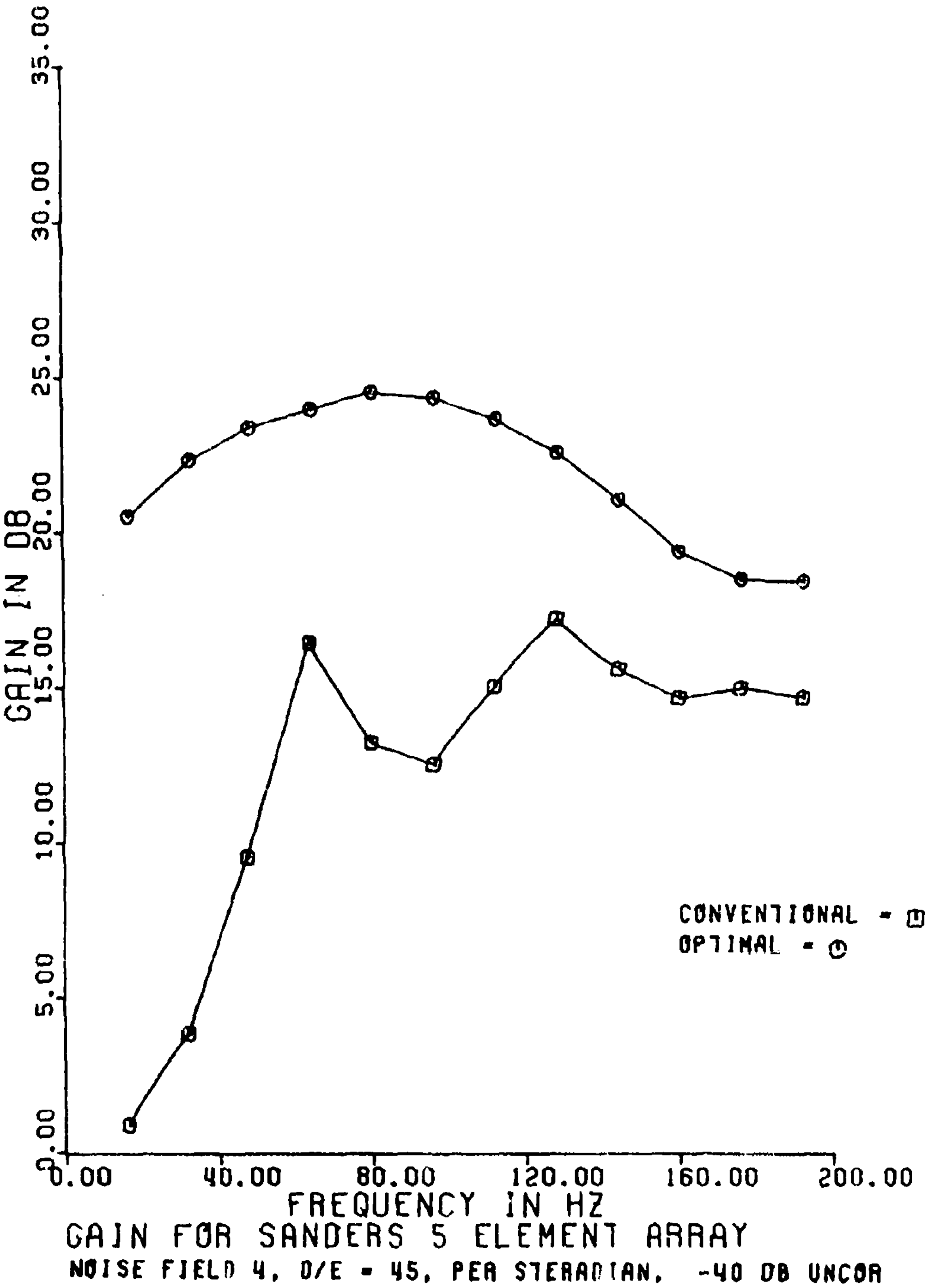

(U) Figure D27. Array gain – noise field 4 – D/E = 75.

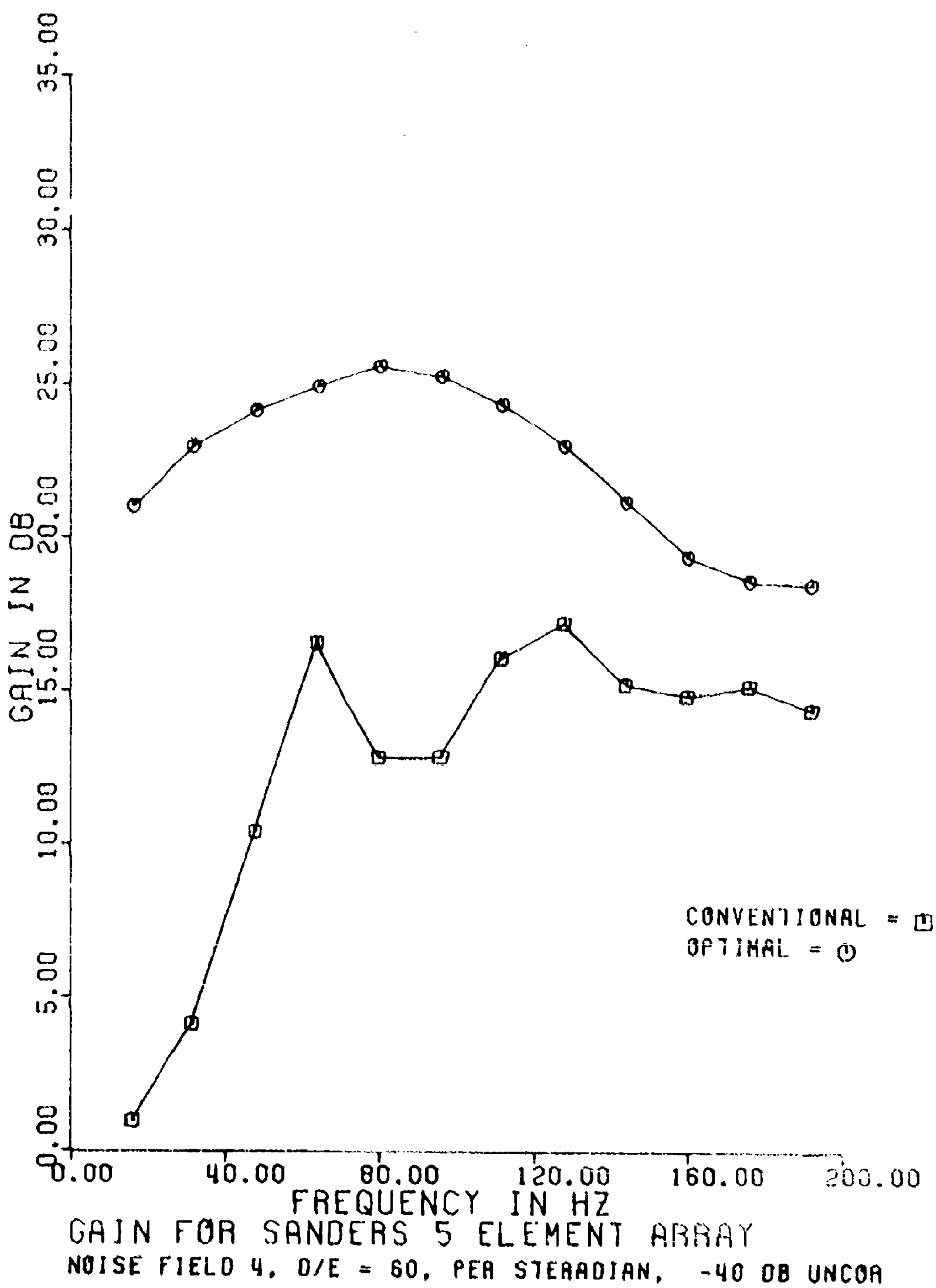

(U) Figure D28. Array gain – noise field 4 D/E = 90.

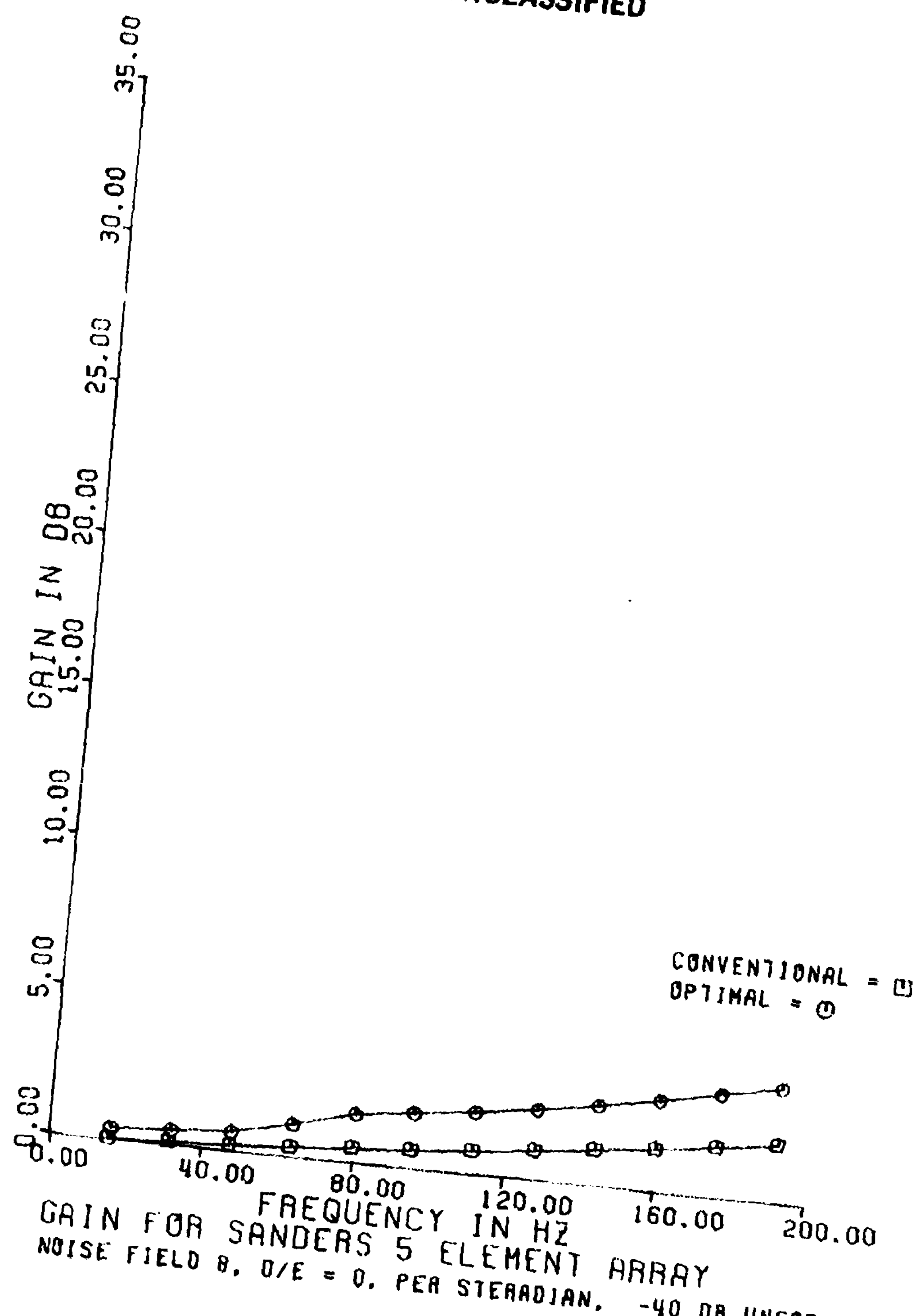

(U) Figure D29. Array gain – noise field 8 – D/E = 0.

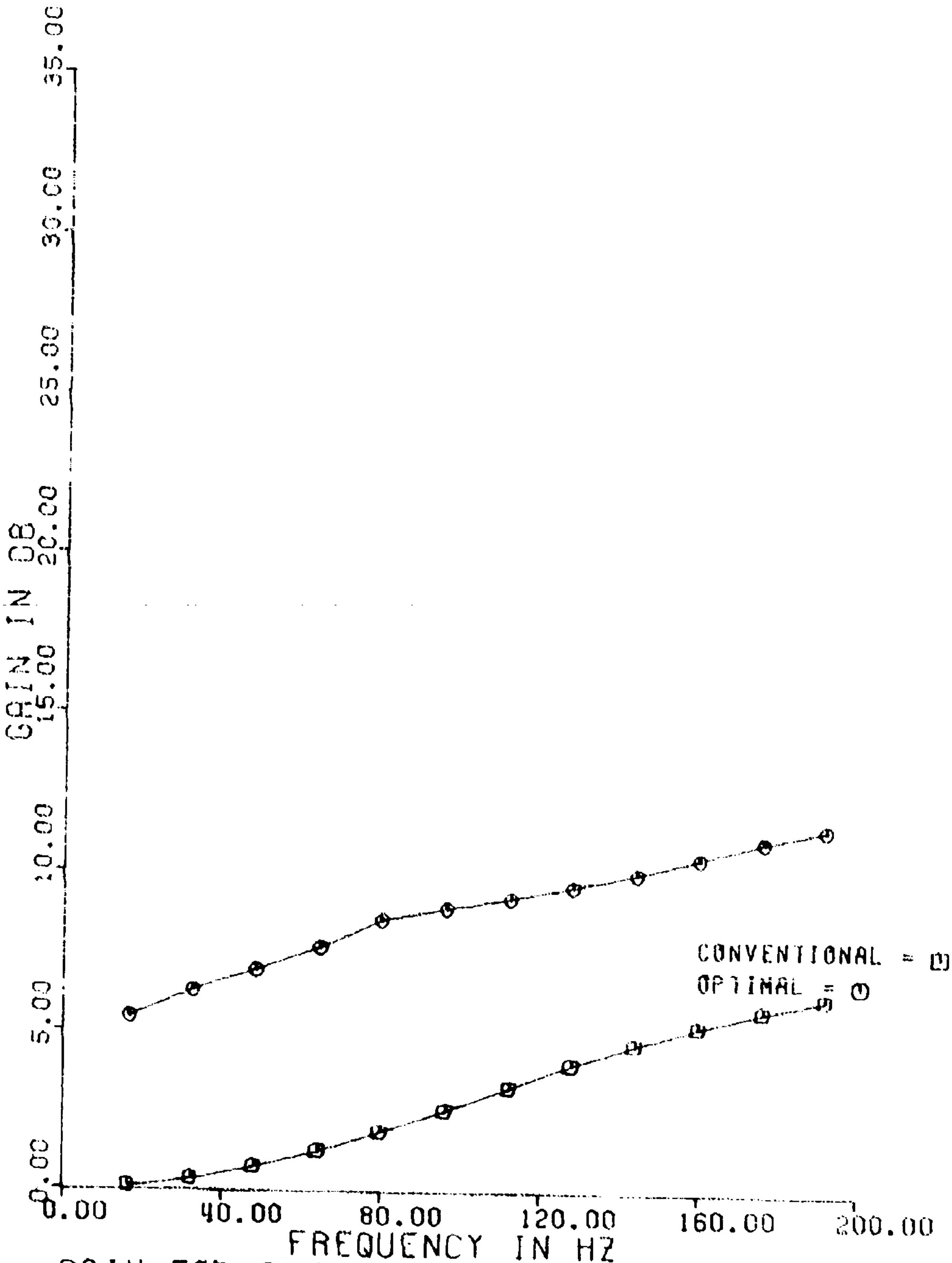

GAIN FOR SANDERS 5 ELEMENT ARRAY

NOISE FIELD 8, D/E = 15, PER STERADIAN, -40 DB UNCOR

(U) Figure D30. Array gain noise field 8 D/E = 15.

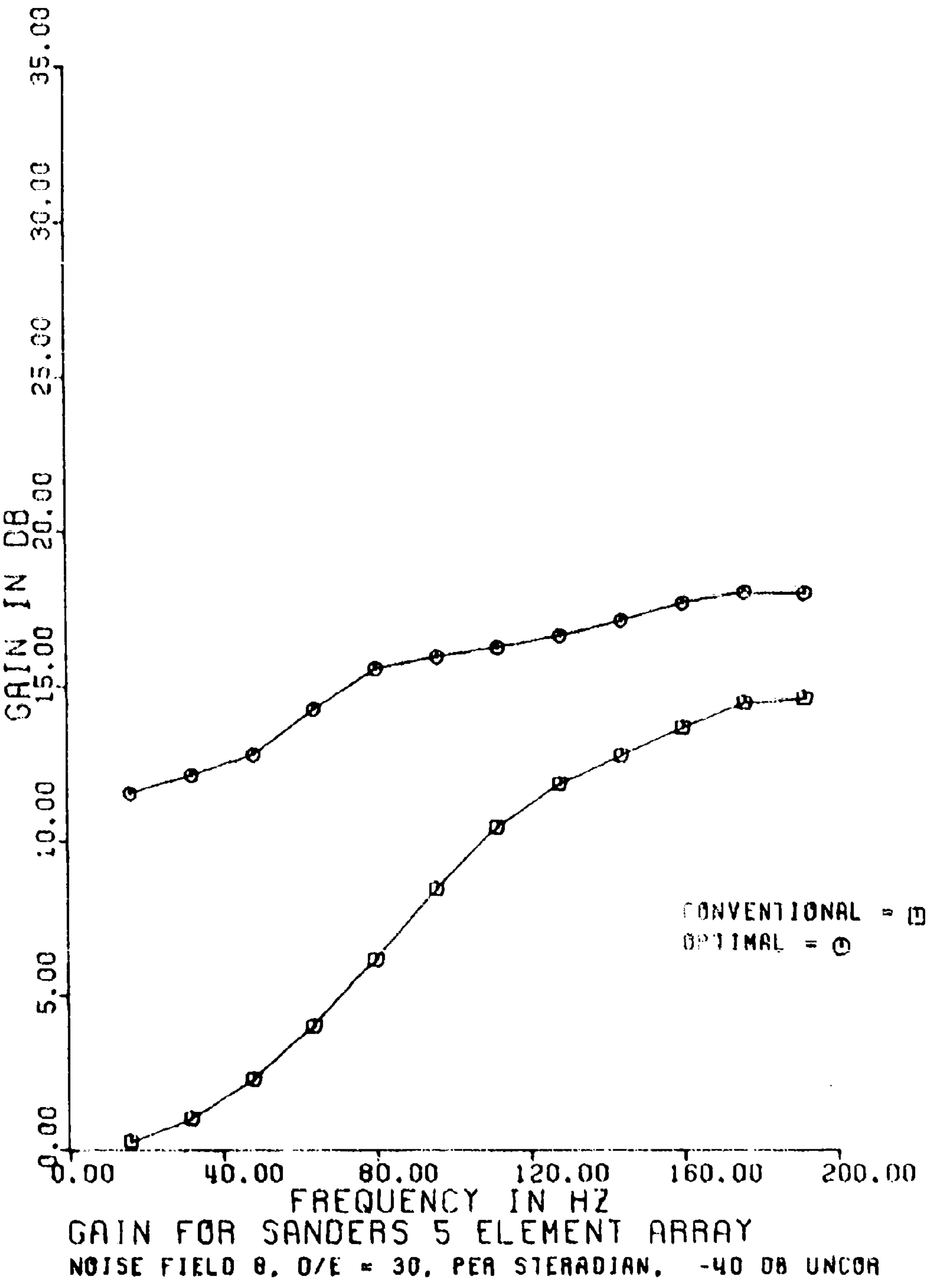

(U) Figure D31. Array gain noise field 8 D/E = 30.

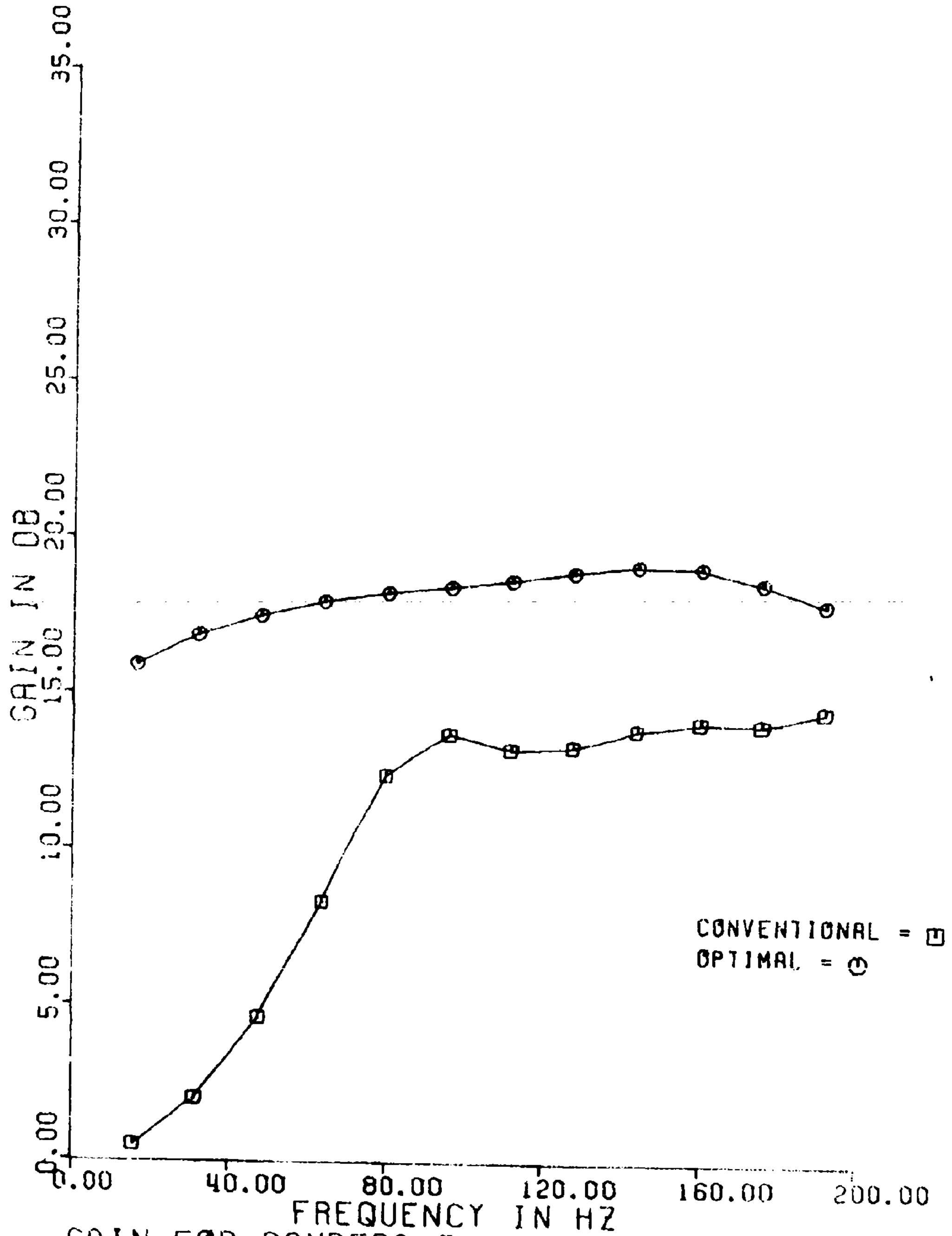

GAIN FOR SANDERS 5 ELEMENT ARRAY
NOISE FIELD 8, D/E = 45, PER STERADIAN, -40 DB UNCOR

(U) Figure D32. Array gain – noise field 8 D/E = 45.

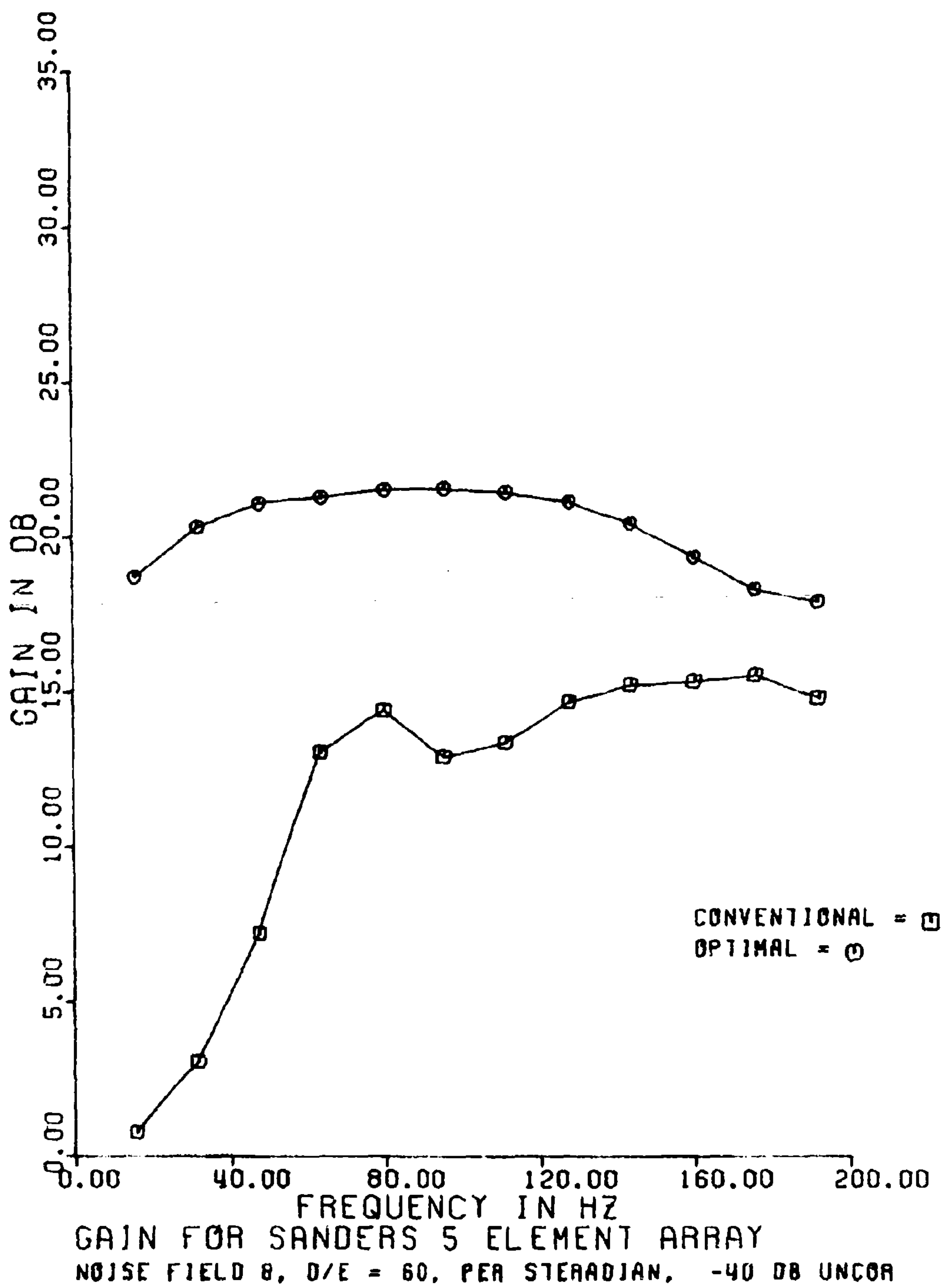

(U) Figure D33. Array gain – noise field 8 D/E = 60.

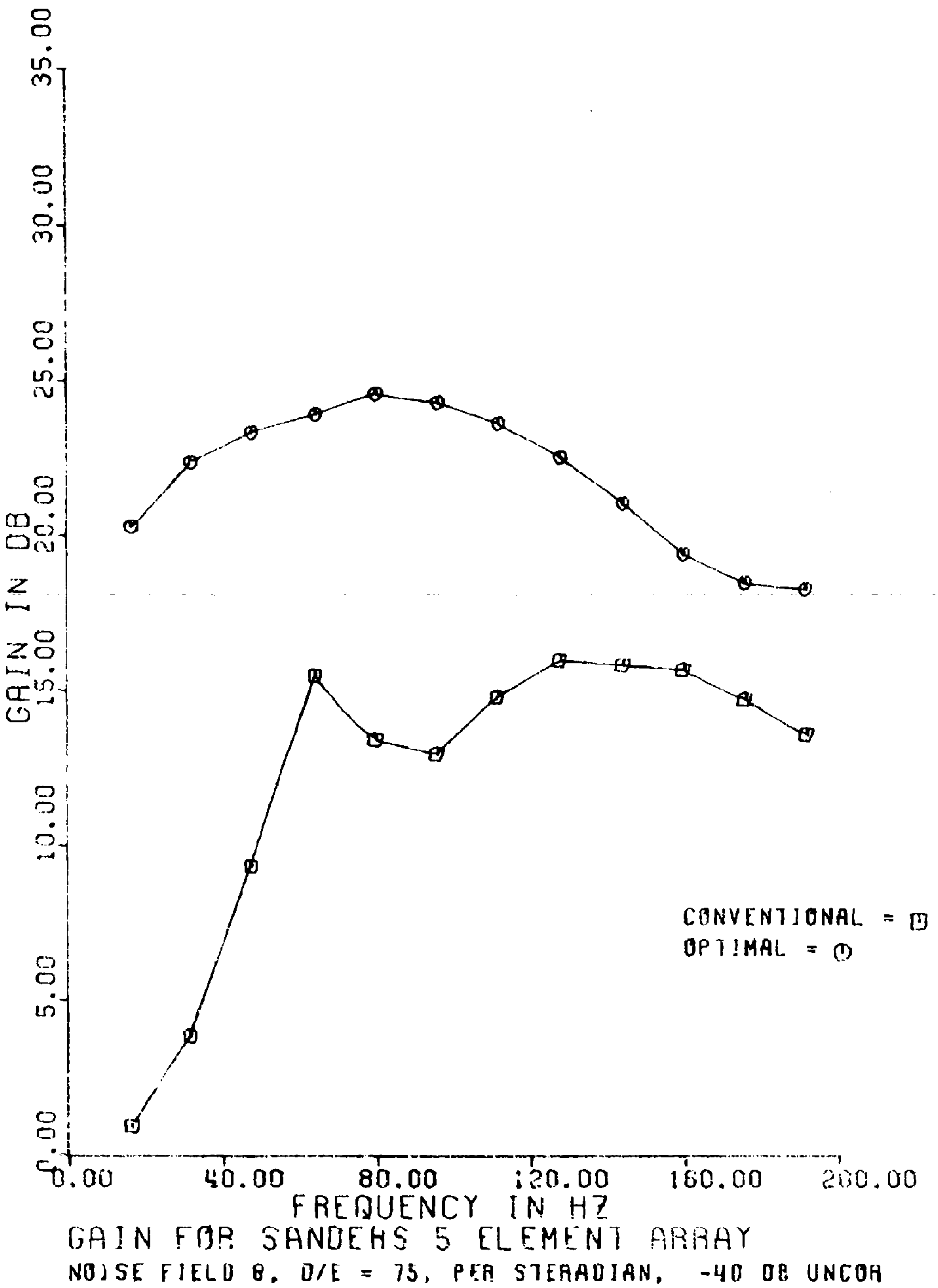

(U) Figure D34. Array gain noise field 8 D/E = 75.

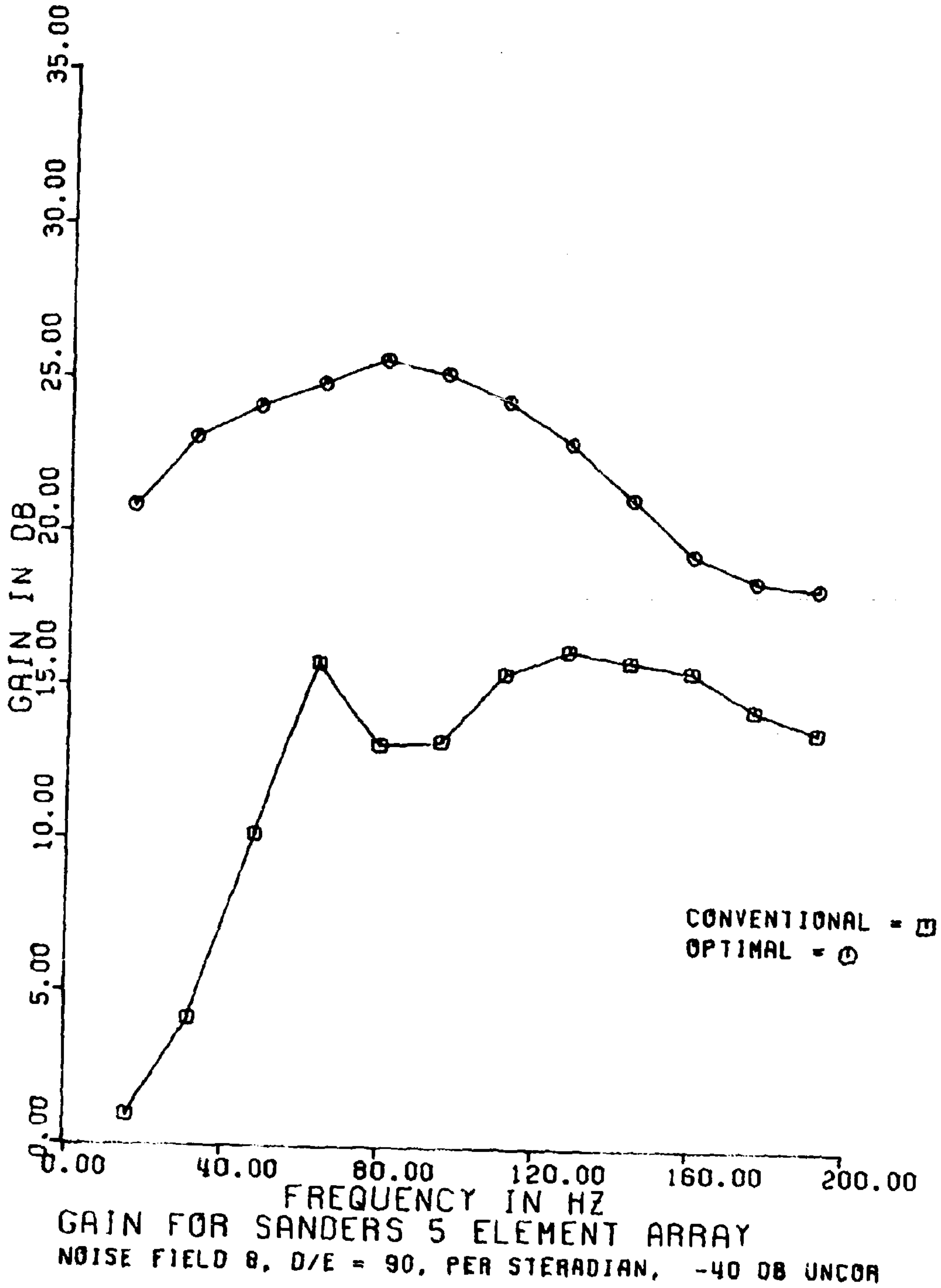

(U) Figure D35. Array gain – noise field 8 – D/E = 90.

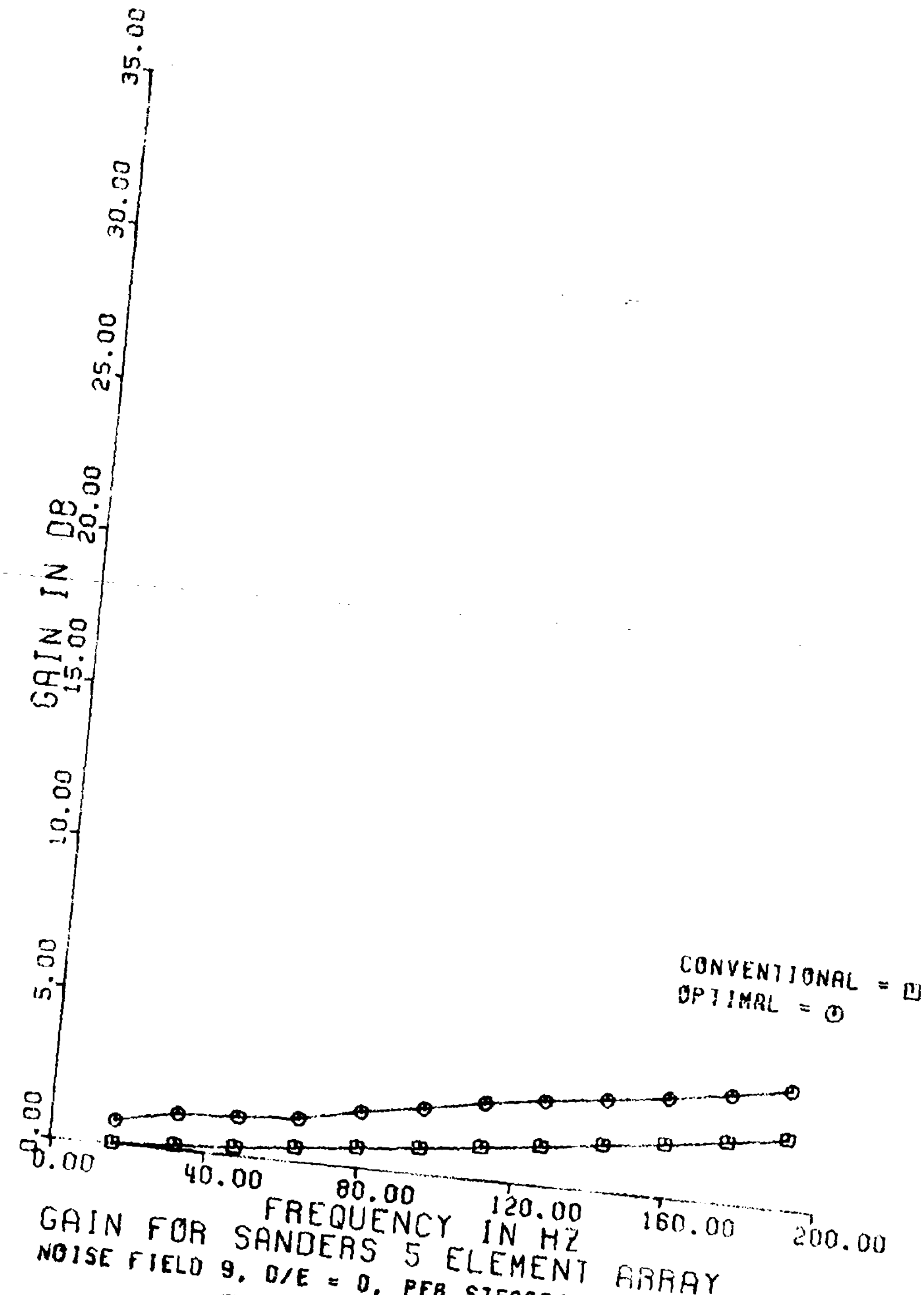

(U) Figure 36. Array gain -- noise field 9 -- D/E = 0.

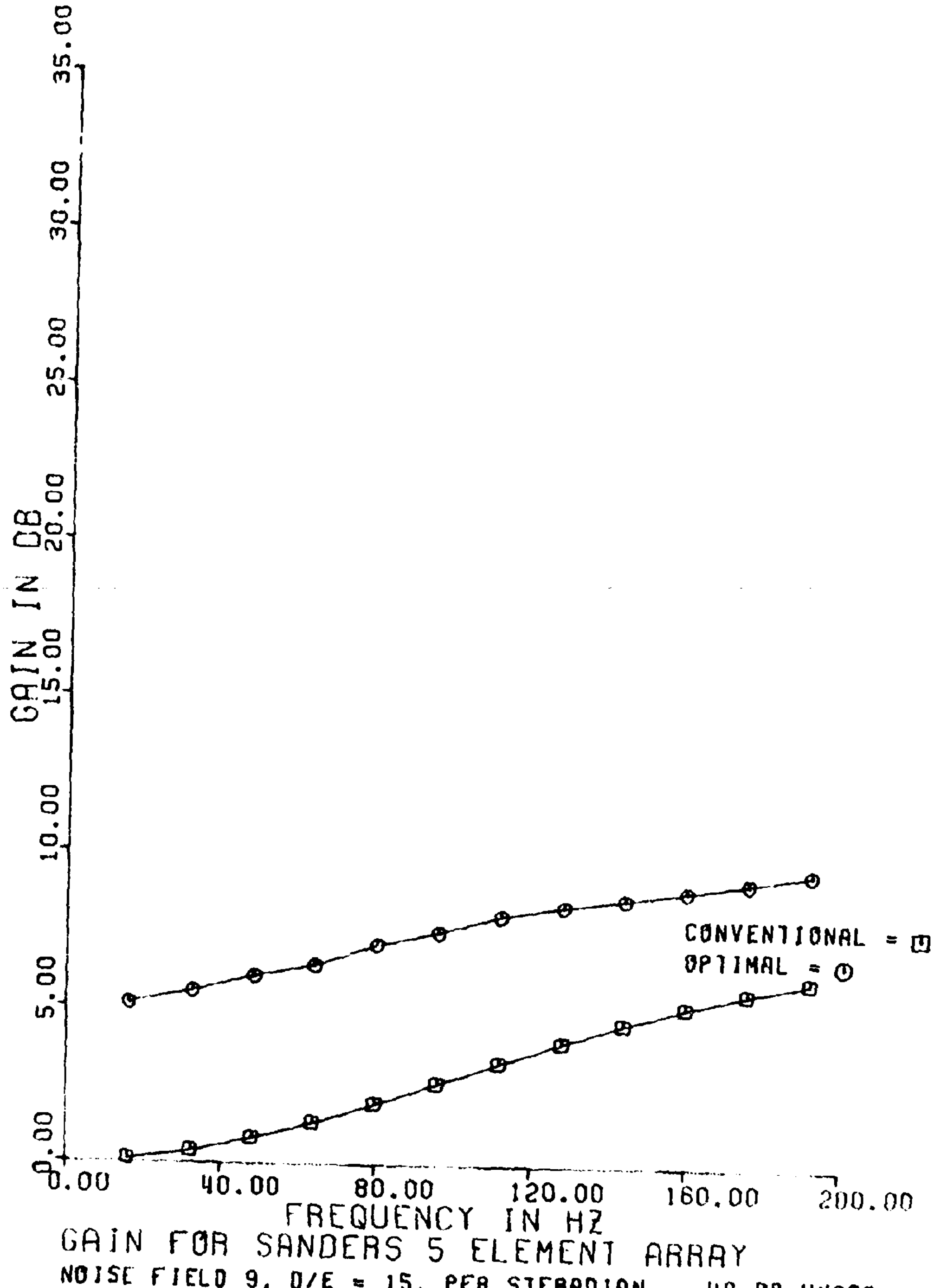

(U) Figure D37. Array gain – noise field 9 – D/E = 15.

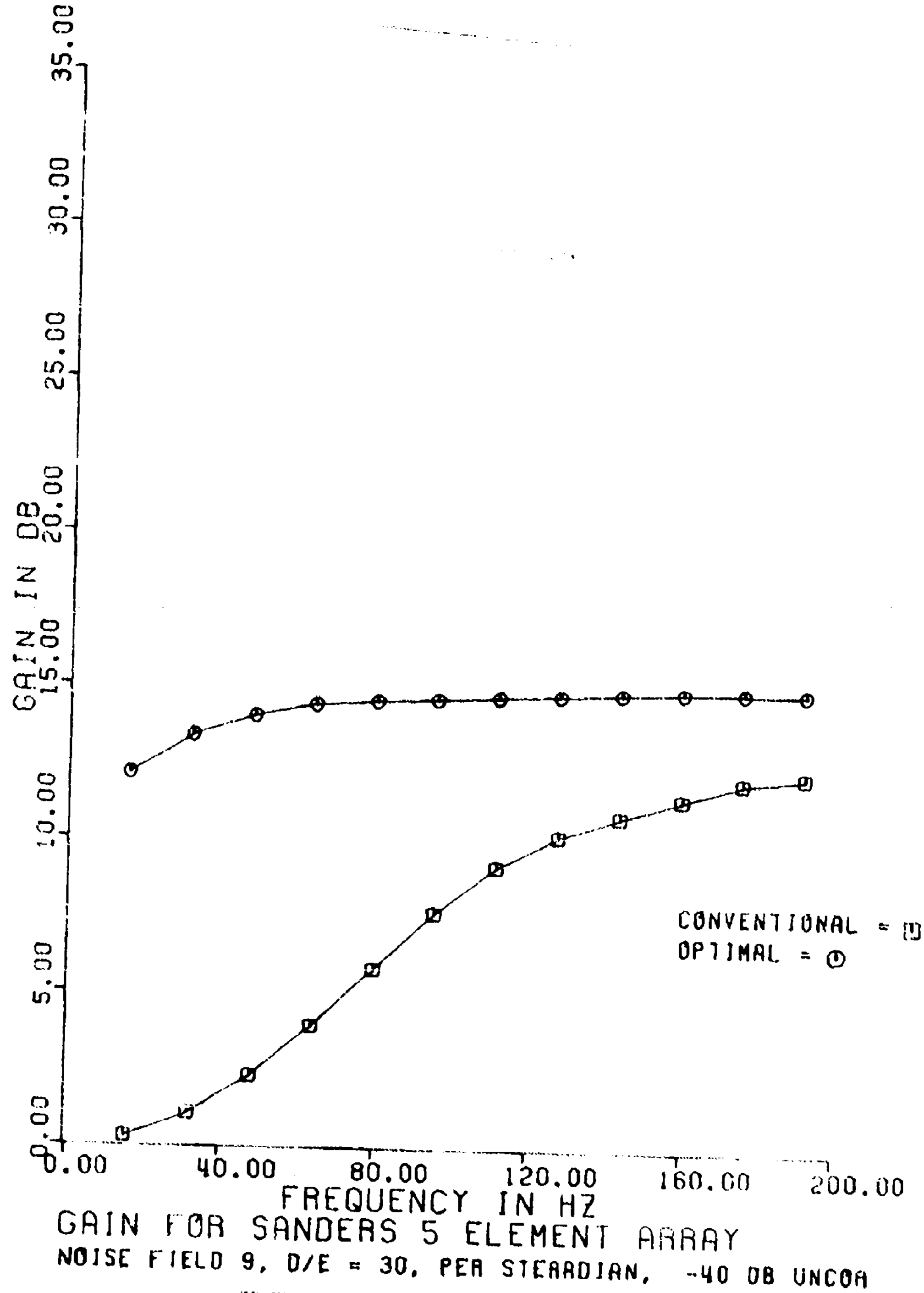

(U) Figure D38. Array gain — noise field 9 — D/E = 30.

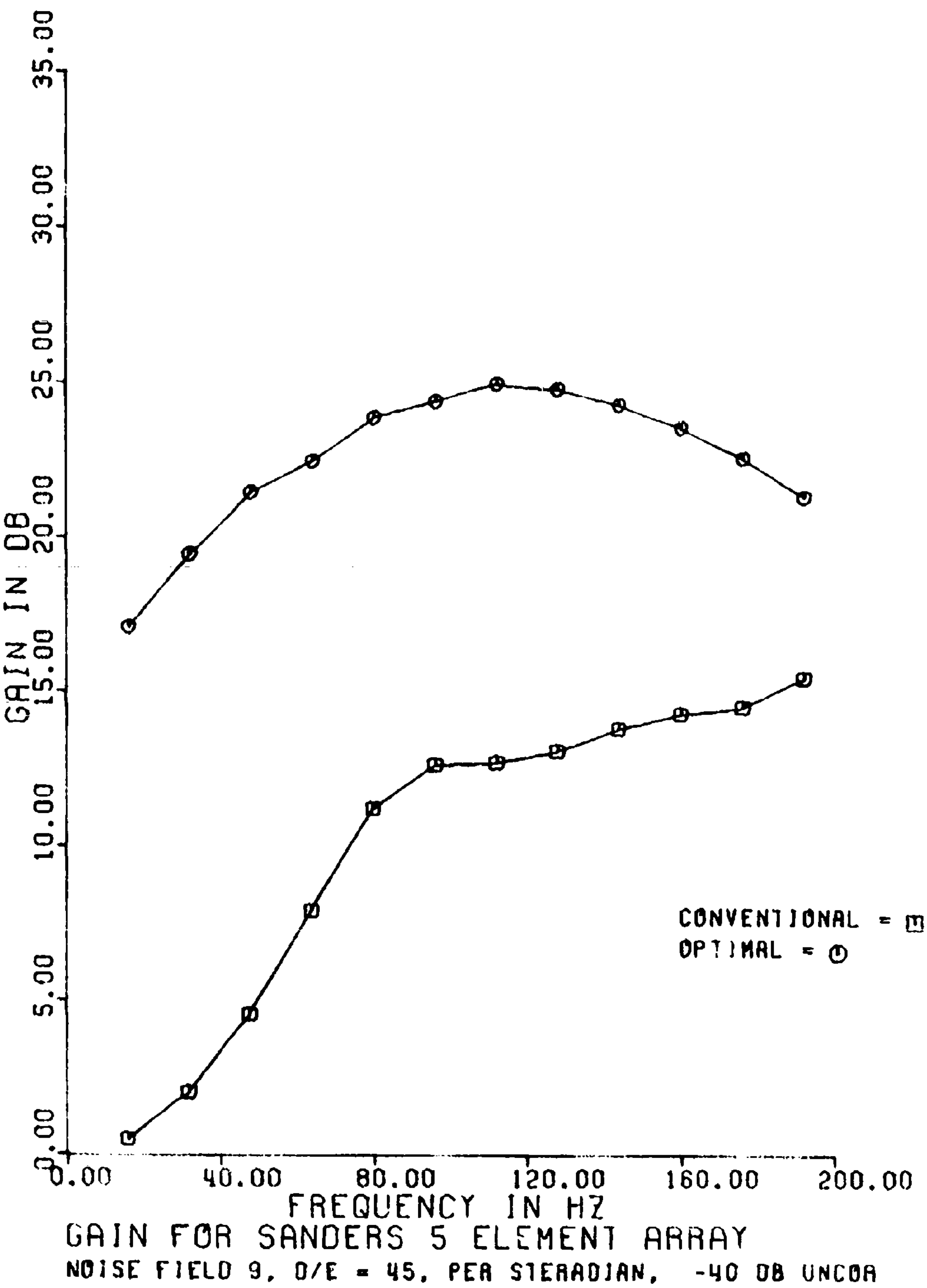

(U) Figure D39. Array gain – noise field 9 – D/E = 45.

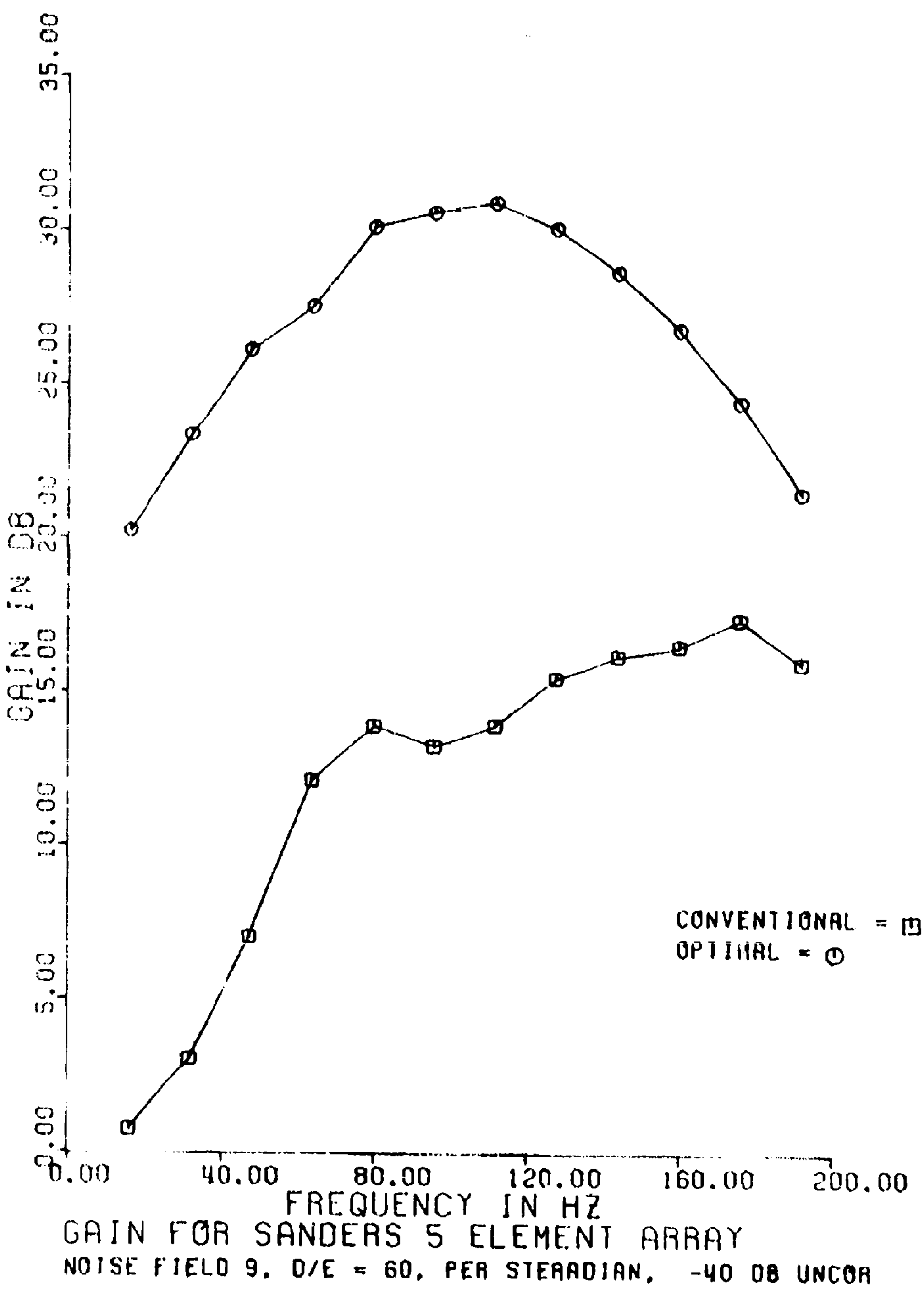

(U) Figure D40. Array gain – noise field 9 -- D/E = 60.

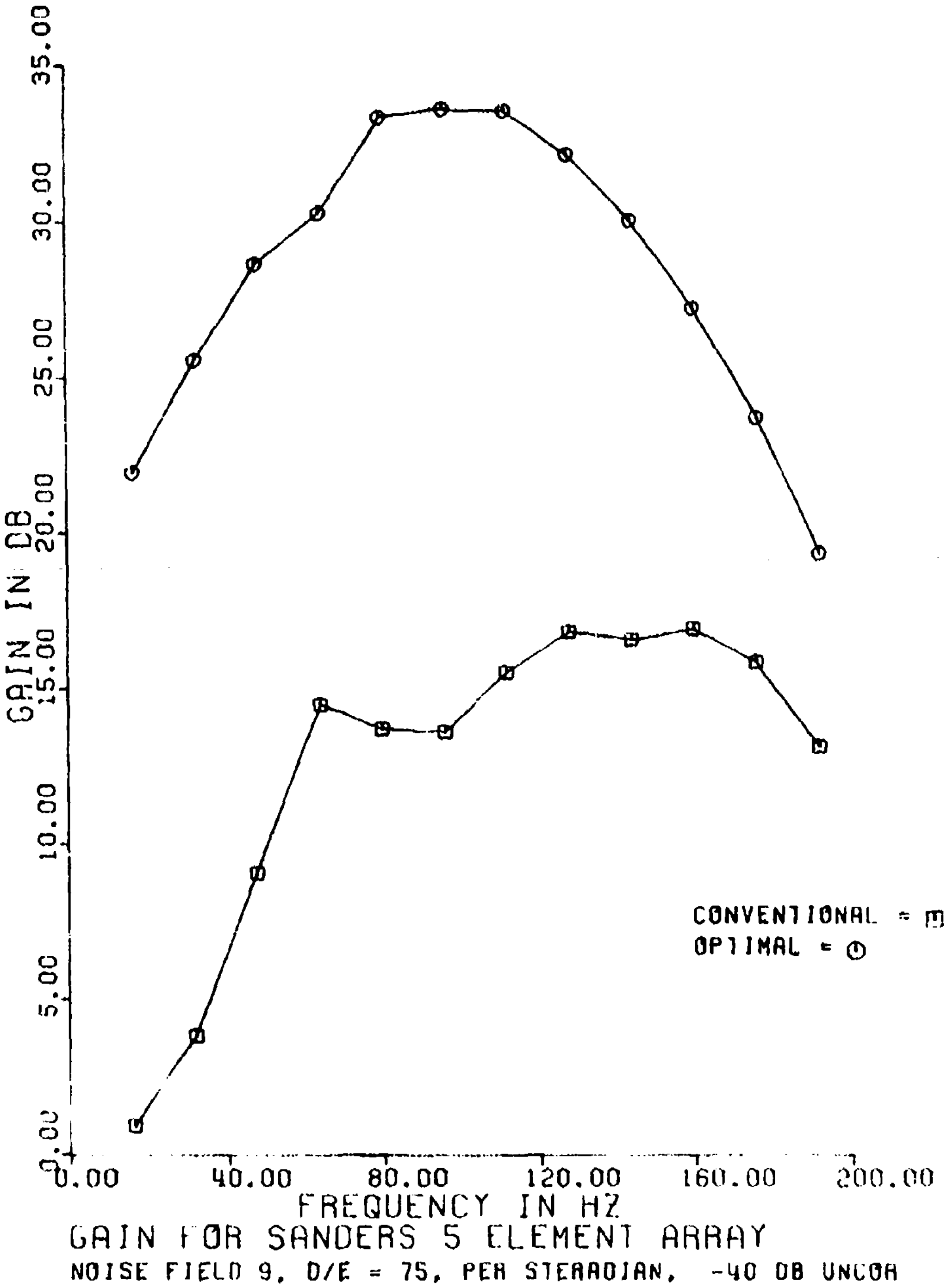

(U) Figure D41. Array gain – noise field 9 – D/E = 75.

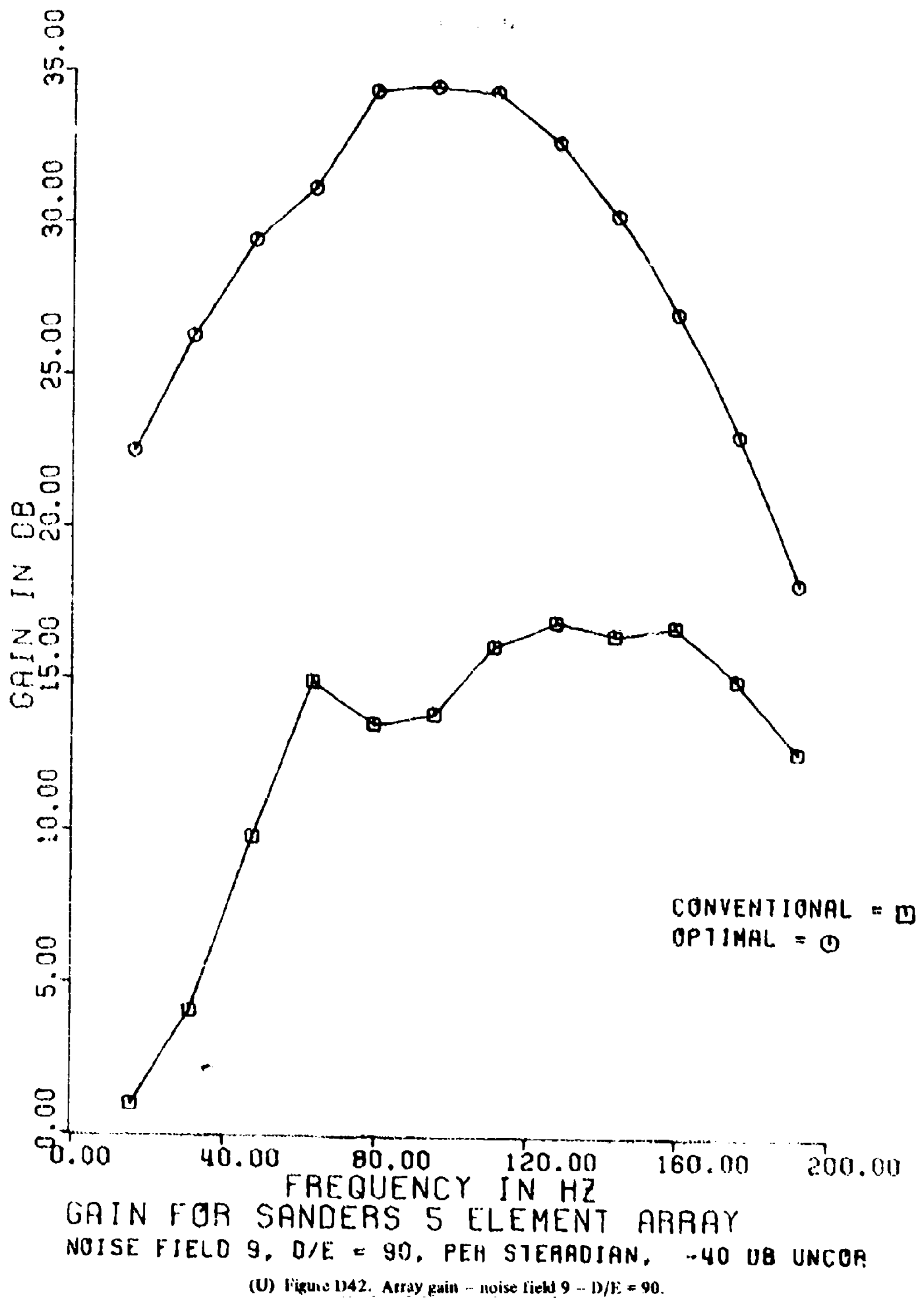

(U) Figure D42. Array gain – noise field 9 – D/E = 90.

INITIAL DISTRIBUTION

1 Assistant Secretary of the Navy (R&D) (ASW)
2 Chief of Naval Operations (NOP-954) (NOP-951)
2 Naval Air Systems Command
    NAIR-53301A (J. M. VonSas)
    NAIR-604
1 Naval Ship Systems Command (NSHP-00V)
1 Office of Naval Research (ONR-469)
2 Anti-Submarine Warfare Systems Project Office (ASW-211)
2 Naval Air Development Center
    Library
    J. Howard
1 Naval Civil Engineering Laboratory
1 Naval Electronics Laboratory Center
1 Naval Missile Center
1 Naval Ordnance Laboratory, White Oak
1 Naval Postgraduate School (Library, Technical Reports Section)
1 Naval Research Laboratory
1 Naval Ship Research and Development Center, Annapolis Division
1 Naval Ship Research and Development Center, Carderock Division
1 Naval Underwater Systems Center, New London Laboratory (J. Kingsbury)
1 Naval Weapons Center (Code 753)
2 Defense Documentation Center
1 Marine Physical Laboratory, Scripps Institution of Oceanography (Dr. V. C. Anderson)
1 Sanders Associate (O. F. Thrasher)

Center Distribution:

131
1311 (2)
50
503 (2)
5053 (10)
506
96
9601

UNCLASSIFIED
Security Classification

DOCUMENT CONTROL DATA - R & D

(Security classification of title, body of abstract and indexing annotation must be entered when the overall report is classified)

1. ORIGINATING ACTIVITY (Corporate author) Naval Undersea Research and Development Center San Diego, California 92132	2a. REPORT SECURITY CLASSIFICATION CONFIDENTIAL 2b. GROUP 4

3. REPORT TITLE

ADAPTIVE BEAMFORMING ANALYSIS FOR DIRECTIONALITY USING DATA FROM A VERTICAL ARRAY IN THE MEDITERRANEAN (U)

4. DESCRIPTIVE NOTES (Type of report and inclusive dates)

Research and Development

5. AUTHOR(S) (First name, middle initial, last name)

Craig G. Anderson
Dorothy A. Anderson
Gerald L. Kinnison

6. REPORT DATE	7a. TOTAL NO. OF PAGES	7b. NO. OF REFS
September 1971	161	4

8a. CONTRACT OR GRANT NO. N00019-70-C-0468 b. PROJECT NO. NAVAIR (533) project number W-2140 and NAVSHIPS (00V) project number F11-121 c. d.	9a. ORIGINATOR'S REPORT NUMBER(S) NUC TP 257 9b. OTHER REPORT NO(S) (Any other numbers that may be assigned this report)

10. DISTRIBUTION STATEMENT

11. SUPPLEMENTARY NOTES	12. SPONSORING MILITARY ACTIVITY Naval Ship Systems Command Naval Air Systems Command Washington, D. C. 20360

13. ABSTRACT

(U) Data were taken from a 5-sensor vertical array in the Ionian Basin. The data were reduced via sophisticated analytical processes to find the vertical directionality of the ambient noise field. The directionality from the measured data was compared to several noise fields simulated a priori. The measured directionality was found not to correspond well to any of the a priori simulated fields.

(U) It was observed that the amount of uncorrelated (circuit) noise has a strong influence on the measured directionality. Large percentages of uncorrelated noise depress the ability of an adaptively processed array to resolve the field. A new simulated noise field was generated to include the same percentage of uncorrelated noise as was reported for the recording instrumentation (10 percent). This simulation was found to compare very closely with the actual array response. Since the high uncorrelated noise probably is a result of the recording rather than the actual field, the directionality was again computed after 10 percent uncorrelated noise was removed from the spectral cross power matrix form of the actual data. The resultant directionality was then compared with that from a simulated field with no uncorrelated noise, which is presented as a candidate directionality model for the Mediterranean Sea ambient noise at 97 Hz.

(U) This report is presented as a prototype example for directionality analysis of data from multi-element arrays (VLAM, FLIP, ACODAC, MODANS, SONODIVER, ITASS, etc.). Adaptive beamforming (ABF) algorithms were employed as the analysis tools. Array gain versus frequency results are also shown for actual and simulated noise fields.

DD FORM 1 NOV 65 1473 (PAGE 1)
0102-014-6600

UNCLASSIFIED
Security Classification

14 KEY WORDS	LINK A		LINK B		LINK C	
	ROLE	WT	ROLE	WT	ROLE	WT
underwater ambient noise						
hydrophone arrays						
adaptive beamforming						

DEPARTMENT OF THE NAVY
OFFICE OF NAVAL RESEARCH
875 NORTH RANDOLPH STREET
SUITE 1425
ARLINGTON VA 22203-1995

IN REPLY REFER TO:

5510/1
Ser 321OA/011/06
31 Jan 06

MEMORANDUM FOR DISTRIBUTION LIST

Subj: DECLASSIFICATION OF LONG RANGE ACOUSTIC PROPAGATION PROJECT (LRAPP) DOCUMENTS

Ref: (a) SECNAVINST 5510.36

Encl: (1) List of DECLASSIFIED LRAPP Documents

1. In accordance with reference (a), a declassification review has been conducted on a number of classified LRAPP documents.

2. The LRAPP documents listed in enclosure (1) have been downgraded to UNCLASSIFIED and have been approved for public release. These documents should be remarked as follows:

   Classification changed to UNCLASSIFIED by authority of the Chief of Naval Operations (N772) letter N772A/6U875630, 20 January 2006.

   DISTRIBUTION STATEMENT A: Approved for Public Release; Distribution is unlimited.

3. Questions may be directed to the undersigned on (703) 696-4619, DSN 426-4619.

B F JR

BRIAN LINK
By direction

Subj: DECLASSIFICATION OF LONG RANGE ACOUSTIC PROPAGATION PROJECT (LRAPP) DOCUMENTS

DISTRIBUTION LIST:

NAVOCEANO (Code N121LC – Jaime Ratliff)
NRL Washington (Code 5596.3 – Mary Templeman)
PEO LMW Det San Diego (PMS 181)
DTIC-OCQ (Larry Downing)
ARL, U of Texas
Blue Sea Corporation (Dr.Roy Gaul)
ONR 32B (CAPT Paul Stewart)
ONR 321OA (Dr. Ellen Livingston)
APL, U of Washington
APL, Johns Hopkins University
ARL, Penn State University
MPL of Scripps Institution of Oceanography
WHOI
NAVSEA
NAVAIR
NUWC
SAIC

Declassified LRAPP Documents

Report Number	Personal Author	Title	Publication Source (Originator)	Pub. Date	Current Availability	Class.
IR 71-2	Fenner, D. F., et al.	SOUND VELOCITY AND BOTTOM CHARACTERISTICS FOR LRAPP ATLANTIC AREAS I, II, AND III (U)	Naval Oceanographic Office	710601	ADC008372; ND	U
T-71-NJ-4508-C	Larsen, H. L., et al.	LRAPP DATA COLLECTION (U)	Tracor, Inc.	710831	AD0517012; ND	U
Unavailable	Anderson, C. G., et al.	ADAPTIVE BEAMFORMING ANALYSIS FOR DIRECTIONALITY USING DATA FROM A VERTICAL ARRAY IN THE MEDITERRANEAN	Naval Undersea Research and Development Center	710901	AD0517696	U
MC PLAN 06	Unavailable	IOMEDEX LRAPP OPERATION ORDER (U)	Maury Center for Ocean Science	710924	ND	U
NRLFR7322	Lawson, W. M.	POSITION-DETERMINING SYSTEM FOR SEA-SPIDER HYDROPHONE ARRAYS	Naval Research Laboratory	711230	ND	U
N00014-71-C-0088	Unavailable	CONTINUATION OF LRAPP FINAL REPORT (U)	Bell Laboratories	720201	AD0520426; NS; ND	U
Unavailable	Unavailable	PARKA II-A EXPERIMENT. VOLUME 2	Maury Center for Ocean Science	720201	AD0596342	U
Unavailable	Unavailable	NOISE POWER MEASUREMENTS FROM THE LAMBDA TOWED ARRAY EXPERIMENT	Texas Instruments, Inc.	720401	ND	U
Unavailable	Anderson, P. R., et al.	LRAPP VERTICAL ARRAY PRELIMINARY DESIGN STUDY, PHASE I	Westinghouse Research Laboratories	720414	AD0900477	U
Unavailable	Unavailable	SUPPLEMENTARY DATA. NOISE POWER MEASUREMENTS FROM THE LAMBDA TOWED ARRAY EXPERIMENT	Texas Instruments, Inc.	720419	ND	U
MC Report 6, Volume 2	Unavailable	PARKA OCEANOGRAPHIC DATA COMPENDIUM-PARKA II-A	Maury Center for Ocean Science	720501	ND	U
MC Report 6, Volume 3	Unavailable	PARKA OCEANOGRAPHIC DATA COMPENDIUM-PARKA II-B	Maury Center for Ocean Science	720501	ND	U
Unavailable	Unavailable	NORLANT 72 PHASE 2 OPERATION PLAN	Naval Underwater Systems Center	720628	AD0521225	U
Unavailable	Unavailable	NORLANT 72 PHASE 2 SCIENTIFIC PLAN	Naval Underwater Systems Center	720628	AD0521226	U
Unavailable	Unavailable	NORLANT 72 PHASE 3 OPERATION PLAN	Naval Underwater Systems Center	720628	AD0521227	U
Unavailable	Unavailable	NORLANT 72 PHASE 3 SCIENTIFIC PLAN	Naval Underwater Systems Center	720628	AD0521228	U
MC PLAN 08	Unavailable	OPERATION PLAN. LRAPP TASSRAP EXERCISE (TEX)	Maury Center for Ocean Science	720701	ND	U
Unavailable	Miller, R. R., III	CURRENT REGIME OF THE MALTESE OCEANIC FRONTAL ZONE	Naval Underwater Systems Center	720906	AD0749706	U